ELECTRON TRANSFER AND ENERGY TRANSFER IN PHOTOACTIVE AND ELECTROACTIVE MOLECULES IN SOLUTION AND AT INTERFACES

by

Xiaohong Zhao

B.S., Chemistry
Northwest Normal University
1982
M.S., Physical Chemistry
Northwest Normal University
1985

Submitted to the Department of Chemistry
in partial fulfillment of the
requirements for the
Degree of

DOCTOR OF PHILOSOPHY

at the

MASSACHUSETTS INSTITUTE OF TECHNOLOGY

September 1994

Signature of
Author _____

Department of Chemistry
June 14, 1994

Certified by

_____

Professor Mark S. Wrighton

Accepted by

_____

Dietmar Seyferth

Chairman, Departmental Committee on Graduate Students

This doctoral thesis has been examined by a committee of the Department of Chemistry as follows:

Professor Robert J. Silbey.....
Chairman

Professor Mark S. Wrighton.....
Thesis Supervisor

Professor Moungi G. Bawendi.....

ELECTRON TRANSFER AND ENERGY TRANSFER IN PHOTOACTIVE AND ELECTROACTIVE MOLECULES IN SOLUTION AND AT INTERFACES

by

Xiaohong Zhao

Submitted to the Department of Chemistry on June 14, 1994 in partial fulfillment of the requirements for the Degree of Doctor of Philosophy in Chemistry

ABSTRACT

Chapter 1

An overview of electron transfer and energy transfer theories is presented. Photoinduced electron transfer and energy transfer at surface-electrolyte interfaces are discussed. A brief review of progress in the fields of photoinduced electron transfer and energy transfer is presented. Molecular-based charge transfer devices and the optimization of the devices with the author's findings in this field are introduced and discussed.

Chapter 2

The laser apparatus assembled for conducting transient absorption and time-resolved emission experiments are described. The bimolecular quenching of the excited state of tetraphenylporphyrin (TPP) by N,N,N',N'-tetramethyl-*p*-phenylenediamine (TMPD) is monitored spectroscopically. The salt effect on the decay kinetics of the charge-separated state, $TPP^{-\cdot}$-$TMPD^{+\cdot}$ is analyzed. Intramolecular quenching of the excited state of $[(4\text{-ferrocenylpyridine})Re(CO)_3\text{-}(1,10\text{-phenanthroline})]^+$ by the ferrocenyl center is also studied. The 4-ferrocenylpyridine complex does not emit light upon photoexcitation, whereas $[(\text{pyridine})Re(CO)_3(1,10\text{-phenanthroline})]^+$ exhibits intense photoluminescence. However, a charge separated-state could not be unambiguously identified in the 4-ferrocenylpyridine complex.

Chapter 3

Inter- and intramolecular quenching of the lowest singlet excited state of three porphyrins by ferrocene derivatives are reported. 5,15-*Bis*(4-tolyl)-2,3,7,8,12,13,17,18-octamethylporphyrin (**1**) and two derivatives of **1** where one of the tolyl methyl groups was replaced by a ferrocenylvinyl group, **2**, or by a ferrocenylethyl group, **3**, were prepared. Porphyrin **2** was

isolated as a mixture of *cis* (73%) and *trans* (27%) isomers. Singlet excited state properties were studied by steady-state emission spectroscopy and by emission lifetime measurements. The relative quantum yields of fluorescence for **2** and **3** compared to **1** are 0.38 and 0.84, respectively. Fluorescence decay lifetimes of **1** and **3** are 15 ns and 14 ns, respectively. Fluorescence of **2** is revealed to be due to the emission of two species (*cis* and *trans* isomers) with lifetimes of 4 ns and 13 ns, respectively. The shorter fluorescence lifetimes and smaller fluorescence quantum yields for **2** and **3** compared to **1** are attributed to quenching of the singlet excited state of the porphyrin by the ferrocenyl centers. However, the fraction of quenching by electron transfer vs. energy transfer could not be quantitatively measured, but the rate constant for quenching is no more than 10^8 s^{-1}, consistent with electron transfer quenching. Intermolecular quenching rate constants for the quenching of the porphyrin singlet excited state by ferrocene derivatives were also found to be consistent with an electron transfer quenching mechanism.

Chapter 4

The Re(I) carbonyl complex $[L'Re(CO)_3(4,4'\text{-}X\text{-}2,2'\text{-}bipyridine)]^+$, **1a** where L'= 4-ethylpyridine and X = $C(O)O\text{-}(CH_2)_3SiCl_3$, was chemically immobilized onto SiO_2, indium tin oxide (ITO), Pt surfaces and high surface area SiO_2. Emission decays and time-resolved emission spectra were obtained for monolayer quantities of **1a** covalently attached to these surfaces. Analysis of the emission decays of **1a** in electrolyte solution on the three flat surfaces allows an evaluation of the contributions of interfacial energy transfer and electron transfer to quenching of photoexcited **1a**. Emission decay profiles fit a single exponential decay. The excited-state lifetime of **1a** is shortest on the conducting and light-absorbing Pt surface, while longer excited-state lifetimes are observed for **1a** on the non-absorbing, insulating SiO_2 surface and the non-absorbing, but conducting ITO surface. The dominant mechanism for quenching by Pt is energy transfer, based on the significant shortening of the emission lifetime of **1a** on Pt compared to that on ITO and SiO_2. The result that the excited-state lifetimes of **1a** on SiO_2 and ITO are very close and can not be distinguished within experimental error is consistent with a small amount of quenching of photoexcited **1a** on ITO by a slow interfacial electron transfer process. The kinetics of the interfacial electron transfer between **1a** and ITO/Pt were examined by cyclic voltammetry and chronoamperometry.

Chapter 5

Intramolecular electron transfer in chromophore end-capped homopolymers and multiblock polymers of electron donors is discussed. A series of chromophore,

[(Re(CO)$_3$(pyridyl)(2,2′-biquinoline)]$^+$, end-capped homopolymers and multiblock polymers were found to have long-lived charge separated states. The homopolymers and multiblock polymers were prepared by ring opening metathesis polymerization (ROMP) of norbornene monomers bearing pendant phenothiazine derivatives or a derivative of N,N,N′,N′-tetramethyl-*p*-phenylenediamine. In some cases methyltetracyclodecane (mtd) was used to introduce a hydrocarbon block. The chromophore was attached to the end of the polymers by quenching a living polymer with [Re(CO)$_3$(2,2′-biquinoline)(pyridine-4-carboxaldehyde)]$^+$. Thus, polymers of the type Re(mtd)$_x$, Re(mtd)$_x$(PTZ)$_y$, Re(mtd)$_x$(TMPD)$_y$, and Re(mtd)$_x$(PTZ)$_y$(TMPD)$_z$ were prepared. A correlation between the electron transfer rate constants and the repeat unit number of an inert spacer block (mtd) which separate a chromophore and electron donor block or electron donor blocks were obtained. Intramolecular chain electron transfer was observed in Re(mtd)$_x$(PTZ)$_y$(TMPD)$_{10}$ (x = 100, 200,y = 10, 50) polymers. Block polymers exhibit higher-order structures. Microphase separation of the blocks which have different building monomers in the solid state was observed. Block segregation and micelle were observed in solution.

Thesis Supervisor: Mark S. Wrighton

Title: Provost and Ciba-Geigy Professor of Chemistry

This thesis is dedicated to my wife, Jie,

my parents and my grandparents

Acknowledgments

First of all, I would like to thank my thesis advisor, Professor Mark Wrighton for allowing me to work for him, for his guidance and forbearance. His wisdom, his dedication to excellence, and his approach to science, have been an inspiration to me. Special thanks to Mark for his great help and patience with my writing thesis. I'd also like to thank Professor Silbey for his generous encouragement and for taking an interest in my research and career. Thanks also to Professor Greene for being a mentor, and to Professor Steinfeld for introducing me to the field of laser spectroscopy. I would like to thank Professor Bawendi for his encouragement.

Special thanks to all at the MIT Laser Research Center I could use many laser and detection facilities to make my thesis possible.

My fellow Wrighton group member Eric Lee started building up the TA apparatus. Eric and I shared the sorrow and joy when the laser systems down and up in Room 6A-220.

I would like to thank all Wrighton group members for their generous help and friendship. I'd thank Drs. Giasson for making the porphyrin-ferrocene molecules, Christ for making surface-derivatizing molecules of photoactive and electroactive, Albagli and Jin-Kyu Lee of the Shrock group for making redox-active ROMP polymers. All help has made this thesis possible.

Ron Duff has been a good friend and has been sharing so much about cars, sound systems, etc. I really enjoyed talks with Helen Tatistcheff and wish her a success at Naval Lab. Doris Kang is helpful for exchanging information about job hunting. Tayhas Palmore impressed me with her hard work and interest in chemistry. I wish good luck to Larry and Maria.

Thanks also go to many Chinese friends of mine at MIT, Hao Li and Ming Zhang who helped me a lot with my quantum class, Changzhu Dou who spent whole night to help me fixing a damaged bicycle, Fuchan Gao, Qi Zhao, Yizu Zhu, and so many others I could not mention here for all the sharing, caring, and the time we spent together.

Finally, I would like to thank my parents and grandparents for their constant support, my wife Jie Cheng for her endless love, her belief in me, her constant support, and her many sacrifices.

Table of Contents

List of Figures

Number Page

Chapter 2

Chapter 3

Chapter 4

Chapter 5

List of Schemes

Number Page

Chapter 1

Chapter 2

Chapter 3

Chapter 4

Chapter 5

List of Tables

Number Page

Chapter 4

Chapter 5

CHAPTER ONE

INTRODUCTION TO PHOTOINDUCED INTERFACIAL ELECTRON TRANSFER AND ENERGY TRANSFER

Photoinduced electron transfer and energy transfer reactions have been extensively studied by numerous researchers with the aim of understanding and utilizing these phenomena as a means of capturing and storing solar energy.[1,2] One approach to solar energy conversion is to model the primary biological processes in photosynthesis.[3] Another approach is to use photoelectrochemical devices to generate electricity or chemical fuels.[4] An impressive illustration of an attempt to model the biological system is a molecular "pentad" where a combination of five donors, chromophores, and acceptors are linked in an ordered fashion in a single molecule. Study of the molecular assemblies which consist of linked donor and acceptor constituents has shown the dependence of photoinduced, intramolecular electron transfer rates on parameters such as driving force, distance, solvent interactions, and molecular geometry,[5-8] providing insight into the factors governing charge separation efficiency in natural and synthetic molecular assemblies for phtoconversion.

One set of model systems is based on transition metal complexes functioning as chromophores.[9] Another is the porphyrin-based systems.[10-16] The interest in using transition metal complexes in a solar energy conversion scheme is due to: (1) their long excited state lifetimes which can be exploited with ease in electron transfer reactions; (2) their photochemical and electrochemical durability; and (3) their strong and tunable absorptivity to optimizing response to the solar spectrum. Similarly, the porphyrin-based systems are not only durable but strongly absorptive in the visible.

Meyer and co-workers have made a Ru(2,2′-bipyridine)$_3^{2+}$-based triad which consists ofa linked phenothiazine derivative as a donor and linked viologen derivative as an acceptor. This triad exhibits a charge-separated state lifetime of 108 ns.[9a] Gust and co-workers have synthesized a porphyrin based, multicomponent charge-separating molecule with a high quantum yield (0.83) and long-lived charge separated state of 55 μs.[11] Recent reviews on photoinduced electron transfer reactions in multicomponent molecular systems can be found in the recent review article by Fox.[2a]

Studies of photoelectrochemical devices have recently focused on semiconductor-based systems, where one or both of the electrodes in an electrochemical cell is a semiconducting photoelectrode. Lewis and co-workers have reported a n-GaAs based photoelectrochemical cell showing 15% solar conversion efficiency.[17] Grätzel and co-workers have demonstrated a dye-sensitized TiO_2-based cell with a 12% solar conversion efficiency.[18] Such semiconductor-based devices are presently much more efficient than molecule-based systems, but molecule-based systems might show some pratical advantages (e.g. cost) with no less theoretical efficiency.[19]

Molecule-based devices consisting of an ordered array of charge separating molecules linking two electrodes is a goal of the Wrighton group.[3] To achieve this goal, it is essential: (1) to design and synthesize appropriate molecular systems as multicomponent redox reagents to extend the lifetime of a charge separated state; (2) to attach appropriate terminal functional

groups to the ends of the molecular system to be orthogonally self-assembled onto electrodes of different materials and to achieve appropriate gap size between two electrodes to accommodate the molecular system; (3) to establish whether photoinduced interfacial electron transfer will compete with energy transfer processes to the electrode which would quench the excited states. The overall situation desired is shown in Scheme 1-1.

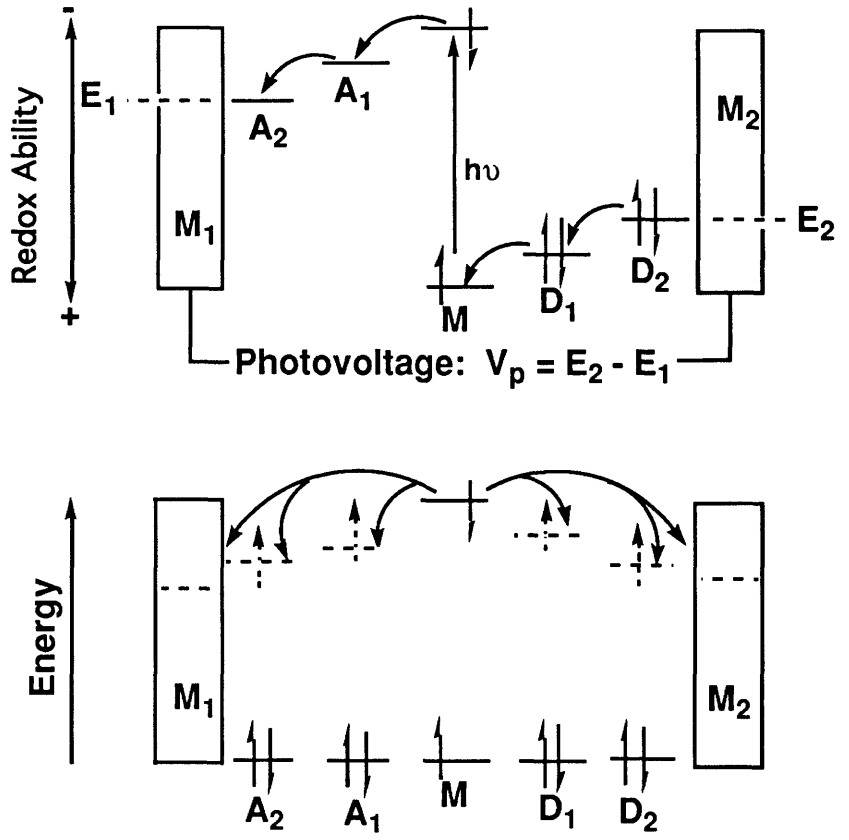

Scheme 1-1. Photoconversion through interfacial electron transfer.

Thesis Overview

Major contributions summarized in this thesis consist of new findings on some established systems and new photophysical results for new photoactive and electroative systems. We have found that interfacial electron transfer always competes with energy transfer for Re(I) complexes bound to Pt or indium tin oxide electrodes immersed in electrolyte media. This critical finding is essential to ultimate success of molecule-based photovoltaic devices like that represented in Scheme 1-1. These findings are summarized in Chapter 4 and 6.

In Chapter 2 we describe the experimental apparatus assembled for conducting transient absorption and time-resolved emission experiments. The procedures used for the studies of intermolecular electron transfer in a porphyrin-tetramethylphenylenediamine system and the intramolecular quenching of Re(I) polypyridyls by a ferrocene moiety are also described. In Chapters 3 and 5 we describe the design and synthesis of multicomponent charge separating molecules, polymers, and the investigation of photoinduced electron transfer in these systems.

The Re(I) terminated phenothiazine and tetramethylphenylene-diamine polymers made by ring-opening metathesis polymerization (ROMP) described in Chapter 5 are the first known polymers to sustain a long-lived, charge-separated state. This new family of macromolecules may yield considerable insight for development of molecule-based systems for photoconversion.

The research projects done in our group have supplied ways and means to achieve the goal of obtaining appropriate gap size between two electrodes to accommodate a molecular system. Large, charge separating polymers may greatly ease the technical requirements for microfabricating the closely spaced electrodes.[20]

The remainder of this chapter provides the necessary background on theories of electron transfer and energy transfer in solution and at electrolyte-surface interfaces needed to interpret the experimental results described in subsequent chapters.

Electron Transfer Theory

The theory of electron transfer has been discussed and reviewed extensively in the literature.[21-31] In the present section, we will briefly describe the theories which serve as the basis for the discussion of the experimental results presented in later chapters. The most widely used and successful theory of electron transfer is that of Marcus,[21,22] which include the assumption that the precursor state (D*-A) must reorganize the nuclear coordinates of both the complex and the surrounding environment to the point where the energy of the reorganized precursor state is the same as that of the successor state immediately following electron transfer.

Within the framework of classical Marcus theory of electron transfer, the unimolecular rate constant k_{et} (in s^{-1}) is given by

$$k_{et} = \kappa_{el}\nu_n \exp\left[-\frac{\left(\lambda + \Delta G^{0'}\right)^2}{4\lambda k_b T}\right], \qquad (1\text{-}1)$$

where λ is the reorganization energy needed to distort the precursor complex and its surroundings to the equilibrium configuration of the successor complex; κ_{el} is the electronic transmission coefficient and ν_n is the frequency of passage (nuclear motion) through the transition state ($\nu_n \cong 10^{13}$ s^{-1}). $\Delta G^{0'}$ is the Gibbs free-energy change in the overall electron transfer reaction, with a correction term ΔG_{corr} to account for any specific interactions (such as Coulombic attraction) between $D^{+\cdot}$ and $A^{-\cdot}$ in the product successor complex, i.e., $\Delta G^{0'} = \Delta G^0 + \Delta G_{corr}$ (usually $\Delta G_{corr} < 0$). Note that eq. (1-1) is a transition-state theory expression with

$$\Delta G^{\ddagger} = \frac{\left(\lambda + \Delta G^{0'}\right)^2}{4\lambda k_b T}. \qquad (1\text{-}2)$$

Thus as $-\Delta G^{0'}$ increases, $\Delta G^{\ddagger}$ decreases, and k_{et} is maximal when $-\Delta G^{0'} = \lambda$. However, in the region where $-\Delta G^{0'} > \lambda$, k_{et} is predicted to *decrease;* this has been called the *inverted region.*[22]

The reorganization energy λ is usually divided into two contributions as follows

$$\lambda = \lambda_i + \lambda_o, \qquad (1\text{-}3)$$

where λ_i arises from critical internal vibrational modes in the precursor complex and is usually represented by a sum of harmonic potential energies,[23] and λ_o accounts for the effect of the

surrounding medium. If a two-sphere dielectric continuum model is assumed[21,22,27], then λ_o is given by

$$\lambda_o = \frac{e^2}{4\pi\varepsilon_0}\left[\frac{1}{2r_D} + \frac{1}{2r_A} - \frac{1}{r_{DA}}\right]\left[\frac{1}{\varepsilon_{op}} - \frac{1}{\varepsilon_s}\right], \qquad (1\text{-}4)$$

where r_D and r_A are the donor and acceptor radii, respectively, r_{DA} is the center-to-center distance of D-A, ε_s is the static dielectric constant.

Treating molecular vibrations as harmonic oscillators, it can be easily shown that the inner sphere reorganization energy is given by[21,27-29]

$$\lambda_i = \sum_k \frac{a_k^r a_k^p}{a_k^r + a_k^p}\left(\frac{1}{2}\Delta Q_k\right)^2, \qquad (1\text{-}5)$$

where a_k^r and a_k^p are the force constants of the normal mode k in the precursor and successor complexes, respectively. ΔQ_k is the displacement in the equilibrium nuclear position. The summation is taken over all the intramolecular vibrational modes. The major contributions to λ_i come from those high frequency modes along which there is a significant distortion. The force constants can obtained from the infrared and Raman spectra. The distortion can be either estimated from the spectral analysis or obtained from the crystallographic data if both oxidation states are stable.[29]

Brunschwig *et al.*[28] have investigated the two contributions to λ and have shown that for a wide variety of transition-metal complexes $\lambda_i \cong 0.2\text{-}0.3$ eV. For most of the large organic D-A

systems considered here, λ_i is not likely to exceed 0.2 eV. λ_o varies from near zero for non-polar solvents where $\varepsilon_{op} \cong \varepsilon_s$ to ≥ 1 eV for polar solvents.

Equation (1-1) is applicable for adiabatic electron transfer, i.e., where $\kappa_{el} \cong 1$. However, many, perhaps most, of the D-A systems studied fall into the class of non-adiabatic electron transfer reactions where $\kappa_{el} << 1$. In the case of non-adiabatic electron transfer, the problem must be treated quantum mechanically. One widely used model, based primarily on earlier work of Jortner,[24,31] assumes a single, averaged effective internal vibrational frequency ν in the precursor complex that contributes to λ_i; the surrounding medium is treated classically as a dielectric continuum. In this semiclassical model k_{et} is given by

$$k_{et} = \frac{2\pi}{\hbar} H_{ps}^2 \left(4\pi\lambda_0 kT\right)^{-1/2} \sum_{m=0}^{\infty} \left(e^{-s} S^m / m!\right) exp\left[-\frac{\left(\lambda_o + \Delta G^{0'} + mh\nu\right)^2}{4\lambda_0 k_b T}\right], \quad (1\text{-}6)$$

where $S = \lambda_i / h\nu$ and H_{ps} is an electronic coupling energy ($H_{ps} = \left\langle \psi_p^0 \middle| \hat{H}_{el} \middle| \psi_s^0 \right\rangle$) where $\hat{H}_{el}$ is the electronic Hamiltonian, and ψ_p^0 and ψ_s^0 are the electronic wave functions for the precursor and successor complexes, respectively. In the high-temperature limit (where $kT >> h\nu$), eq.(1-6) reduced to

$$k_{et} = \frac{2\pi}{\hbar} H_{ps}^2 \left(4\pi\lambda_0 kT\right)^{-1/2} exp\left[-\frac{\left(\lambda_o + \Delta G^{0'}\right)^2}{4\lambda_0 k_b T}\right], \quad (1\text{-}7)$$

which is the same as eq.(1-1) with

$$\kappa_{el}\nu_n = \frac{2\pi}{\hbar} H_{ps}^2 \left(4\pi\lambda_0 kT\right)^{-1/2}. \qquad (1\text{-}8)$$

When a high-frequency mode makes an important contribution to λ, eq.(1-1) is a good approximation in the normal region, but an expression such as eq.(1-7) is better in the inverted region.[30]

Interfacial Electron Transfer

The one-electron, and outer-sphere electron transfer reactions at electrodes have been theoretically studied for decades.[22,32-35] In considering interfacial electron transfer process involving a reversible molecular redox couple, it is important to be mindful of the following: (1) as a donor or acceptor of the redox complex, electronic states of a metal are a continuum, and therefore forward and back interfacial electron transfer rate constants, k_f and k_b, will be sums of the individual rates for each electronic state of the metal weighted by the Fermi-Dirac probability of occupancy (f_+) or vacancy (f_-) of that state; (2) the electron might tunnel a long distance with the tunneling rate determined by the electronic coupling between the metallic states of the electrode and the redox molecule, i.e., when the reaction is nonadiabatic; (3) the reduction and oxidation states of the redox complex have similar structures, and the dominant contribution to the activation barrier is the reorganization of the solvent,[36] which can treated classically.

The rate constants k_f and k_b can thus be written as

$$k_{f,b} = \sum_i f_{\pm}(\varepsilon_i)\ \upsilon_i\ \exp\left[-\Delta G^{\ddagger}_{f,b}(\varepsilon_i) / \left(k_b\ T\right)\right], \qquad (1\text{-}9)$$

where $-e\varepsilon_i$ is the energy of the ith metallic state, and the Fermi-Dirac probabilities are

$$f_{\pm}(\varepsilon_i) = \left\{1 + \exp\left[\pm e(\varepsilon_i - E) / \left(k_b T\right)\right]\right\}^{-1}. \qquad (1\text{-}10)$$

The prefactor υ_i is determined by the electronic coupling between the ith metallic state and the redox molecule. The activation free energies are given by the Marcus theory[32]

$$\Delta G^{\ddagger}_{f,b}(\varepsilon_i) = \left[\lambda \pm e(\varepsilon_i - E^{0'})\right]^2 / \left(4\lambda\right) \qquad (1\text{-}11)$$

where λ is the reorganization energy defined in a similar way as that for the electron transfer in solution. Here, we assume that the same reorganization energy applies to both the forward and back reactions.

Substituting eq.(1-10) and eq.(1-11) into eq.(1-9), we can obtain

$$k_{f,b} = \upsilon\rho\left(k_b T\right)\sum_i \frac{\exp\left\{-\left[x - \frac{\lambda \pm e(E - E^{0'})}{k_b T}\right]^2\left[\frac{k_b T}{4\lambda}\right]\right\}}{\left\{1 + \exp(x)\right\}}\,\Delta x \qquad (1\text{-}12)$$

Defining

$$\rho_i = \frac{1}{e\Delta\varepsilon_i} = \frac{1}{e\left(\varepsilon_i - \varepsilon_j\right)}, \quad x = \frac{e\left(\varepsilon_i - E\right)}{k_b T},$$

and making the simplifying assumption that both the electronic coupling and density of metallic states are independent of energy, eq.(1-12) can be recast as

$$k_{f,b} = \upsilon\rho(k_bT)\sum_i \frac{\exp\left\{-\left[x - \frac{\lambda \pm e(E - E^{0'})}{k_bT}\right]^2\left[\frac{k_bT}{4\lambda}\right]\right\}}{\{1 + \exp(x)\}}\ \Delta x. \qquad (1\text{-}13)$$

It is straightforward to convert the above summation into an integral as

$$k_{f,b} = \upsilon\rho(k_bT)\int_{-\infty}^{\infty} \frac{\exp\left\{-\left[x - \frac{\lambda \pm e(E - E^{0'})}{k_bT}\right]^2\left[\frac{k_bT}{4\lambda}\right]\right\}}{\{1 + \exp(x)\}}\ dx. \qquad (1\text{-}14)$$

At moderate reaction free energies and temperatures [$e(E-E^{0'}) \ll \lambda$, $k_bT \ll \lambda$], the integrations for k_b and k_f are both much less than $(4\pi\lambda/k_bT)^{1/2}$, normally activated, and follow opposing exponential dependencies on potential. At very negative reaction free energy for the forward electron transfer or at very positive reaction free energy for the back electron transfer, the integration is equal to $(4\pi\lambda/k_bT)^{1/2}$ and is temperature independent. To make the integration equal to unity, we can rewrite eq.(1-14) as

$$k_{f,b} = \upsilon\rho\,(4\pi\lambda k_bT)^{1/2}\,\Omega_{f,b}(\lambda,\ E - E^{0'},\ T), \qquad (1\text{-}15)$$

where $\Omega_{f,b}(\lambda,\ E - E^{0'},\ T)$ is rewritten as

$$\Omega_{f,b} = \left(k_bT/4\pi\lambda\right)^{1/2}\int_{-\infty}^{\infty} \frac{\exp\left\{-\left[x - \frac{\lambda \pm e(E - E^{0'})}{k_bT}\right]^2\left[\frac{k_bT}{4\lambda}\right]\right\}}{\{1 + \exp(x)\}}\ dx.$$

Energy Transfer

Molecular energy transfer, well known for a long time, had been theoretically and experimentally studied by many researchers. We are concerned here mainly with the electronic excitation energy transfer between molecules. Theoretical studies of the electronic excitation energy transfer have been developed by Förster[37] and Dexter.[38] Förster developed a physical model, based on coulombic interaction between a donor and an acceptor, with which energy transfer results from long range dipole-dipole or quadrupole-quadrupole interaction between the energy donor and acceptor. Dexter elaborated the other mechanism---the exchange interaction model. The Dexter energy transfer mechanism requires orbital overlap of the donor and acceptor. The rate of the coulombic energy transfer (Förster mechanism) is given as

$$k_{cl} = \left(\frac{1}{\tau_0}\right)\left(\frac{R_0}{R}\right)^6, \qquad (1\text{-}16)$$

where τ_0 is the fluorescence decay time of the excited state of the donor, and

$$R_0 = \left[\frac{9000(\ln 10)K^2 q}{128\pi^5 n^4 N}\int f(\tilde{\nu})\,\varepsilon_q(\tilde{\nu})\,\frac{d\tilde{\nu}}{\tilde{\nu}^4}\right]^{1/6}. \qquad (1\text{-}17)$$

In eq.(1-17) q is the fluorescence quantum yield of the excited state of the donor and R_0 is called the "critical transfer distance" where the rate of the energy transfer becomes the same as the rate of the decay of the excited state of the donor.

The rate of the Dexter exchange energy transfer is given by

$$k_{ex} = k_0 \exp(-2R/L), \qquad (1\text{-}18)$$

where R is the distance and L is the Bohr radius of the donor and acceptor.[39]

Interfacial Energy Transfer

Interfacial energy transfer may occur when the excited molecule is immobilized on a surface. The process has been extensively modeled by different theories.[40-43] The Chance-Prock-Silbey model[44,45] has been successfully applied to interfacial energy transfer between metal or semiconducting surfaces and the excited molecule, mainly in a vacuum. This model treats the photoexcited molecule as a point oscillating dipole located above a metal of dielectric constant $\varepsilon(\omega)$, which is separated from a dielectric ambient at an infinitely sharp boundary shown in Scheme 1-2. The oscillating dipole has a dipole moment given by

$$\mu = \exp(-i\omega t - bt/2). \qquad (1\text{-}19)$$

The dielectric ambient accommodating the dipole has a real refractive index n_1 and a propagation constant $k_1 = 2\pi n_1/\lambda$. The refractive index of the metal is complex as $\tilde{n}_2$ $(\equiv n_2 + iK_2)$, and a propagation constant is given by $k_2 = 2\pi\tilde{n}_2/\lambda$. Within this framework, the total emission decay rate of the excited molecule can be separated into radiative and nonradiative components, the latter representing the rate of energy transfer to the metal by

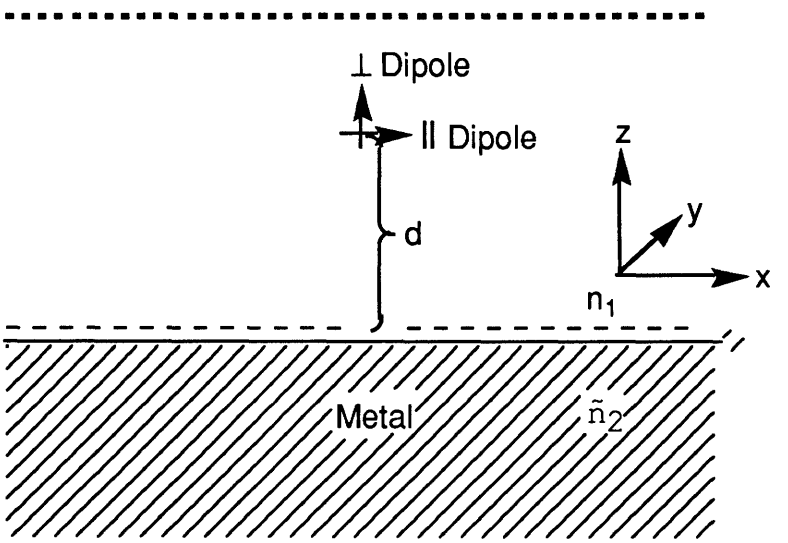

Scheme 1-2. Geometry of the dipole-metal system; d is the distance from the diploe to the surface. The dashed lines represent the two planes through which the flux is computed.

using the energy flux method. The energy flux method requires a negligible shift in the emission frequency caused by a metal and the intrinsic damping of the dipole. In the case of a vertical dipole, the total energy flux through planes parallel to the metal surface, above and below the dipole, can be calculated by using the complex Poynting vector.[46,47] Because the total energy flux divided by the energy of the dipole is equal to the total damping rate constant without considering the intrinsic nonradiative decay, the normalized rate constant for nonradiative energy transfer to the metal can be written as[45]

$$\hat{b}_{ET} = 3q \, \mathrm{Im} \int_{1}^{\infty} B e^{-2l\hat{d}} \tau^3 d\tau \qquad (1\text{-}20)$$

where $\tau = \eta/k_1$, $\hat{b}_{ET} = b_{et}/b^0$ ($b^0 = b_r^0 + b_{nr}^0 = 1/\tau^0$), $B \equiv \varepsilon_2/(\varepsilon_1 m + \varepsilon_2 l)$, $\hat{d} = k_1 d$, $m \equiv -i\left(k_1^2 - \eta^2\right)^{1/2}$, $l \equiv -i\left(k_1^2 - \eta^2\right)^{1/2}$, and q is the quantum yield of the emission.

To obtain the energy transfer rate constant for small $\hat{d}$, we just multiply eq.(1-20) by d^3 (because the integral is proportional to d^{-3}) and then let d approach zero. This leads to

$$\lim_{d \to 0} \hat{b}_{ET} = \frac{3q}{4\hat{d}^3} \mathrm{Im}\left(\frac{-k_1^2}{k_1^2 + k_2^2}\right) \qquad (1\text{-}21)$$

for a vertical dipole and

$$\lim_{d \to 0} \hat{b}_{ET} = \frac{3q}{8\hat{d}^3} \mathrm{Im}\left(\frac{-k_1^2}{k_1^2 + k_2^2}\right) \qquad (1\text{-}22)$$

for a horizontal dipole. If we define

$$\hat{b}_{ET} = \beta d^{-3} \, , \qquad (1\text{-}23)$$

we can write

$$\beta = \frac{3q}{32} \frac{\lambda^3 \theta}{\pi^3 n_1} \left[\frac{n_2 K_2}{\left(n_1^2 + n_2^2 - K_2^2\right)^2 + 4 n_2^2 K_2^2}\right], \qquad (1\text{-}24)$$

where $k_1 = 2\pi n_1/\lambda$, $k_2 = 2\pi \tilde{n}_2/\lambda$, and $\tilde{n}_2 = n_2 + iK_2$. θ is a parameter for orientation of the dipole and equals 1 for a horizontal dipole, 2 for a vertical dipole, and 4/3 for randomly oriented dipoles. Unlike the dimensionally reduced Förster transfer rate constant expression, the Chance-Prock-Silbey model

gives a specific β parameter only in terms of the optical constants of the two media. If the emission is a broad band, eq.(1-24) may be rewritten as an integral over the emission spectrum, which is analogous to the Förster expression, as following

$$\beta_{tot} = \frac{\int_{\omega_1}^{\omega_2} \beta(\omega) I_{EM}(\omega) d\omega}{\int_{\omega_1}^{\omega_2} I_{EM}(\omega) d\omega} \qquad (1\text{-}25)$$

where β_{tot} is the value of β integrated over the emission band and $I_{EM}(\omega)$ is the normalized emission intensity at a specific frequency.

References

1. Wrighton, M. S. *Comments Inorg. Chem.* **1985**, *4(5)*, 269.

2. (a) Fox, M. A. *Chem. Rev.* **1992**, *92*, 365. (b) Wasielewski, M. R. *Chem. Rev.* **1992**, *92*, 435. (c) Mayer, T. J. *Acc. Chem. Res. 1989, 22(5)*, 163. (d) *Photoinduced Electron Transfer;* Fox, M. A.; Chanon, M., Ed.; Elsevier: Amsterdam, 1988.

3. Wrighton, M. S. *In Fine chemicals for the Electronics Industry;* Banfield, P., Ed.; Royal Soc. Chem.: London, 1986; pp. 53-69.

4. (a) Lewis, N. S. *Ann. Rev. Phys. Chem.* **1991**, *42*, 543. (b) *Heterogeneous Photoinduced Electron Transfer;* Gratzal, M., Ed.; CRC Publishers: Boca Raton, FL, 1988.

5. (a) Ulstrup, J. *Charge Transfer Processes in Condensed Media;* Springer-Verlag: Berlin, 1979. (b) Devault, D. *Quantum-Mechanical Tunnelling in Biological Systems;* Cambridge Univ. Press: Cambridge, ed.2, 1984. (c) Newton, M. D.; Sutin, N. *Annu. Rev. Phys. Chem.* **1984**, *35*, 437. (d) Closs, G. L.; Miller, J. R. *Science* **1988**, *240*, 440.

6. (a) Marcus, R. A. *Annu. Rev. Phys. Chem.* **1966**, *15*, 155. (b) Marcus, R. A.; Sutin, N. *Biochim. Biophys. Acta* **1985**, *811*, 265. (c) Fox, M. A. *Adv. Photochem.* **1986**, *13*, 237. (d) Mikkelsen, K. V.; Ratner, M. A. *Chem. Rev.* **1987**, *87*, 113.

7. (a) Isied, S. S. *Prog. Inorg. Chem.* **1984**, *32*, 443. (b) Meyer, T. J.; Taube, H. in *Comprehensive Coordination Chemistry;* Wilkinson, G.; Gillard, R. D.; McCleverty, J. A., Ed.: Pergamon Press: London, 1987, Vol.1, P331.

8. Connoly, J. S.; Bolton, J. R. In *Photoinduced Electron Transfer;* Eds. Fox, M. A.; Chanon, M. Elsevier: Amsterdam, **1988**, Part D, P303.

9. (a) Mecklenburg, S. L.; Reek, B. M.; Schoonover, J. R.; McCafferty, D. G.; Wall, C. G.; Ericson, B. W.; Meyer, T. J. *J.*

Am. Chem. Soc. **1993**, *115*, 5479. (b) Jones, W. E.; Bignozzi, C. A.; Chen, P.; Meyer, T. J. *Inorg. Chem.* **1993**, *32*, 1176. (c) Scott, J. R.; Willie, A.; McLean, M.; Stayton, P. S.; Sligar, S. G.; Durham, B.; Millet, F. *J. Am. Chem. Soc.* **1993**, *115*, 6820. (d) MacQeen, D. B.; Shanze, K. S.; *J. Am. Chem. Soc.* **1991**, *113*, 7470.

10. (a) Wiederrecht, G. P.; Watanabe, S.; Wasielewski, M. R. *Chem. Phys.* **1993**, *176*, 601. (b) Gosztola, D.; Wasielewski, M. R. *J. Phys. Chem.* **1993**, *97*, 9599. (c) Wasielewski, M. R.; Gaines, G. L.; Wiederrecht, G. P.; Svec, W. A.; Niemczyk, M. P. *J. Am. Chem. Soc.* **1993**, *115*, 10442. (d) Johnson, D. G.; Niemczyk, M. P.; Minsek, D. W.; Wiederrecht, G. P.; Svec, W. A.; Gaines, G. L.; Wasielewski, M. R. *J. Am. Chem. Soc.* **1993**, *115*, 5692. (e) Wasielewski, M. R.; Gaines, G. L.; Niemczyk, M. P.; Gosztola, D.; Svec, W. A. *Pure Appl. Chem.* **1992**, *64*, 1319. (f) Oneil, M. P.; Niemczyk, M. P.; Svec, W. A.; Gosztola, D.; Gaines, G. L.; Wasielewski, M. R. *Science*, **1992**, *257*, 63. (g) Vergelt, F. J.; Koehorst, R. B. M.; Schaafsma, T. J.; Lambry, J. C.; Martin, J. L.; Johnson, D. G.; Wasielewski, M. R. *Chem. Phys. Lett.* **1991**, *182*, 107. (h) Gaines, G. L.; Oneil, M. P.; Svec, W. A.; Niemczyk, M. P.; Wasielewski, M. R. *J. Am. Chem. Soc.* **1991**, *113*, 2774. (i) Hofstra, U.; Schaafsma, T. J.; Sanders, G. M.; Van Dijk, M.; Van der Plas, H. C.; Johnson, D. G.; Wasielewski, M. R. *Chem. Phys. lett.* **1988**, *151(1-2)*, 169. (j) Wasielewski, M. R. Photochem. Photobiol. 1988, 47, 923. (k) Wasielewski, M. R. Niemczyk, M. P.; Svec, W. A.; Pewitt, E. B.

J. Am. Chem. Soc. **1985**, *107*, 1080. (l) ibid. 1985, 107, 5562. (m) Wasielewski, M. R.; Niemczyk, M. P. *J. Am. Chem. Soc.* **1984**, *106*, 5043.

11. (a) Lee, S. J.; Degraziano, J. M.; Macpherson, A. N.; Shin, E. J.; Kerrigan, P. K.; Seely, G. R.; Moore, A. L.; Moore, T. A.; Gust, D. *Chem. Phys.* **1993**, *176*, 321. (b) Gust, D.; Moore, T. A.; Moore, A. L.; Macpherson, A. N.; Lopez, A.; Degraziano, J. M.; Gouni, I.; Bittersmann, E.; Seely, G. R.; Gao, F.; Nieman, R. A.; Ma, X. C. C.; Demanche, L. J.; Hung, S. C.; Luttrull, D. K.; Lee, S. J.; Kerrigan, P. K. *J. Am. Chem. Soc.* **1993**, *115*, 11141. (c) Gust, D.; Moore, T. A.; Moore, A. L.; Leggett, L.; Lin, S.; Degraziano, J. M.; Hermant, R. M.; Nicodem, D.; Craig, P.; Seely, G. R.; Nieman, R. A. *J. Phys. Chem.* **1993**, *97*, 7926. (d) Gust, D.; Moore, T. A.; Moore, A. L. *Acc. Chem. Res.* **1993**, *26*, 198. (e) Gust, D.; Moore, T. A.; Moore, A. L.; Devadoss, C.; Liddell, P. A.; Hermant, R.; Nieman, R. A.; Demanche, L. J.; Degraziano, J. M.; Gouni, I. *J. Am. Chem. Soc.* **1992**, *114*, 3590. (f) Gust, D.; Moore, T. A.; Moore, A. L.; Gao, F.; Luttrull, D. K.; Degraziano, J. M.; Ma, X. C. C.; Makings, L. R.; Lee, S. J.; Trier, T. T.; Bittersmann, E.; Seely, G. R.; Woodward, S.; Bensasson, R. V.; Rougee, M.; Deschryver, F. C.; Vanderauweraer, M. *J. Am. Chem. Soc.* **1991**, *113*, 3638. (g) Gust, D.; Moore, T. A.; Moore, A. L.; Ma, X. C. C.; Nieman, R. A.; Seely, G. R.; Belford, R. E.; Lewis, J. E. *J. Phys. Chem.* **1991**, *95*, 4442. (h) Gust, D.; Moore, T. A.; Moore, A. L.; Makings, L. R.; Seely, G. R.; Ma, X.; Trier, T. T.; Gao,

F. *J. Am. Chem. Soc.* **1988**, *110*, 7567. (i) Land, E. J.; Lexa, D.; Bensasson, R. V.; Gust, D.; Moore, T. A.; Moore, A. L.; Liddell, P. A.; Nemeth, G. A. *J. Phys. Chem.* **1987**, *91*, 4831. (j) Gust, D.; Moore, T. A.; Makings, L. R.; Liddell, P. A.; Nemeth, G. A.; Moore, A. L. *J. Am. Chem. Soc.* **1986**, *108*, 8028.

12. Liu, J. Y.; Bolton, J. R. *J. Phys. Chem.* **1992**, *96*, 1718. (b) Schmidt, J. A.; Liu, J. Y.; Bolton, J. R.; Archer, M. D.; Gadzekpo, V. P. Y. *J. Chem. Soc., Faraday Trans 1*, **1989**, *85*, 1027. (c) Schmidt, J. A.; McIntosh, A. R.; Weedon, A. C.; Bolton, J. R.; Connolly, J. S.; Hurley, J. K.; Wasielewski, M. R. *J. Am. Chem. Soc.* **1988**, *110*, 1733. (d) Archer, M. D.; Gadzekpo, V. P. Y.; Bolton, J. R. *Croat. Chem. Acta* **1987**, *60*, 577. (e) Archer, M. D.; Gadzekpo, V. P. Y.; Bolton, J. R.; Schmidt, J. A.; Weedon, A. C. *J. Chem. Soc., Faraday Trans 2*, **1986**, *82*, 2305. (f) Bolton, J. R.; Ho, T. F.; Liauw, S.; Siemiarczuk, A.; Wan, C. S. K.; Weedon, A. C. *J. Chem. Soc., Chem. Commun.* **1985**, *(9)*, 559.

13. (a) Leland, B. A.; Joran, A. D.; Felker, P. M.; Hopfield, J. J.; Zewail, A. H.; Dervan, P. B. *J. Phys. Chem.* **1985**, *89*, 5571. (b) Joran, A. D.; Leland, B. A.; Geller, G. G.; Hopfield, J. J.; Dervan, P. B. *J. Am. Chem. Soc.* **1984**, *106*, 6090.

14. Danielson, E.; Elliot, C. M.; Merkert, J. W.; Meyer, T. J. *J. Am. Chem. Soc.* **1987**, *109*, 2519.

15. Penfield, K. W.; Miller, J. R.; Paddon-Row, M. N.; Cotsaris, E.; Oliver, A. M.; Hush, N. S. *J. Am. Chem. Soc.* **1987**, *109*, 5061.

16. (a) McMahon, R. J.; Forcé, R. K.; Patterson, H. H.; Wrighton, M. S. *J. Am. Chem. Soc.* **1988**, *110*, 2670. (b) Forcé, R. K.; McMahon, R. J.; Yu, J.; Wrighton, M. S. *Spectrochim. Acta* **1989**, *45A(1)*, 23.

17. (a) Tufts, B. J.; Abraham, I. L.; Santangelo, G. N.; Ryba, L. G.C.; Lewis, N. S. *Nature*, **1987**, *326*, 861. (b) Lewis, N. S. *Acc. Chem. Res.* **1990**, *23*, 176.

18. O'Regan, B.; Grätzel, M. *Nature*, **1991**, *353*, 737.

19. Parkinson, B. *Acc. Chem. Res.* **1984**, *17*, 431.

20. Gardner, T. J. Ph.D. Thesis, Massachusetts Institute of Technology, September, 1993.

21. (a) Marcus, R. A. *J. Chem. Phys.* **1956**, *24*, 966. (b) Marcus, R. A. *Faraday Discus. Chem. Soc.* **1960**, *29*, 21. (c) Marcus, R. A. *Ann. Rev. Phys. Chem.* **1966**, *15*, 155. (d) Marcus, R. A. *Faraday Discus. Chem. Soc.* **1982**, *74*, 7. (e) Marcus, R. A. *J. Phys. Chem.* **1989**, *93*, 3078.

22. Marcus, R. A. *J. Chem. Phys.* **1965**, *43*, 679.

23. Marcus, R. A.; Sutin, N. *Biochim. Biophys. Acta* **1985**, *811*, 265.

24. (a) Kestner, N. R.; Logan, J.; Jortner, J. *J. Phys. Chem.* **1974**, *78*, 2148. (b) Jortner, J. *J. Chem. Phys.* **1976**, *64*, 4860. (c) Jortner, J. Phil. Mag. 1979, B40, 317.

25. (a) Hush, N. S. *Trans. Faraday Soc.* **1961**, *57*, 557. (b) Hush, N. S. *Prog. Inorg. Chem.* **1967**, *8*, 391. (c) Hush, N. S. *Electrochim. Acta* **1968**, *13*, 1005.

26. *Photoinduced Electron Transfer*; Fox, M. A.; Chanon, M., Ed.; Elsevier: Amsterdam, 1988.

27. (a) Sutin, N. *J. Photochem.* **1979**, *10*, 19. (b) Sutin, N. *Acc. Chem. Res.* **1982**, *15*, 275. (c) Prog. Inorg. Chem. 1983, 30, 441. (e) Sutin, N.; Brunschwig, B. S.; Creutz, C.; Winkler, J. R. *Pure Appl. Chem.* **1988**, *60*, 1817.

28. Brunschwig, B. S.; Ehrenson, S.; Sutin, N. *J. Phys. Chem.* **1986**, *90*, 3657.

29. (a) Brunschwig, B. S.; Logan, J.; Newton, M. D.; Sutin, N. *J. Am. Chem. Soc.* **1980**., *102*, 5798. (b)Brunschwig, B. S.; Creutz, C.; Macartney, D. H.; Sham, T-K.; Sutin, N. *Faraday Discus. Chem. Soc.* **1982**, *74*, 113.

30. Siders, P.; Marcus, R. A. *J. Am. Chem. Soc.* **1981**, *103*, 748.

31. Ulstrup, J.; Jortner, J. *J. Chem. Phys.* **1975**, *63*, 4358.

32. Newton, M. D.; Sutin, N. *Annu. Rev. Phys. Chem.* **1984**, *35*, 437.

33. Levich, V. G. In *Advances in Electrochemistry and Electrochemical Engineering;* Delahay, P., Ed.; Interscience: New York, 1966; Vol. 4, p 249.

34. Ratner, M. A. *J. Phys. Chem.* **1990**, *94*, 4877, and references therein.

35. (a) Schmickler, W. *J. Electroanal. Chem.* **1986**, *204*, 31. (b) Morgan, J. D.; Wolynes, P. G. *J. Phys. Chem.* **1987**, *91*, 874. (c) Zusman, L. D. *Chem. Phys.* **1987**, *112*, 53. (d) Mishra, A. K.; Rangarajan, S. K. *J. Phys. Chem.* **1987**, *91*, 3417. (e) Sebastian, K. L. *J. Chem. Phys.* **1989**, *90*, 5056. (f) Chidsey, C. E. *Science,* **1991**, 251, 919.

36. Gennett, T.; Milner, D. F.; Weaver, M. J. *J. Phys. Chem.* **1985**, *89*, 2787.

37. (a) Förster, T. Ann. Phys. 1948, 2, 55. (b) Förster, T. *Faraday Discus. Chem. Soc.* **1959**, *27*, 7. (c) Förster, T. In *Comparative Effect of Radiation;* Burton, M.; Kirby-Smith, J. J.; Magee, J. L., Ed.; Wiley: New York, 1965; p 300. (d)

Förster, T. In *Modern Quantum Chemistry;* Sinanoğlu, O., Ed.; Part III, Academic: New York, 1965; p 93.

38. Dexter, D. L. *J. Chem. Phys.* **1953**, *21*, 836.

39. Wilkinson, F. In *Photoinduced Electron Transfer;* Part A; Fox, M. A.; Chanon, M., Ed.; Elsevier: New York, 1989; pp 207-227.

40. Morawitz, H. *Phys. Rev.* **1969**, *187*, 1792.

41. Tews, K. H. *Ann. Phys. Leipz.* **1973**, *29*, 97.

42. (a) Ritchie, R. *Phys. Rev.* **1957**, *106*, 874. (b) Ritchie, R. *Surf. Sci.* **1973**, *34*, 1.

43. (a) Stern, E.; Ferrell, R. *Phys. Rev.* **1958**, *111*, 1214. (b) Ferrell, R. *Phys. Rev.* **1960**, *120*, 130.

44. (a) Chance, R. R.; Prock, A.; Silbey, R. *J. Chem. Phys.* **1974**, *60*, 2184, 2744. (b) *ibid.*, **1976**, *65*, 2527. (c) *ibid.*, **1977**, *66*, 1765. (d) Chance, R.R.; Prock, A.; Silbey, R. In *Advances in Chemical Physics;* Rice, S.A.; Prigogine, I. Ed., Wiley: New York, 1978; vol. 37, p1.

45. Chance, R. R.; Prock, A.; Silbey, R. *J. Chem. Phys.* **1975**, *62*, 2245.

46. Sommerfeld, A. *Partial Differential Equations of Physics;* Academic: New York, 1949.

47. Stratton, J. *Electromagnetic Theory;* McGraw-Hill: New York, 1941.

CHAPTER TWO

EXPERIMENTAL METHODS AND EXAMPLES OF CHARGE SEPARATING SYSTEMS.

In this chapter we summarize the experimental techniques, transient absorption and time-resolved emission spectroscopy, which are used to study photoinduced electron transfer and energy transfer in different media. We also describe the major experimental apparatus which make the techniques available. Studies of inter- and intramolecular electron transfer reactions by the techniques will be discussed.

Transient absorption spectroscopy[1] is one of most widely used spectroscopic techniques to monitor transient species such as neutral radicals, radical ions, excited states, and exciplexes. Photoinduced electron transfer reactions can be followed by (1) capturing the transient absorption spectrum of the radical ions produced from the reaction at a specific delay time after the excitation pulse; and/or (2) recording the change of optical density of the radical ions versus time at a fixed wavelength.

The photoinitiation of electron transfer reactions is accomplished by a combination of a Quanta-Ray DCR-3 Nd:YAG laser with a 3-5 ns 10 Hz pulsed output at 1064 nm, which can be doubled to 532 nm or tripled to 355 nm, and a Quanta-Ray RS-1 Raman shifter (working medium: H_2). The Raman shifter converts the laser lines from the YAG laser to either Stokes or anti-Stokes lines. The 416 nm line is the most often used one, and is the first Stokes shift of 355 nm output from the YAG laser.

The transient absorption spectrum is obtained by an EG&G 1421 double-intensified optical multichannel analyzer (OMA) with a white light probe. The OMA detector is gated at a gate width

of 10 ns through a EG&G 1302 fast pulser and is triggered with a delayed pulse from a SRS Model DG535 digital delay/pulse generator. The data acquisition and scanning of the detector are synchronized and controlled with an EG&G 1463 controller and EG&G 1461 detector interface.

The white light source is a high pressure Xenon arc lamp powered by a super-quiet OLIS XL150 power supply. The probe light is collimated and focused into the sample so that it overlaps spatially with the excitation laser beam through the length of the sample, and then directed into the entrance of the detector by a f-matched focal lens, see Figure 2-1. An electronically controlled Uniblitz model T132 shutter is used to chop the CW probe light to protect some samples from photo-degradation.

To measure the time dependence of photogenerated transients, the optical density at a specific wavelength is monitored by a Thurlab DET2-Si photodiode with a 1 ns rise time. The photovoltage signal from the detector is collected on a LeCroy 8088 transient digitizer with 742 ps resolution. The monochromatic probes are CW lasers, a Coherent Innova 70-4 Ar^+ laser tunable between 458 and 515 nm, or a Coherent Innova 90-K Kr^+ laser tunable between 356 and 676 nm. The probe beam is blocked by a shutter between scans to avoid depleting photodiode voltage, see Figure 2-2.

Identification of the radical ions produced from the electron transfer reaction can be accomplished by comparing the transient absorption spectra of the intermediates to the known

spectra of the radical ions or excited state. Kinetics of the formation and disappearance of the electron transfer intermediates can be measured with sub-nanosecond resolution by monitoring the absorbance change over time at a specific wavelength with the photodiode. The collimation of the excitation and probe laser beams are achieve by a broad band dichroic mirror. A long pass filter and interference filter are used to remove excitation light.

Time-resolved emission spectra can be conveniently acquired by the OMA photodiode array detector gated with a gate width of 10 ns and triggered with a delayed pulse relative to the excitation laser pulse. In the measurement of the transient emission spectra of photoactive molecules immobilized on flat surfaces, emission signals are collected by a set of lenses which are f-matched with the spectrograph of the detector at a specific angle to the excitation in order to eliminate the perturbation from the reflected excitation light (Figure 2-3). Appropriate filters are inserted into the optical path to suppress the excitation and scattered light. Emission decays at a specific wavelength can be monitored by a Hamamatsu R446 photomultiplier (PMT) with a 2.7 ns rise time and recorded by the transient digitizer shown in Figure 2-4. Emission signals are detected through a SA model DH-10 double grating monochromator. The PMT is negatively biased by a Fluke model 405B regulated high voltage power supply. All lifetimes are determined by averaging at least three independent measurements.

Simple relative emission quantum yield and lifetime measurements provide important quantatative information regarding electron transfer rates in linked chromophore-donor (or acceptor) "diads". Forward electron transfer rates can be determined by comparing steady state or transient emission of a chromophore alone to that of the linked chromophore-donor/acceptor assembly. The rate is determined according to eq. (2-1), where τ is emission lifetime and ϕ is emission intensity.

$$k_f = 1/\tau_{linked} - 1/\tau_{chromophore} = 1/\phi_{linked} - 1/\phi_{chromophore} \quad (2\text{-}1)$$

Back electron transfer from the reduced chromophore to the oxidized donor can be measured spectroscopically, provided the charge separated state is sufficiently long lived and has a distinct absorption. If the back electron transfer is faster than the forward electron transfer, then no build up of the charge separated state can be detected.

In this chapter bimolecular quenching of the excited state of tetraphenyl-porphyrin (TPP) by N,N,N',N'-tetramethyl-*p*-phenylenediamine (TMPD) is described, where the charge separated state, $TPP^{-\cdot}$-$TMPD^{+\cdot}$, is less well studied.[2] A salt effect[6,7] on enhancing separation of the contact radical ion pair, $TPP^{-\cdot}$-$TMPD^{+\cdot}$, is investigated. Intramolecular quenching of the excited state of $[(pyridine)Re(CO)_3(1,10\text{-phenanthroline})]^+$ by ferrocene is also presented in this chapter.

Experimental

Transient absorption apparatus. The transient absorption apparatus was assembled at the MIT Laser Research Center, which is a National Science Foundation Regional Instrumentation Facility. Transient absorption spectra were acquired following a laser excitation pulse of 416 nm (1mJ/pulse) from a Quanta-Ray RS-1 Raman shift laser pumped by a Quanta-Ray DCR-3 Nd:YAG laser (third harmonic, 3 ns FWHM) for the TPP-TMPD system and a laser excitation pulse of 355 nm (1mJ/pulse) from a Quanta-Ray DCR-3 Nd:YAG laser (third harmonic, 3 ns FWHM) for the Re(I)-ferrocene system. The Raman shifter output was separated by a prism, and the desired wavelength was sent through an aperture and interference filter to completely isolate a pump wavelength. The data acquisition and scanning of the detector were synchronized and controlled with an EG&G 1463 controller and EG&G 1461 detector interface.

A 150 W high pressure Xenon arc lamp provided the broad band probe light. Transient spectra were obtained by an EG & G 1421 OMA diode array detector gated through a EG & G Model 1302 fast pulser. The delay time from the laser pulse leading edge to sampling pulse falling edge was controlled by a SRS Model DG535 digital delay/pulse generator. Each transient absorption spectrum was obtained by averaging 250 scans.

Electrochemical measurements. Electrochemical experiments were carried out at 293 K. The working electrode was a modified Pt mirror with an immersed area of ~1 cm^2. Pt wire was the counter-electrode and oxidized Ag wire was the

quasi-reference. The electrolyte solution was purged with Ar prior to voltammetry and was blanketed with Ar during voltammetry. Linear sweep cyclic voltammograms were recorded using a Pine Instruments RDE 4 bipotentiostat.

Fluorescence measurements. Fluorescence spectra were recorded on a Perkin Elmer MPF-44 spectrophotofluorimeter using a 1 cm fused silica fluorescence cell. Solutions with the same absorbance (A ≅ 0.1 at 413 nm) were prepared for TPP in tetrahydrofuran (THF). The spectra were recorded after the solutions were deoxygenated by purging with solvent-saturated Ar for 30 minutes. Concentrations of a quencher in THF were controlled to vary from 0 to 2×10^{-2} M.

Materials. TMPD (Aldrich) was purified by vacuum sublimation prior to use. TPP (Aldrich) was used as supplied. [n-Bu_4N]PF_6 was recrystallized twice from ethanol. THF was distilled over CaH_2. Acetonitrile (CH_3CN) was distilled over P_2O_5.

{*fac*-(4-ferrocenylpyridine)Re(CO)$_3$(1,10-phenanthroline)}$^+CF_3SO_3^-$, b, and {*fac*-(pyridine)Re(CO)$_3$(1,10-phenanthroline)}$^+CF_3SO_3^-$, a. Molecules **a** and **b** were synthesized by Dr. Charles Christ and have been characterized by proton NMR, IR, and UV/vis spectroscopy.[3]

Results and Discussion

Bimolecular Quenching of Tetraphenylporphyrin (TPP) by N,N,N',N'-Tetramethyl-*p*-phenylenediamine (TMPD). A Stern-Volmer quenching[4] study shows that TMPD quenches excited TPP at a fast rate, Figure 2-5. From the Stern-Volmer slope and lifetime of the singlet excited state of TPP (15.6 ns), we find quenching to occur at essentially the diffusion-controlled quenching rate, 2.3×10^{10} $M^{-1}s^{-1}$.

Photoexcitation of TPP in the presence of TMPD produced a transient absorption spectrum with the characteristic absportions[5] at about 448 nm for $TPP^{-\cdot}$, and 570 nm and 620 nm for $TMPD^{+\cdot}$ in the presence and absence of [*n*-Bu_4N]PF_6, shown in Figure 2-6 and Figure 2-7, respectively. The transient absorption measured at 450 nm decays in the presence or absence of [*n*-Bu_4N]PF_6. In the absence of 0.1 M [*n*-Bu_4N]PF_6, the decay fits a single exponential with a rate constant of 4.1×10^5 s^{-1}, Figure 2-8. In the presence of 0.1 M [*n*-Bu_4N]PF_6, the decay occurs with second order, equal concentration kinetics with a rate constant of 2.7×10^{10} $M^{-1}s^{-1}$ typical for diffusion-controlled recombination processes, Figure 2-9. The observation of differing kinetics suggests that the transient electron transfer intermediates in the TPP-TMPD system without electrolytes are contact ion pairs (CIP), $TPP^{-\cdot}$-$TMPD^{+\cdot}$ and those in the system with electrolytes are salt-counterion ion pairs (SCIP) of $TPP^{-\cdot}$ and $TMPD^{+\cdot}$ which are solvent-separated. The contact ion pair forms from the solvent-separated ion pair

(SSIP), symbolized as $TPP^{-}\cdot \| TMPD^{+}\cdot$ within several hundred ps following photolysis.[6] The formation of the contact ion pair was prevented by electrolytes through the ion-pair exchange mechanism[6,7] shown in Scheme 2-1.

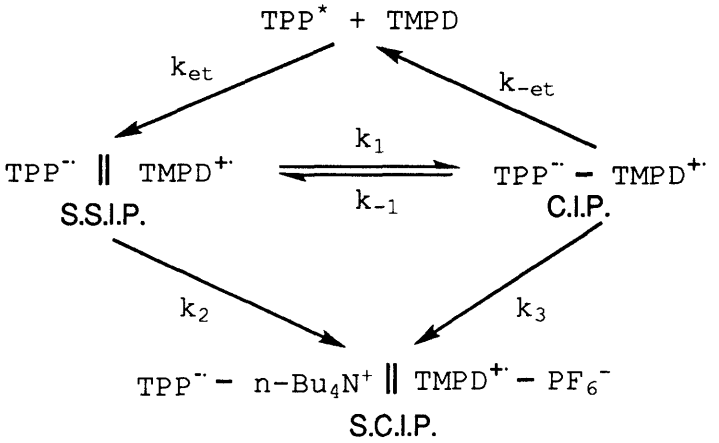

Scheme 2-1. Kinetics of the electron transfer reactions in TPP/TMPD systems with or without adding electrolytes.

The much higher energies of the lowest excited singlet state (~ 4.33 eV) and the lowest triplet state (3.07 eV)[8] of TMPD compared to those for TPP, singlet (~ 1.86 eV) and triplet (1.43 eV),[9] indicates that the energy transfer quenching of the excited TPP by TMPD is thermodynamically unfavorable. Accordingly, the quenching of the excited TPP by TMPD, eq. (2-2), is exclusively an electron transfer process. Equation (2-3) gives the driving force for the electron transfer

$$TPP + TMPD \xrightarrow{h\nu} TPP^{*} + TMPD \xrightarrow{k_{et}} TPP^{\cdot -} + TMPD^{+\cdot} \qquad (2\text{-}2)$$

quenching process, ΔG^0 where $E_{h\nu}$ is the energy of lowest singlet excited state, $E_{h\nu}$ is ~ 1.86 eV above the ground state. The $E_{1/2}$ for the TMPD redox system is

$$\Delta G^0 = E_{1/2}\ (TMPD^{+}\cdot/TMPD) - E_{h\nu} - E_{1/2}\ (TPP/TPP^{-}\cdot) \qquad (2\text{-}3)$$

0.10 V vs. SCE and $E_{1/2}$ for TPP redox system is -1.05 V vs. SCE. Substituting the values of $E_{h\nu}$, $E_{1/2}$ ($TMPD^{+}\cdot$/TMPD), and $E_{1/2}$ (TPP/$TPP^{-}\cdot$) into eq. (2-3), the driving force for the electron transfer process can be determined to be ~ 0.71 eV. The 0.71 eV driving force is adequate to drive a diffusion-controlled bimolecular electron transfer reaction.

Intramolecular electron transfer in Re(I)-phenanthroline donor-chromophore diad molecules. [(pyridine)$Re(CO)_3$(1,10-phenanthroline)]$^{+}CF_3SO_3^{-}$, **a**, and [(4-ferrocenylpyridine)$Re(CO)_3$(1,10-phenanthroline)$\}^{+}CF_3SO_3^{-}$, **b**, were prepared to investigate the possibility of intramolecular electron transfer quenching of the lowest excited state of the Re(I) complex by the ferrocenyl center. Relatively little ground-state electronic interaction between the electron donor (ferrocene) and the Re(I)-phenanthroline chromophore occurs as a comparison of the UV/vis spectra of **a** and **b** show. The absorption spectrum of **b** (Figure 2-10) in the region shown is sum of the absorption spectra of **a** and ferrocene. No additional bands due to charge transfer were observed. The cyclic voltammograms of **a** and **b** were recorded in CH_3CN using 0.1 M [n-

$Bu_4N]PF_6$ as electrolyte, and the halfwave potentials are -1.14 V and +0.75 V (vs Ag) corresponding to the reduction of phenanthroline ligand and the oxidation of ferrocene attached to Re(I)-phenanthroline center by a pyridyl linkage. Thus, the spectral and electrochemical properties are as expected.

Emission spectra of dilute, deoxygenated solutions of **a** and **b** in CH_3CN were recorded at room temperature and show single emission bands centered 549 nm. Relative quantum yield of the fluorescence of **b** compared to **a** is 0.04 as shown in Figure 2-11. The decrease in the emission intensity of **b** is attributed to intramolecular quenching of the Re(I) excited state by the ferrocenyl center. The emission lifetime of **a** was determined by time-resolved emission spectroscopy as τ_0 =1.582 μs[10] and the emission lifetime of **b** was measured as τ = 89 ns. From the relative quantum yield of emission of **b**, the emission lifetime of **b** can be estimated to be about 63 ns which is in reasonable agreement with the emission lifetime of **b** measured by time-resolved emission spectroscopy. Since the energy (~ 2.3 eV)[10] of the lowest triplet excited state of the chromophore is significantly higher than that (~ 1.7 eV)[11] of ferrocene, energy transfer is a viable pathway for the emission quenching of Re(I)-phenanthroline chomophore. However, the electron transfer quenching is also possible with an estimated driving force of ~1.0 eV. Thus, transient absorption spectroscopy has been used to establish the quenching mechanism.

The transient absorption spectra following 3 ns pulsed laser (355 nm) excitation of **b** in CH_3CN was monitored with an OMA

detector with 10 ns gate width and were composed of a negative band around 550 nm due to emission and a featureless broad band between 350-500 nm (Figure 2-12). The decay lifetime of the emission signal at 550 nm measured from the OMA detector is same as the emission lifetime of **b** measured by the PMT within experimental error. The transient absorption spectra of **a** in CH_3CN excited at 355 nm was quite similar with that of **b** while the decay of the negative band at 550 nm due to emission gave a lifetime of about 1.6 μs, as shown in Figure 2-13.

To identify the transient species produced from the intramolecular quenching, we need to know the spectra of the excited state of the Re chromophore, **a**, the one-electron reduced Re(I)-phenanthroline complex, and the one-electron oxidized ferrocene. The transient absorption of **a** supplies the absorption spectrum of the excited state of the Re(I) chromophore. Transient absorption detection of ferrocenium is not feasible due to the low absorptivity of ferrocenium (λ_{max} = 617 nm, ε = 340 $M^{-1}cm^{-1}$). To obtain the authentic absorption spectrum of the one-electron reduced Re(I)-phenanthroline complex, the transient absorption of the intermolecular system of **a** and TMPD in CH_3CN excited at 416 nm was measured, since TMPD is known to quench exclusively by electron transfer. The transient absorption spectrum (Figure 2-14) for the Re(I)-phenanthroline/TMPD system shows peaks for $TMPD^{+}\cdot$. but no peaks were found between 350-500 nm which could be assigned to the one-electron reduced Re(0) species. Thus, we have not been able to distinguish the excited Re species and the one-electron reduced Re species. Therefore,

we cannot unambiguously conclude that the ferrocenyl group quenches by electron transfer.

Conclusions

Transient absorption and transient emission laser systems were assembled, and we demonstrated our ability to detect transient species by absorption and emission spectroscopy. Intermolecular quenching of photoexcited TPP by TMPD produced charge separated TMPD radical cations and TPP radical anions. Added electrolyte was found to enhance the formation of the solvent-separated species from the contact ion pair. Intramolecular quenching of photoexcited Re(I)-phenanthroline by a ferrocenyl center was studied. The relative contribution of electron and energy transfer to the quenching process could not be determined because the charge separated state of the Re(I) system could not be distinguished from the excited state.

References

1. (a) Porter, G. In *Techniques of Organic Chemistry*; 2nd ed.; Friess, S. L.; Lewis, E. S.; Weissberger, A., Ed.; Wiley-Interscience: New York, 1963; Vol. 8, Part 2. (b) Porter, G.; West, M. A. In *Techniques in Chemistry, Investigation of Rates and Mechanisms of Reactions*; Weissberger, A.; Hawkins, G. G., Ed.; Wiley-Interscience: New York, 1973; Part2. (3) Rabek, J. F. *Experimental Methods in Photochemistry and Photophysics*; Wiley-Interscience: New York, 1982; Part 2, Chapter 23.

2. Wasielewski, M. R.; Gaines, G. L.; O'Neil, M. P.; Svec, W. A.; Niemczyk, M. P. *J. Am. Chem. Soc.* **1990**, *112*, 4559.

3. Christ, C.; Wrighton, M. S. unpublished results.

4. Turro, N. J. *Modern Moecular Photochemistry*; Benjamin/Cummings: Menlo Park CA, 1978.

5. (a) Peychal-Heiling, G.; Wilson, G. S. *Anal. Chem.* **1971**, *43*, 550. (b) Pott, G. T.; Kommandeur, J. *J. Chem. Phys.* **1967**, *47*, 395.

6. Simon, J. D.; Peters, K. S. *J. Am. Chem. Soc.* **1982**, *104*, 6142.

7. (a) Kawanishi, Y.; Kitamura, N.; Tazuke, S. *J. Phys. Chem.* **1986**, *90*, 6034. (b) Simon, J. D.; Su, S. *J. Phys. Chem.* **1988**,

92, 2395. (c) Galán, M.; Dominguez, M.; Andreu, R.; Moyá, M. L.; Sánchez, F. *J. Chem. Soc. Faraday Trans.* **1990**, *86*, 937.

8. Kimura, K.; Tsubomura, H. *Mol. Phys.* **1966**, *11*, 349.

9. Moore, T. A.; Benin, D.; Roderick, T. *J. Am. Chem. Soc.* **1982**, *104*, 7356.

10. Luong, J. C. Ph.D. Thesis, Massachusetts Institute of Technology, Sept. 1981.

11. Scott, D. R.; Becker, R. S. *J. Chem. Phys.* **1961**, *35*, 516.

Figure 2-1. Transient absorption apparatus for identification of transient species produced following photoexcitation.

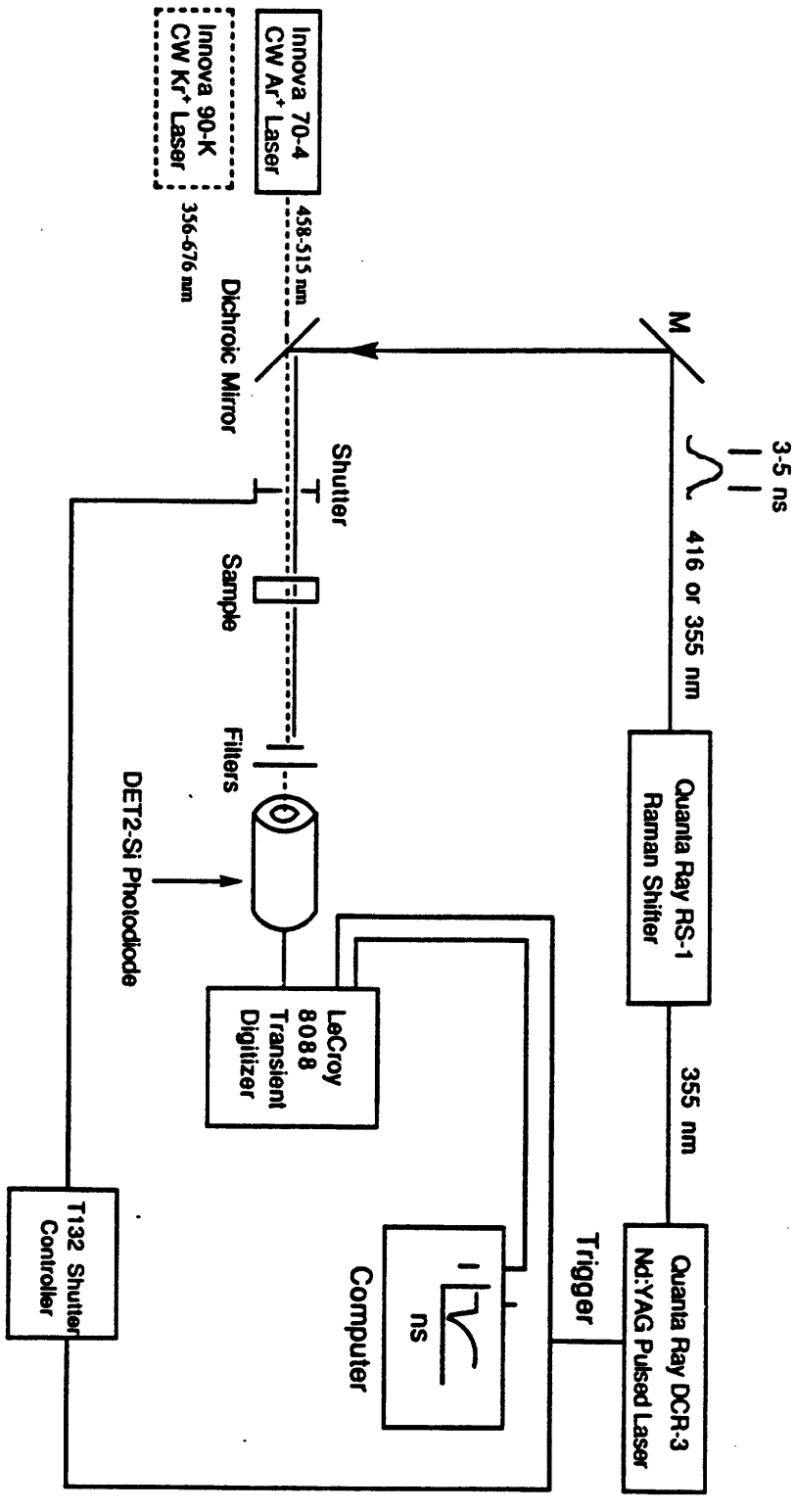
Innova 70-4
CW Ar+ Laser
Innova 90-K
CW Kr+ Laser
458-515 nm
356-676 nm
Dichroic Mirror
M
3-5 ns
416 or 355 nm
Quanta Ray RS-1
Raman Shifter
355 nm
Quanta Ray DCR-3
Nd:YAG Pulsed Laser
Trigger
Shutter
Sample
Filters
DET2-Si Photodiode
LeCroy
8088
Transient
Digitizer
ns
Computer
T132 Shutter
Controller

Figure 2-2. Transient emission apparatus for recording transient emission spectra from solution or monolayer samples following photoexcitation.

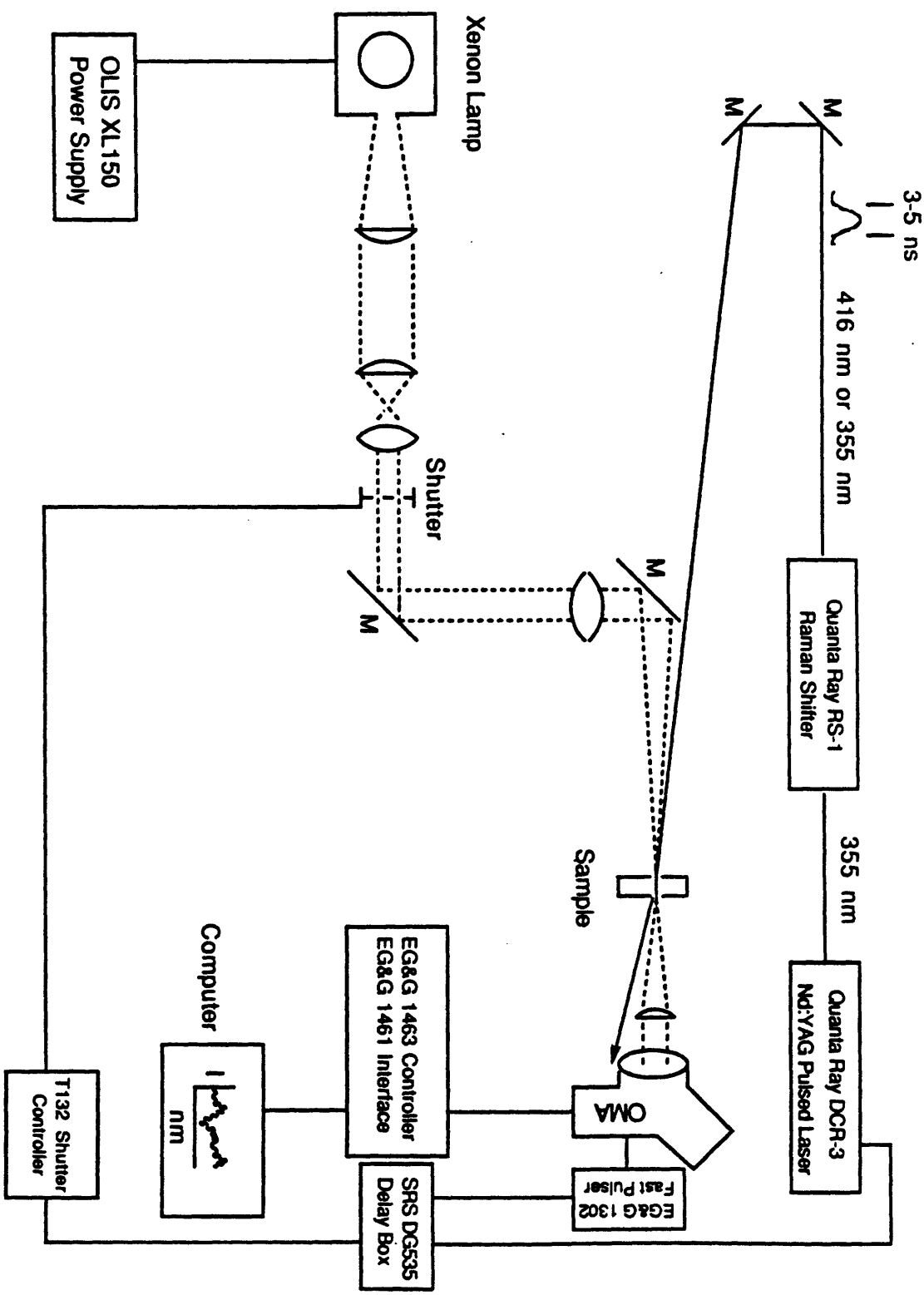
3-5 ns
416 nm or 355 nm
355 nm
M
M
M
M
Xenon Lamp
OLIS XL150
Power Supply
Shutter
Quanta Ray RS-1
Raman Shifter
Quanta Ray DCR-3
Nd:YAG Pulsed Laser
Sample
OMA
EG&G 1302
Fast Pulser
EG&G 1463 Controller
EG&G 1461 Interface
SRS DG535
Delay Box
Computer
nm
T132 Shutter
Controller

Figure 2-3. Single wavelength transient absorption apparatus for following kinetics of photoinduced electron transfer reactions.

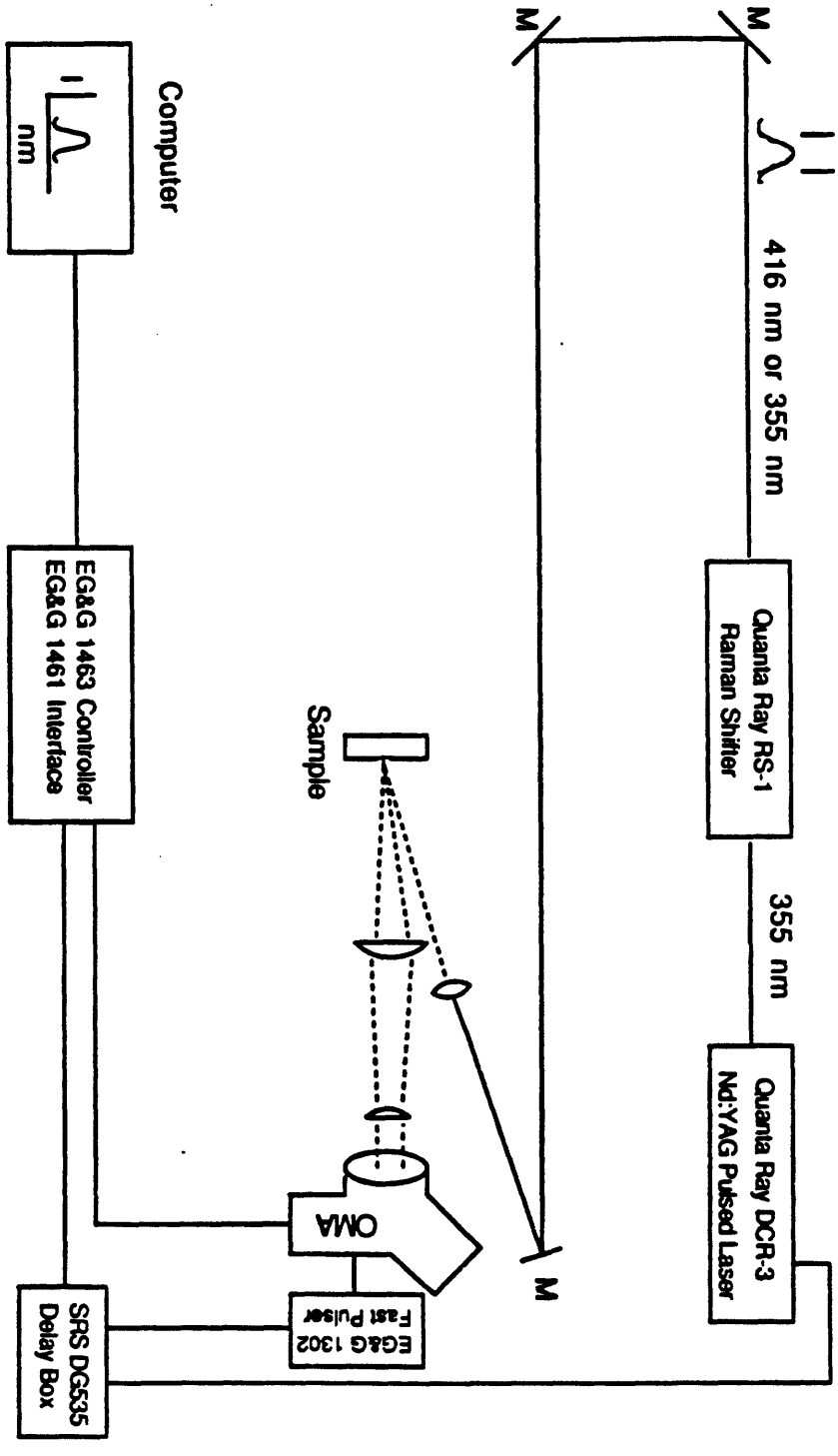
3-5 ns
416 nm or 355 nm
M
M
M
Quanta Ray RS-1
Raman Shifter
355 nm
Quanta Ray DCR-3
Nd:YAG Pulsed Laser
Sample
OMA
EG&G 1302
Fast Pulser
SRS DG535
Delay Box
EG&G 1463 Controller
EG&G 1461 Interface
Computer
nm

Figure 2-4. Single wavelength emission apparatus for measuring lifetimes of emission decays from solution or monolayer samples following photoexcitation.

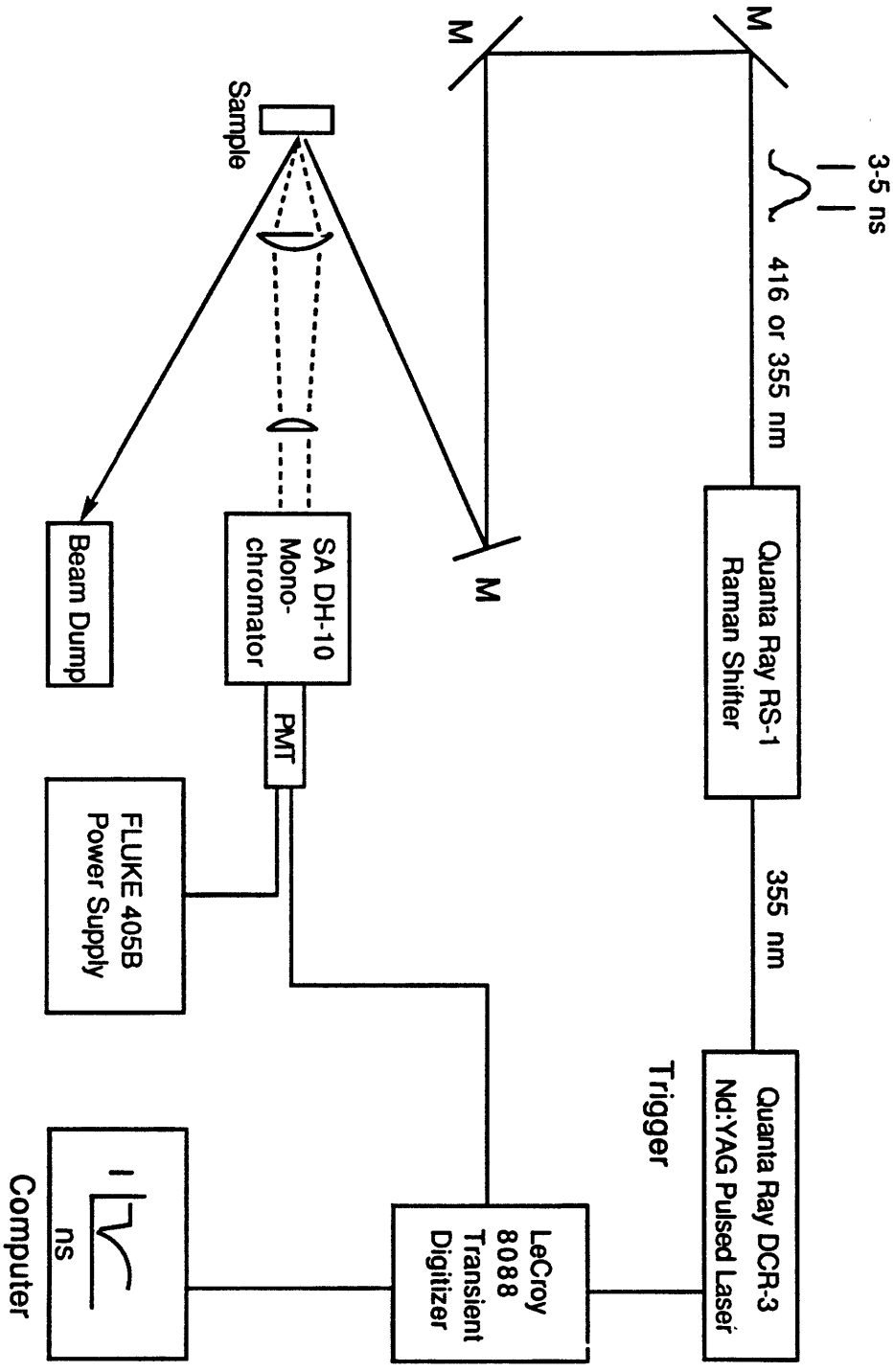
M
M
M
Sample
3-5 ns
416 or 355 nm
Quanta Ray RS-1
Raman Shifter
355 nm
Quanta Ray DCR-3
Nd:YAG Pulsed Laser
Trigger
SA DH-10
Mono-
chromator
PMT
Beam Dump
FLUKE 405B
Power Supply
LeCroy
8088
Transient
Digitizer
ns
Computer

Figure 2-5. Stern-Volmer plot for quenching of the fluorescence of TPP by TMPD in THF at room temperature.

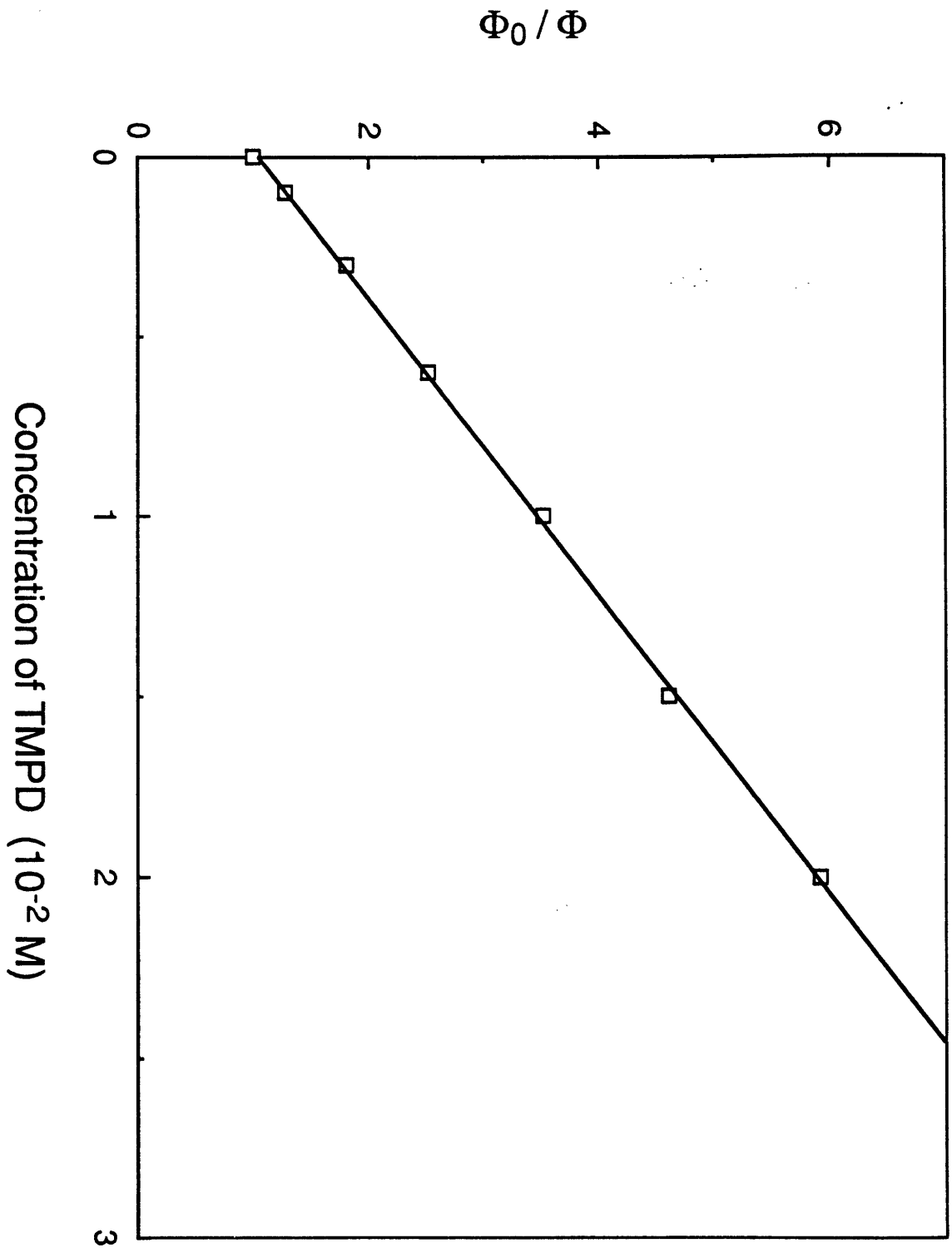
Φ_0 / Φ
0
2
4
6
0
1
2
3
Concentration of TMPD (10^{-2} M)

Figure 2-6. Transient absportion taken 100 ns after a 10 ns, 1 mJ/pulse, 416 nm excitation of TPP in THF/0.1 M [*n*-BuN_4]PF_6 with 0.1 M TMPD. The inset shows the second-order kinetics of diffusion-controlled back electron transfer.

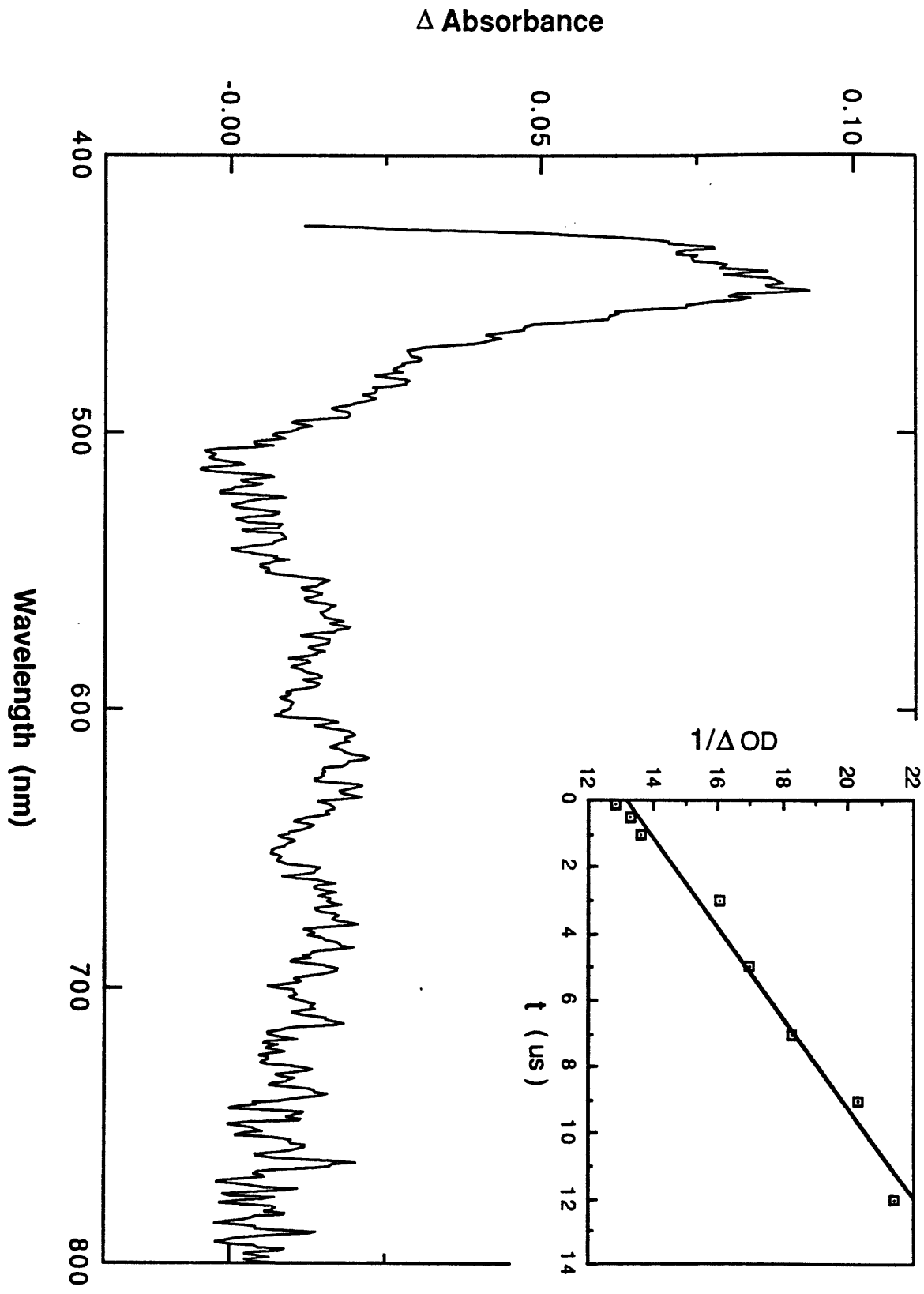
Δ Absorbance
-0.00
0.05
0.10
400
500
600
700
800
Wavelength (nm)
1/Δ OD
12
14
16
18
20
22
0
2
4
6
8
10
12
14
t (us)

Figure 2-7. Transient absorption taken 100 ns after a 10 ns, 1 mJ/pulse, 416 nm excitation of TPP in THF with 0.1 M TMPD containing no added electrolyte. The inset shows the first-order kinetics of back electron transfer.

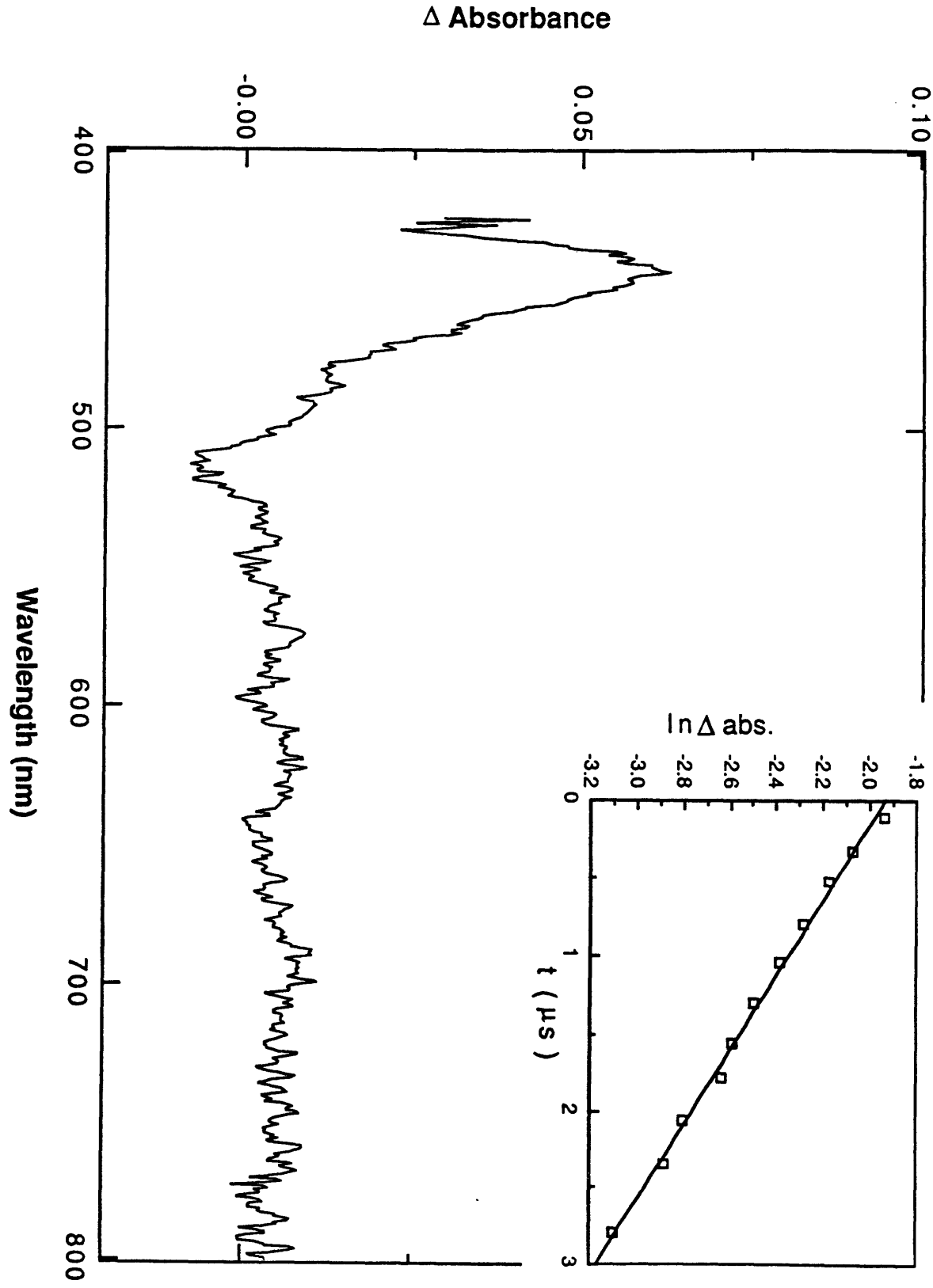
Δ Absorbance
-0.00
0.05
0.10
400
500
600
700
800
Wavelength (nm)
ln Δ abs.
-3.2
-3.0
-2.8
-2.6
-2.4
-2.2
-2.0
-1.8
0
1
2
3
t (μs)

Figure 2-8. A comparison between the kinetic fit to a second-order machanism and that to a first-order machanism (inset) with atransient absorption deay at 416 nm of TPP-TMPD/THF/0.1M [*n*-BuN_4]PF_6 system.

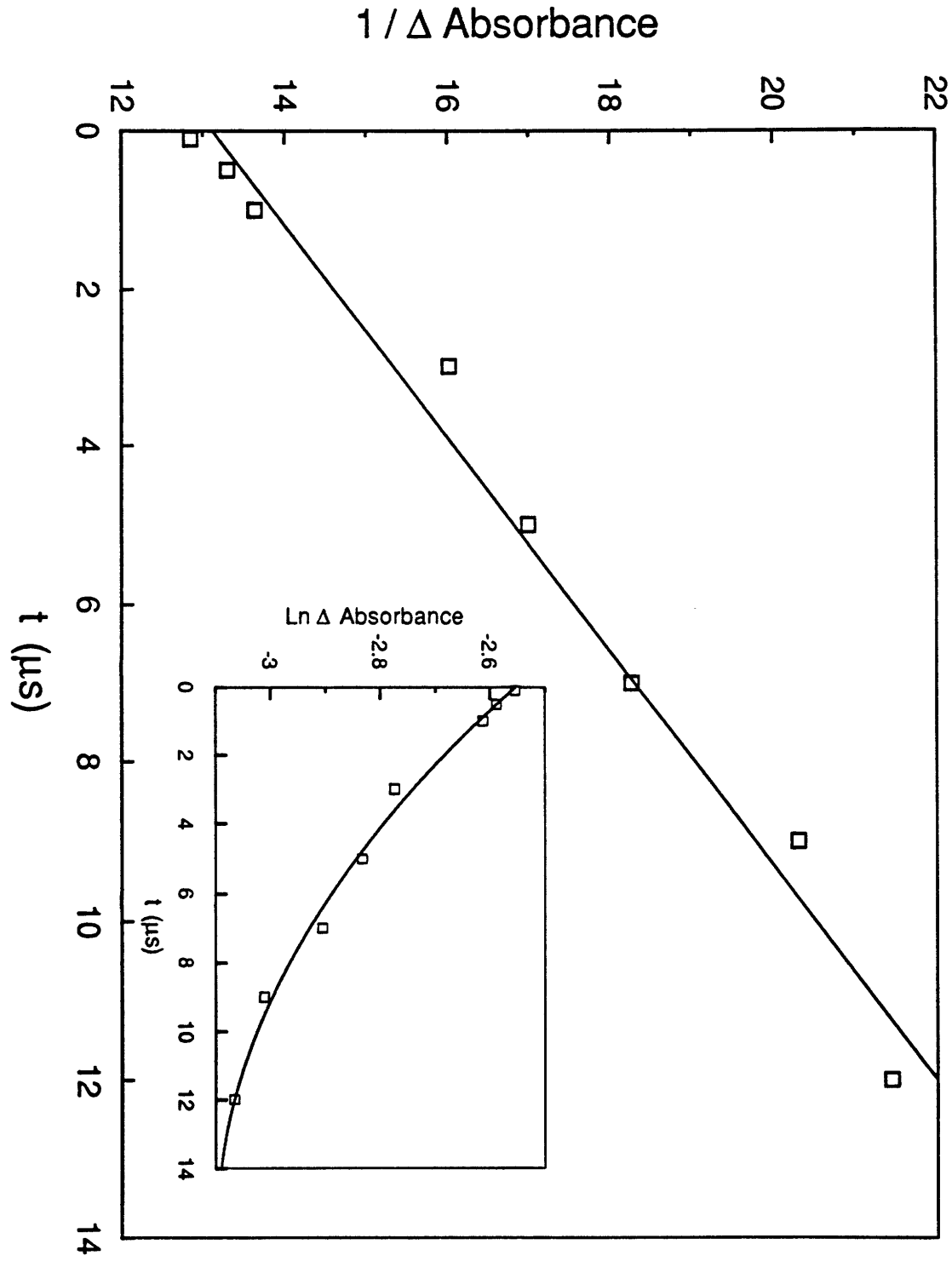
1 / Δ Absorbance
12
14
16
18
20
22
0
2
4
6
8
10
12
14
t (μs)
Ln Δ Absorbance
-3
-2.8
-2.6
0
2
4
6
8
10
12
14
t (μs)

Figure 2-9. A comparison between the kinetic fit to a first-order machanism and that to a second-order machanism (inset) with a transient absorption decay at 416 nm of TPP-TMPD/THF (no added electrolyte) system.

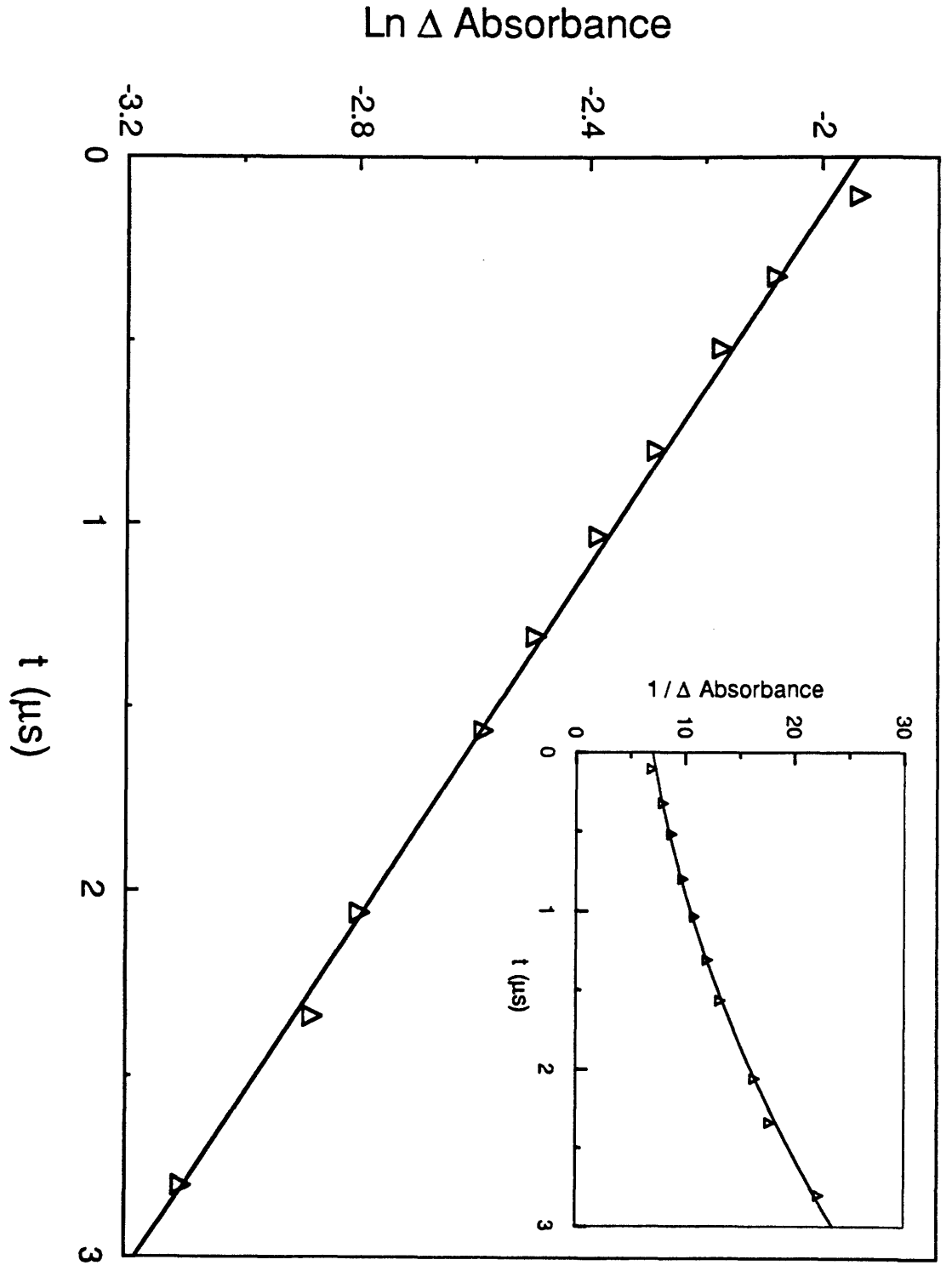
Ln Δ Absorbance
-3.2
-2.8
-2.4
-2
0
1
2
3
t (μs)
1 / Δ Absorbance
0
10
20
30
0
1
2
3
t (μs)

Figure 2-10. UV/vis absorption spectra of [(4-ferrocenylpyridine)$Re(CO)_3$(1,10-phenanthroline)]$^+$ (**b**) in CH_3CN. The inset shows an UV/vis spectra of [(pyridine)$Re(CO)_3$(phenanthroline)]$^+$ (**a**) in CH_3CN.

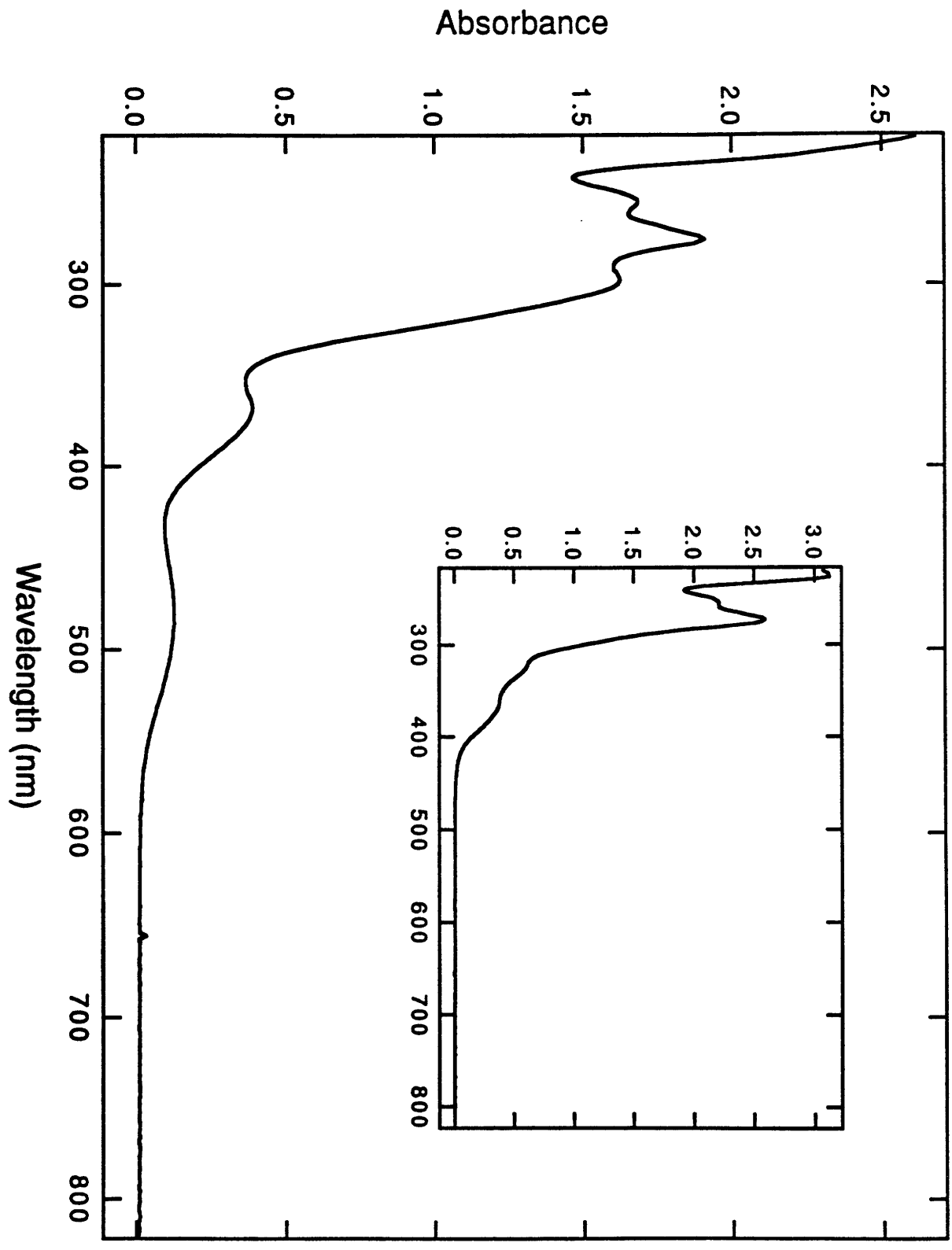
Absorbance
0.0
0.5
1.0
1.5
2.0
2.5
Wavelength (nm)
300
400
500
600
700
800
0.0
0.5
1.0
1.5
2.0
2.5
3.0
300
400
500
600
700
800

Figure 2-11. Relative emission intensity of **a** (———) and **b** (·····) in deoxygenated CH_3CN at room temperature ($\lambda_{exc} = 370$ nm). The two samples were measured under identical conditions (matched absorbance at 370 nm), therefore the relative emission intensities represent relative emission quantum yields.

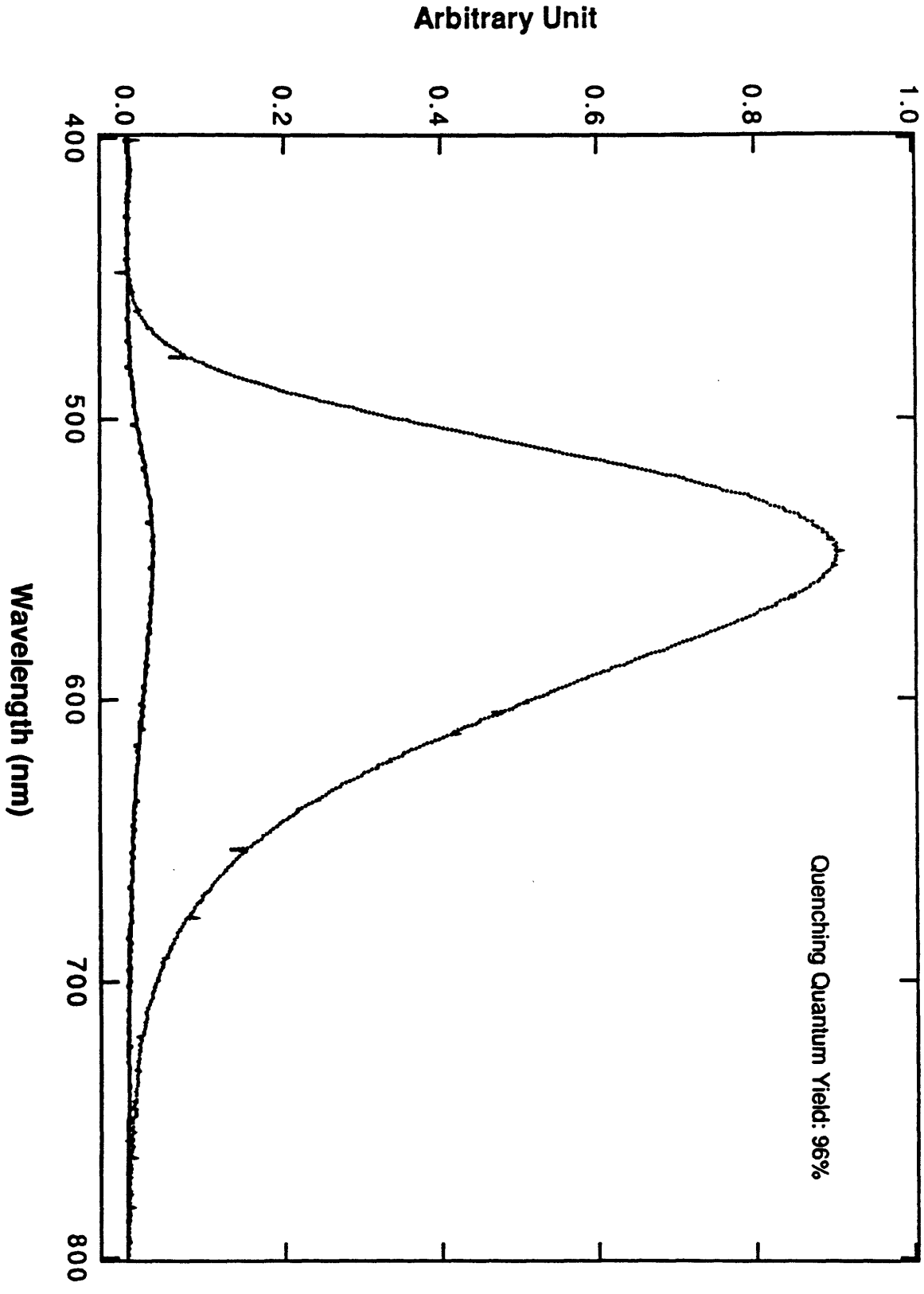
Arbitrary Unit
0.0
0.2
0.4
0.6
0.8
1.0
400
500
600
700
800
Wavelength (nm)
Quenching Quantum Yield: 96%

Figure 2-12. Transient absorption of [(4-ferrocenylpyridine)$Re(CO)_3$(1,10-phenanthroline)]$^+$ (**b**) in CH_3CN at indicated times following 3 ns, 355 nm excitation pulse.

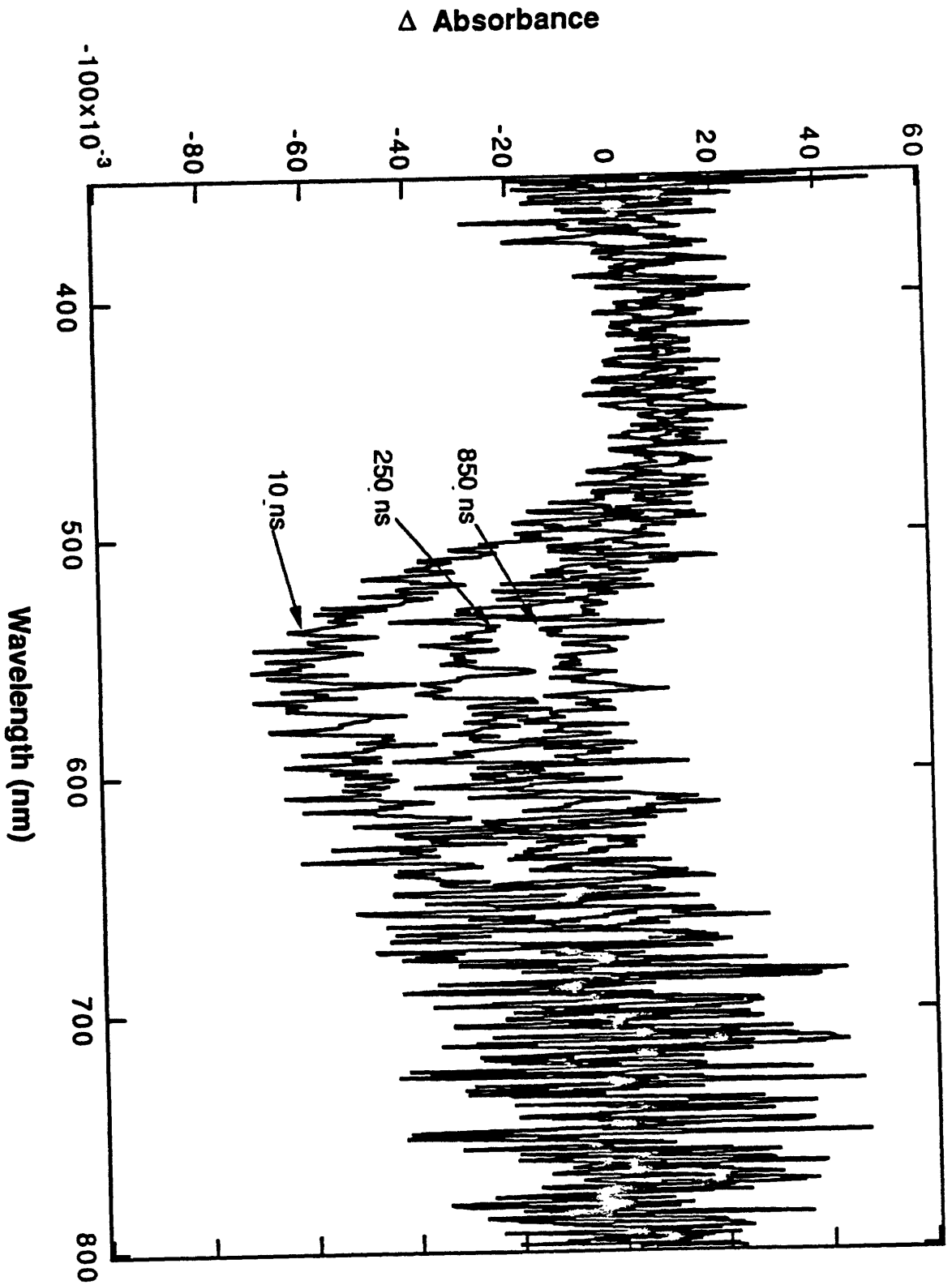
Δ Absorbance
-100x10-3
-80
-60
-40
-20
0
20
40
60
400
500
600
700
800
Wavelength (nm)
10 ns
250 ns
850 ns

Figure 2-13. Transient absorption of [(pyridine)Re(CO)$_3$(1,10-phenanthroline)]$^+$ (**a**) in CH_3CN at indicated times following 3 ns, 355 nm excitation pulse.

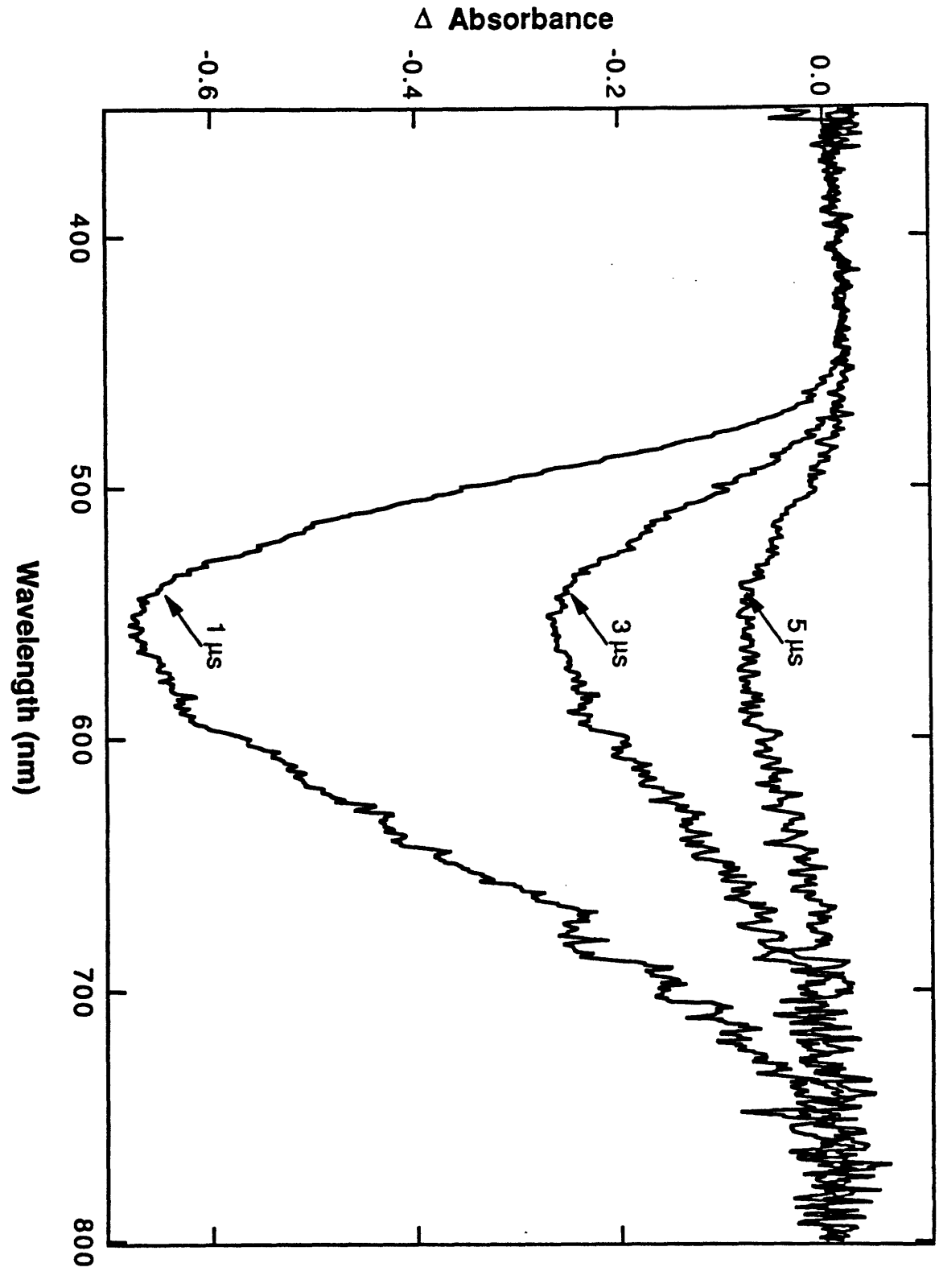
Δ Absorbance
0.0
-0.2
-0.4
-0.6
400
500
600
700
800
Wavelength (nm)
1 μs
3 μs
5 μs

Figure 2-14. Transient absorption of [(pyridine)Re(CO)$_3$(1,10-phenanthroline)]$^+$ (**a**) in CH_3CN with 0.1 M TMPD at indicated times following 3 ns, 416 nm excitation pulse.

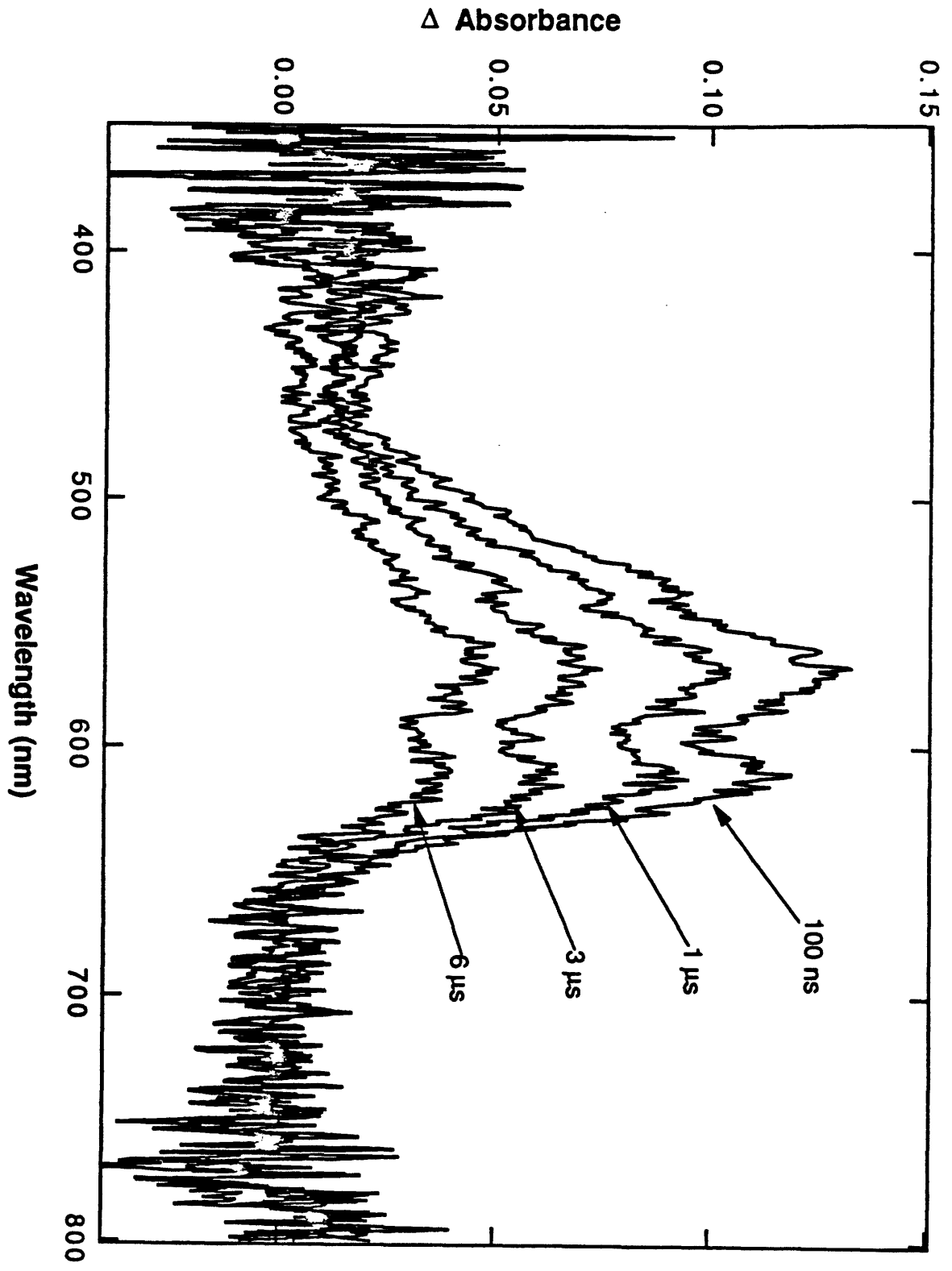
Δ Absorbance
0.00
0.05
0.10
0.15
400
500
600
700
800
Wavelength (nm)
6 µs
3 µs
1 µs
100 ns

CHAPTER THREE

INTER- AND INTRAMOLECULAR QUENCHING OF THE SINGLET EXCITED STATE OF PORPHYRINS BY FERROCENE

A key strategy to build molecule-based efficient and durable optical energy conversion devices is to extend the lifetime of a charge separated state by synthesizing multicomponent redox molecules. In this chapter a series of porphyrins **1-3** (see Scheme 3-1), two of them having linked ferrocenyl centers, were studied as linked chromophore-donor systems. The porphyrin/ferrocene system is attractive because the porphyrin chromophore absorbs over most of the solar spectrum,[1] its singlet excited state can be reduced by ferrocene according to thermodynamic arguments, and the ferrocenyl centers can be reversibly oxidized. This series of molecules allows us to address questions concerning the quenching mechanism of porphyrins and ferrocenes and the effect of the different linking groups in **2** and **3** on quenching rate.

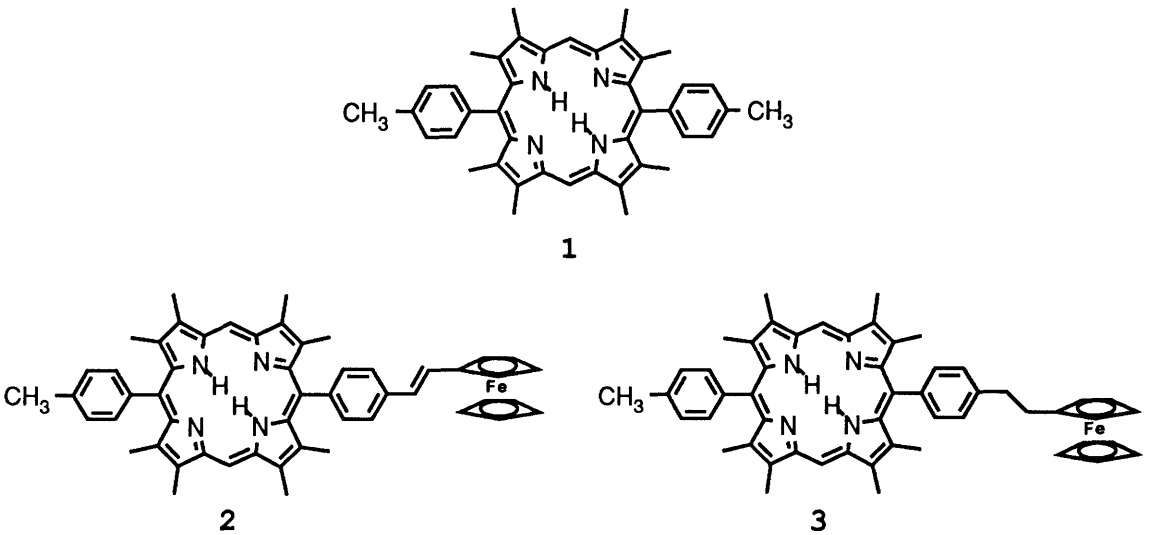

Scheme 3-1. Structures of porphyrins **1**, **2**, and **3**.

There have been several reports of ferrocene substituted porphyrins in the literature.[2-5] The preparation of a porphyrin-ferrocene-quinone assembly was described by Beer and Kurem.[2] Intramolecular quenching of porphyrin fluorescence was observed, but the quenching was attributed to rapid intramolecular electron transfer from the excited porphyrin chromophore to the quinone acceptor. It is likely that the ferrocene center employed was incapable, thermodynamically, of reducing the singlet excited state of the porphyrin chromophore. Maiya, Barbe, and Kadish[3] observed that ferrocene quenches the triplet excited state of a metallo-porphyrin. Although the authors did not rule out quenching by an electron transfer mechanism, the data were interpreted in terms of an energy transfer mechanism. Quenching of the triplet excited state of porphyrin by an energy transfer mechanism is likely since ferrocene has a low-lying triplet excited state. Here, we present results consistent with the conclusion that ferrocenyl centers can reduce the porphyrin singlet excited state intermolecularly and intramolecularly. Others have claimed that ferrocene reduces the lowest excited state of UO_2^{2+}.[6] It has been recently shown that ferrocene can serve as an electron donor to the lowest excited state of Cr(2,2'-bipyridine)$_3^{3+}$ [7] and can quench excited Ru(II) polypyridyls by both electron donation and energy transfer.[8] The different linking groups in **2** and **3** are found to give significantly different quenching rates.

Experimental

Synthesis of Porphyrins 1, 2, and 3. Porphyrin **1-3** were made by Richard Giasson in the Wrighton group.[9]

Fluorescence spectra and Stern-Volmer experiments. Fluorescence spectra were recorded on a Perkin Elmer MPF-44 spectrophotofluorimeter using a 1 cm optical glass cell. Solutions with the same absorbance (A = 0.040 at 504 nm) were prepared for porphyrins **1, 2** and **3** in 2-MTHF. The spectra were recorded after the solutions were deoxygenated with 2-MTHF saturated Ar for 30 min. Additional spectra were recorded after bubbling the solutions with 2-MTHF saturated air and 2-MTHF saturated oxygen for 30 min. These additional data were used in the Stern-Volmer analysis for the quenching of porphyrins **1, 2** and **3** fluorescence by oxygen.

The Stern-Volmer experiments using ferrocene as quencher were performed in 2-MTHF. Concentration of porphyrins **1, 2** and **3** is constant within a set of solutions (A = 0.050 at 504 nm) and concentration of ferrocene varies from 0 to 2 x 10^{-2} **M**. Samples were subjected to three freeze-pump-thaw cycles and sealed under vacuum in 1 cm Pyrex tubes.

The Stern-Volmer experiments using both oxygen and ferrocene derivatives as quenchers were performed in THF. Solutions containing the same concentration of porphyrin **1** (A = 0.040 at 628 nm) were prepared. One of the solutions contained no ferrocene derivative. The others contained

known concentrations of one of the following ferrocene derivatives: octamethylferrocene; ferrocene; phenylferrocene; acetylferrocene; or diacetylferrocene. A 1 cm optical glass cell was used. Spectra were recorded for each solution after purging 30 min with THF saturated Ar, after purging 30 min with THF saturated air, and after purging 30 min with THF saturated oxygen.

Fluorescence lifetime measurements. Time resolved fluorescence measurements were done at the MIT Laser Research Center, which is a National Science Foundation Regional Instrumentation Facility. Excitation light of 588 nm was produced by a Coherent 590 cavity-extended dye laser synchronously pumped by the second harmonic of a Coherent Antares 76-S mode-locked Nd-YAG laser (70 ps FWHM, 76 MHz). The repetition rate of the dye laser was reduced to 1 MHz using a cavity dumper. The output of the dye laser has a 5 ps pulse width. Fluorescence was collected at a right angle to the excitation beam and sent through a magic angle polarizing filter and monochromator to select out the 700 nm emission. A microchannel plate PMT (Hamamatsu R1564-U-07, 90 ps transit time spread) detected the fluorescence; the time difference between this signal and a reference signal from a photodiode monitoring the incident beam was converted into a voltage via a time-to-amplitude converter. This voltage was sent to a multichannel analyzer and stored in a microcomputer. The overall temporal response of the TCPC system was 150 ps.

Transient absorption experiments. Transient absorption experiments were performed at the MIT Laser Research Center. Transient absorption signals were acquired following a laser excitation pulse of 416 nm (1mJ/pulse) from a Quanta-Ray RS-1 Raman shift laser pumped by a Quanta-Ray DCR-3 Nd:YAG laser (third harmonic, 3 ns FWHM). The Raman shifter output was separated by a prism, and the desired wavelength was sent through an aperture and interference filter to completely isolate a pump wavelength.

A 150 W high pressure Xenon arc lamp, which was powered by a super-quiet OLIS XL150 power supply, provided the broad band probe light. Transient spectra were obtained by an EG & G 1421 OMA diode array detector gated through a EG & G Model 1302 fast pulser. The delay time from the laser pulse leading edge to the sampling pulse falling edge was controlled by a SRS Model DG535 digital delay/pulse generator. The data acquisition and scanning of the detector were synchronized and controlled with an EG&G 1463 controller and EG&G 1461 detector interface. Each transient absorption spectrum was obtained by averaging 250 scans.

Results

Optical Absorption and Emission Properties of 1, 2 and 3. Absorption spectra of **2** and **3** are nearly identical to that of **1**, Figure 3-1, as is expected due to the low absorptivity of the ferrocene chromophore (l_{max} = 440 nm, e =

90 $M^{-1}cm^{-1}$)[10] compared to porphyrin. No additional bands due to charge transfer or perturbation of the porphyrin chromophore were observed. This indicates relatively little ground-state electronic interaction between the electron donor (ferrocene) and electron acceptor (porphyrin) subunits.

Emission spectra of dilute, deoxygenated solutions of **1**, **2** and **3** in 2-methyltetrahydrofuran, 2-MTHF, were recorded at room temperature. All three species show two emission bands centered at 630 nm and 698 nm. Relative quantum yields of fluorescence of **2** and **3** compared to **1** are 0.38 and 0.84, respectively, Figure 3-1. The decrease in fluorescence intensity in **2** and **3** is attributed to intramolecular quenching of the porphyrin singlet state by the ferrocenyl centers.

Intermolecular quenching of fluorescence of porphyrins **1**, **2** and **3** by added ferrocene was observed in 2-MTHF at room temperature, Figure 3-2. Stern-Volmer analysis[11] yields linear plots with $k_q t$ values of 48.3 $\mathbf{M^{-1}}$, 23.1 $\mathbf{M^{-1}}$ and 45.1 $\mathbf{M^{-1}}$ for **1**, **2** and **3**, respectively. Assuming that the porphyrins are quenched at the same rate by ferrocene, the ratio of the Stern-Volmer constants, $k_q t$, is equal to the ratio of the lifetimes. The value of $\mathbf{t_2/t_1}$ obtained by this method is 0.48, and that of $\mathbf{t_3/t_1}$ is 0.93. These are in agreement, within experimental error, with the relative quantum yields of fluorescence.

Oxygen was also shown to quench the fluorescence of porphyrins **1**, **2** and **3** by comparing the intensity of emission

of solutions saturated with either Ar (0% O_2), air (20% O_2) or pure O_2 (100% O_2), Figure 3-3. The value of $\mathbf{t_2/t_1}$ obtained from the ratio of Stern-Volmer constants for O_2 quenching is 0.48, and that of $\mathbf{t_3/t_1}$ is 0.86. These values are in agreement with the values obtained for the relative quantum yields of fluorescence, and for the intermolecular quenching with ferrocene.

The fluorescence lifetimes of **1**, **2** and **3** were directly measured by the time-correlated single-photon-counting technique in 2-MTHF at room temperature, Figure 3-4. Fluorescence of **1** and **3** showed single exponential decays with lifetimes of 15 ns and 14 ns, respectively. Fluorescence of **2** showed a double exponential decay consistent with a short-lived species having a lifetime of 4 ns and a longer-lived species with a lifetime of 13 ns. The results for **2** are consistent with the presence of *cis* and *trans* isomers in solution, but definitive assignment of a lifetime to a given species depends on isolation of the pure isomers.

Transient Absorption Spectroscopy. The transient absorption spectra following a 10 ns pulsed laser excitation of **1**, **2** and **3** were monitored with an optical multichannel analyzer with a 10 ns gate width. The transient spectrum of **1** was of the triplet state[12] between 430-480 nm which decayed at a single exponential rate of 9.5×10^4 s^{-1}, shown in Figure 3-5. Transient spectra of **2** and **3** showed a similar broad absorption band between 430-480 nm with single exponential decay rates of 4.7×10^5 s^{-1} and 2.1×10^5 s^{-1} respectively,

as shown in Figures 3-6 and 3-7. The spectrum of reduced porphyrin[12] overlaps with that of the porphyrin excited state, so we are unable to unambiguously assign the transient absorption spectra of **2** and **3**. If we assume the transient absorptions are due to triplet states and that triplet state lifetimes for all porphyrins excluding ferrocene quenching are the same, we can calculate intramolecular triplet state quenching rate constants of 3.8×10^5 s^{-1} for **2** and 1.2×10^5 s^{-1} for **3**. Ferrocene has a low-lying triplet excited state and is known to be an effective triplet quencher.[13]

An important non-radiative process in excited state porphyrin is intersystem crossing. A possible quenching mechanism of **2** and **3** singlet excited states is enhanced intersystem crossing relative to **1** due to the pendant ferrocene. The fluorescence quantum yield of porphyrins[14] is 0.1 to 0.2, less than the intersystem crossing quantum yield of 0.6 to 0.8, so any additional intersystem crossing that significantly affects singlet emission intensity should have a small but measurable effect on triplet state population. The transient absorption spectra show that the absolute concentration of triplet **2** and **3** following excitation is no greater than for **1**, indicating that little or no enhancement of intersystem crossing is taking place.

Intermolecular Quenching of 1 by Ferrocene Derivatives. Stern-Volmer quenching constants were obtained for a series of ferrocene derivatives with a wide range of oxidation potentials. Some ferrocene derivatives, such as

diacetylferrocene, absorb significant amounts of excitation light at the concentrations needed to quench the porphyrin chromophore, a problem that requires cumbersome correction techniques with traditional Stern-Volmer methods. We report here a new technique that provides for a simple, direct measure of the Stern-Volmer constant even under conditions in which the quencher attenuates the intensity of the excitation light.

A stock solution of porphyrin in THF was made. An aliquot was removed and mixed with a known amount of ferrocene derivative. This solution was divided into three samples and the fluorescence intensity in O_2, air, and Ar saturated solvent was measured. A Stern-Volmer constant, k_qt, was generated for the quenching of that solution's fluorescence by O_2. This was repeated for aliquots of the porphyrin solution with different concentrations of ferrocene derivative, including a solution with no ferrocene derivative, Fig. 3-8a. Comparing the Stern-Volmer constants of the solutions with a given concentration of ferrocene derivative to the solution without ferrocene derivative allows the ratios of the fluorescence lifetimes to be determined: $SV_{(oxy)0}/SV_{(oxy)[Fc]} = k_{q(oxy)}t_0/k_{q(oxy)}t_{[Fc]} = t_0/t_{[Fc]}$. Plotting t_0/t for various concentrations of ferrocene derivative provides the Stern-Volmer plot for quenching of porphyrin fluorescence by that ferrocene derivative, Figure 3-8b.

The singlet excited state of porphyrin **1** was quenched by ferrocene derivatives with oxidation potentials between

0.00 V to +0.85 V vs. SCE. Using the measured lifetime of 15 ns for porphyrin **1**, intermolecular quenching rate constants were calculated for five ferrocene derivatives, Figure 3-9.

Discussion

Steady state emission spectroscopy and Stern-Volmer analyses were used to probe the quenching of the porphyrin singlet excited state by the ferrocenyl moieties in porphyrins **2** and **3**. The ratio of lifetimes of porphyrin **3** to **1**, $\mathbf{t_3/t_1}$, obtained by these methods, ranges from 0.84 to 0.93. The ratio of the lifetimes obtained by direct measurement ($\mathbf{t_3/t_1}$ = 14 ns/15 ns = 0.93) is in good agreement with the results from relative fluorescence and intermolecular quenching. Using the relationship $k_3 = 1/\mathbf{t_3} - 1/\mathbf{t_1}$ and fluorescence lifetimes of 15 ns for porphyrin **1** and 14 ns for porphyrin **3**, a rate constant of 4.8×10^6 s^{-1} can be obtained for the quenching of the porphyrin excited singlet state by the attached ferrocenyl center.

The ratio of lifetimes of porphyrin **2** to **1**, $\mathbf{t_2/t_1}$, obtained by steady state techniques, ranges from 0.38 to 0.48. Time resolved fluorescence decay shows two species present in solution with lifetimes of 4 ns ($\mathbf{t_2/t_1}$ = 0.26) and 13 ns ($\mathbf{t_2/t_1}$ = 0.87). Using a steady state $\mathbf{t_2/t_1}$ average of 0.43, the relative contribution to total quenching by the fast and

slow components can be calculated to be 72:28. The ratio of *cis*:*trans* isomers in solution as determined by NMR is 73:27. Assuming the two quenching rates are due to the two isomers, the fluorescence lifetimes correspond to quenching rate constants of 1.8×10^8 s^{-1} for the *cis* isomer and 1.0×10^7 s^{-1} for the *trans* isomer.

Intermolecular quenching of porphyrin **1** with a series of ferrocene derivatives shows that the quenching rate constant increases as the ferrocene oxidation potential becomes less positive. This pattern follows that expected for electron transfer as the rate of electron transfer quenching increases as the driving force for electron transfer increases.[8] However, the quenching pattern is not in complete accord with an electron transfer mechanism because considerable quenching still takes place when there is no driving force for electron transfer. The quenching rate pattern of the five ferrocene derivatives is also not compatible with an exclusively energy transfer quenching mechanism, because the energy levels of the singlet excited state of the best ferrocene quenchers are higher or equal to those of the worst quencher. It should be noted that acetylferrocene (λ_{max} = 455 nm, ε = 420 $M^{-1}cm^{-1}$)[15] and diacetylferrocene (λ_{max} = 470 nm, ε = 440 $M^{-1}cm^{-1}$)[15] have significantly lower energy singlet excited states than octamethylferrocene and ferrocene (λ_{max} = 440 nm, ε = 90 $M^{-1}cm^{-1}$).[10,15] Thus, energy transfer may dominate the quenching mechanism for these quenchers since electron transfer is not thermodynamically favorable.

Several arguments support charge transfer as the dominant quenching mechanism of the porphyrin singlet excited state by the ferrocenyl centers in **2** and **3**. First, thermodynamic arguments support the assignment of the quenching mechanism to electron transfer from the ferrocenyl moiety to the excited porphyrin. In high dielectric constant solvents, the sum of the redox potentials for oxidation of a donor and the reduction of an acceptor is a good estimate of the energy level of the radical-ion pair of a charge separated species.[16] Thus, for compounds **2** and **3**, the energy level of the charge separated state is, respectively, 1.90 eV and 1.86 eV above the ground state. Since the lowest singlet excited state of these porphyrins is 1.97 eV above the ground state, the photoinduced intramolecular electron transfer reaction is exothermic by 0.07 eV (1.6 kcal mol^{-1}) and 0.11 eV (2.5 kcal mol^{-1}), respectively, for **2** and **3**, schedule 3-2. Second, the singlet excited state of ferrocene (2.46 eV)[10] is above that of the porphyrin chromophore (1.97 eV), thus quenching by energy transfer would be endothermic (0.49 eV or 11.3 kcal mol^{-1}). Third, triplet yields of **2** and **3** are not larger than for **1**, ruling out quenching due to enhanced intersystem crossing. Therefore, we conclude that the ferrocene centers in **2** and **3** quench the singlet excited state of the porphyrins by an electron transfer mechanism.

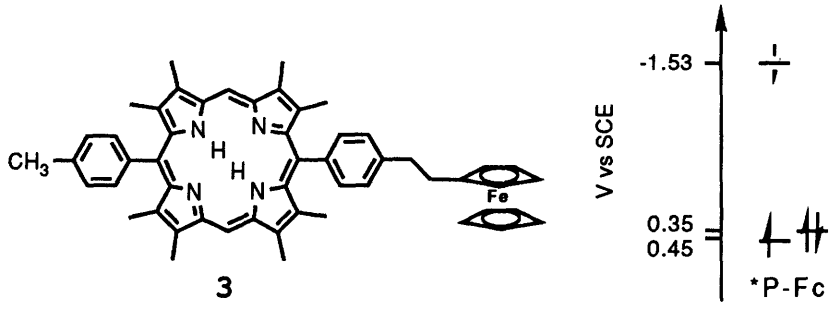

3

Scheme 3-2. Energetics for photoinduced electron transfer of **3**.

The driving force for the forward electron transfer is ~0.1 eV. Back electron transfer is favoured by ~1.9 eV. For the charge separated state to be built up, the back electron transfer must be slower than the forward electron transfer. Although our forward electron transfer rate is modest for both **2** and **3**, the back electron transfer driving force is well inside the inverted region and so back electron transfer rate may, in fact, be slower than the forward. However, porphyrin and ferrocene have no good spectroscopic handles to identify the charge separated state. The extinction coefficients of ferrocene and ferrocenium absorptions are low (λ_{max} = 440 nm, ε = 90 $M^{-1}cm^{-1}$ and λ_{max} = 617 nm, ε = 340 $M^{-1}cm^{-1}$),[17] and the absorption of reduced porphyrin overlaps with that of triplet state porphyrin. Unlike $Ru(bpy)_3^{2+}$ and Fc or viologen, or Re chromophores and PTZ or viologen, with porphyrin-ferrocene system we cannot derive back electron transfer rates.

Conclusions

Forward electron transfer rates of **2** and **3** show an interesting effect from linking groups: All three linked molecules **2***cis*, **2***trans* and **3** have a donor separated by the same number of atoms from the chromophore. Quenching in the ethyl linked assembly **3** is half as fast as the vinyl *trans* linked **2***trans*, despite the somewhat greater driving force of **3**. The quencher held *trans* to the chromophore, **2***trans*, quenches an order of magnitude slower than that in the *cis* geometry, **2***cis*.

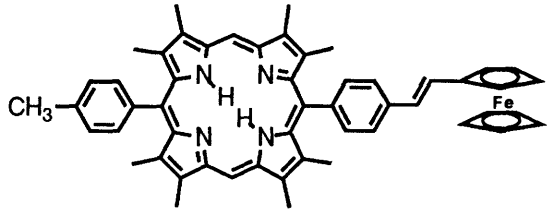

2

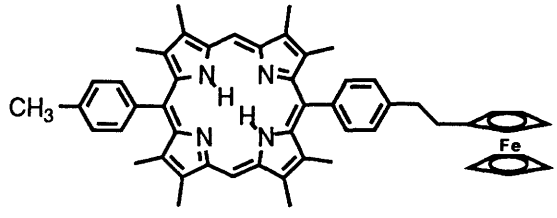

3

k_q*cis* = 1.8×10^8 s^{-1} k_q = 4.8×10^6 s^{-1}

k_q*trans* = 1.0×10^7 s^{-1}

At these low driving forces for electron transfer, both the geometric arrangement of the porphyrin and ferrocene, and the nature of the linking group, greatly alter the quenching rate.

References

1. Felton, R.H. **The Porphyrins**, *5*, Chapt. 3, Dolphin, D., Ed., Academic Press, **1978**.
2. Beer, P.D.; Kurek, S.S. *J. Organomet. Chem.* **1989**, C6-C8, 366.
3. Maiya, G.B.; Barbe, J.-M.; Kadish, K.M. *Inorg. Chem.* **1989**, *28*(13), 2524.
4. Schmidt, E.S.; Calderwood, T.S.; Bruice, T.C. *Inorg. Chem.* **1986**, *25*(20), 3718.
5. Wollmann, R.G.; Hendrickson, D.N. *Inorg. Chem.* **1977**, *16*(12), 3079.
6. Traverso, O.; Rossi, R.; Magon, L.; Cinquantini, A.; Kemp, T.J. *J.C.S. Dalton* **1878**, 569.
7. Lee, S.; Bakac, A.; Espenson, J.H. *Inorg. Chem.* **1989**, *28*, 1367.
8. Lee, E.J.; Wrighton, M.S. *J. Am. Chem. Soc.* **1991**, *113*, 8562.
9. Giasson, R.; Lee, E. J.; Zhao, X.; Wrighton, M. S. *J. Phys. Chem.* **1993**, *97*, 2596.
10. Sohn, Y.S.; Hendrickson, D.N.; Gray, H.B. *J. Am. Chem. Soc.* **1971**, *93*, 3603.
11. Stern, O.; Volmer, M. *Physik Z.* **1919**, *90*, 183.
12. (a) Bonnet, R.; Lambert, C.; Land, E.J.; Scourides, P.A.; Sinclair, R.S. *Photochem. Photobiol.* **1983**, *38*, 1.

(b) Peychal-Heiling, G.; Wilson, G.S. *Anal. Chem.* **1971**, *43*, 550.

13. Weller, A.Z. *Physik Chem. (Munich)* **1982**, *133*, 93.

14. (a) Harriman, A. *J.C.S. Faraday I*, **1980**, *76*, 1978.
(b) Moore, T.A.; Benin, D.; Tom, R. *J. Am. Chem. Soc.* **1982**, *104*, 7356.

15. Rosenblum, M. *Chemistry of the Iron Metallocenes: Ferrocene, Ruthenocene, Osmocene;* Interscience: New York, 1965; p 40, 86.

16. Weller, A.Z. *Physik Chem. (Munich)* **1982**, *133*, 93.

17. Zhao, X. Ph.D. Thesis, Chapter 2, Massachusetts Institute of Technology, Sept. 1994.

Figure 3-1. Relative fluorescence intensity of **1** (——), **2** (- - -) and **3** (—·—) in deoxygenated 2-methyl THF at room temperature (λ_{exc} = 504 nm). All three samples were measured under identical conditions, therefore the relative intensities represent relative emission quantum yields. The inset shows the absorption spectrum of **1** in THF.

Figure 3-2. Stern-Volmer plot for the quenching of the flourescence of porphyrin **1, 2** and **3** by ferrocene in 2-methyl THF at room temperature.

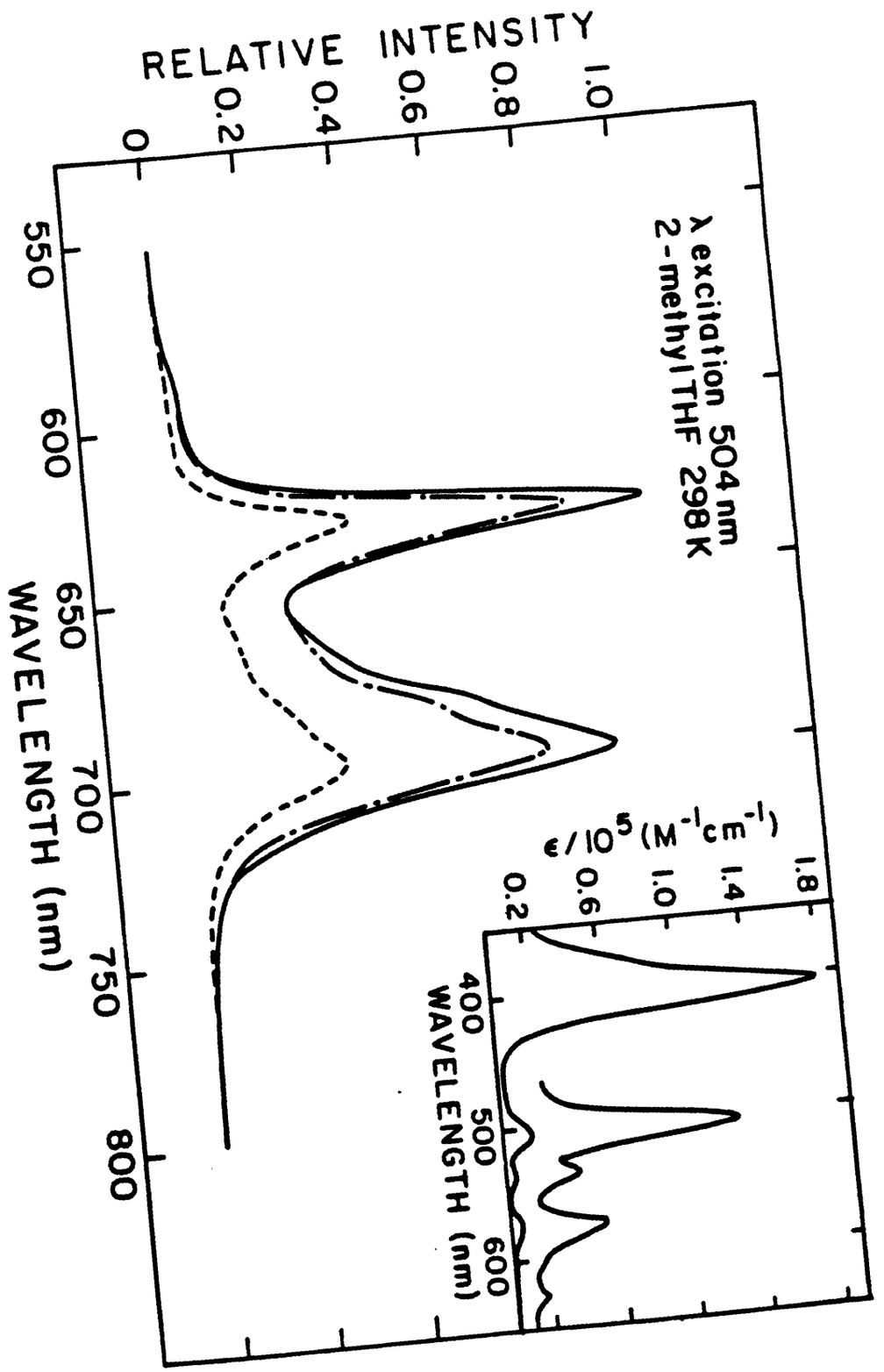
RELATIVE INTENSITY
0
0.2
0.4
0.6
0.8
1.0
λ excitation 504 nm
2-methyl THF 298K
550
600
650
700
750
800
WAVELENGTH (nm)
ε/10^5 (M^-1 c E^-1)
0.2
0.6
1.0
1.4
1.8
400
500
600
WAVELENGTH (nm)

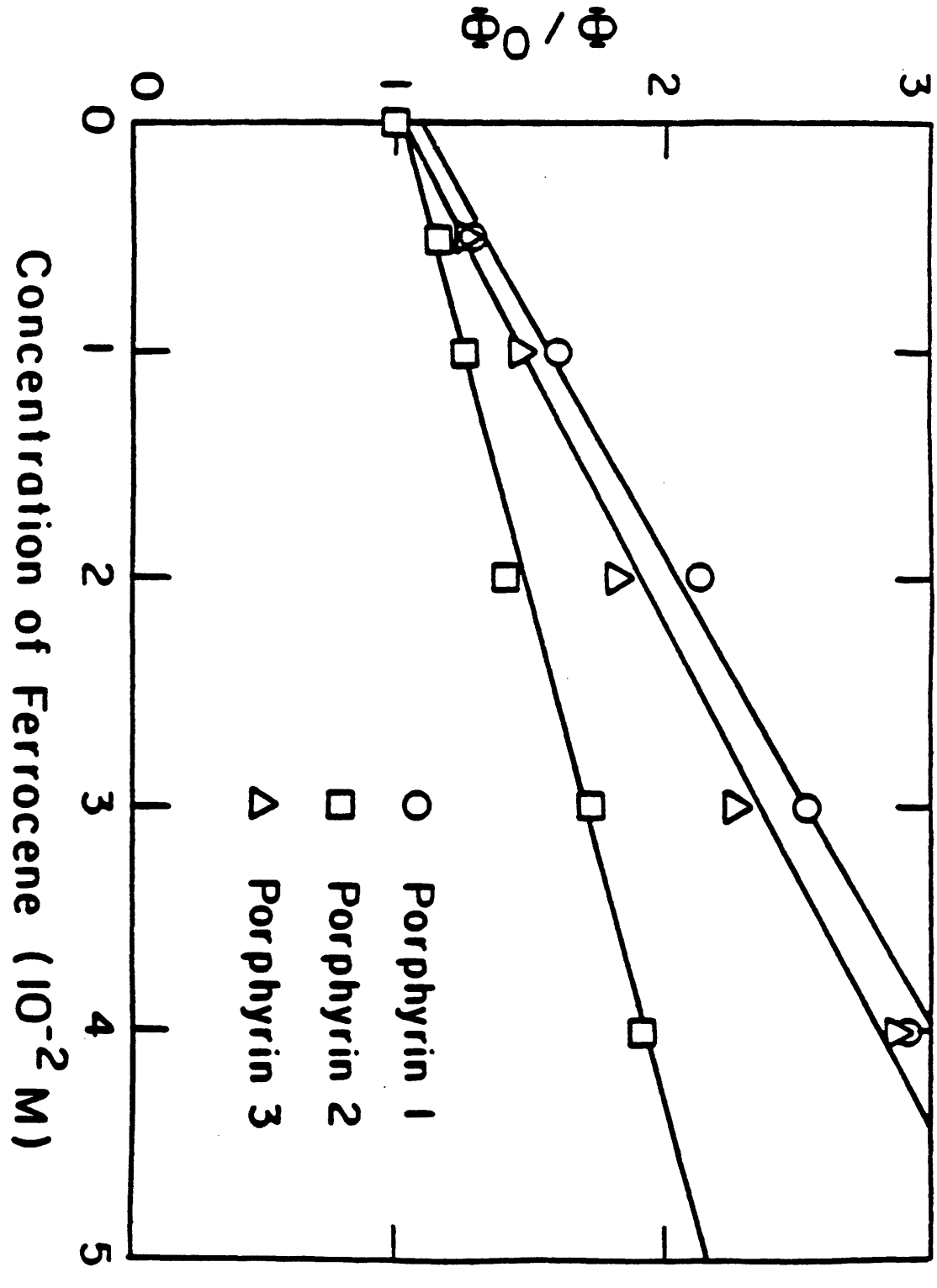
Φ_0 / Φ
0
1
2
3
0
1
2
3
4
5
Concentration of Ferrocene (10^{-2} M)
O Porphyrin 1
□ Porphyrin 2
Δ Porphyrin 3

Figure 3-3. Stern-Volmer plot for the quenching of the flourescence of porphyrin **1**, **2** and **3** by oxygen in 2-methyl THF at room temperature. The solutions were saturated with Ar (0% O_2), air (20% O_2) of pure O_2 (100% O_2).

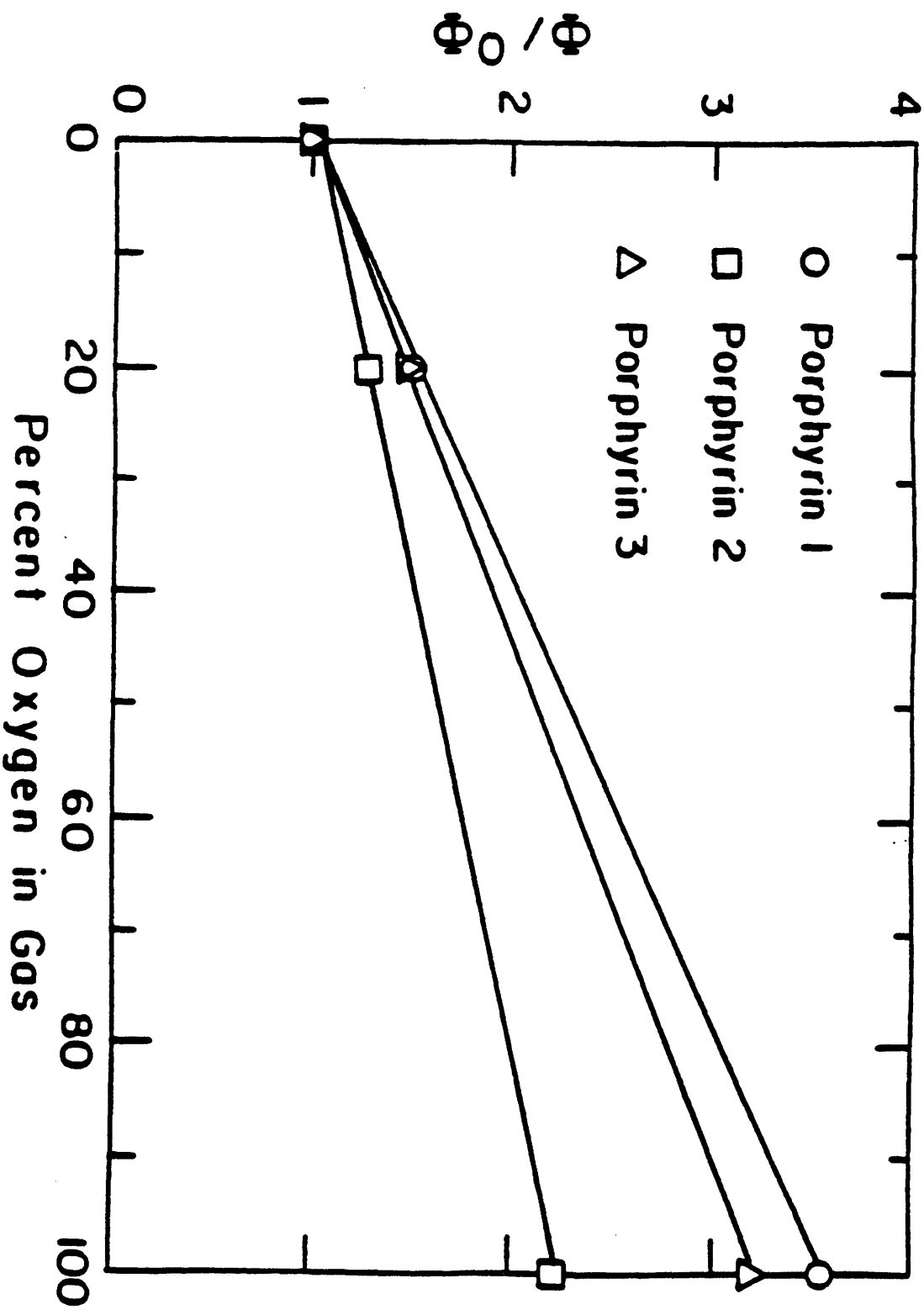
Φ/Φ0
0
1
2
3
4
0
20
40
60
80
100
Percent Oxygen in Gas
O Porphyrin 1
□ Porphyrin 2
△ Porphyrin 3

Figure 3-4. Fluorescence decays of **1**, **2**, and **3** in degassed 2-MTHF at room temperature.

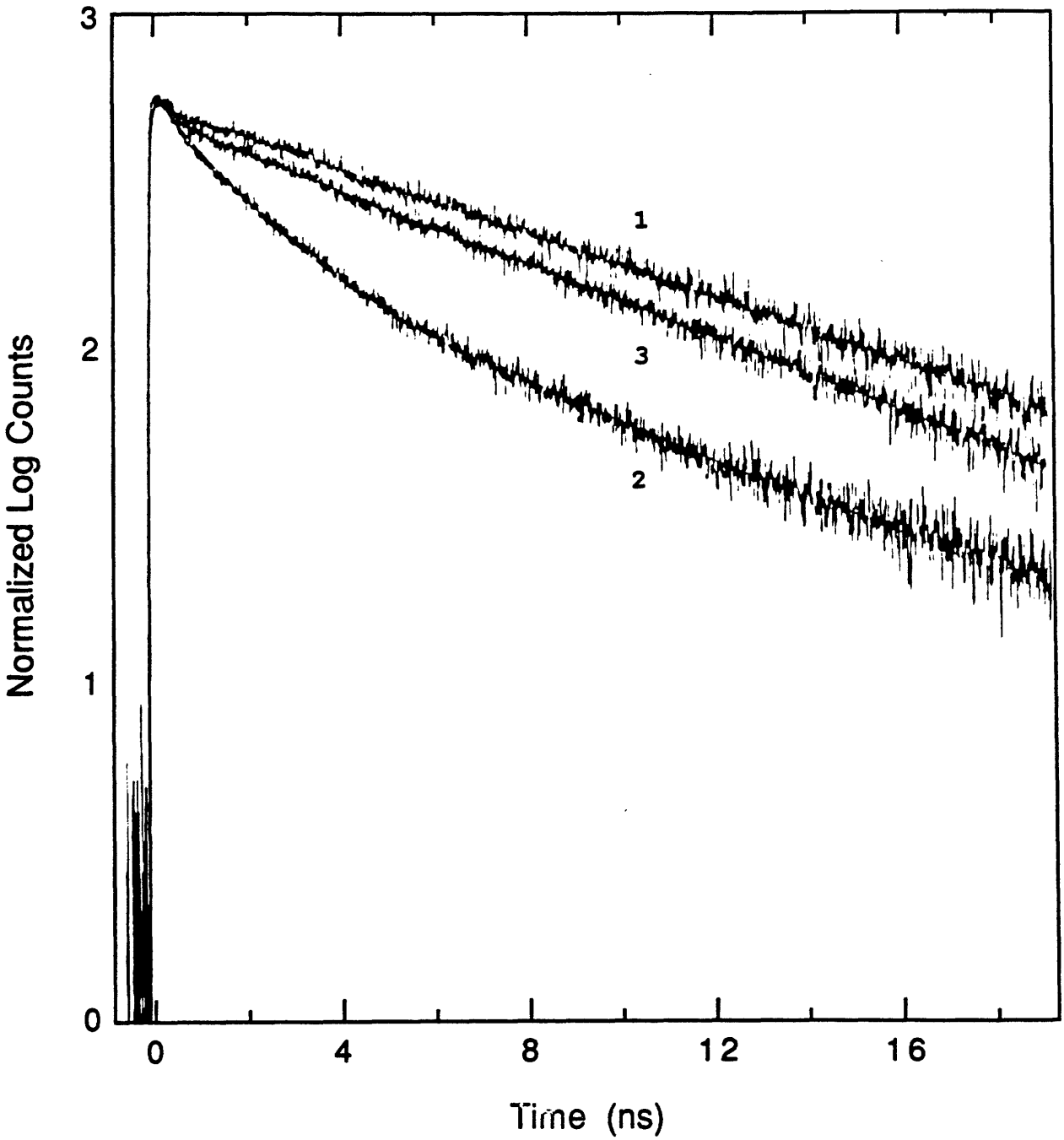
3
2
1
0
Normalized Log Counts
1
3
2
0
4
8
12
16
Time (ns)

Figure 3-5. Transient absorption spectrum of **1** in THF excited at 416 nm and recorded at a delay time of 500 ns. The inset shows the absorption decay at 440 nm.

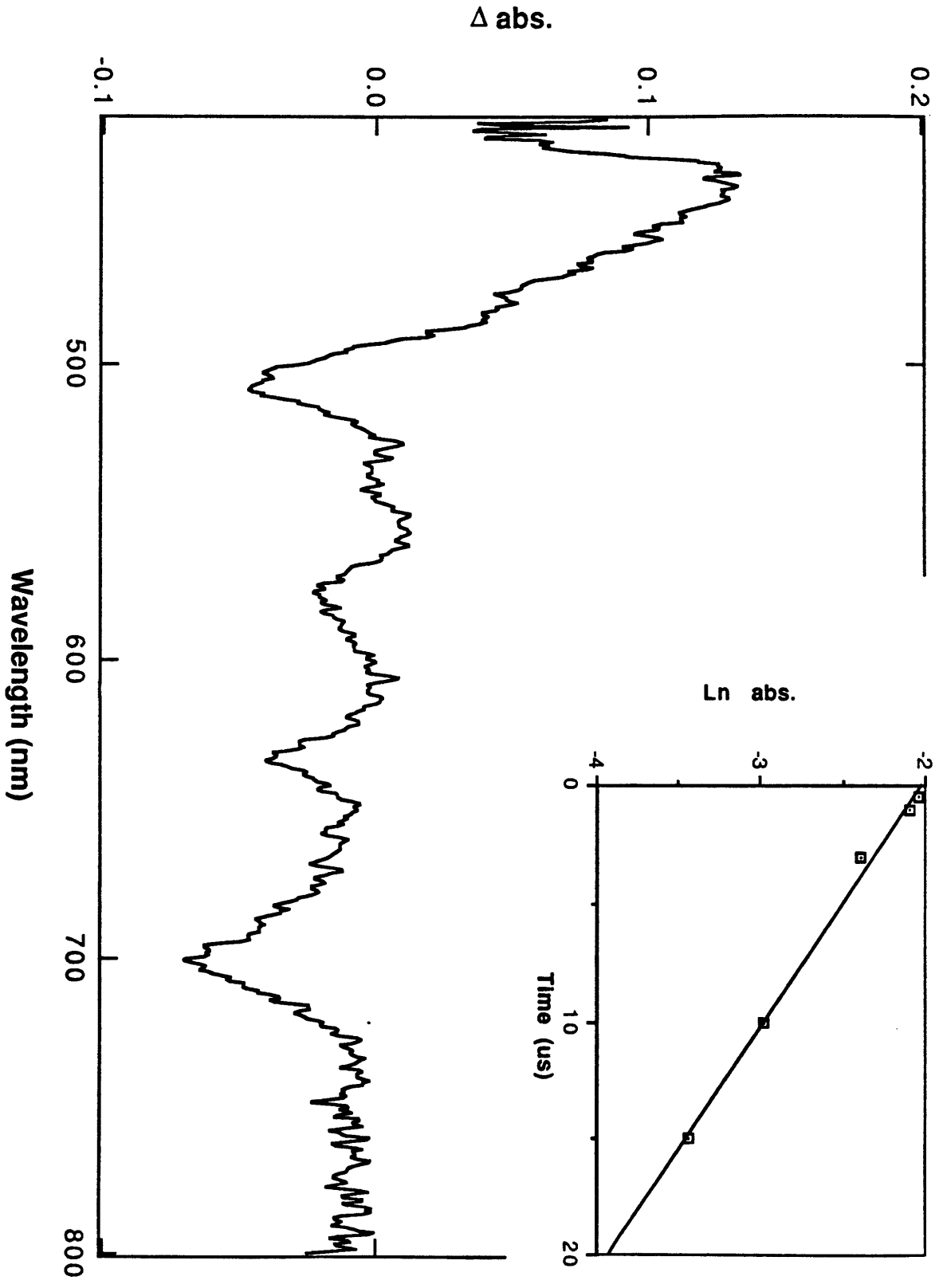
Δ abs.
-0.1
0.0
0.1
0.2
500
600
700
800
Wavelength (nm)
Ln abs.
-4
-3
-2
0
10
20
Time (us)

Figure 3-6. Transient absorption spectrum of **2** in THF excited at 416 nm and recorded at a delay time of 100 ns. The inset shows the absorption decay at 440 nm.

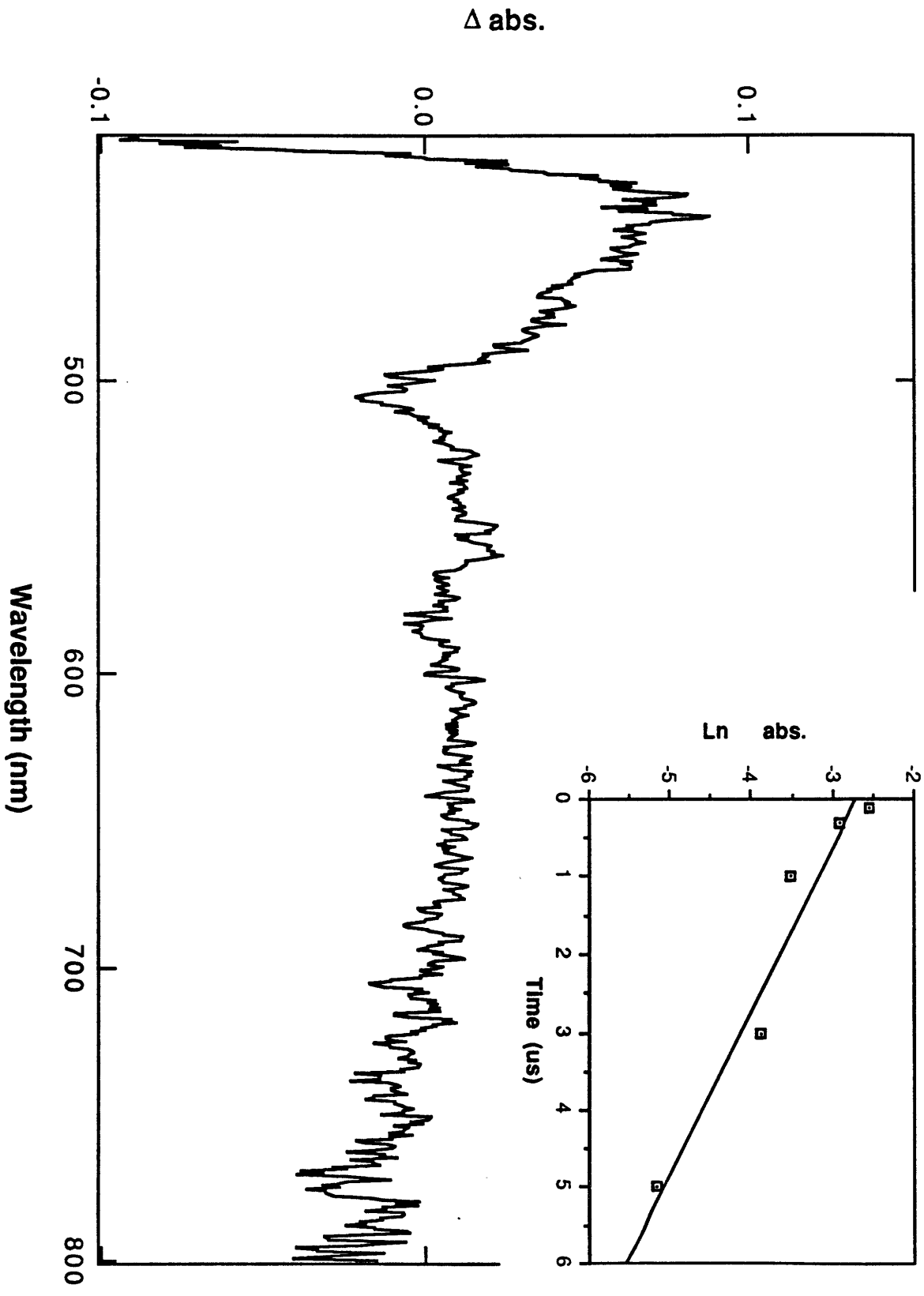
Δ abs.
-0.1
0.0
0.1
500
600
700
800
Wavelength (nm)
Ln abs.
-6
-5
-4
-3
-2
0
1
2
3
4
5
6
Time (us)

Figure 3-7. Transient absorption spectrum of **3** in THF excited at 416 nm and recorded at a delay time of 100 ns. The inset shows the absorption decay at 440 nm.

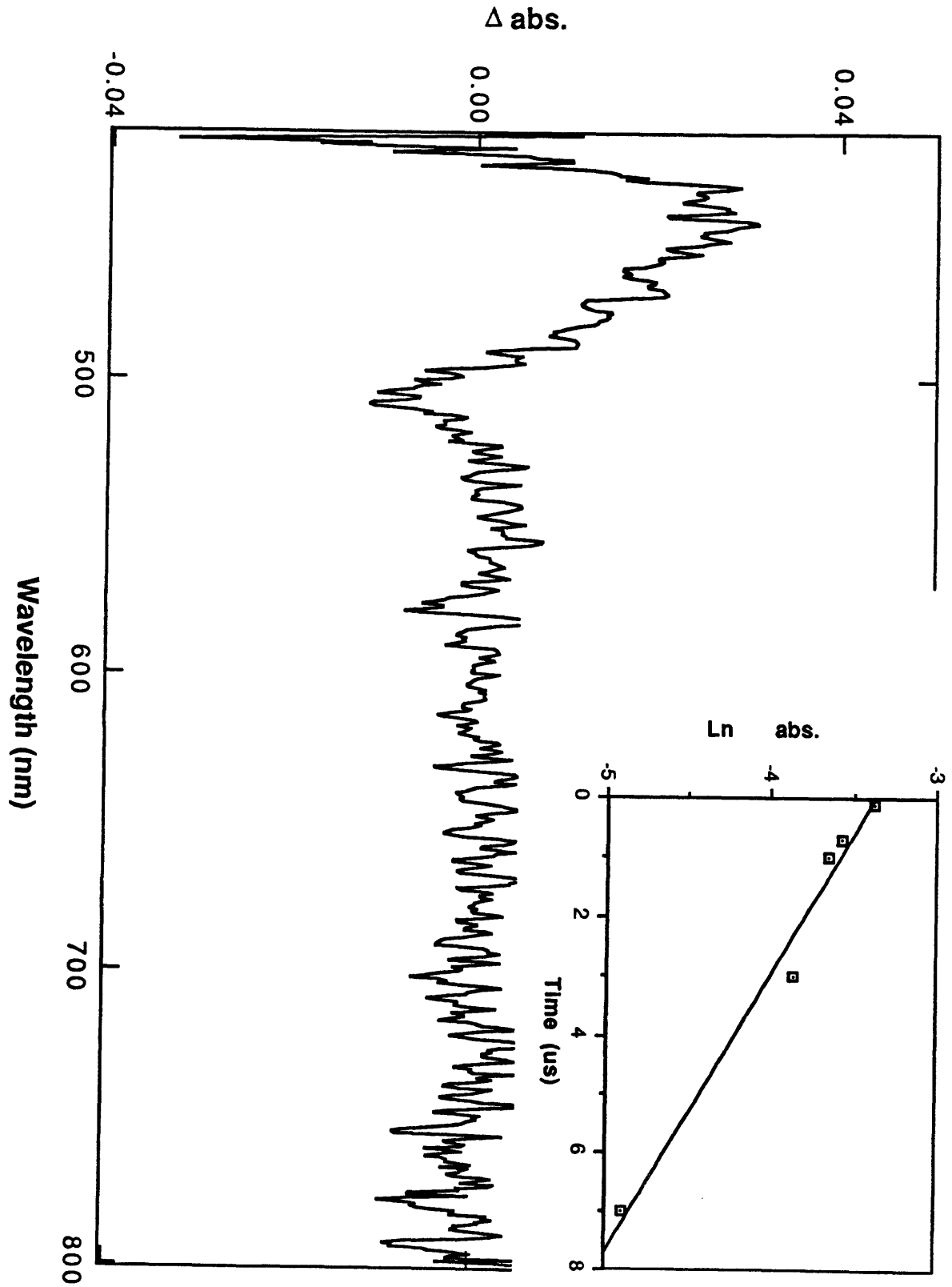
Δ abs.
-0.04
0.00
0.04
500
600
700
800
Wavelength (nm)
Ln abs.
-5
-4
-3
0
2
4
6
8
Time (us)

Figure 3-8. (a) Stern-Volmer plot of O_2 quenching of porphyrin **1** with various concentrations of ferrocene in solution. (b) Ratio of Stern-Volmer constant versus ferrocene concentrations gives a Stern-Volmer plot for quenching of porphyrin **1** by ferrocene.

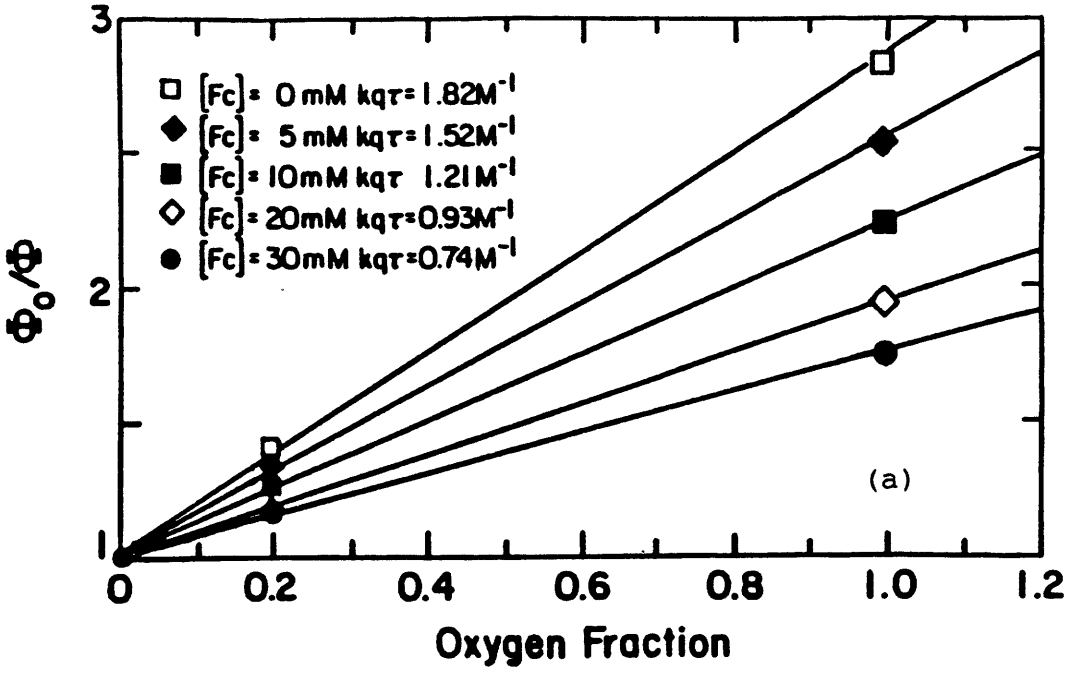
[Fc] = 0 mM kqτ = 1.82M⁻¹
[Fc] = 5 mM kqτ = 1.52M⁻¹
[Fc] = 10mM kqτ 1.21M⁻¹
[Fc] = 20mM kqτ = 0.93M⁻¹
[Fc] = 30mM kqτ = 0.74M⁻¹
Φ₀/Φ
(a)
Oxygen Fraction

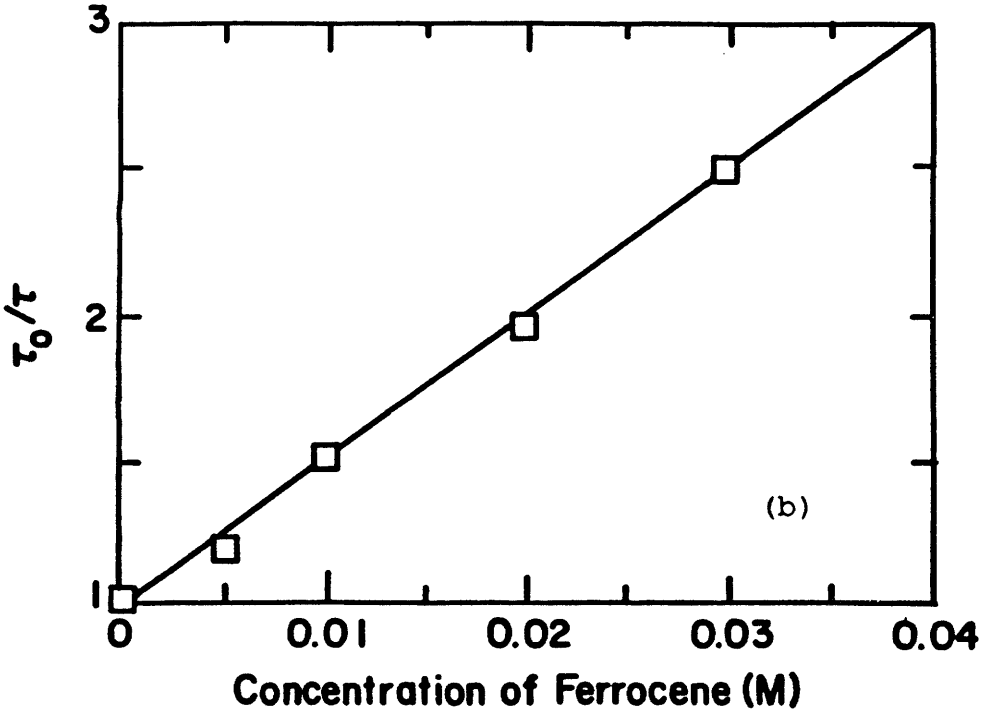
τ₀/τ
(b)
Concentration of Ferrocene (M)

Figure 3-9. Quenching constant for the quenching of porphyrin **1** fluorescence as a function of the oxidation potential of the ferrocene derivatives (vs SCE in CH_3CN containing 0.1 M [*n*-Bu_4N]ClO_4).

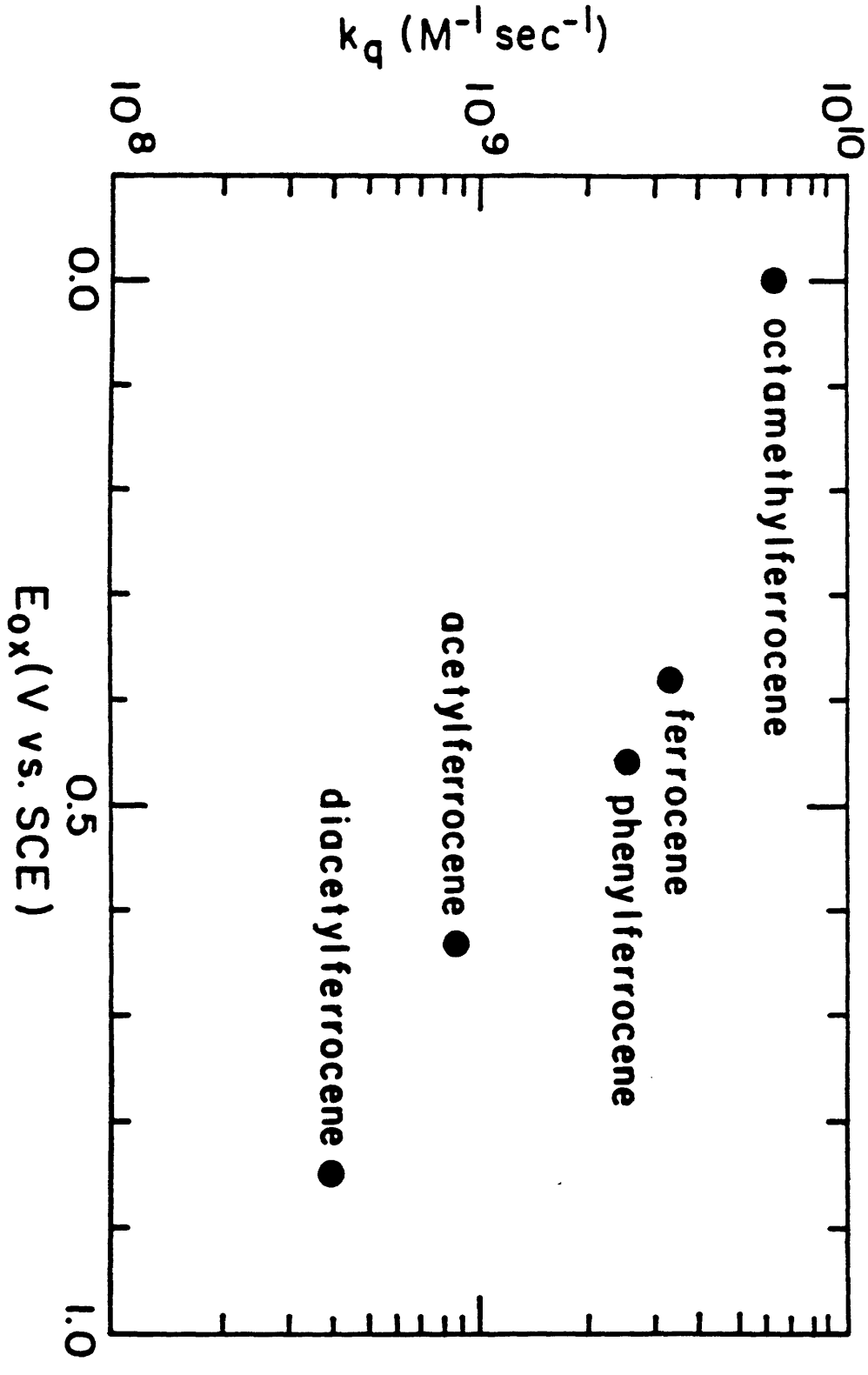
k_q (M^{-1} sec^{-1})
10^8
10^9
10^{10}
0.0
0.5
1.0
E_{ox}(V vs. SCE)
octamethylferrocene
ferrocene
phenylferrocene
acetylferrocene
diacetylferrocene

CHAPTER FOUR

PHOTOINDUCED ENERGY TRANSFER AND ELECTRON TRANSFER BETWEEN SURFACE-CONFINED RE(I) COMPLEXES AND SURFACES

Abstract

The Re(I) carbonyl complex $[L'Re(CO)_3(4,4'-X-2,2'-bipyridine)]^+$, **1a** where L'= 4-ethylpyridine and X = $C(O)O-(CH_2)_3SiCl_3$, was chemically immobilized onto SiO_2, indium tin oxide (ITO), Pt surfaces and high surface area SiO_2. Emission decays and time-resolved emission spectra were obtained for monolayer quantities of **1a** covalently attached to these surfaces. Analysis of the emission decays of **1a** in electrolyte solution on the three flat surfaces allows an evaluation of the contributions of interfacial energy transfer and electron transfer to quenching of photoexcited **1a**. Emission decay profiles fit a single exponential decay. The excited-state lifetime of **1a** is shortest on the conducting and light-absorbing Pt surface, while longer excited-state lifetimes are observed for **1a** on the non-absorbing, insulating SiO_2 surface and the non-absorbing, but conducting ITO surface. The dominant mechanism for quenching by Pt is energy transfer, based on the significant shortening of the emission lifetime of **1a** on Pt compared to that on ITO and SiO_2. The result that the excited-state lifetimes of **1a** on SiO_2 and ITO are very close and can not be distinguished within experimental error is consistent with a small amount of quenching of photoexcited **1a** on ITO by a slow interfacial electron transfer process. The kinetics of the interfacial electron transfer between **1a** and ITO/Pt were examined by cyclic voltammetry and chronoamperometry.

Introduction

In this chapter we present a study of interfacial quenching processes for the photoexcited Re(I) carbonyl complex, $[L'Re(CO)_3(4,4'\text{-}X\text{-}2,2'\text{-bipyridine})]^+$, **1a**, where L'= 4-ethylpyridine and X = $C(O)O\text{-}(CH_2)_3SiCl_3$, chemically immobilized on surfaces. The critical measurements are time-resolved emission spectroscopy. Chemically immobilizing chromophores on surfaces can be useful as well characterized systems for studying interfacial processes.[1] We have previously reported the characterization of electrodes modified with **1a** by electrochemical methods, UV/vis, IR and emission spectroscopy and the study of the charge-separated state of a species related to **1a** on high surface area SiO_2.[2]

Interfacial quenching of excited states of molecules anchored on conducting substrates by electron and energy transfer plays a central role in such diverse processes as photoelectrochemistry, photocatalysis, and imaging. Interfacial energy transfer can compete with photoinduced interfacial electron transfer in an organized electrode-confined molecular assembly designed to achieve vectorial electron transfer following light absorption. Therefore, the efficiency of the assembly for electricity or fuel generation is often determined by competition between these two processes.

Harris[3] and other researchers[4] have studied photoinduced energy transfer between adsorbed atoms or molecules and metal surfaces as a function of the distance between them in a vacuum. Frank[5] used steady-state fluoresence spectroscopy to

investigate the quenching process of organic self-assembled monolayers on an aluminum surface. However, few well-defined experimental systems[1,6,7] have been available to study the kinetic properties of photoinduced electron transfer and energy transfer between electrode surfaces and monolayers.

In our study, the rate constant of photoinduced interfacial energy transfer is determined by comparing the emission decays of **1a** on Pt and ITO knowing that (a) the photoinduced electron transfer rates at Pt- and ITO-electrolyte interfaces are almost identical and are slow compared to the photoinduced interfacial energy transfer; (b) ITO does not quench the photoexcited **1a** by energy transfer. The rate constant of the photoinduced interfacial electron transfer can be estimated by comparison of emission decays of **1a** on ITO and SiO_2, because SiO_2 is inert to both energy and electron transfer quenching. The kinetics of interfacial electron transfer quenching of **1a** on ITO and Pt were also studied by electrochemical methods. Similar electrochemical studies for alkanethiol monolayers with pendant ferrocenyl centers or Ru^{3+} or other redox centers on metal surfaces have been reported.[8-10]

Experimental Section

Materials. The preparation of **1a** and $[L'Re(CO)_3(4,4'\text{-}X\text{-}2,2'\text{-bipyridine})]^+$, **1b**, where L'= 4-ethylpyridine and X = $C(O)OCH_2CH=CH_2$, is described in Scheme 4-1. ITO on a glass was obtained from Delta Technologies and fabricated into

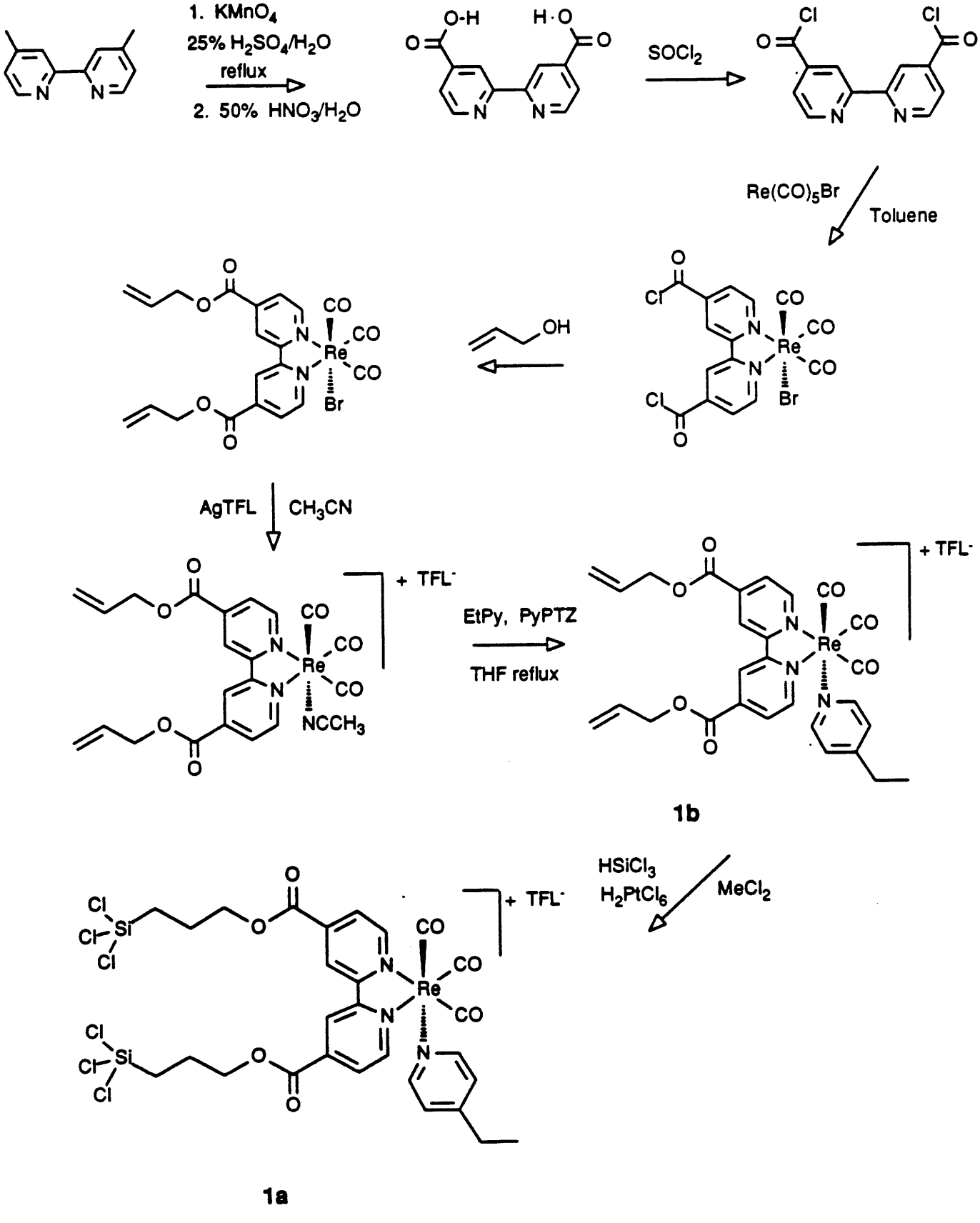
1. KMnO4
25% H2SO4/H2O
reflux
2. 50% HNO3/H2O
SOCl2
Re(CO)5Br
Toluene
AgTFL
CH3CN
+ TFL-
EtPy, PyPTZ
THF reflux
HSiCl3
H2PtCl6
MeCl2
1b
1a

electrodes. Pt electrodes were made by evaporating approximately 50 Å Ti and then 1000 Å of Pt onto Si wafers. The various spectroscopic-grade solvents (EM Science) were used as received. [*n*-Bu_4N]PF_6 (Aldrich) was recrystallized from ethanol. High surface area SiO_2 (400 m^2/g) was obtained from Alfa and was dried for 72 hours at 200 °C in vacuo.

Sample Preparation. **1a** was immobilized on the pretreated Pt, ITO, and glass surfaces by siloxy linkage as shown in Scheme 4-2. Pt electrodes were pretreated by immersing them in 1:1 HCl/CH_3OH for 30 min, then in concentrated H_2SO_4 for 30 min, and were sonicated in OmniSolv H_2O for 10 min. The electrodes were then cleaned in O_2 plasma for 10 minutes, and finally were derivatized by soaking in 0.1 to 1 mM solutions of **1a** in CH_2Cl_2 for 2-20 minutes. ITO and glass surfaces were pretreated by immersion in 10 M NaOH for 10 minutes and then sonicating them in H_2O and CH_3OH for 10 minutes. They were then derivatized by soaking in 0.1 to 1 mM solutions of **1a** in CH_2Cl_2 for 2-20 minutes. The modified surfaces were rinsed thoroughly with CH_2Cl_2 to avoid emission from free **1a** in solution.

The immobilization of **1a** on high surface area SiO_2 was carried out by stirring the pretreated high surface area SiO_2 in 1×10^{-4}-1×10^{-3} M CH_2Cl_2 solutions of **1a** under N_2 atmosphere overnight, and then washing successively with CH_3CN, hexane, and CH_2Cl_2.

The surface coverages of **1a** on ITO and Pt electrodes were controlled by adjusting the concentration of the derivatizing

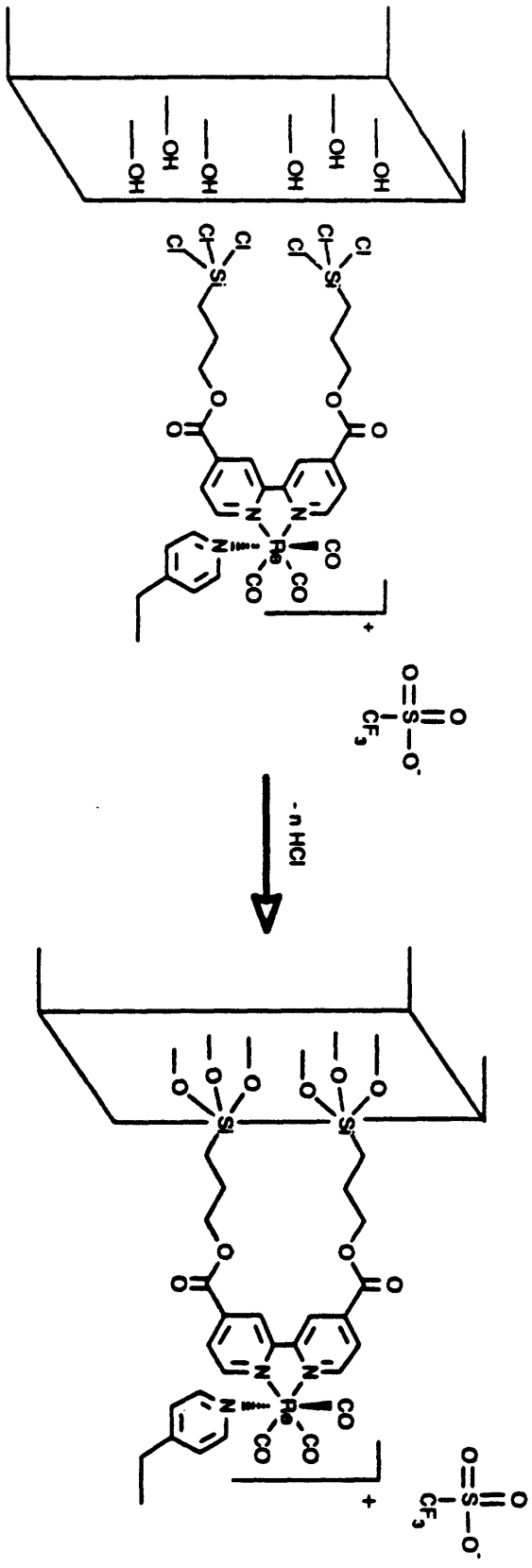
- n HCl

solutions and the immersion time. Surface coverages were determined by integration of slow sweep cyclic voltammograms. All electrochemical and emission measurements were made in 0.1 M [*n*-Bu_4N]PF_6/CH_2Cl_2 or CH_3CN or 0.1 M LiCl/H_2O. All measurements were carried out at room temperature. Measurements of the emission decays were made with both degassed and air-saturated samples.

Transient Emission Experiments. Transient emission signals were acquired following a laser pulse excitation of 416 nm (1mJ/pulse) from a Quanta-Ray RS-1 Raman shift laser pumped by a Quanta-Ray DCR-3 Nd:YAG laser (third harmonic, 3 ns FWHM). Emission signals were collected by a set of lenses which are f-matched with the spectrograph of the detector at a specific angle to the excitation in order to eliminate the perturbation from the reflected excitation light. Emission decays at a specific wavelength were monitored by a Hamamatsu R446 photomultiplier (PMT) with a 2.7 ns rise time and recorded by a LeCroy 6880A transient digitizer. Emission signals were monochromated by a SA model DH-10 double monochromator. The PMT was negatively biased by a Fluke model 405B regulated high voltage power supply. All lifetimes are determined by averaging at least three independent measuements.

Transient emission spectra were acquired by an EG&G 1421 OMA diode array detector gated with a gate width of 10 ns through a EG&G 1302 fast pulser. The delay time from laser pulse leading edge to sampling pulse falling edge was controlled by a SRS Model DG535 digital delay/pulse generator.

The data acquisition and scanning of the detector were synchronized and controlled with an EG&G 1463 controller and EG&G 1461 detector interface. The output from the OMA detector was interfaced to an IBM PC.

Steady State Emission Measurements. Emission and excitation spectra were recorded on a MPF-44 spectrophotofluorimeter. The emission spectra were corrected for the instrument response by a calibration curve generated using GE tungsten standard lamp.

Electrochemical Measurements. Electrochemical experiments were carried out at room temperature. The working electrode was the derivatized electrode with an immersed area of ~1 cm^2. Pt wire was the counterelectrode, and oxidized Ag wire was the quasi-reference. The electrolyte solution was purged with Ar prior to voltammetry and chronoamperometry and was blanketed with Ar during experiments. Linear sweep cyclic voltammograms and chronoamperometry curves were recorded using one channel of a Pine Instruments RDE4 bipotentiostat. In the chronoamperometry experiments the potentiostat was driven by a Princeton Applied Research Model 175 programmer, and signals were recorded on a Hi-Techniques IQ 300 or Nicolet 4094B digital oscilloscope.

FTIR Measurements. Reflectance FTIR (RFTIR) spectra were obtained at 2 cm^{-1} resolution on an Nicolet 60 SX FTIR spectrometer equipped with a Specac IR polarizing filter and a Spectra-tech reflectance-absorbance apparatus operated with a grazing angle of 78^o.

Results and Discussion

Emission Quantum Yield Measurements. The relative emission quantum yield of **1a**, q, was measured by integrating the corrected emission spectrum relative to $[Ru(bpy)_3](PF_6)_2$ in H_2O as a standard (ϕ_r = 0.042 at 298 K).[23] q was determined to be 0.030 by using eq. 4-1 where A is the absorbance at the excitation wavelength, I is the integrated area of the

$$q = \phi_r \frac{A_r\ I_s}{A_s\ I_r}\left(\frac{n_s}{n_r}\right)^2 \qquad (4\text{-}1)$$

emission band, and n is refractive index. Subscripts r and s indicate reference and sample solutions respectively.

Reflectance FTIR Spectra of 1a on Pt. The reflectance FTIR spectra of the monolayers on Pt demonstrate that the CO stretching frequency (2040 cm^{-1}) of the surface-confined **1a** is identical to that (2038 cm^{-1}) of the solution analog at 2 cm^{-1} resolution, as shown in Figure 4-1. RFTIR spectra of **1a** on ITO and SiO_2 could not be obtained due to the interference from internal reflections in the glass substrates.

Electrochemistry of 1a Chemically Immobilized on Pt and ITO Electrodes. Electrochemical methods such as cyclic voltammetry and chronoamperometry provide simple and reliable ways to measure the surface coverage, and interfacial electron transfer rates between electroactive monolayers and electrode surfaces. Consequently, kinetic data for interfacial electron

transfer can be used to estimate the rate constants of the photoinduced electron transfer between Pt or ITO electrodes and the surface-confined Re(I) complex.

Reversible Cyclic Voltammetry. Cyclic voltammetry shows a reversible one-electron redox wave for the bipyridine-diester moiety at -0.75 V vs. SCE for both Pt and ITO electrode-confined **1a**. Integration of cyclic voltammetric waves for the electrodes gives uncorrected coverage of $\sim 3 \times 10^{-10}$ mol/cm^2 for ITO and $3\text{-}15 \times 10^{-10}$ mol/cm^2 for Pt. Coverage of **1a** were estimated to be monolayer or submonolayer when surface roughness was taken into account.[11] Figure 4-2 shows typical cyclic voltammograms for **1a** at monolayer coverage on Pt and ITO. At sufficiently slow scan rates (10-50 mV/s), the cyclic voltammogram shows that the formal potential of the redox centers (-750 mV vs SCE) is close to the formal potential of a solution analog, **1b** (-760 mV vs SCE); the peak splitting (ΔE_p) is small (ca. 10 mV) within experimental uncertainty ($\pm$ 4 mV), and the peak half-widths (ΔE_{fwhm}) are 95-105 mV. The characteristics of the CV indicate that the local environment around each redox center is quite uniform. At higher scan rates, the anodic and cathodic peak positions are substantially separated. Peak splitting can be used to calculate the apparent standard rate constant (k^0_{app}), which is the electron transfer rate constant at zero overpotential, if the transfer coefficient, α, is known.[12] The apparent standard rate constant provides only a qualitative method for following electron transfer kinetics compared to chronoamperometry.[10]

It has been reported that short chain trichlorosilane derivatives form less ordered, and less closely packed monolayer than other surface derivatizing agents.[13] However, our data are consistant with monolayer coverages from **1a**. We cannot, of course, establish the uniformity of coverage, since cyclic voltammogram does not reveal the lateral distribution of the redox centers. Nonetheless, the cyclic voltammogram is consistent with uniform coverage and we assume it be so.

Chronoamperometry. Interfacial electron transfer rate constants can be measured by chronoamperometry. At a given overpotential ($\eta = E-E^0$), the current, i, follows a simple exponential decay:[14]

$$i = k_{app} Q \exp(-k_{app} t) \qquad (4\text{-}2)$$

where k_{app} is the apparent rate constant which is the sum of the forward and backward electron-transfer rate constants ($k_f + k_b$) and Q is the charge passed to convert the redox centers from one oxidation state to the other. Therefore, a plot of log (current) vs time should be linear with a slope of $-k_{app}$, provided that all of the redox centers have the same apparent rate constant. Such plots of **1a** on ITO at different final potentials are shown in Figure 4-3 and those of **1a** on Pt shown in Figure 4-4. Similar experiments for non-derivatized Pt and ITO show only a current transient for double layer charging with decay to zero current within 3 ms. The measured rate constants vs applied overpotentials on the ITO and Pt electrodes, Tafel

plots, are shown in Figure 4-5 and Figure 4-6. Tafel plots were used to estimate the maximum rate constants for the interfacial electron transfer processes between the Re(I) centers and ITO or Pt surfaces. These rate constants indicate approximately how fast the photoinduced interfacial electron transfer can be. The overpotential limits are imposed by the decay rate of the signal, and the onset of sample degradation. Because negative overpotentials cause degradation of monolayers of **1a**, the transient currents were measured only at positive overpotentials.

Tafel plots can be fit to Eq. 4-3, derived from Marcus theory[15] in order to extract such parameters as solvent reorganization energy, λ, and prefactor, $\upsilon\rho$. These values are given for the "best fit" in Figures 4-5 and 4-6. As we have discussed in Chapter One, assuming that the same reorganization energy applies to both the forward and backward reactions, and that the electronic coupling υ and the density of metallic states ρ are independent of energy, the interfacial electron transfer rate constants could be written as

$$k_{f,b} = \upsilon\rho(4\pi\lambda k_B T)^{1/2}\Omega_{f,b}(\lambda,\ E-E^{0\prime},T) \qquad (4-3)$$

where k_B is the Boltzmann constant, T the absolute temperature, and $\Omega_{f,b}(\lambda,\ E-E^{0\prime},\ T)$ are activation factors which are independent of the electronic coupling and the density of states and are given by

$$\Omega_{f,b}\ (\lambda,\ E\text{-}E^{0'},\ T) = C^{1/2}\int_{-\infty}^{\infty} g(x)\,dx$$

where $C = (k_B T/4\pi\lambda)$, $x = \dfrac{e(\varepsilon_i - E)}{k_b T}$ and

$$g(x) = \frac{\exp\left\{ -C\pi \left[x - \dfrac{\lambda \pm e(E\text{-}E^{0'})}{k_B T} \right]^2 \right\}}{1 + \exp(x)}$$

λ and $\upsilon\rho$ can be used to calculate k_f and k_b for the interfacial electron transfer between the surface-confined **1a** and Pt or ITO.

Transient Emission Spectra and Emission Lifetimes of 1a Immobilized on SiO_2 (Glass), ITO, and Pt and High Surface Area SiO_2. The corrected emission and excitation spectra of **1a** on Pt electrode in CH_2Cl_2/0.1 M [*n*-Bu_4N]PF_6 are shown in Figure 4-7. The excitation wavelength is 416 nm, close to the maximum for the Re $\rightarrow$ 2,2′-bipyridine charge transfer band of the Re(I) complex. The inset is the corrected emission and excitation spectra of the solution analog, **1b**, under the same conditions. Figure 4-7 shows that the Re(I) center has the same emission and excitation spectra in solution and on electrodes. This corroborates the RAFTIR data for **1a** on Pt which show that the carbonyl absorption peaks do not shift within experimental error of 2 nm.

The corrected, time-resolved emission spectra of **1a** on SiO_2, ITO, Pt, high surface area SiO_2 and in CH_2CH_2/0.1 M [*n*-Bu_4N]PF_6 were acquired following laser flash (3 ns pulse width) excitation of **1a** on the surfaces at 416 nm and were monitored with a time-resolution of 10 ns. The emission maxima and

profiles of **1a** on the surfaces did not change with time, showing again that the localized interaction between the surface-confined **1a** and the surfaces are weak. Figures 4-8a, 4-8b, and 4-8c show the time-resolved emission spectra of **1a** on the SiO_2, ITO, and Pt surfaces, respectively. The spectra of **1a** under all circumstances are essentially the same.

The emission decays of **1a** on the SiO_2 (glass), ITO, and Pt surfaces immersed in air-saturated CH_2Cl_2/0.1 M [*n*-Bu_4N]PF_6 solution are shown in Figure 4-9, 4-10, and 4-11, respectively. The emission lifetimes were obtained by a nonlinear least-squares fitting of the decays and could be expressed with a single-exponential function. Each decay curve is the average of 20 scans to improve the signal-to-noise ratio. The repeatability of the transient emission data was verified by making several independent measurements on different electrodes, Table I. Some scatter was observed in lifetime measurements. Error analysis might not be appropriate in describing these variations, since the value for each electrode results from the average of 20 independent data acquisitions. The variations are more likely the result of the effect of differing surface morphology.

Interestingly, the emission lifetimes of **1a** on high surface area SiO_2 in CH_2Cl_2/0.1 M [*n*-Bu_4N]PF_6 at 600 nm and 580 nm were both found to be 318 ns, in contrast to the lifetime of only ~160 ns on flat SiO_2 glass.

Emission maxima (E_{em}), and lifetimes (τ) from **1a** immobilized on SiO_2 (glass), ITO, and Pt in CH_2Cl_2/0.1 M

[*n*-Bu_4N]PF_6 at room temperature are listed in Table I. The lifetimes of the emission decays shown in Figure 4-9, 4-10, and 4-11 are listed in Table I as sample 1 of the modified SiO_2, ITO and Pt surfaces.

The solvent dependence of the emission decays of **1a** on SiO_2, ITO, and Pt surfaces was investigated in CH_2Cl_2, CH_3CN, and H_2O. The results show that the emission lifetimes of **1a** on SiO_2, ITO, and Pt surfaces and its solution analog **1b** decrease as $\tau(CH_2Cl_2) > \tau(CH_3CN) > \tau(H_2O)$. The emission decays of **1a** on SiO_2, ITO, and Pt in H_2O are scattered over a wide range. Table 4-2 shows one data set among several.

Interfacial Electron Transfer and Energy Transfer at Surface-Electrolyte Interfaces. The photoinduced electron transfer and energy transfer at surface-electrolyte interfaces occur competitively when photoactive molecules are immobilized on a conducting, light-absorbing surface. Our strategy to deconvolute the photoinduced interfacial electron transfer from the energy transfer is to use the modified ITO electrode as a surface inert toward energy transfer and to use the modified SiO_2 surface as a surface inert toward both interfacial processes. The energetics for energy transfer are unfavorable for ITO and both energy transfer and electron transfer are energetically unfavorable on SiO_2.

Interfacial Electron Transfer at Metal(or Conducting Metal Oxide)-Electrolyte Interfaces. As predicted by interfacial electron transfer theories,[15-18] an electron can be transferred from the surface-confined **1a** to the electrode and *vice versa*.

Because of the dilute surface density of charge-separated states and the opacity of the Pt electrode, photoinduced interfacial electron transfer processes on ITO and Pt electrodes could not be monitored by transient absorption spectroscopy. However, time-resolved emission spectroscopy could be used successfully because of its unique sensitivity. In addition, the photoinduced interfacial electron transfer rates can be inferred from electrochemical measurements when the effects of the presence of the hole on Re(I) are taken into consideration.

From the lifetime of the excited state of **1a** in solution, 339 ns, the rate constant for relaxation was calculated to be 2.95×10^6 s^{-1}. Using our electrochemical results, the formalism[19] (eq. 4-3) derived from Marcus theory was used to estimate the interfacial electron transfer rate constants at an over-potential of +750 mV. The forward interfacial electron transfer rate constants are ~2.5×10^3 s^{-1} for ITO and ~8.2×10^3 s^{-1} for Pt, and the backward rate constants are approximately zero for both ITO and Pt with an upper limit of 10^{-3} s^{-1}. For photoinduced electron transfer, the potential imposed at the electrode was zero so that the overpotential ($\eta = E-E^0$) was equal to $-E^0$ (+750 mV). Therefore, the photoinduced electron transfer rate constant (k_f) for both ITO and Pt should not be more than 8×10^3 s^{-1}, assuming that the presence of the hole on Re(I) hinders transport from bipyridyl moiety to metal substrates. The quenching processes of the photoexcited **1a** on ITO will be dominated by the hole-electron recombination. Consequently, the emission lifetime of **1a** on ITO should be

close to that of **1a** on SiO_2. This is consistent with the experimental emission lifetime measurements.

Because the quenching processes of the excited state of the surface-confined **1a** on ITO consists of radiative (k_r), nonradiative (k_n) relaxation processes, and the forward interfacial electron transfer process (k_f, Eq. 4-3), the observed emission decay rate constant can be written as

$$1/\tau_{obs} = k_r + k_n + k_f; \qquad (4\text{-}4a)$$

or

$$k_f = 1/\tau_{obs} - 1/\tau_0 \qquad (4\text{-}4b)$$

where $1/\tau_0 = k_r + k_n$. The observed electron transfer rate constant, k_f, is obtained from the difference between the decay rate constant of **1a** on the ITO electrode and the decay rate constant, $1/\tau_0$, of the surface-confined **1a** on SiO_2 (Eq. 4-4b). The data from Table 4-1 and Figures 4-9 and 4-10 show that the emission decays of **1a** on SiO_2 and ITO surfaces are the same within experimental error. Because the experimental error of the decay measurements is 1-2 ns, we can estimate the upper-limit of the interfacial electron transfer rate as

$$k_f^{max} = 1/\tau_{obs} - 1/(\tau_0 + 2) \cong 10^4\ s^{-1}.$$

Because Pt likely gives both electron transfer and energy transfer, the difference between the decay rate of **1a** on Pt and the decay rate, $1/\tau_0$, of the surface-confined **1a** on SiO_2 (Eq. 4-

4b) is the sum of the rates of the two processes, energy and electron transfer with energy transfer dominant.

As observed by other researchers,[20] a decrease in the emission lifetimes of **1a** on SiO_2 and ITO surfaces was observed, in comparison to **1a** in solution. The origin of the decrease in lifetime is not well understood. The most likely reason is self quenching by the high surface concentration of Re(I) centers. The relatively long-lived excited **1a** on high surface area SiO_2 likely signals low coverage (and little self quenching).[26]

Interfacial Energy Transfer of **1a** at Pt-Electrolyte Interfaces. It has been experimentally[1,2] and theoretically[21,22] shown that over short distance, a photoexcited molecule can transfer energy nonradiatively to an absorbing medium. The large absorbtivity of Pt at frequencies in the visible range makes photoinduced interfacial energy transfer between photoexcited **1a** and Pt electrode to occur likely. The visible transparency of ITO and SiO_2 makes energy transfer not viable. From our chronoamperometry results we expect that photoinduced interfacial electron transfer rates between **1a** and ITO and Pt would be similar, so the energy transfer rate constant can be calculated from the difference between the decay rate of **1a** on the Pt electrode and on ITO by following Eq. 4-5:

$$1/\tau_{obs} = k_r + k_n + k_f + k_{ET}. \qquad (4\text{-}5a)$$

Eq. 4-5a can be rewritten as

$$k_{ET} = 1/\tau_{obs} - 1/\tau_0' \qquad (4\text{-}5b)$$

where k_{ET} is the interfacial energy transfer rate constant, τ_{obs} is the emission decay lifetime of **1a** on Pt, and τ_0' is the emission decay lifetime of **1a** on ITO. Substituting the values of τ_{obs} and τ_0' into Eq. 4-5b, k_{ET} is calculated to be 2×10^7 s^{-1}.

The Chance-Prock-Silbey model,[21] as we have discussed in Chapter One, has been successfully applied to interfacial energy transfer between metal or semiconducting surfaces and excited molecules, mainly in a vacuum. This model treats the photoexcited molecule as a point oscillating dipole located above a metal of dielectric constant $\tilde{\varepsilon}(\omega)$, which is separated from a dielectric ambient at an infinitely sharp boundary. Within this framework, the total emission decay rate of the excited molecule can be separated into radiative and nonradiative components, the latter representing the rate of energy transfer to the metal.

In our experiment the excited molecule, as the oscillating dipole, is on a semi-infinite half space with a different dielectric constant as shown in Scheme 4-3. The medium surrounding surface-confined **1a**, region I, is CH_2Cl_2/0.1 M [*n*-Bu_4N]PF_6, and the half space is Pt metal, region II. The d is defined as the distance between the surface-confined **1a** and Pt surface shown in Scheme 3. The interfacial energy transfer rate normalized to the decay rate in the absence of energy transfer, $\hat{b}_{ET}$, is given by

$$\hat{b}_{ET} = \beta d^{-3} \qquad (4\text{-}6)$$

Here d is defined as above and β can be written[26a] as

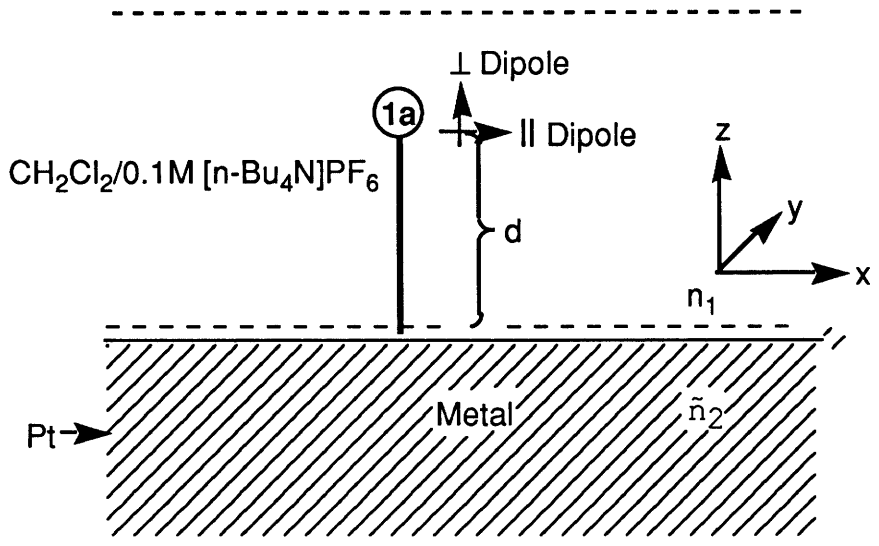

Scheme 3. Geometry of the dipole-over metal mirror model.

$$\beta = \frac{3\,q}{32}\,\frac{\lambda^3\,\theta}{\pi^3\,n_1}\left[\frac{n_2\,K_2}{\left(n_1^2 + n_2^2 - K_2^2\right)^2 + 4n_2^2\,K_2^2}\right], \qquad (4\text{-}7)$$

where q, the emission quantum yield of **1a** in CH_2Cl_2, was found to be 0.030 and n_1, n_2, and K_2 are optical constants for CH_2Cl_2 and Pt separately. λ is the wavelength of the emission maximum, and θ is a parameter varying with orientation and equal to 1 for a dipole parallel to the surface, 2 for a dipole perpendicular to the surface, and 4/3 for randomly oriented dipoles. Because the emission is not confined to a narrow band, Eq. (4-7) should be written as an integral over the emission spectrum as follows

$$\beta_{tot} = \frac{\int_{\omega_1}^{\omega_2} \beta(\omega)\, I_{EM}(\omega)\, d\omega}{\int_{\omega_1}^{\omega_2} I_{EM}(\omega)\, d\omega}, \qquad (4\text{-}8)$$

where β_{tot} is the value of β integrated over the emission band and $I_{EM}(\omega)$ is the normalized emission intensity at a specific frequency. Knowing the values of the optical constants[24] for CH_2Cl_2 and Pt at different emission frequencies (n_1=1.424, n_2=2.23, and K_2=3.92 at 600 nm), we calculated the value of β_{tot} to be 3.32×10^5 Å^3. Thus, we can use the experimental value of b_{ET} ($b_{ET}=\hat{b}_{EI}\, b_0$) to estimate the distance between the surface-confined Re(I) center and the Pt surface. Rewriting Eq. 4-6 gives

$$d = \left(\frac{\beta}{k_{ET}\, \tau_0}\right)^{-3}, \qquad (4\text{-}9)$$

Substituting the values of β, k_{ET}, and τ_0 to eq. (4-9), gives $d \approx 36$ Å. From the molecular structure of **1a**, the distance in an idealized representation between the Re(I) center and the oxygen atom of the siloxyl linkage is about 13 Å. The thickness of the oxide overlayer on Pt would then be estimated to be 23 Å which is in agreement with the results of ellipsometric measurements.[25] However, it should be realized that **1a** is a very hydralytically unstable molecule and that $d \approx 36$ Å likely reflects an average Pt-Re distance for oligomeric material on the surface.

Conclusion

Emission decays of **1a** immobilized on SiO_2, ITO, Pt surfaces and on high surface area SiO_2 in CH_2Cl_2/0.1 M [*n*-Bu_4N]PF_6 can be fitted by a single exponential. The rate constants of the photoinduced interfacial energy transfer were obtained by comparing the emission decays of **1a** on Pt to those on ITO, which is inert toward energy transfer. Interfacial electron transfer as estimated by chronoamperometry, was quite slow and does not competes with the much faster radiative and non-radiative processes of the Re(I) centers. The conclusion that the photoinduced interfacial electron transfer was slow is also supported by the closeness of the emission lifetimes of **1a** on ITO and SiO_2. The short lifetime on Pt indicates significant energy transfer to Pt and we estimate an average Pt-Re(I) distance of 36 Å. The emission lifetimes of **1a** on SiO_2, ITO, and Pt surfaces decrease in the order $\tau(CH_2Cl_2) > \tau(CH_3CN) > \tau(H_2O)$, just as its solution analogue **1b** does in these solvents.

References

1. Hashimoto, K.; Hiramoto, M.; Sakata, T.; Muraki, H.; Takemura, H.; Fujihira, M. *J. Phys. Chem.* **1987**,91,6198.

2. Charles Jr., C.S.; Palmore, T.R.; Lee, E.; Zhao, X.; Yu, J.; Wrighton, M.S. *Inorg. Chem.* **1992**, 31, 4439.

3. (a) Peterson, E.S.; Harris, C.B. *J. Chem. Phys.* **1989**, 91, 2683. (b) Hane, J.K.; Prisant, M.G.; Harris, C.B. Meyer, G.J.; Leung, L.K.; Ellis, A.B. *J. Phys. Chem.* **1989**, 93, 7975. (c) Waldek, D.H.; Alivisatos, A.P.; Harris, C.B. *Surface Sci.* **1985**, 158, 103. (d) Alivisatos, A.P.; Waldeck, D.H.; Harris, C.B. *J. Chem. Phys.* **1985**, 82, 541. (e) Whitmore, P.M.; Alivisatos, A.P.; Harris, C.B. *Phys. Rev. Lett.* **1983**,50,1092. (f) Whitmore, P.M.; Robota, H.J.; Harris, C.B. *J. Chem. Phys.* **1982**, 77, 1560.

4. (a) Avouris, Ph.; Demuth, J.E.; Schmeisser, D. *J. Chem. Phys.* **1983**, 79, 488. (b) Avouris, Ph.; Demuth, J.E. *ibid,* 75, 4783. (c) Rossetti, R.; Brus, L.E. *J. Chem. Phys.* **1982**, 76, 1146.

5. Chen, S.H.; Frank, C.W. *Langmuir,* **1991**, 7, 1719.

6. Hidalgo-Luangdilok, C.; Bocarsly, A.B. *Inorg. Chem.* **1990**, 29, 2894.

7. Gust, D.; Moore, T.A.; Moore, A.L.; Luttrull, D.K.; DeGraziano, J.M.; Boldt, N.J.; Van der Auweraer, M.; DeSchryver, F.C. *Langmuir* **1991**, 7, 1483.

8. (a) Chidsey, C.E.D.; Bertozzi, C.R.; Putvinski, T.M.; Mujsce, A.M. *J. Am. Chem. Soc.* **1990**, *112*, 4301. (b) Chidsey, C.E.D. *Science* **1991**, *251*, 919.

9. (a) Creager, S.E.; Collard, D.M; Fox, M.A. *Langmuir* **1990**, *6*, 1617. (b) Creager, S.E.; Rowe, G.K. *Anal. Chim. Acta* **1991**,*246*, 233. (c) Collard, D.M.; Fox, M.A. *Langmuir* **1991**, 7, 1192.

10. Finklea, H.O.; Hanshew, D.D. *J. Am. Chem. Soc.* **1992**, *114*, 3173.

11. The surface roughness was estimated to be about 8 times higher than that of the ideal flat ones such as Au for Pt electrodes by SEM.

12. Laviron, E. *J Electroanal. Chem.* **1979**, 101, 19.

13. Tillman, N.; Ulman, A.; Schildkraut, J.S.; Penner, T.L. *J. Am. Chem. Soc.* **1988**, *110*, 6136.

14. Creager, S.E.; Weber K. *Langmuir* **1993**, 9, 844.

15. Marcus, R.A.; *J. Chem. Phys.* **1965**, 43, 679.

16. Levich, V.G. *in Advances in Electrochemistry and Electrochemical Engineering,* P. Delahay, Ed. Interscience, New York, NY, **1966**, vol. 4, pp.249.

17. Hush, N.S. *Electrochim. Acta,* **1968**, 113, 1005.

18. (a)Schmickler, W. *J. Electroanal. Chem.* **1986**, 204, 31. (b) Morgan, J.D.; Wolynes, P.G. *J. Phys. Chem.* **1987**, 91, 874. (c) Zusman, L.D. *Chem. Phys.* **1987**, 112, 53. d) Mishra, A.K.; Rangarajan, S.K. *J. Phys. Chem.* **1987**, 91, 3417. (e) Sebastian, K.L. *J. Chem. Phys.* **1989**, 90, 5056.

19. Chidsey, C.E. *Science,* **1991**, *251*, 919.

20. (a) Liang, Y.; Ponte Goncalves, A.M. *J. Phys. Chem.* **1985**, 89, 3290. (b) Kajiwara, T.; Hasimoto, K.; Kawai, T.; Sakata, T. *J. Phys. Chem.* **1982**, 86, 4516.

21. (a) Chance, R.R.; Prock, A.; Silbey, R. *J. Chem. Phys.* **1975** *62*, 2245. (b) Chance, R.R.; Prock, A.; Silbey, R. *in Advances in Chemical Physics,* Rice, S.A.; Prigogine, I. Eds., Wiley: New York, **1978**, vol. 37, p1.

22. (a) Kuhn, H. *Pure Appl. Chem.* **1965**, *11*, 345. (b) Kuhn, H. *J. Chem. Phys.* **1970**, *53*, 101.

23. Van Houten, J.; Watts, R.J. *J. Am. Chem. Soc.* **1976**, 98, 4853.

24. *CRC Handbook of Chemistry and Physics*, 72nd Edition, D.R. Lide, Editor, **1993**, **12**-100.

25. Gottesfeld, S.; Maia, G.; Floriano, J.B.; Tremiliosi-Filho, G.; Ticianelli, E.A.; Gonzalez, E.R. *J. Electrochem. Soc.* **1991**, 3219.

26. *Handbook for Optical Constants of Solids*, E. D.Palik, Editor, pp 749-763, Academic Press (1985).

Table 4-1: Emission maxima(E_{em}) and lifetimes(τ) of **1a** chemically immobilized on SiO_2, ITO, and Pt surfaces in CH_2Cl_2/0.1 M [*n*-Bu_4N]PF_6. τ values in parenthesis are those from the degassed samples.

Sample		free **1a**	**1a** on electrodes		
			SiO_2	ITO	Pt
A	Eem(nm)	602	602	604	603
	τ(ns)	280(339)	110(161)	107(155)	33(36)
B	Eem(nm)		602	602	602
	τ(ns)		93(136)	115(166)	31(34)
C	Eem(nm)		596	604	602
	τ(ns)		101(148)	92(133)	36(40)
D	Eem(nm)		602	605	601
	τ(ns)		103(151)	109(158)	29(31)

Table 4-2: Lifetimes (ns) of **1b** in CH_2Cl_2 and **1a** immobilized on SiO_2, ITO, and Pt surfaces in CH_2Cl_2/0.1 M [*n*-Bu_4N]PF_6/CH_2Cl_2 or /CH_3CN, and 0.1 M LiCl/H_2O. λ_{ex} =416 nm; λ_{em} =600 nm.

solvent	**1b**	SiO_2	ITO	Pt
CH_2Cl_2	280	110	107	33
	339 (degassed)			
CH_3CN	94	82	78	26
	156 (degassed)			
H_2O	55 (degassed)	48	29?	16
	49			

Figure 4-1: (a) FTIR spectrum of **1a** in CH_2Cl_2. (b) Reflectance FTIR spectrum of **1a** on Pt.

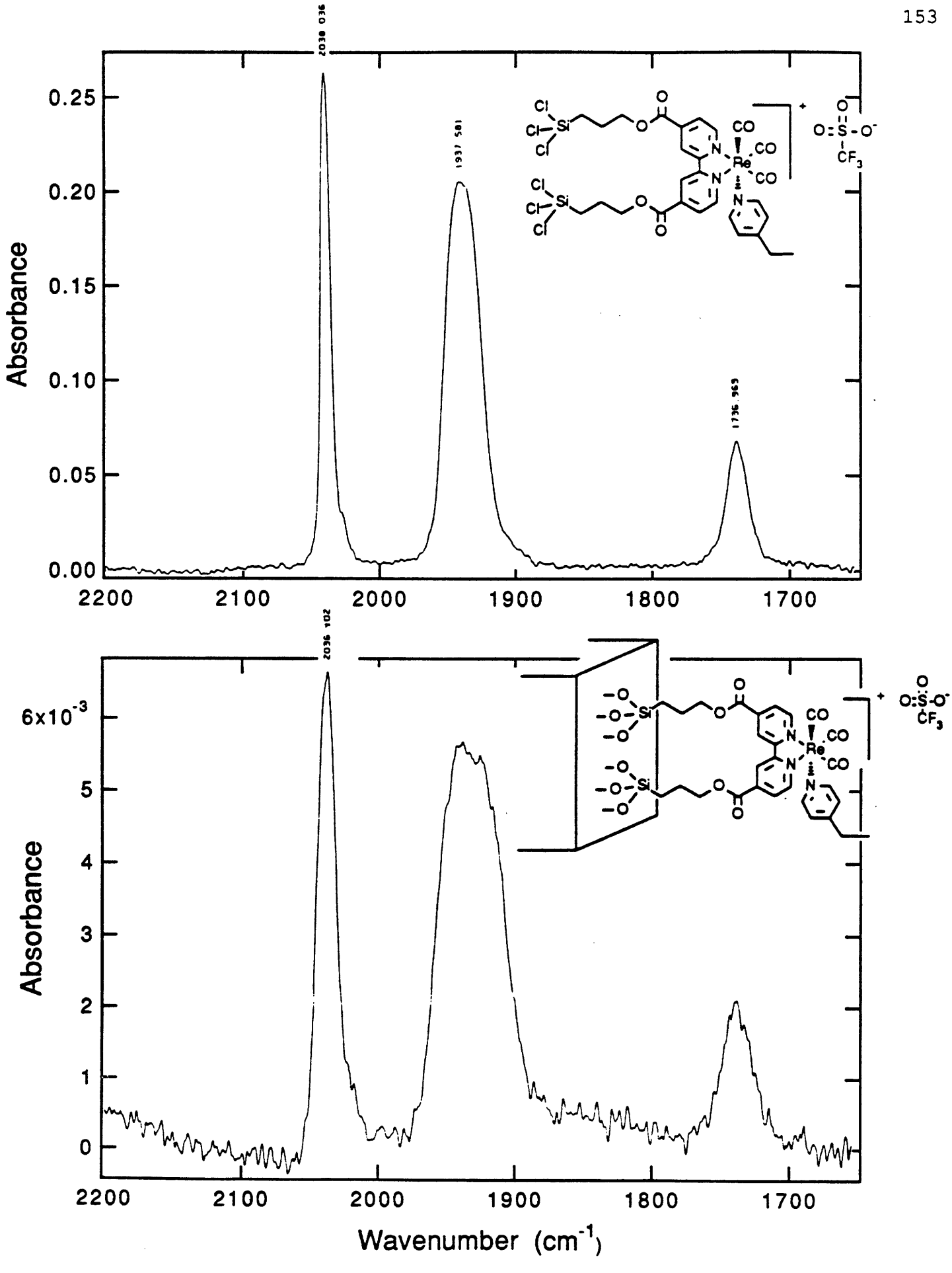
2038 036
1937 581
1736 969
0.25
0.20
0.15
0.10
0.05
0.00
Absorbance
2200
2100
2000
1900
1800
1700
2036 102
6x10-3
5
4
3
2
1
0
Absorbance
Wavenumber (cm-1)

Figure 4-2: Reversible cyclic voltammograms of **1a** monolayers on ITO (a) and Pt (b). All cyclic voltammograms were acquired in CH_2Cl_2/0.1 M [*n*-Bu_4N]PF_6 at 50 mV/s with an immersed electrode area of ~1.0 cm^2.

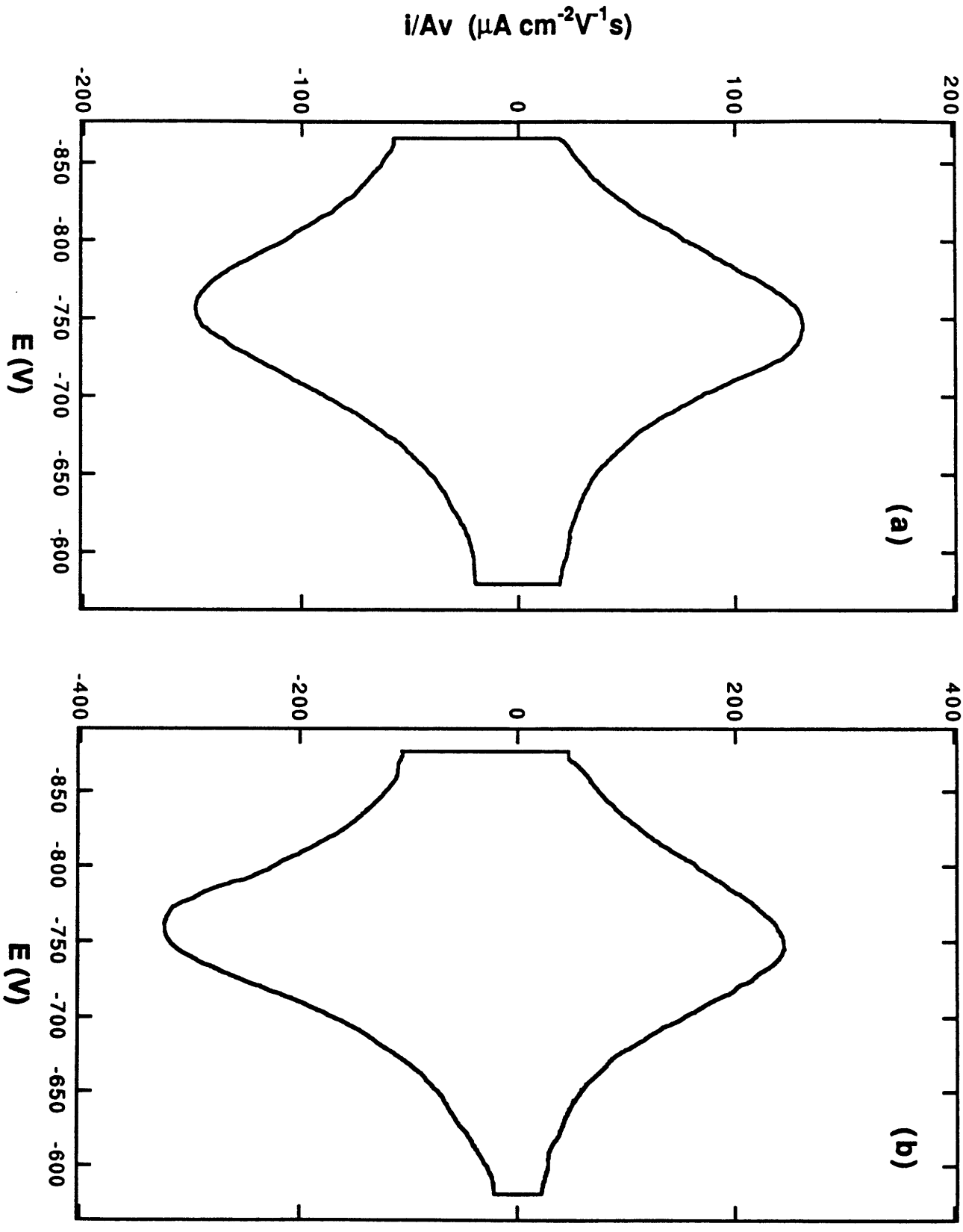
i/Av (μA cm-2V-1s)
-200
-100
0
100
200
E (V)
-850
-800
-750
-700
-650
-600
(a)
-400
-200
0
200
400
E (V)
-850
-800
-750
-700
-650
-600
(b)

Figure 4-3: Log (current) vs time following potential steps to various potentials (dashed) and linear regression fits to the linear portions (solid) for ITO electrodes derivatized with **1a**. Over potential, decay lifetime: (a) +260 mV, 4.7 ms; (b) +110 mV, 17.2 ms; (c) +60 mV, 25.8 ms.

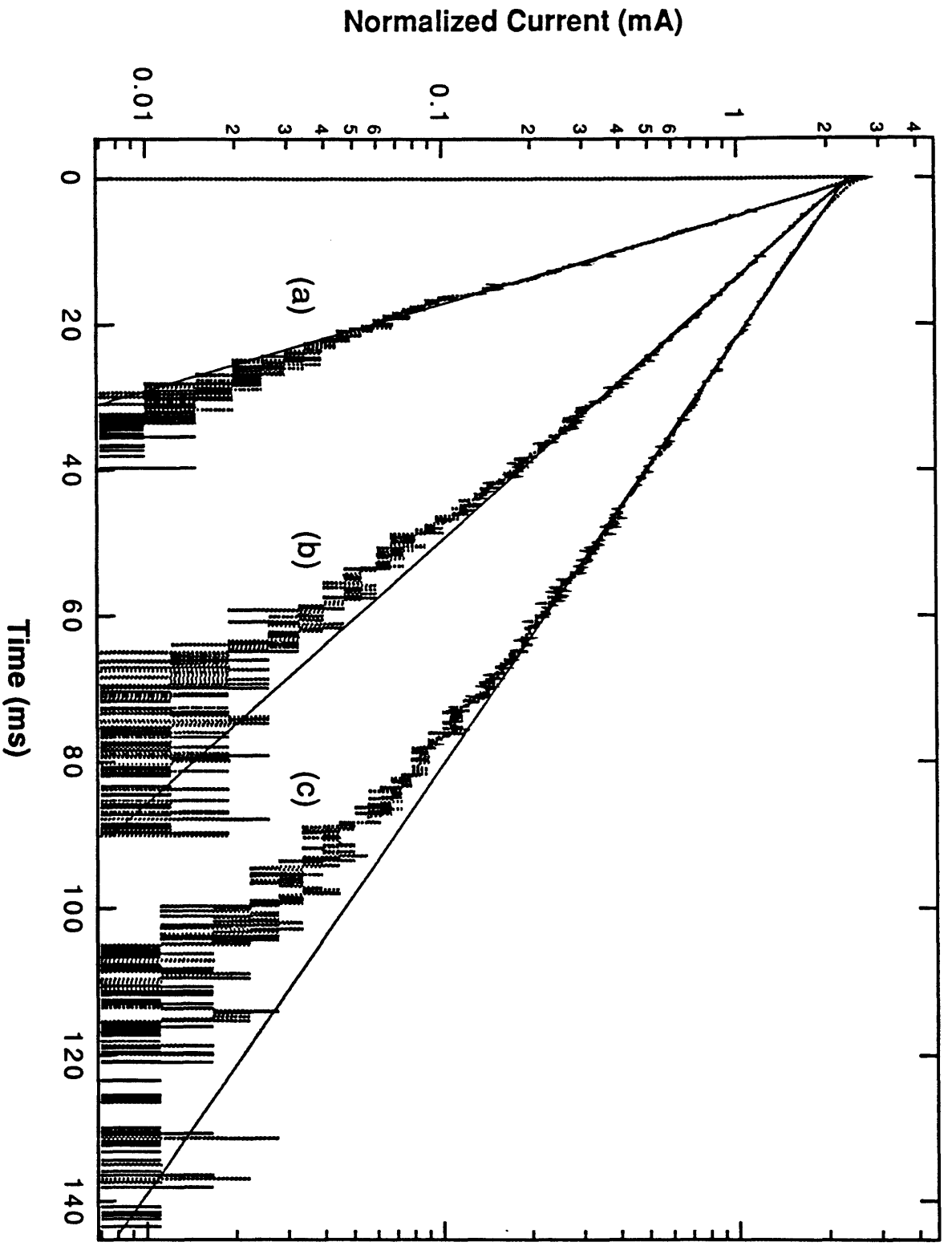
Normalized Current (mA)
0.01
0.1
1
Time (ms)
0
20
40
60
80
100
120
140
(a)
(b)
(c)

Figure 4-4: Log (current) vs time following potential steps to various potentials (dashed) and linear regression fits to the linear portions (solid) for Pt electrodes derivatized with **1a**. Over potential, decay lifetime: (a) +260 mV, 10.9 ms; (b) +110 mV, 32.1 ms; (c) +60 mV, 47.3 ms.

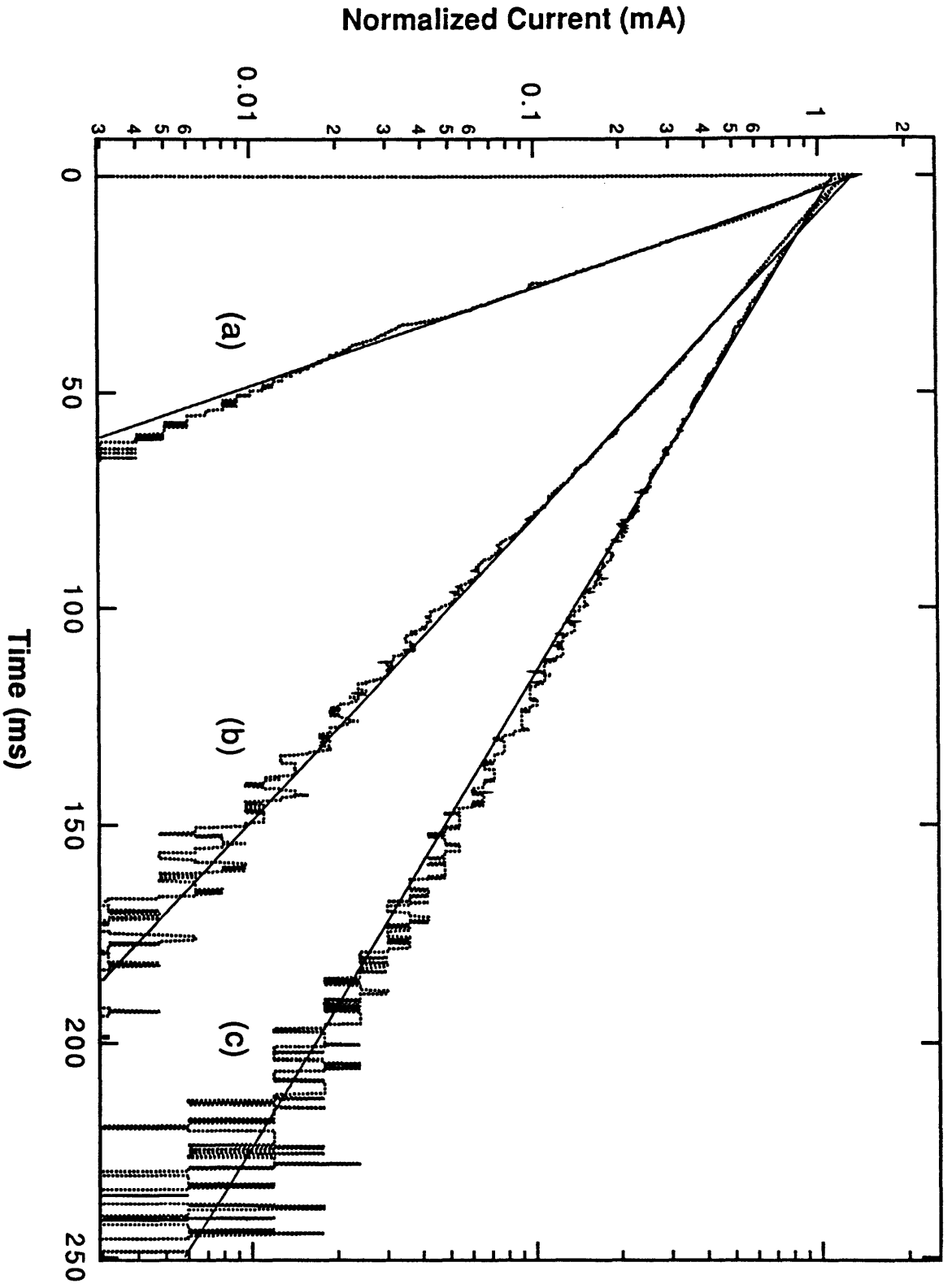
Normalized Current (mA)
0.01
0.1
1
Time (ms)
0
50
100
150
200
250
(a)
(b)
(c)

Figure 4-5: Tafel plots for reduction of **1a** at monolayer coverage on ITO in CH_2Cl_2/0.1 M [*n*-Bu_4N]PF_6. The theoretical Tafel curve fit to the data set for **1a** on ITO is shown for λ = 0.21 eV. The other theoretical Tafel curves are shown for specific λ values which have larger λ and $\upsilon\rho$ above the fit curve and less λ and $\upsilon\rho$ under the fit curve.

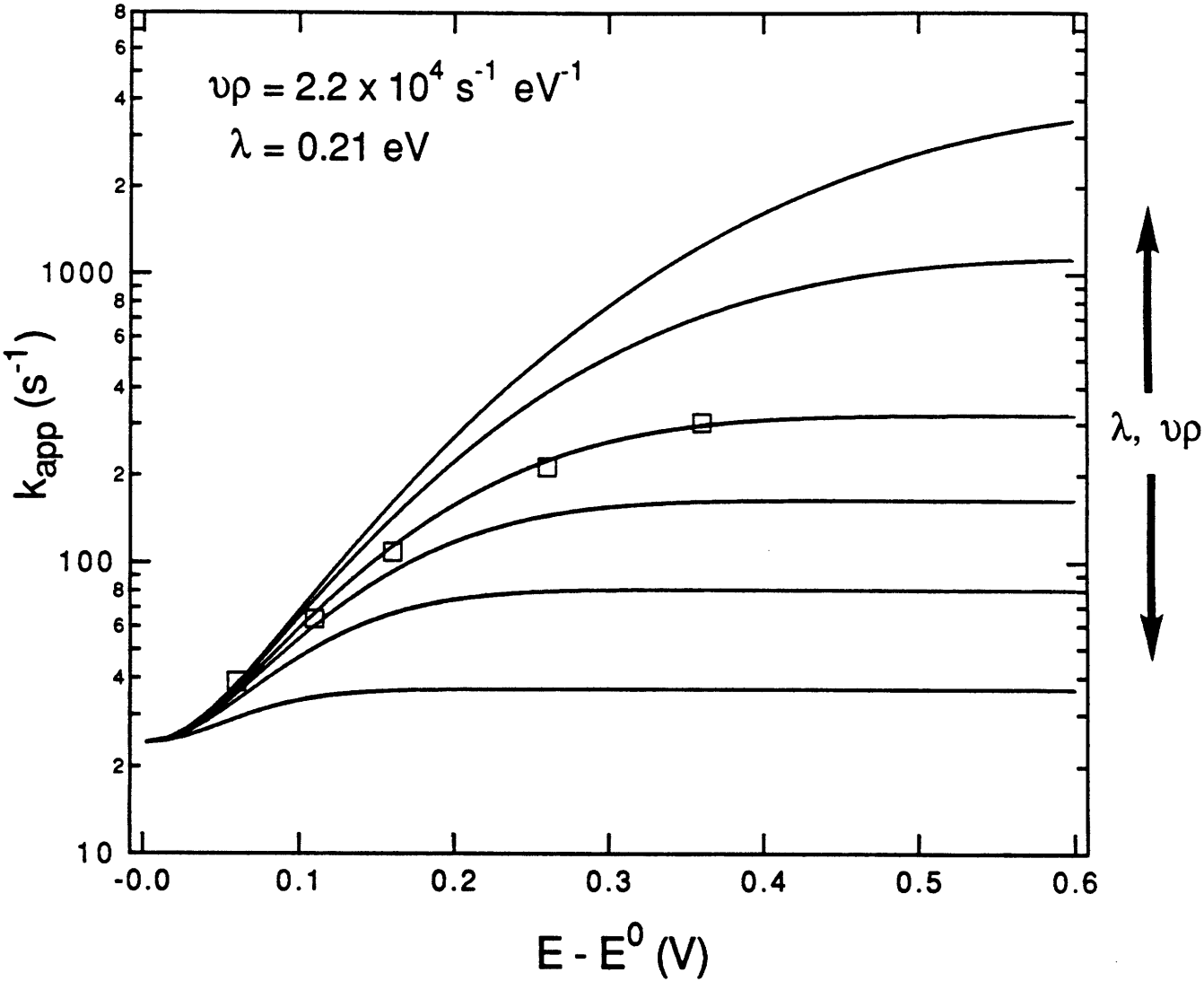
υρ = 2.2 x 10^4 s^-1 eV^-1
λ = 0.21 eV
k_app (s^-1)
1000
100
10
-0.0
0.1
0.2
0.3
0.4
0.5
0.6
E - E^0 (V)
λ, υρ

Figure 4-6: Tafel plots for reduction of **1a** at monolayer coverage on Pt in CH_2Cl_2/0.1 M [*n*-Bu_4N]PF_6. The theoretical Tafel curve fit to the data set for **1a** on Pt is shown for λ = 0.23 eV.

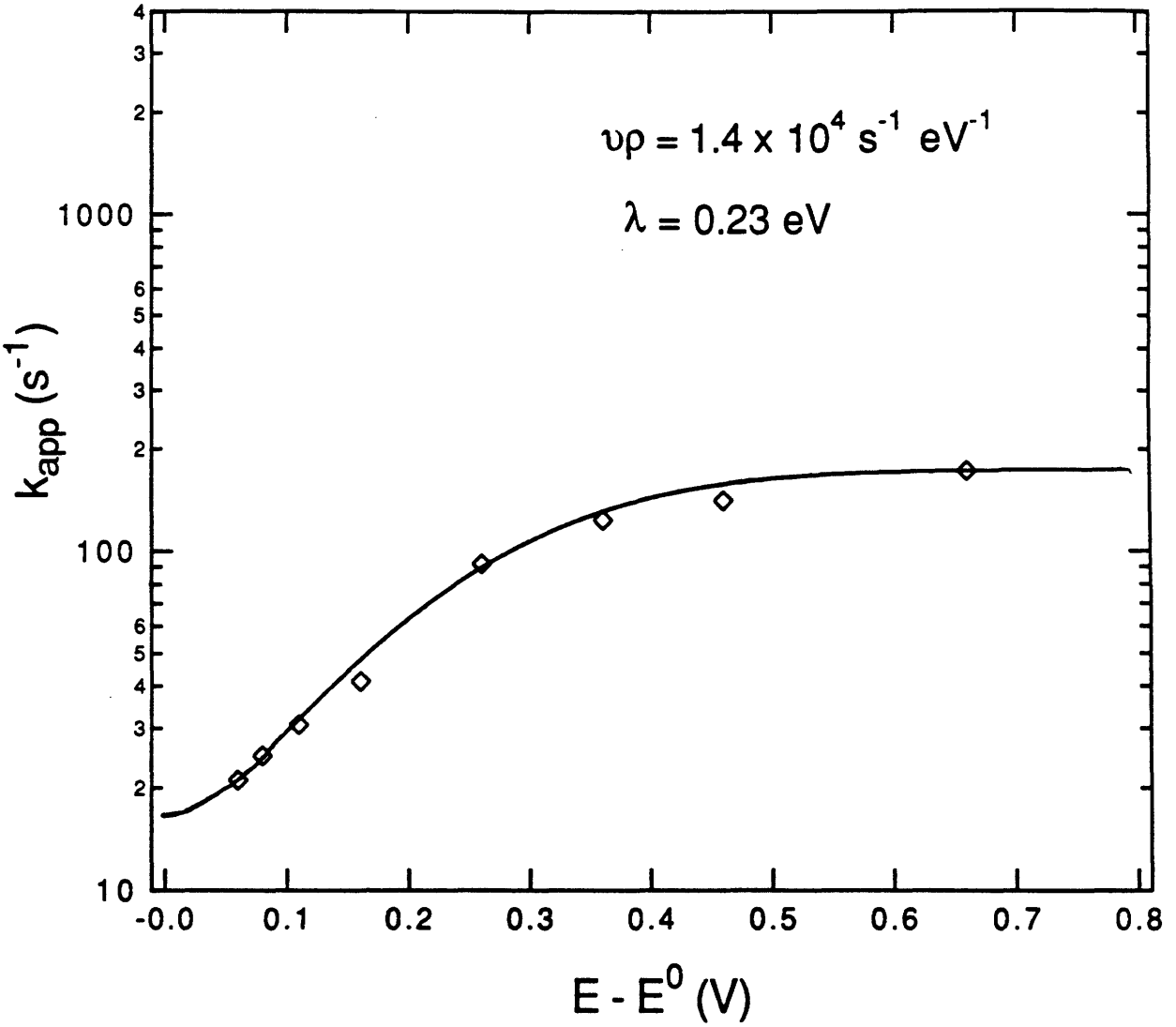
υρ = 1.4 x 10^4 s^-1 eV^-1
λ = 0.23 eV
k_app (s^-1)
E - E^0 (V)
1000
100
10
-0.0
0.1
0.2
0.3
0.4
0.5
0.6
0.7
0.8

Figure 4-7: Corrected emission and excitation spectra of **1a** on a Pt electrode in CH_2Cl_2/0.1 M [*n*-Bu_4N]PF_6. The excitation wavelength for the Re complexes was 416 nm, close to the maxima of their lowest absorption bands. Inset: the corrected emission and excitation spectra of the solution analog, **1b**, under the same conditions.

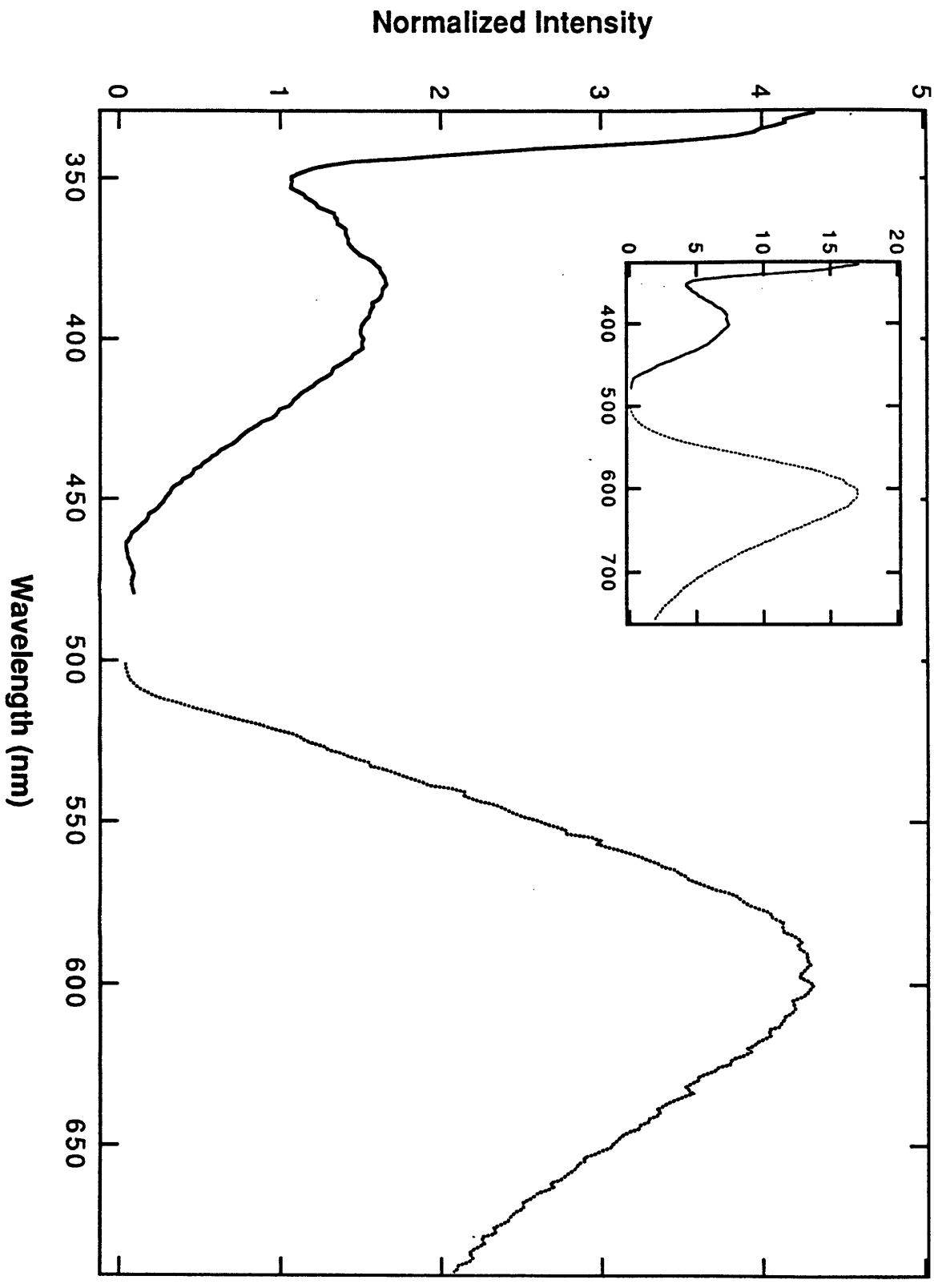
Normalized Intensity
0
1
2
3
4
5
350
400
450
500
550
600
650
Wavelength (nm)
0
5
10
15
20
400
500
600
700

Figure 4-8: Time-resolved emission spectra of **1a** on (a) SiO_2, (b) ITO, and (c) Pt surfaces in CH_2Cl_2/0.1 M [n-Bu_4N]PF_6. The emission spectra (——) is for the spectra with delay time of 10 ns; emission spectra (·····) for the spectrum with delay time of 40 ns; Emission spectra (-----) for the spectrum with delay time of 80 ns.

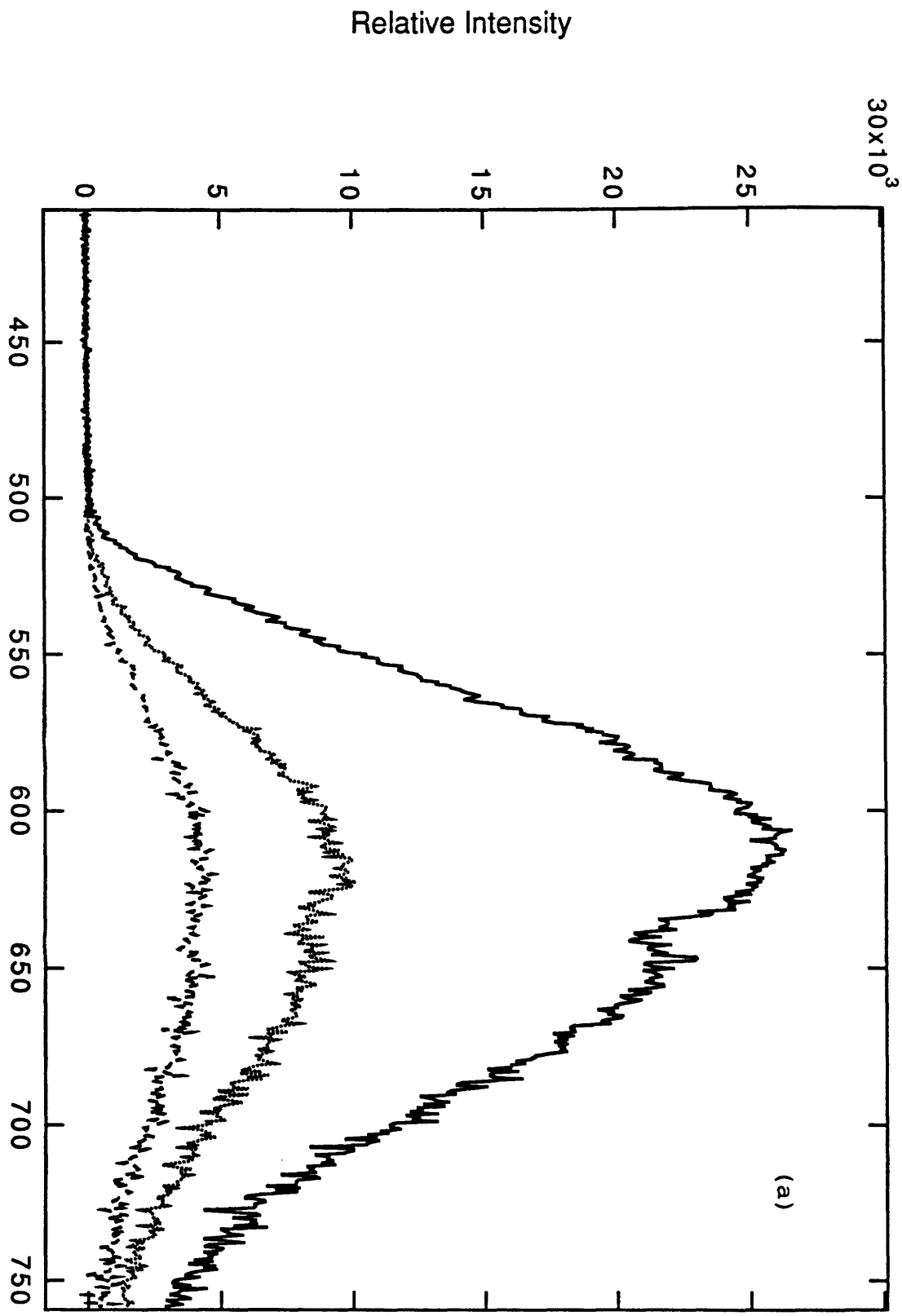

Emission of 1a on glass at 10, 20, and 80ns

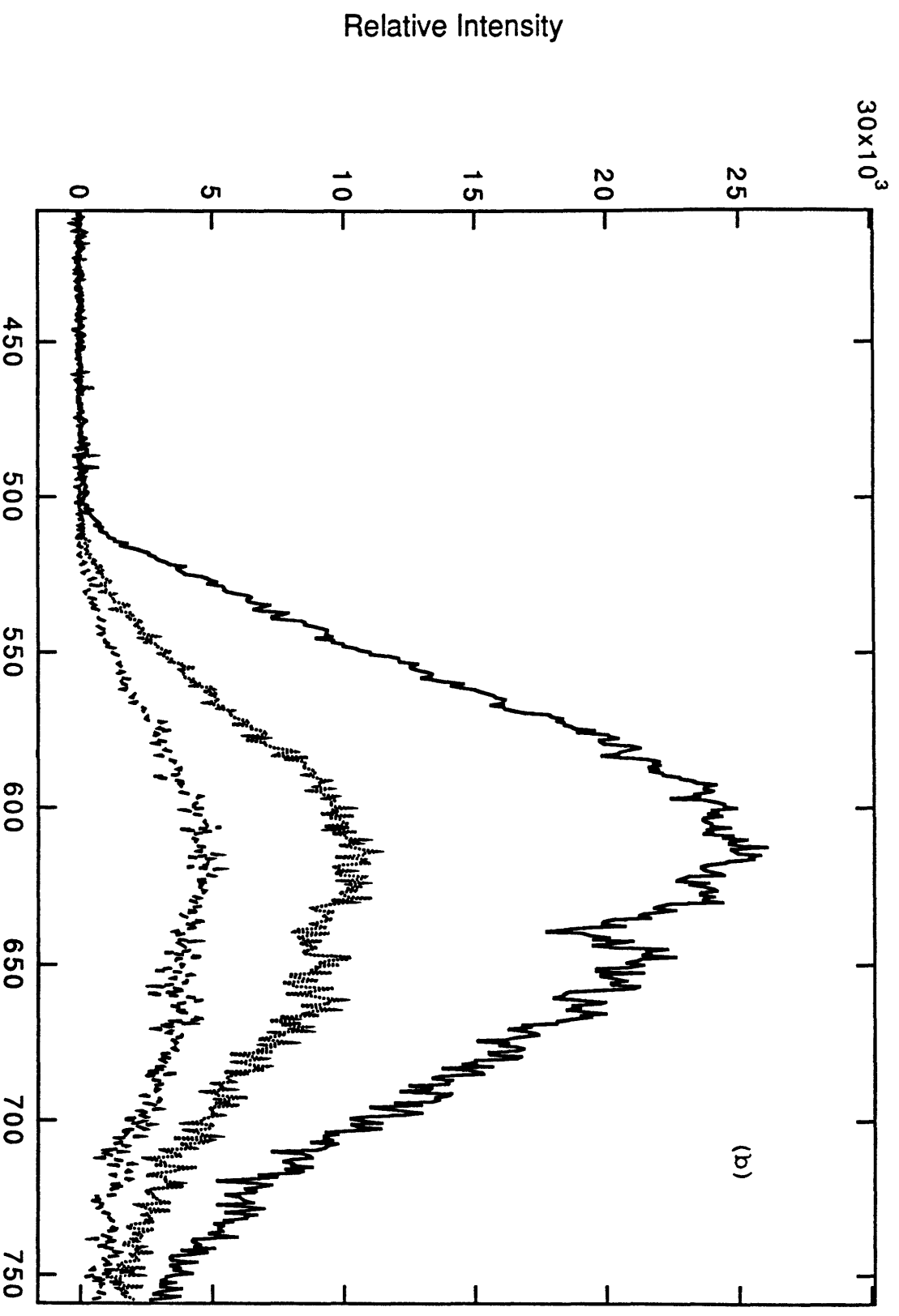

Emission of 1a on ITO at 10, 20, and 80ns

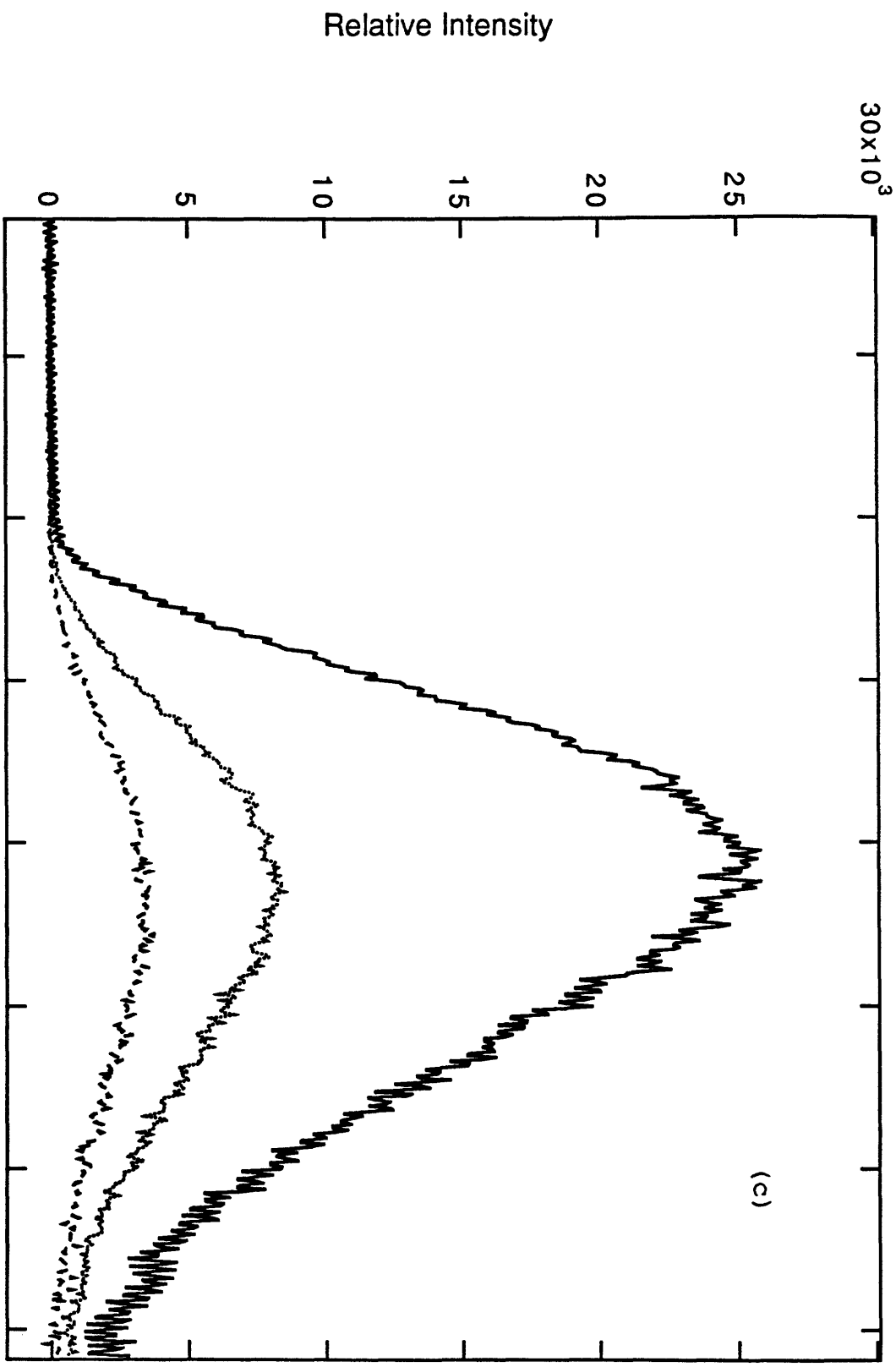

Emission of 1a on Pt at 10, 20, and 80ns

Figure 4-9: Emission decay (dotted) of **1a** on a SiO_2 (glass) surface in CH_2Cl_2/0.1 M [*n*-Bu_4N]PF_6. Emission decay was monitored at 600 nm. The nonlinear least-squares fit (solid) is also shown.

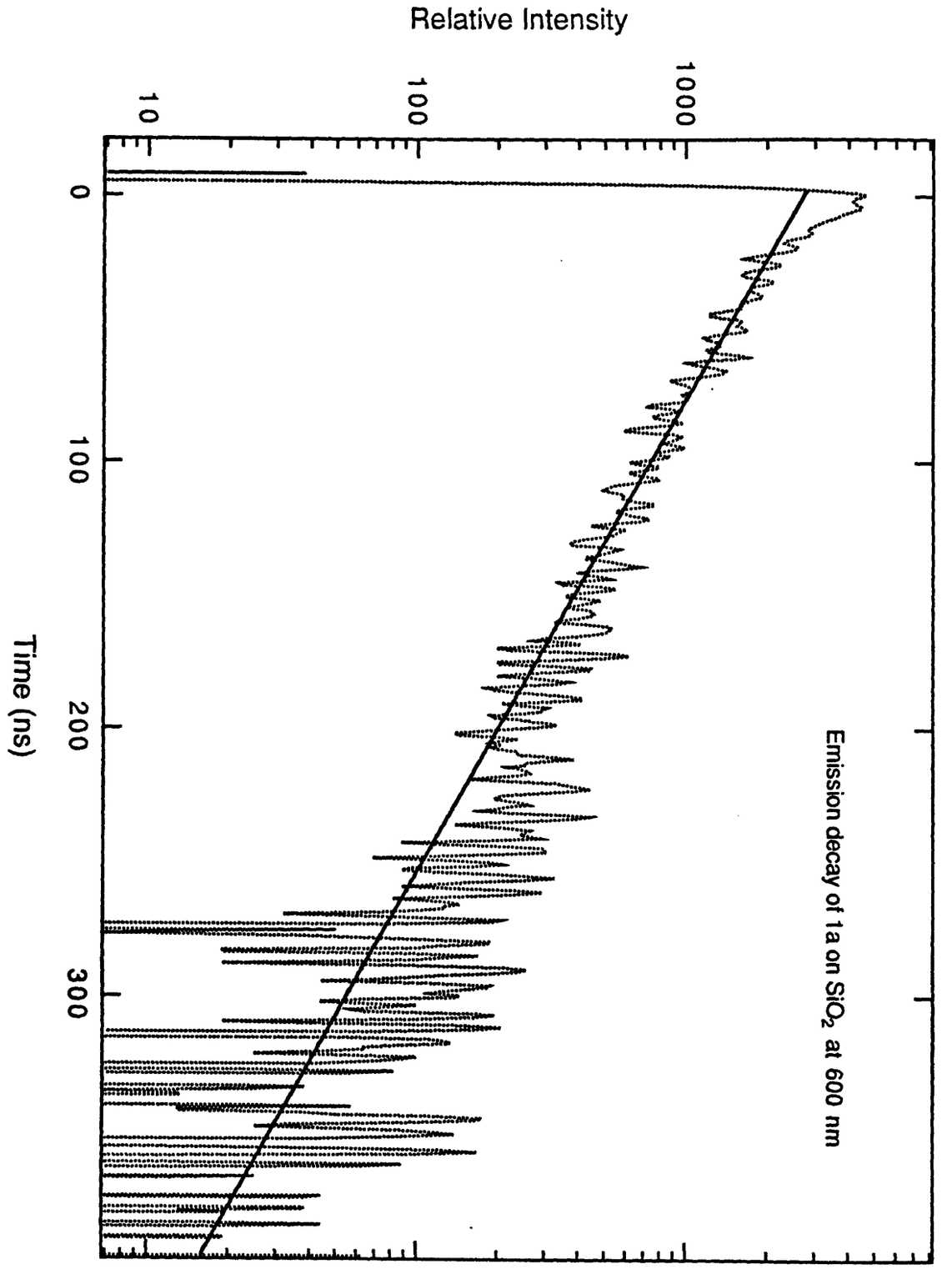
Relative Intensity
10
100
1000
0
100
200
300
Time (ns)
Emission decay of 1a on SiO_2 at 600 nm

Figure 4-10: Emission decay (dotted) of **1a** on an ITO surface in CH_2Cl_2/0.1 M [*n*-Bu_4N]PF_6. Emission decay was monitored at 600 nm. The nonlinear least-squares fit (solid) is also shown.

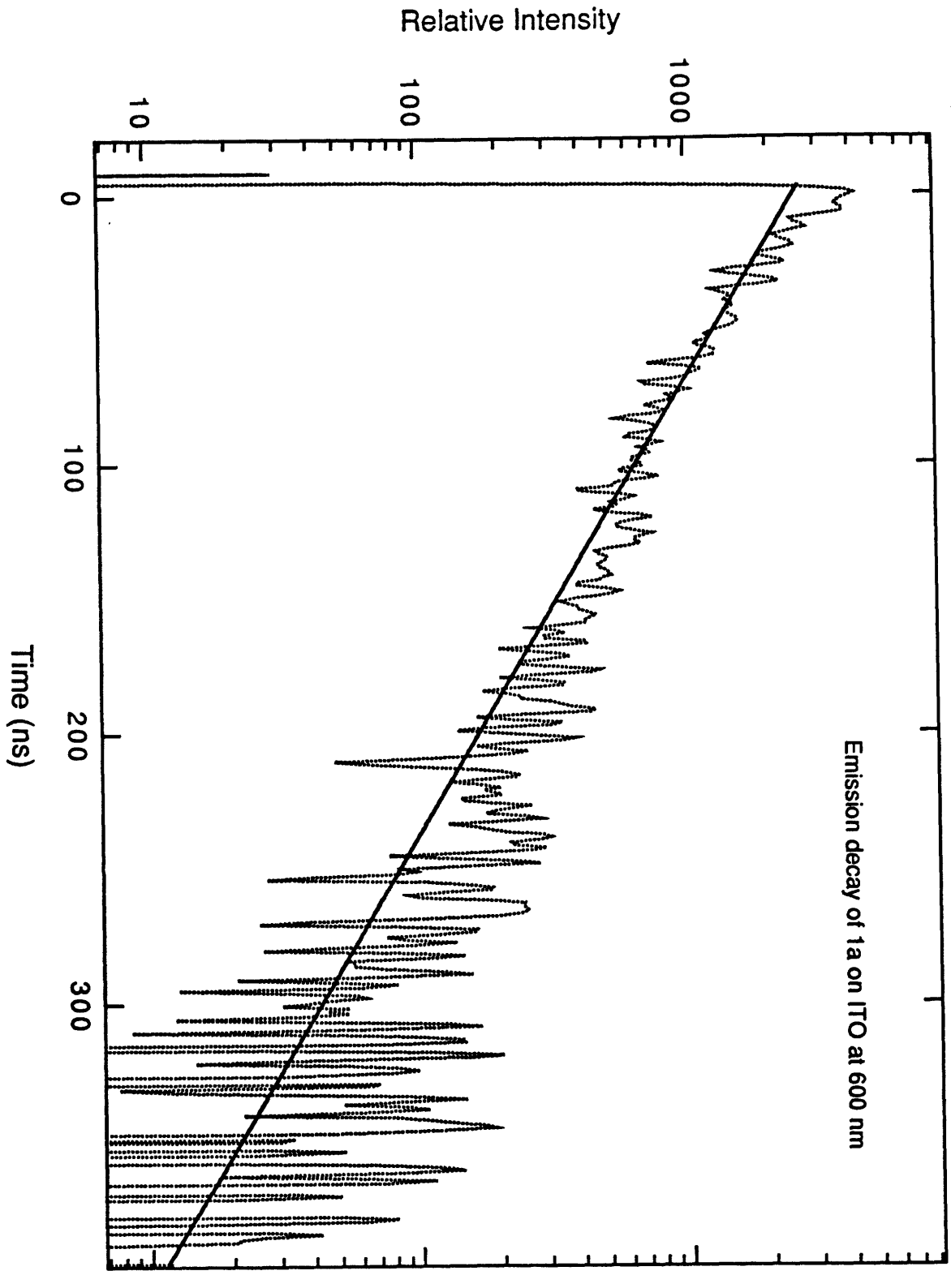
Relative Intensity
10
100
1000
0
100
200
300
Time (ns)
Emission decay of 1a on ITO at 600 nm

Figure 4-11: Emission decay (dotted) of **1a** on Pt surface in CH_2Cl_2/0.1 M [*n*-Bu_4N]PF_6. The nonlinear least-squares fit (solid) is also shown.

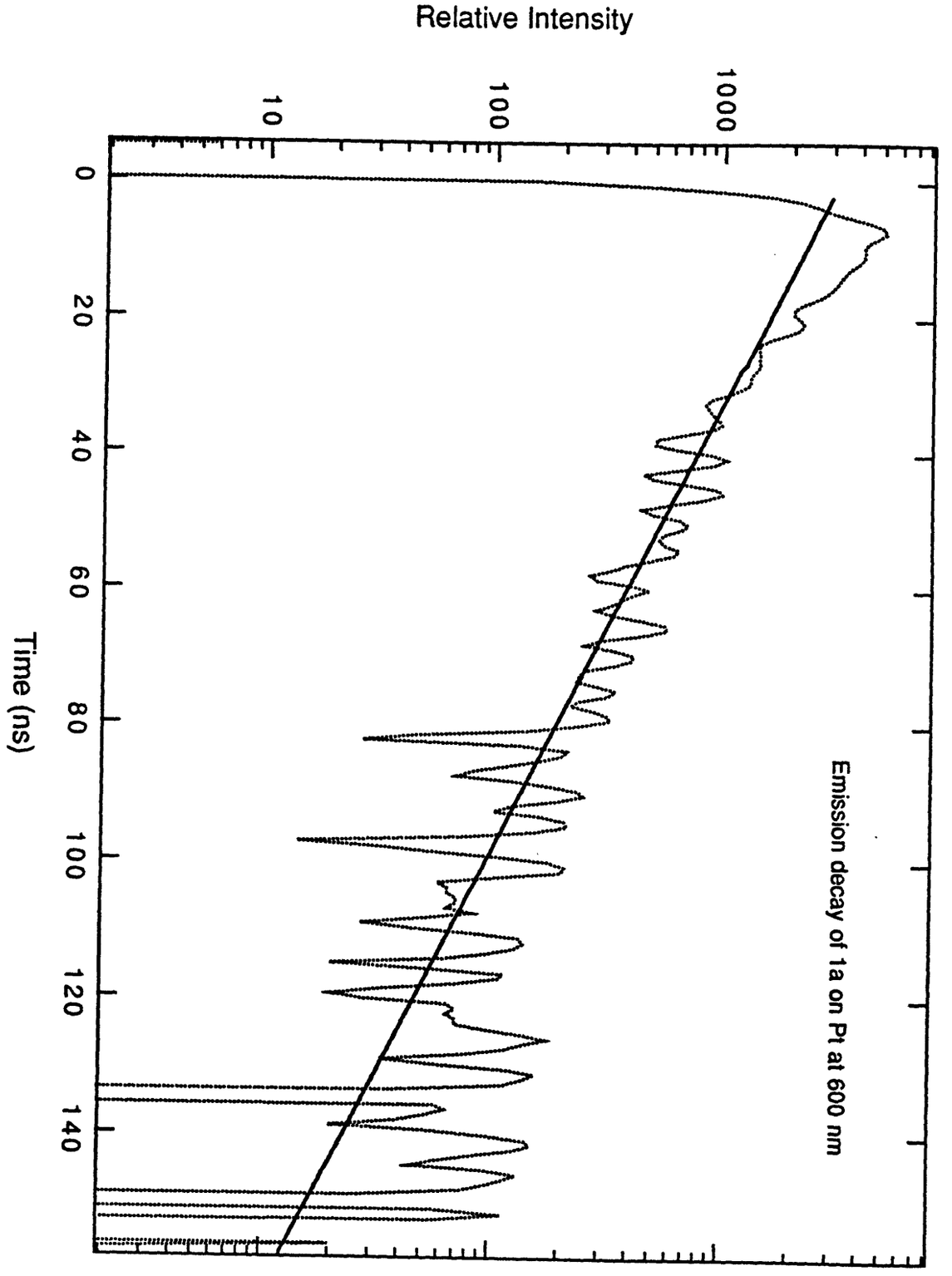
Relative Intensity
10
100
1000
0
20
40
60
80
100
120
140
Time (ns)
Emission decay of 1a on Pt at 600 nm

CHAPTER FIVE

INTRAMOLECULAR ELECTRON TRANSFER IN CHROMOPHORE END-CAPPED HOMOPOLYMERS AND MULTIBLOCK POLYMERS OF ELECTRON DONORS.

In this chapter we present the design and photophysical characterization of chromophore end-capped homopolymers, and di- and triblock polymers of electron donors. Polymers prepared by ring opening metathesis polymerization (ROMP) of norbornene derivatives offer a wide range of materials having an ordered arrangement of redox centers. Studies of the molecular materials in solution and as cast films of some of the polymerspolymers are described.

As discussed in Chapter One, one objective in preparing synthetic analogues of the photosynthetic apparatus is to effect unidirectional transport of electrons within a molecular system following photoexcitation. The unidirectional transport can be achieved by arranging a sequence of downhill electron transfer events following photoexcitation, by ordering a set of redox reagents according to formal potential. Further, long-lived charge separation might be achieved by providing a sequence of isoenergetic electron transfer events to allow an electron to diffuse following primary electron transfer to or from a photoexcited center. The synthesis of such molecular systems and the studies of their photophysics and photochemistry would be important for understanding the phenomena and utilizing molecular systems for durable and efficient photoenergy conversion or molecular electronic devices.

The importance of multiblock charge-separating polymers for electron transfer studies stems from the ability to control the arrangement of the subunits, such as the chromophore, spacer, and electron donor (or acceptor) blocks and the repeat unit

number of each block. Such systems may have features in common with natural photosynthetic systems.[1] The objective is to effect electron transfer reactions as shown in Scheme 5-1.

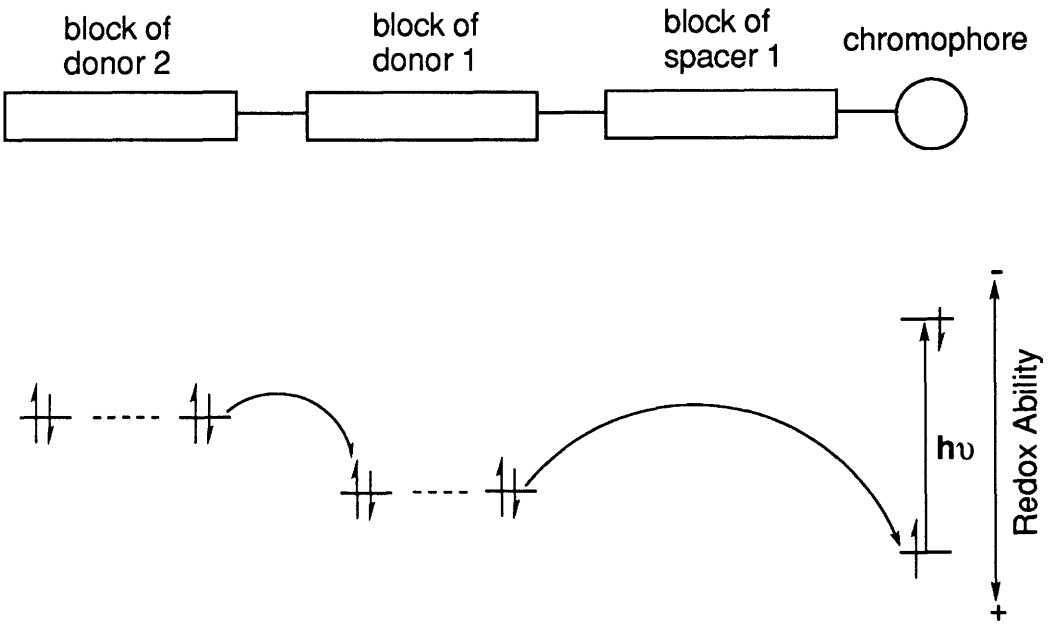

Scheme 5-1. Photoinduced chain electron transfer in a multiblock charge-separating polymer with two blocks of different electron donors. The sequence of events is (1) light absorption; (2) electron transfer from a subunit of dinor block1; (3) "self-quenching" among subunits of donor 1; (4) electron transfer from a subunit of donor 2 and (5) "self quenching" among subunits of donor 2.

A long term objective of the Wrighton group is to span a pair of microelectrodes with a molecular "wire" capable of charge separation, in order to build a molecule-based photovoltaic device.[2] Multiblock charge-separating polymers can, in principles, be readily synthesized in ~ 100 nm dimensions to

span such a gap, but the structures of the polymers from ROMP are not rigid. The prospect of bridging two electrodes with such polymers is, therefore, low, but charge separation as in Scheme 5-1 coupled with phase separation of the blocks may yield ways to exploit the molecules in device application.

In this study we have successfully extended the charge-separated state lifetime by nearly 20 fold in polymers compared to appropriate model molecules and obtained a correlation between the electron transfer rate constants and the number of repeat units in an inert spacer block which separates a chromophore and an electron donor block. We have observed microphase separation of multiblock polymers prepared by ROMP of norbornene derivatives containing pendant redox centers. Evidence for block segregation and micelle formation was observed in solution as well.

The chromophore used as the end-cap to a polymer ensemble is a Re(I)-biquinoline complex, $[Re(CO)_3(biq)(pyridyl)]^+$ (biq = 2,2′-biquinoline), in which the 2,2′-biquinoline ligand yields a low energy Re $\rightarrow$ 2,2′-biquinoline lowest excited state associated with visible absorption.[13] Thus, the chromophore can be optically excited while avoiding absorption by the rest of the polymer. The basic unit of the electron donor blocks in the multiblock polymers are derivatives of phenothiazine (PTZ) and N,N,N′,N′-tetramethyl-*p*-phenylenediamine (TMPD) which are durable upon one-electron oxidation and are transparent to visible light.

Model chromophore-donor "diad" compounds **I, II** and **III** shown in Scheme 5-2, were made to investigate the behavior of such species following photoexcitation. Electron transfer

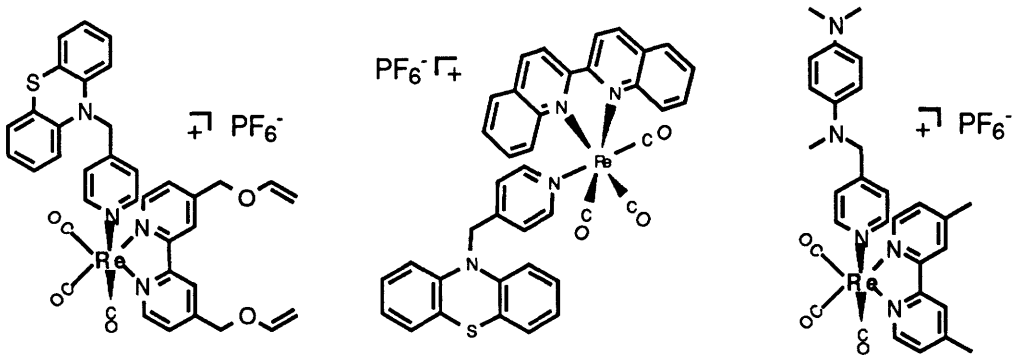

I **II** **III**

Scheme 5-2. Molecular structures of model "diad" **I, II,** and **III**.

quenching of a photoexcited chromophore usually results in rapid back electron transfer from the reduced chromophore to the oxidized donor. If the back electron transfer rate is faster than the forward electron transfer rate, no charge-separated state will accumulate precluding spectroscopic characterization. Molecules with PTZ attached to Re(I) centers via pyridine are known to possess long lived, spectroscopically identifiable charge-separated states.[3,4] These molecules, similar to **I**, were first made and studied by Meyer and co-workers.[3] TMPD[5] was similarly attached to a $Re(CO)_3(Me_2bpy)$pyridyl (Me_2bpy = 4,4'-dimethyl-2,2'-bipyridine) chromophore, **III**. Compound **III** is the first example of TMPD attached to a metal polypyridyl chromophore. These three compounds all show a slower back

electron transfer rate than forward electron transfer, and allow us to spectroscopically identify and monitor the decay kinetics of the charge-separated state.

The polymers studied, Scheme 5-3, were prepared by ROMP of appropriate norbornene monomers.[6] The living ROMP technique allows the preparation of copolymers with blocks that have a predetermined average length (repeat unit number) of various units in a well-controlled sequence. The number of repeat units in a given block has a relatively narrow dispersity, and block with as few as 5 repeat units per block can be made. The Re(I) chromophore was incorporated as an end group via a Wittig-like capping reaction of the living polymer with the 4-pyridinecarboxaldehyde (pyr-CHO) functional group in the complex $[Re(CO)_3(biq)(pyr\text{-}CHO)]^+PF_6^-$. The homopolymers $Re(PTZ)_{25}$, $Re(TMPD)_{25}$, a series of diblock polymers $Re(mtd)_n(PTZ)_{10}$ (n = 5, 20, 50, 100, 200), $Re(mtd)_{50}(PTZ)_m$ (m = 5, 10, 25, 50), $Re(mtd)_x(TMPD)_y$ (x = 25, 110, y = 5, 10), and the series of triblock polymers $Re(mtd)_x(PTZ)_y(TMPD)_z$ (x = 100, 200, y = 10, 50, z = 10) were prepared. In addition, $Re(mtd)_n$ (n = 5, 20, 50, 100, 200) polymers were also prepared as non-donor-containing model polymers. The conformation of these polymers in solution is unknown. It is generally believed that repeat units with the same structure associate together in a block. Conformations with the Re(I) chromophore adjacent to the donor blocks would not, therefore, be the optimum arrangement for long-lived charge-separated states to be generated. Rather, the use of a spacer block should prove fruitful.

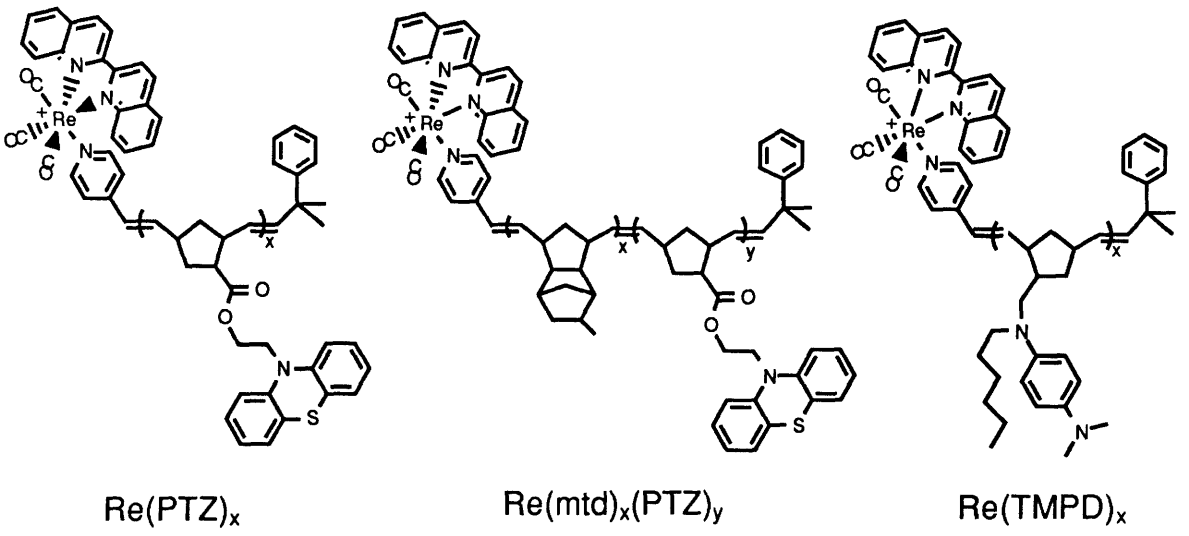

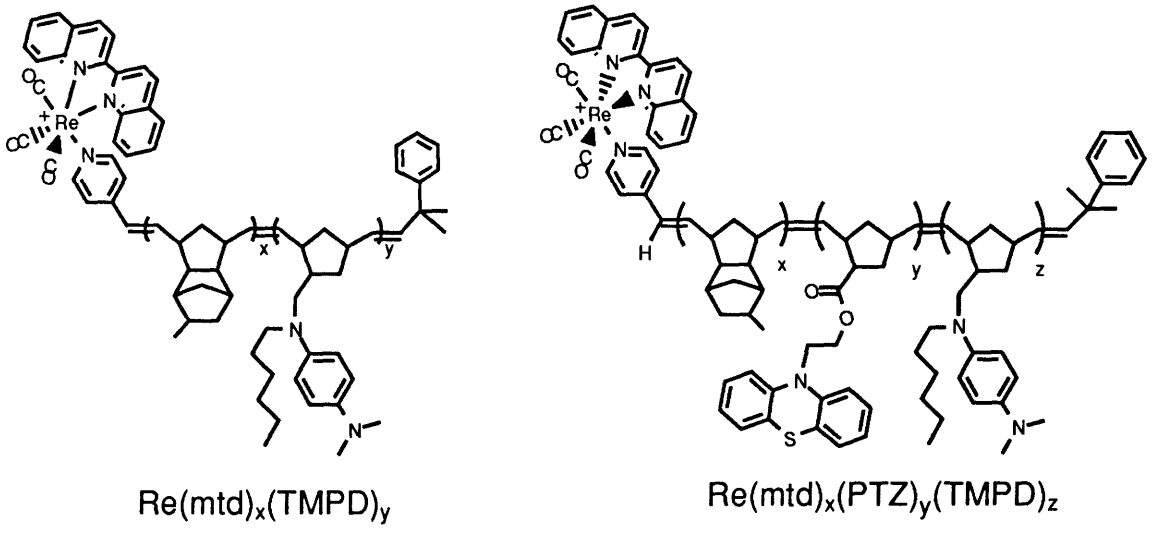

Scheme 5-3. Polymers prepared by ROMP and quenched to yield the Re(I)-capped molecules.

There have been several reports about photoinduced electron transfer in polymeric systems.[7,8] Random co-polymers of Ru and Os chromophores have been prepared, and the energy transfer between adjacent repeat units studied.[9,10] Murray and co-workers have electropolymerized chromophores and redox units onto electrode surfaces and observed photocurrent.[11] Other groups have made polymers of chromphore repeat units and have

demonstrated electron transfer to acceptors in solution.[12] The polymers described in this chapter are polymers capable of separating charge along their backbone following photoexcitation, making them a potentially important new family of macromolecules.

Experimental

Synthesis. The model compounds **I, II, III,** and the polymers were synthesized by Dr. David Albagli in the Wrighton group and Jin-Kyu Lee of the Shrock group.[13]

Sample Preparation. Samples for all time-resolved emission and transient absorption measurements were prepared in a custom-made glass apparatus that allowed for freeze-pump-thaw degassing (4 cycles, 10-4 Torr) in one arm followed by transfer of the solution into a 1.00 cm path length fused silica fluorescence cuvette within the apparatus.

Transient Absorption Experiments. Transient absorption spectra were acquired following a laser excitation pulse at 416 nm (2-5 mJ/pulse) from a Quanta-Ray RS-1 Raman shift laser pumped by a Quanta-Ray DCR-3 Nd:YAG laser (third harmonic, 3 ns FWHM). The Raman shifter output was separated by a prism, and the desired wavelength was sent through an aperture and interference filter to isolate a pump wavelength. The data acquisition and scanning of the detector were synchronized and controlled with an EG&G 1463 controller and EG&G 1461 detector interface.

A 150 W high pressure Xenon arc lamp provided the broad band probe light. Transient spectra were obtained by an EG & G 1421 OMA diode array detector gated through an EG & G Model 1302 fast pulser. The delay time from laser pulse leading edge to sampling pulse falling edge was controlled by an SRS Model DG535 digital delay/pulse generator. An electronically controlled Uniblitz model T132 shutter was used to chop the CW probe light to protect some samples from photo-degradation.

Transient absorption decay at a specific wavelength was monitored by a Thurlab DET2-Si photodiode with a 1 ns rise time. The photovoltage signal from the detector was collected on a LeCroy 8088 transient digitizer with 742 ps resolution. Photoexcitation was carried out by the laser system supplying a 5 ns, 2-5 mJ/pulse, 416 nm pump pulse. The optical density decays at the wavelength range, where the charge separated states have a strong characteristic absorption, were probed by the CW Ar^+ and Kr^+ ion lasers at 515 nm and 568 nm separately. The probe beam was blocked by a shutter between scans to avoid depleting photodiode voltage.

Transient Emission Experiments. Transient emission signals were monitored at a 90° angle to the excitation beam following a laser pulse excitation of 416 nm (~0.05 mJ/pulse) from a Quanta-Ray RS-1 Raman shift laser pumped by a Quanta-Ray DCR-3 Nd:YAG laser (third harmonic, 3 ns FWHM). Emission signals were collected by a set of lenses which was f-matched

with the spectrograph of the detector, and were monochromated by a SA model DH-10 double grating monochromator. Emission decays at a specific wavelength were monitored by a Hamamatsu R446 photomultiplier (PMT) with a 2.7 ns rise time and recorded by a LeCroy 6880A transient digitizer with 742 ps resolution. The PMT was negatively biased by a Fluke model 405B regulated high voltage power supply. All lifetimes were determined by averaging at least seven independent measurements.

Results and Discussion

Linked Re-PTZ molecules. Complete quenching of the emission of the Re(I) centers in **I** and **II**, even at very low concentration (ruling out intermolecular quenching), is attributed to intramolecular quenching of the MLCT triplet state, ^{3}(MLCT), of the Re(I) centers by the PTZ moiety. Because the energy of the lowest $^3(\pi\pi^*)$ state for PTZ (2.64 eV)[14] is much higher than that of the ^{3}(MLCT) for the Re(I)-based chromophore (2.02 eV), intramolecular energy transfer is thermodynamically unfavorable. Therefore, intramolecular quenching of the ^{3}(MLCT) state of the Re(I) center with PTZ is dominated by electron transfer.

Transient absorption confirms the identity of the intermediate state produced by photoexcitation of **I** to be the charge separated state. The transient absorption spectrum is dominated by the $PTZ^{+\cdot}$ absorption, as indicated in Figure 5-1. The absorption decay at 515 nm, where $PTZ^{+\cdot}$ absorbs, provides a

measure of the lifetime of the charge-separated state, as shown in Figure 5-2. The lifetime of the charge-separated state was found to be 23 ns. Compound **II** is a model molecule for the redox polymers capped with the Re(I) chromophore. The transient absorption of **II** in THF at 515 nm, where $PTZ^{+\cdot}$ absorbs, was measured, and the charge-separated state lifetime was determined to be 15 ns, as indicated in Figure 5-3.

The energetics for electron transfer are as shown in Scheme 5-4 and Scheme 5-5. The forward electron transfer for **I** is exothermic by 0.42 eV and by 0.45 eV for **II**.[15] The excited state electron transfer processes involving an electron transfer from the PTZ unit to Re occur within the 3 ns excitation pulse. The back electron transfer from the reduced α-diimine ligand to $PTZ^{+\cdot}$ has a much slower rate constant, 4.3×10^7 s^{-1}. This slower rate is presumably caused by the large driving force which puts the reaction in the so-called Marcus inverted region.[3] The rate constant of the back electron transfer from the reduced 2,2′-biquinoline unit in **II** to $PTZ^{+\cdot}$, 6.3×10^7 s^{-1}, is slightly larger than that for **I**. This is consistant with a smaller driving force (1.57 eV, see Scheme 5-5) for the reaction which is still in the inverted region, and possibly to other factors related to structural difference between **I** and **II**.

The spectroscopic accessibility of the charge separated states of **I** and **II** is made possible by the much slower back electron transfer rates associated with the inverted region effect compared to the forward electron transfer rates. The slower back electron transfer rate may also be because the

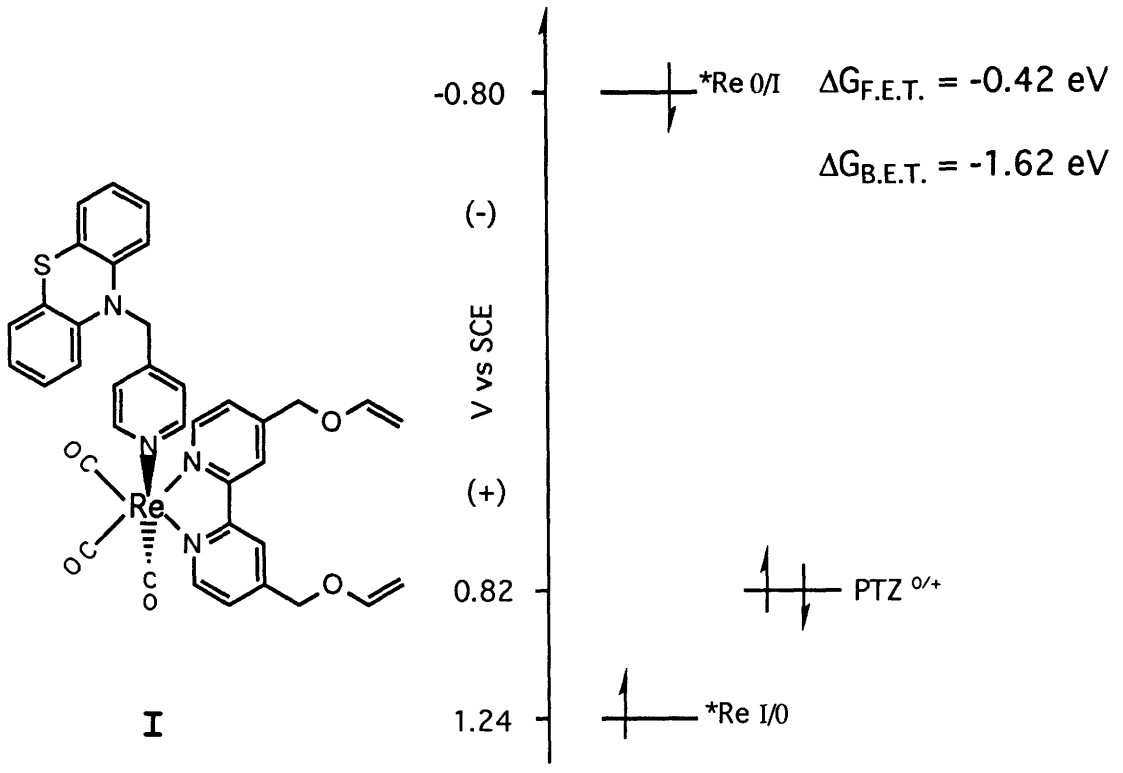

Scheme 5-4. Energetics for photoinduced electron transfer in **I**.

forward electron transfer is from PTZ which is directly bonded to Re(I) whereas the back electron transfer is from $bpy^{-\cdot}$ or $biq^{-\cdot}$ to $PTZ^{+\cdot}$. Thus, the electron may travel over a longer distance in the back electron transfer process. However, it is not clear if the back electron transfer is through space or through the metal center.

The model compounds **I** and **II** show that PTZ linked to Re(I) can have long lived charge-separated states. PTZ block copolymers terminated with the Re(I) chromophore should be good polymeric systems for extending lifetimes of charge-separated states.

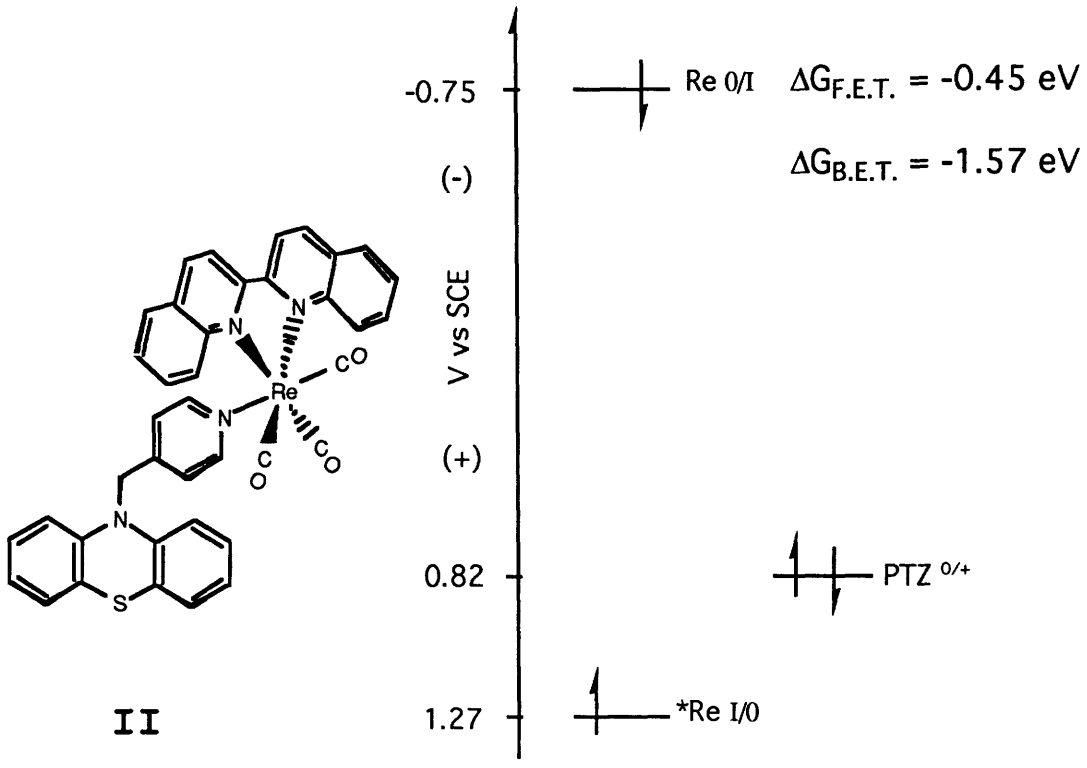

II

Scheme 5-5. Energetics for photoinduced electron transfer in **II**.

Linked Re-TMPD molecules. Molecule **III** is the first example of a TMPD-like molecule covalently attached to a Ru(II)- or Re(I)-based chromophore. TMPD is a good electron donor with a large ($\Delta\varepsilon \approx 10^4$ $M^{-1}cm^{-1}$) visible absorption change upon oxidation.[5] Complete quenching of emission of the Re(I) center in **III**, even at very low concentration (ruling out intermolecular quenching), is attributed to intramolecular electron transfer quenching of the MLCT triplet state of Re(I) center by TMPD. This conclusion follows from the much higher energy (3.07 eV)[16] of the $^3(\pi\pi^*)$ state of TMPD over that (2.02 eV) of the ^{3}(MLCT) state of the Re(I) ruling out energy transfer. The thermodynamic viability of the electron transfer

process suggests that electron transfer is responsible for the quenching of the Re(I) luminescence.

Chemical and electrochemical oxidation of **III** in CH_3CN were studied, and the absorption spectrum of the oxidized **III** either by adding $Fe(n^5\text{-}C_5H_5)^{2+}$ or by electrochemical oxidation at 0.4 V vs SCE in CH_3CN/0.1 M $[n\text{-}Bu_4N]PF_6$ are shown in Figure 5-4. A characteristic $TMPD^{+\cdot}$ absorption bands are observed. The forward electron transfer driving force for **III** is greater than that for Re-MePTZ system by 0.7 eV, and the back electron transfer is less energetic by the same amount, Scheme 5-6. A charge-separated state is observed via detection of the transient absorption spectrum of $TMPD^{+\cdot}$ following photoexcitation of **III** at 416 nm, as shown in Figure 5-5.

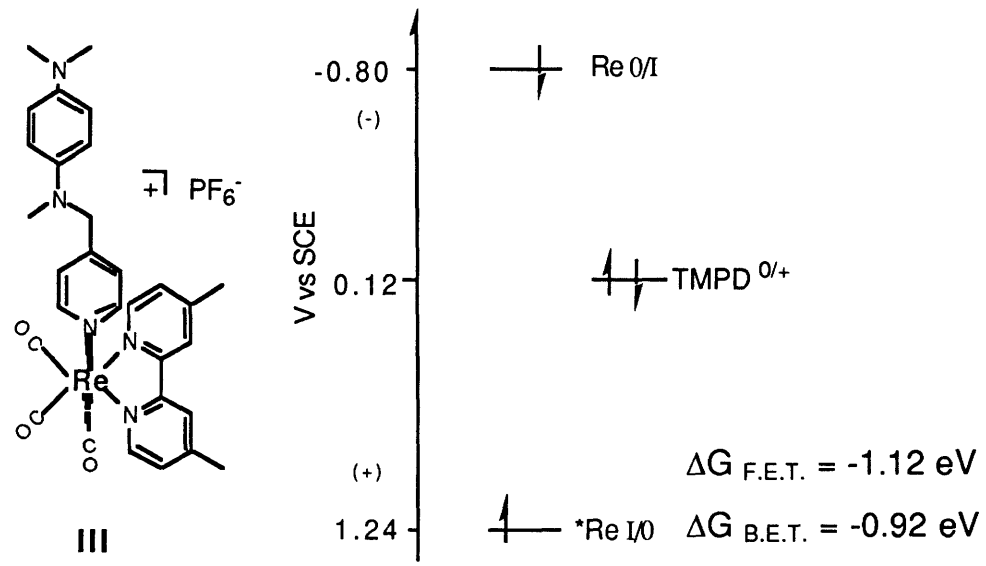

Scheme 5-6. Energetics for photoinduced electron transfer in **III**.

This indicates that the forward electron transfer rate is still faster than the back electron transfer rate. The charge-separated state has a lifetime of ~6 ns obtained by monitoring the absorption decay of **III** in THF at 568 nm, where $TMPD^{+\cdot}$ strongly absorbs.

Model compound **III** shows that TMPD linked to a Re(I) chromophore may have a relatively long-lived charge-separated state with a lifetime regulated by the energetics of the back electron transfer. TMPD block copolymers terminated with a Re(I) chromophore are predicted to perform as good polymeric systems for extending charge separated-state lifetimes. An ordered PTZ-TMPD multiblock copolymer terminated with a Re(I) chromophore (adjacent to the PTZ block) would be good polymeric system for further extending charge-separated state lifetimes by an intramolecular electron transfer, because TMPD is a more potent electron donor than PTZ and could be used to collect an oxidizing equivalent from the $PTZ^{+\cdot}$ produced in an initial electron transfer event to the PTZ block..

Re-PTZ homopolymers and diblock polymers. Emission spectra in toluene were recorded at room temperature for $Re(mtd)_x$ (x = 5, 20, 50, 100, 200), $Re(mtd)_{50}(PTZ)_x$ (x = 5, 10, 25, 50) and $Re(mtd)_x(PTZ)_{10}$ (x = 5, 20, 50, 100, 200) (cf. Scheme 5-3). All samples show one, broad emission band with a maximum at ~ 620 nm. The emission spectra of $Re(mtd)_x(PTZ)_{10}$ in toluene are shown in Figure 5-6. All emission studies were done at a sufficiently low concentration to rule out intermolecular

quenching processes. Complete intramolecular quenching of emission of the Re(I) center in $Re(PTZ)_{25}$ was observed, whereas emission of the Re(I) center of $Re(mtd)_x(PTZ)_{10}$ and $Re(mtd)_{50}(PTZ)_x$ is partially quenched. The quenching is attributed to intramolecular electron transfer quenching of the MLCT triplet state of the Re(I) centers by a unit of PTZ in the PTZ block. Because the energy of the lowest $^3(\pi\pi^*)$ state for PTZ (2.64 eV[14]) is much higher than that of the ^{3}(MLCT) for the Re-based chromophore (2.02 eV), intramolecular energy transfer is thermodynamically unfavorable. Therefore, we conclude intramolecular quenching of the ^{3}(MLCT) state of the Re(I) center with the PTZ block to be dominated by electron transfer as in the model complexes **I** and **II**. Relative quantum yields of emission of the PTZ-containing polymers compared to $Re(mtd)_{25}$ are listed in Table 5-1 showing that the relative emission quantum yield decreases with the repeat unit number of the mtd block interposed between the Re(I) center and PTZ block. The emission lifetimes, Table 5-1, are in accord with the relative emission quantum yield data.

Emission lifetimes were also determined for toluene solution of all model polymers, $Re(mtd)_x$ (x = 5, 20, 50, 100, 200), a homopolymer, $Re(PTZ)_{25}$, block polymers, $Re(mtd)_x(PTZ)_{10}$, (x = 5, 20, 50, 100, 200) and $Re(mtd)_{50}(PTZ)_x$ (x = 5, 10, 25, 50). The emission lifetimes of the $Re(mtd)_x$ polymers in toluene are included in Table 5-2 and are similar to the lifetime of the chromphore, $[(pyridine)Re(CO)_3(2,2'\text{-biquinoline})]^+$ in CH_3CN. $Re(mtd)_5$ has a somewhat shorter emission lifetime, and that may

be due to the relatively small amount of hydrocarbon oligomer derived from only five units of mtd. The $Re(mtd)_x(PTZ)_y$ polymers show shorter lifetimes and tend to show shorter lifetimes for larger y and smaller x. The incomplete quenching suggests that polymer chain dynamics[17] govern the quenching efficiency, and further study is required to understand the quenching rates. However, the qualitative effects are in accord with expectation.

Detection of charge-separated species following photoexcitation of $Re(mtd)_x(PTZ)_y$ by transient absorption is possible. Photoexcitation of $Re(PTZ)_{25}$ produces an absorption change similar to that in model compounds **I** and **II**, as shown in Figure 5-7. The transient absorption of $Re(mtd)_x$ only show the excited state absorption which is different from that of the charge-separated species. The absorption decay of the charge-separated state at 515 nm was monitored, and the lifetime of the charge-separated state was found to be 38 ns in toluene as shown in Figure 5-7. The longer lifetime is due to either (a) greater distance between the chromphore and donor, or (b) delocalization of the "hole" along the PTZ polymeric block via a series.of "self-exchange" events among the PTZ units of the PTZ block.

Unlike $Re(PTZ)_{25}$, PTZ blocks in $Re(mtd)_x(PTZ)_y$ did not completely quench the photoexcited Re(I) center. Emissions precluded acquisition of transient absorption data in the first 50 ns following pulse excitation, but the transient absorption spectra ultimately show the spectral fingerprint of $PTZ^{+\cdot}$ and much longer lifetimes of charge-separated states with increasing

x in $Re(mtd)_x(PTZ)_y$. As an example, photoexcitation of $Re(mtd)_{100}(PTZ)_{10}$ gives the transient absorption of the charge-separated state shown in Figure 5-8 and the charge-separated state lifetime of 111 ns, almost a ten-fold increase in lifetime over the original model compound **II**. Photoexcitation of $Re(mtd)_{50}(PTZ)_5$ produces the transient absorption of the charge-separated state and the charge-separated state lifetime of 95 ns, Figure 5-9. The charge-separated state lifetimes, τ_{cs}, of the polymers are listed in Table 5-2 and increase with increasing x and decrease with increasing y in $Re(mtd)_x(PTZ)_y$. The decrease of the charge-separated lifetimes with the repeat unit number of PTZ block could be caused by shorter average distance between the Re(I) center and the PTZ block.

As in forward electron transfer quenching measured by emission lifetimes, polymer chain dynamics play a role in the back electron transfer (measured by transient absorption decays). The charge-separated state lifetimes of the $Re(mtd)_x(PTZ)_y$ diblock polymers increase with the repeat unit number of mtd spacer block and then show saturation behavior when the repeat unit number, or polymer chain length, approaches ~100. This suggests that the intramolecular back electron transfer rates are limited by polymer chain dynamics.[17] The presence of the mtd spacer block obviously affects the forward and back electron transfer rates between Re(I) and PTZ.

Re-TMPD homopolymers and diblock polymers. Emission of the Re(I) center of $Re(TMPD)_{25}$ in toluene was completely quenched.

The complete quenching of the emission is attributed to intramolecular electron transfer and is believed to be driven by the same energetics as in model compound **III**. Intramolecular energy transfer is not viable because the energy (2.02 eV) of the ^{3}(MLCT) state of Re(I) center, is much lower than that (3.07 eV)[16] of the triplet state of TMPD. Consequently, the quecching of the ^{3}(MLCT) state for $Re(TMPD)_{25}$ is dominated by intramolecular electron transfer.

A redox-inactive mtd block was interposed between the Re(I) and TMPD block to make $Re(mtd)_x(TMPD)_y$ polymers. Unlike $Re(TMPD)_{25}$, $Re(mtd)_{25}(TMPD)_5$ and $Re(mtd)_{110}(TMPD)_{10}$ did not completely quench the emission of the Re(I) center. Emission lifetimes of diblock polymers $Re(mtd)_{25}(TMPD)_5$ and $Re(mtd)_{110}(TMPD)_{10}$ were measured in toluene and found to be 92 ns and 111 ns, respectively.

Photoexcitation of $Re(TMPD)_{25}$ produces an absorption change nearly identical to that in the model compound **III**, Figure 5-10. The absorption decay of the charge-separated state at 568 nm, where $TMPD^{+\cdot}$ strongly absorbs, was monitored, and the lifetime of the charge-separated state was found to be 14 ns in toluene, Figure 5-10. The lifetime of the charge-separated state in the polymers compared to **III** is extended by either greater distance between the chromophore and donor, or delocalization of the "hole" along the TMPD units of the TMPD block.

The transient absorption spectra of $Re(mtd)_x(TMPD)_y$ diblock polymers in toluene were recorded with delay times longer than

50 ns after pulsed excitation. All the transient absorption spectra show the spectral fingerprint of $TMPD^{+\cdot}$ and much longer lifetimes of charge-separated states than **III**. For example, the transient absorption of the charge separated state of $Re(mtd)_{25}(TMPD)_5$ following photoexcitation at 416 nm was obtained, and the charge separated state lifetime was determined to be 92 ns, Figure 5-11. Photoexcitation of $Re(mtd)_{110}(TMPD)_{10}$ also produces the charge-separated transient detected by absorption. The charge-separated state lifetime was found to be 105 ns, which represents almost a 20-fold increase in lifetime over the model compound **III**. The charge-separated state lifetimes of $Re(mtd)_x(TMPD)_y$ are listed in Table 5-3.

In the same way as in the $Re(mtd)_x(PTZ)_y$ polymers, the presence of the mtd spacer block affects the forward and back electron transfer rates between Re(I) and the TMPD block. Interestingly, the charge-separated lifetime of $Re(mtd)_{110}(TMPD)_{10}$ is very close to that of $Re(mtd)_{100}(PTZ)_{10}$. This again indicates that the intramolecular back electron transfer rates are limited by the polymer chain dynamics instead of the electron transfer energetics, since the PTZ had a ~0.7 eV more favorable back electron transfer reaction.

Re-PTZ-TMPD triblock polymers. Incorporation of two different electron donors into a multiblock polymer should, in principle, allow the second redox group to transfer an electron to the first, as indicated in Scheme 5-7. This second step

should separate the hole and electron at greater distances and allow for a longer lived charge-separated state.

In Scheme 5-7 k_2 must be faster than k_{b1} (or k_{b2}) for the $TMPD^{+\cdot}$ to be observed. With $Re(PTZ)_{25}$, k_1 is very fast ($\sim 10^9$ s^{-1}) and k_{b1} is 2.63×10^7 s^{-1}. For $Re(mtd)_5(PTZ)_{10}$, which has a shortest mtd block, k_{b1} is more than two times slower, 1.22×10^7 s^{-1}. This is the rate with which intramolecular, sequential electron transfer must compete.

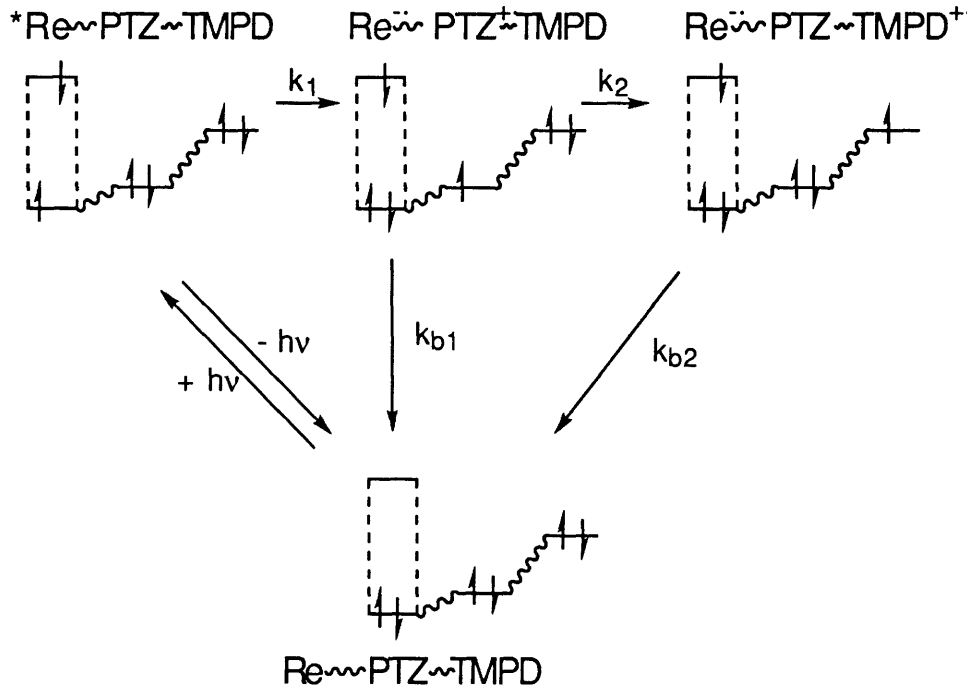

Scheme 5-7. Photoinduced electron transfer in a copolymer with two blocks of different electron donors.

$Re(mtd)_{100}(PTZ)_{10}(TMPD)_{10}$, $Re(mtd)_{100}(PTZ)_{50}(TMPD)_{10}$, and $Re(mtd)_{200}(PTZ)_{10}(TMPD)_{10}$ were made. Emission from the Re(I) chromophore is only partially quenched in all cases. The

emission lifetimes of three triblock polymers in toluene are listed along with those of the model polymers in Table 5-4. All three triblock polymers show transient absorption consistent with a combination of $PTZ^{+\cdot}$ and $TMPD^{+\cdot}$ following photoexcitation. The transient absorption spectra of the charge-separated state for $Re(mtd)_{100}(PTZ)_{10}(TMPD)_{10}$ at different times following photoexcitation are shown in Figure 5-12. The absorption decays of three triblock polymers were monitored at 515 nm, where $PTZ^{+\cdot}$ strongly absorbs while $TMPD^{+\cdot}$ weakly absorbs, and at 568 nm, where $TMPD^{+\cdot}$ strongly absorbs and $PTZ^{+\cdot}$ does not absorb. The lifetime of $PTZ^{+\cdot}$ and $TMPD^{+\cdot}$ for $Re(mtd)_{100}(PTZ)_{10}(TMPD)_{10}$ were found to be 85 and 88, respectively, Figure 5-12. The decay lifetimes at different monitoring wavelengths are listed in Table 5-4. Based on the absorption decay data at 568 nm, there is no evidence for sequential electron transfer as suggested in Scheme 5-7. Such sequential electron transfer has been detected in a series of bimolecular processes in solution, Figure 5-14.[18] Thus, while $PTZ^{+\cdot}$ in the polymer should oxidize TMPD units we find no evidence for it; rather $TMPD^{+\cdot}$ appears as a primary electron transfer product. This secondary structure of the polymer allows the TMPD units to effectively quench the Re-centered excited state by electron transfer.

Cast films of Re-PTZ and Re-TMPD polymers. Most of the polymers investigated can be made into cast films either as free standing films or on a glass slide. Some films show good uniformity and smoothness. The emission of the Re(I) center in

cast films of $Re(PTZ)_{25}$, $Re(mtd)_{100}(PTZ)_{10}$, and $Re(mtd)_{100}(PTZ)_{10}(TMPD)_{10}$ was quenched by more than 90% compared to the chromophore. Transient absorption of the cast films of the polymers were measured at room temperature. Photoexcitation of the cast film of $Re(mtd)_{100}(PTZ)_{10}(TMPD)_{10}$, produced the charge-separated state which is dominated by $PTZ^{+\cdot}$ and $TMPD^{+\cdot}$ absorption bands, as shown in Figure 5-15. A double exponential absorption decay at 515 nm for $PTZ^{+\cdot}$ was observed with τ_{CS}^{1} = 35 ns and τ_{CS}^{2} = 191 ns. The faster decay could correspond to "intrastrand" electron transfer between $PTZ^{+\cdot}$ and an adjacent TMPD. On the other hand, the slower decay could be correspondent to the "interstrand" back electron transfer from the reduced Re(0) center or TMPD to $PTZ^{+\cdot}$. "Strand" separation, or block segregation, for the tri-block polymers are supported by X-ray diffraction measurements.[19] The charge-separated states for both $Re(PTZ)_{25}$ and $Re(mtd)_{100}(PTZ)_{10}$ cast films were observed and found to have single exponential decays. The charge separated state lifetimes of the cast films are included in Table 5-5.

Conclusion

A series of chromophore end-capped homopolymers and multiblock polymers based on **II** and **III** were synthesized by ring-opening metathesis polymerization and found to have long-lived charge-separated states. $Re(mtd)_x(PTZ)_y$ diblock polymers were found to sustain charge-separated state

lifetimes up to nearly an order of magnitude greater than that of their model compound, **II**. Both forward and back electron transfer rates in $Re(mtd)_x(PTZ)_y$ polymers increase with the number of PTZ units in a PTZ block and decrease with the number of mtd units in a mtd block. The intramolecular forward and back electron transfer rates are limited by polymer chain dynamics at a specific polymer chain length. Photoexcitation of $Re(mtd)_x(TMPD)_y$ diblock polymers produced charge-separated states with lifetimes up to nearly 20 time longer than that of **III**. Cast films of some polymers were studied by transient emission and absorption spectroscopy, and charge-separated states of some redox polymers in the solid state are demonstrated.

In this chapter we have demonstrated the examples of structurally well-controlled polymers capable of separating charge upon photoexcitation. These polymers have shown great potential in fundamental electron transfer and polymer chain dynamics, and as molecular units for photoenergy conversion or molecular electronic devices. However, we have not been able to observe sequential electron transfer in multiblock polymers which might duplicate the photosynthetic Z-scheme of vectorial electron transfer. The secondary structure of ROMP products permits direct communication of the chromophore and several blocks in a multiblock system. In principle, we should take advantage of phase separation in a multiblock system and further work on such systems should prove useful.

References

1. (a) Meyer, T. J. *Acc. Chem. Res.* **1989**, *22*, 163. (b) Photoinduced Electron Transfer; Fox, M. A., Channon, M., Eds.; Elsevier: New York, 1988. (c) Supramolecular Photochemistry; Scandola, F., Balzani, V., Eds.; Ellis Horwood Ltd.; Chesson, 1991. (d) Wasielewski, M. R. *Chem. Rev.* **1992**, *92*, 435. (e) Marchi, M.; Gehlen, J. N.; Chandler, D.; Newton, M. *J. Am. Chem. Soc.* **1993**, *115*, 4178.

2. Wrighton, M. S. *Comments Inorg. Chem.* **1985**, *4*, 269.

3. (a) Chen, P.; Duesing, R.; Tapolsky, G.; Meyer, T. J. *J. Am. Chem. Soc.* **1989**, *111*, 8305. (b) Meyer, T. J. *Acc. Chem. Res.* **1989**, *22*, 163. (c) Chen, P.; Curry, M.; Meyer, T. J. *Inorg. Chem.* **1989**, *28*, 2271. (d) Cooley, L. F.; Headford, C. E. L.; Elliot, C. M.; Kelley, D. F. *J. Am. Chem. Soc.* **1988**, *110*, 6673. (e) Danielson, E.; Elliot, C. M.; Merkert, J. W.; Meyer, T. J. *J. Am. Chem. Soc.* **1987**, *109*, 2519. (f) Chen, P.; Westmoreland, T. D.; Danielson, E.; Schanze, K. S.; Anthon, D.; Neveux, P. E., Jr.; Meyer, T. J. *Inorg. Chem.* **1987**, *26*, 1116. (g) Schnoover, J. R.; Strouse, G. F.; Chen, P.; Bates, W. D.; Meyer, T. J. *Inorg. Chem.* **1993**, *32*, 2618.

4. Christ, C. S.; Yu, J.; Zhao, X.; Palmore, G. T.; Wrighton, M. S. *Inorg. Chem.* **1992**, *31*, 4439.

5. (a) Rao, P. S.; Hayon, E. J. Phys. Chem. 1975, 79, 1063. (b) Albrecht, A. C.; Simpson, W. T. *J. Am. Chem. Soc.* **1955**, *77*, 4454.

6. (a) Schrock, R. R. *Acc. Chem. Res.* **1990**, *23*, 158. (b) Grubbs, R. H.; Tumas, W. *Science*, **1989**, *243*, 907.

7. (a) Albagli, D.; Bazan, G.; Schrock, R. R.; Wrighton, M. S. *J. Am. Chem. Soc.* **1993**, *115*, 7328. (b) Albagli, D.; Bazan, G.; Schrock, R. R.; Wrighton, M. S. *J. Am. Chem. Soc.* **1992**, *114*, 4150. (c) Albagli, D.; Bazan, G.; Schrock, R. R.; Wrighton, M. S. *J. Phys. Chem.* in press.

8. (a) Fox, M. A.; Jones, W. E., Jr.; Watkins, D. M. *Chem. Eng. News* **1993**, *71*, 38. (b) Guillet, J. E. *Pure Appl. Chem.* **1991**, *63*, 917. (c) Webber, S. E. *Chem. Rev.* **1990**, *90*, 1469. (d) Morishima, Y.; Kobayashi, T.; Furui, T.; Nozakura, S. *Macromolecules* **1987**, *20*, 1707. (e) Itoh, Y.; Morishima, Y.; Nozakura, S. *Photochem. & Photobiol.* **1984**, *39*, 603. (f) Itoh, Y.; Morishima, Y.; Nozakura, S. *Photochem. & Photobiol.* **1984**, *39*, 451.

9. (a) Jones, W. E., Jr.; Younathan J. N;Strouse, G. F.; Meyer, T. J. *J. Am. Chem. Soc.* **1993**, *115*, 7363. (b) Baxter, S. M.; Jones, W. E., Jr.; Danielson, E.; Worl, L. A.; Strouse, G. F.; Younathan J. N; Meyer, T. J. *Coordination Chem. Rev.* **1991**, *111*, 47. (c) Worl, L. A.; Strouse, G. F.; Younathan J. N; Baxter, S.

M.; Meyer, T. J. *J. Am. Chem. Soc.* **1990**, *112*, 7571. (d) Younathan J. N; McClanahan, S. F.; Meyer, T. J. *Macromolecules* **1989**, *22*, 1048. (e) Margerum, L. D.; Meyer, T. J. Murray, R. W. *J. Phys. Chem.* **1986**, *90*, 2696.

10, (a) Forster, R. J.; Vos, J. G. *Macromolecules* **1990**, *23*, 4372. (b) Webber, S. E.; Batteas, J. D.; Kamioka, K.; Chatterjee, P. K. *J. Phys. Chem.* **1991**, *95*, 960.

11. Murray, R. W. *Ann. Rev. Mater. Sci.* **1984**, *14*, 145.

12. Ennis, P. M.; Kelly, J. M. *J. Phys. Chem.* **1989**, *93*, 5735.

13. Albagli, D.; Lee, J.; Zhao, X.; Lee, E. J.; Schrock, R. R.; Wrighton, M. S. unpublished data.

14. (a) Moroi, Y.; Braun, A. M.; Grätzel, M. *J. Am. Chem. Soc.* **1979**, *101*, 567. (b) Maestri, M.; Grätzel, M. *Ber. Bunsenges. Phys. Chem.* **1977**, *81*, 504.

15. The cyclic voltammetry of $Re(CO)_3(biq)(pyr)$ was studied by Dr. Luong in our laboratory and found to have two reduction waves with $E_{1/2}$ = -0.7 V and $E_{1/2}$ = -1.0 V. The details can be referred in Leong's Ph.D. thesis, Massachusetts Institute of Technology, Sept. 1981.

16. Kimura, K.; Tsubomura, H. *Mol. Phys.* **1966**, *11*, 349.

17. Wilemski, G.; Fixman, M. *J. Chem. Phys.* **1974**, *60*, 866.

18. Lee, E. J. Ph.D. Thesis, Massachusetts Institute of Technology, Aug. 1993.

19. Supplementary X-ray diffraction experimental results for $Re(mtd)_x(PTZ)_y(TMPD)_z$ can obtained upon request.

Table 5-1. Relative emission quantum yields (Φ_{em}) and emission lifetimes (τ_{em}) of Re(mtd)x(PTZ)y polymers.

Sample	Φ_{em}	τ_{em} (ns)
$Re(mtd)_{25}$	1.00	146
$Re(mtd)_{100}(PTZ)_{10}$	0.91	105
$Re(mtd)_{50}(PTZ)_{10}$	0.80	99
$Re(mtd)_{20}(PTZ)_{10}$	0.38	55
$Re(mtd)_{5}(PTZ)_{10}$	0.13	33
$Re(PTZ)_{25}$	0.00	---

Table 5-2. Emission and Charge-Separated State Lifetimes (ns) in $Re(mtd)_x(PTZ)_y$ Block Polymers

Sample[a]	τ_{em}[b]	τ_{CS}[b]	**Sample**[a]	τ_{em}[b]	τ_{CS}[b]
$Re(CO)_3(biq)$	155	--	$Re(mtd)_{50}(PTZ)_5$	120	95
Re(biq)(PTZ) **(II)**	0	15	$Re(mtd)_{50}(PTZ)_{10}$	99	93
$Re(PTZ)_{25}$	0	38	$Re(mtd)_{50}(PTZ)_{25}$	98	89
			$Re(mtd)_{50}(PTZ)_{50}$	93	74
$Re(mtd)_5$	111	--	$Re(mtd)_5(PTZ)_{10}$	33	82
$Re(mtd)_{20}$	147	--	$Re(mtd)_{20}(PTZ)_{10}$	55	91
$Re(mtd)_{50}$	146	--	$Re(mtd)_{50}(PTZ)_{10}$	99	93
$Re(mtd)_{100}$	146	--	$Re(mtd)_{100}(PTZ)_{10}$	105	110
$Re(mtd)_{200}$	163	--	$Re(mtd)_{200}(PTZ)_{10}$	123	111

a Cf. Scheme 5-3.

b τ_{em} of Re(biq) and τ_{cs} of **II** were measured in CH_3CN and τ_{em} and τ_{cs} of all polymers were measured in toluene.

Table 5-3. Emission and Charge-Separated State Lifetimes (ns) in $Re(mtd)_x(TMPD)_y$ Block Polymers compared to model molecules and polymers.

Sample[a]	τ_{em}[b]	τ_{CS}[b]	**Sample**[a]	τ_{em}[b]	τ_{CS}[b]
Re(biq)	155	--	Re(biq)(TMPD)	--	6
$Re(mtd)_{25}$	146	--	$Re(mtd)_{25}(TMPD)_5$	92	91
$Re(mtd)_{100}$	146	--	$Re(mtd)_{110}(TMPD)_{10}$	111	105
$Re(TMPD)_{25}$	--	14			

a Cf. Scheme 5-3.

b τ_{em} of Re(biq) and τ_{cs} of Re(biq)(TMPD) were measured in CH_3CN and τ_{em} and τ_{cs} of all polymers were measured in toluene.

Table 5-4. Charge-separated state lifetimes (τ_{CS}) of $Re(mtd)_x(PTZ)_y(TMPD)_z$ triblock polymers with two electron donors compared to τ_{em} and τ_{cs} of model polymers and $Re(mtd)_x(PTZ)_y$ diblock polymers.

Sample[a]	τ_{em}[b] (ns)	τ_{CS} (ns)[b] 515 nm	τ_{CS} (ns)[b] 568 nm
$Re(mtd)_{100}$	146	--	--
$Re(mtd)_{100}(PTZ)_{10}$	105	110	--
$Re(mtd)_{110}(TMPD)_{10}$	111		105
$Re(mtd)_{100}(PTZ)_{10}(TMPD)_{10}$	101	85	88
$Re(mtd)_{100}(PTZ)_{50}(TMPD)_{10}$	96	83	87
$Re(mtd)_{200}$	163	--	--
$Re(mtd)_{200}(PTZ)_{10}$	123	111	--
$Re(mtd)_{200}(PTZ)_{10}(TMPD)_{10}$	116	103	103

a Cf. Scheme 5-3.

b τ_{em} of Re(biq) and τ_{cs} of Re(biq)(TMPD) were measured in CH_3CN and τ_{em} and τ_{cs} of all polymers were measured in toluene.

Table 5-5. Charge-separated state lifetimes (τ_{CS})* of the cast films of $Re(PTZ)_{25}$, $Re(mtd)_{100}(PTZ)_{10}$, $Re(mtd)_{100}(PTZ)_{10}(TMPD)_{10}$, and $Re(mtd)_{100}(PTZ)_{50}(TMPD)_{10}$.

Sample	τ_{CS} (ns)	
$Re(PTZ)_{25}$	37	
$Re(mtd)_{100}(PTZ)_{10}$	121	
	τ_{CS}^1 (ns)	τ_{CS}^2 (ns)
$Re(mtd)_{100}(PTZ)_{10}(TMPD)_{10}$	35	191

* Charge-separated state lifetimes (τ_{CS}) of the cast films were measured at 515 nm.

Figure 5-1. Broad band transient absorption spectrum of **I**. The spectrum was taken 5 ns after a 3 ns 355 nm excitation of I in CH_3CN/0.1M [*n*-Bu_4N]PF_6.

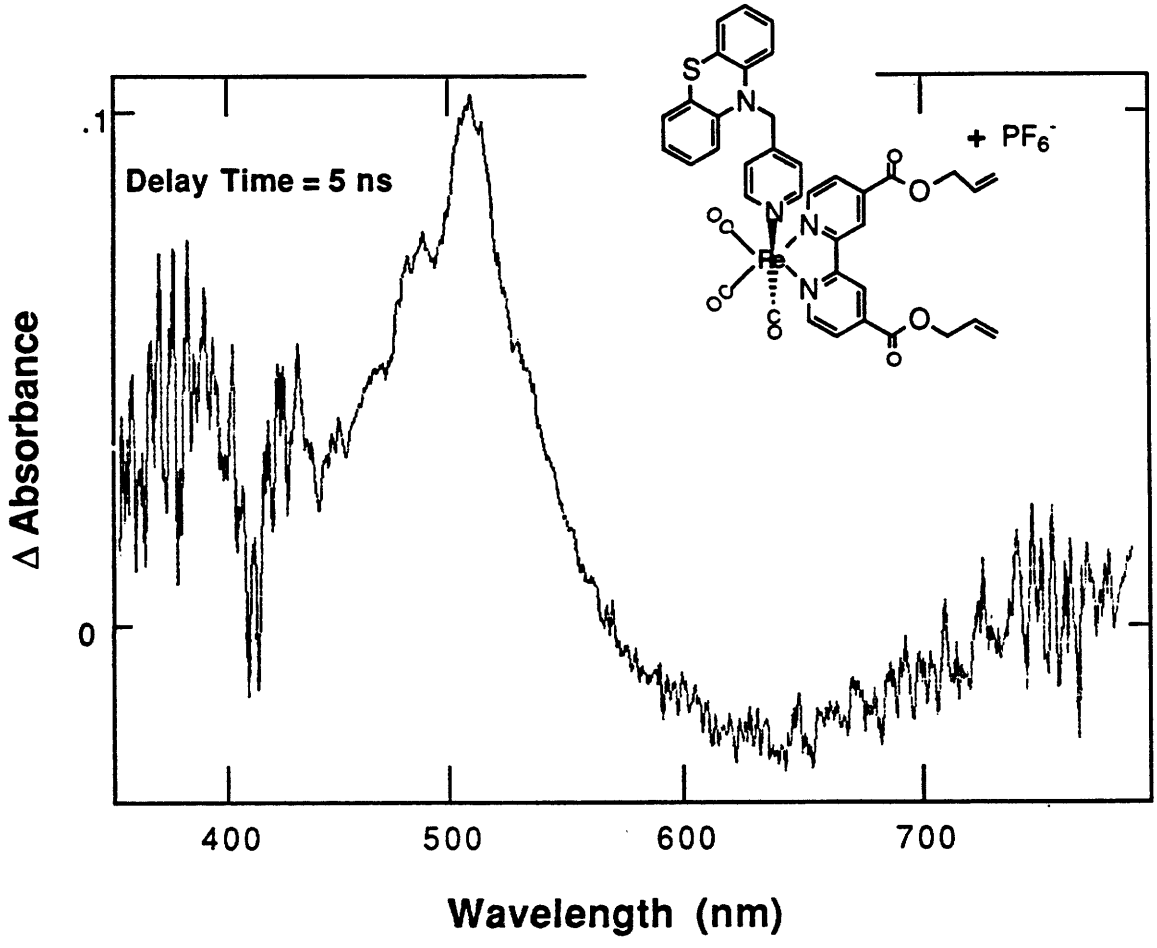
Delay Time = 5 ns
.1
0
Δ Absorbance
400
500
600
700
Wavelength (nm)
+ PF6-

Figure 5-2. Transient absorption decay at 515 nm following 3 ns 355 nm excitation of **I**. Fitting the decay curve gives the lifetime of the charge-separated state of 23 ns.

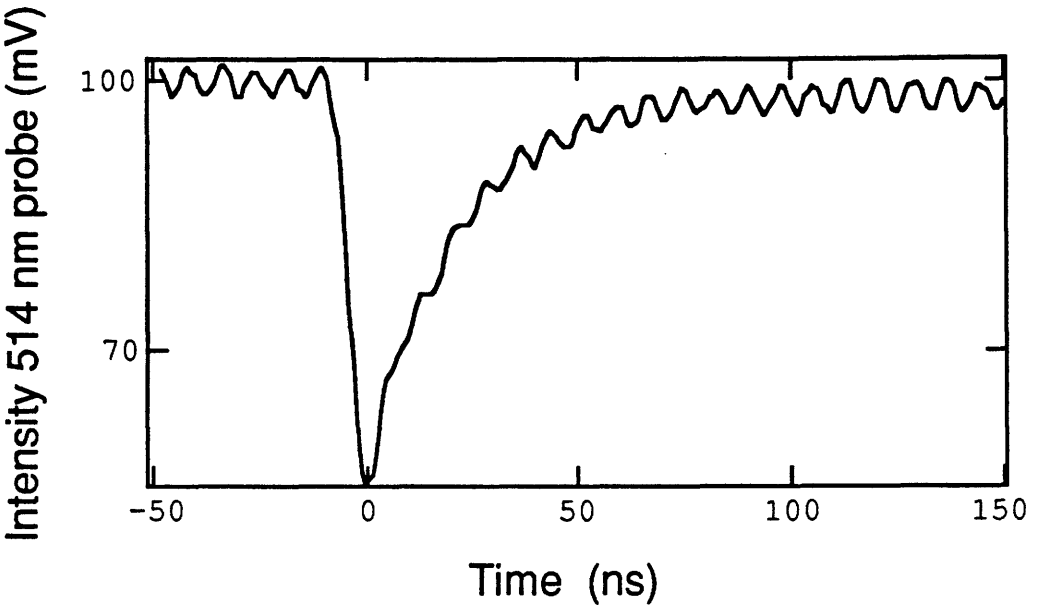
Intensity 514 nm probe (mV)
100
70
-50
0
50
100
150
Time (ns)

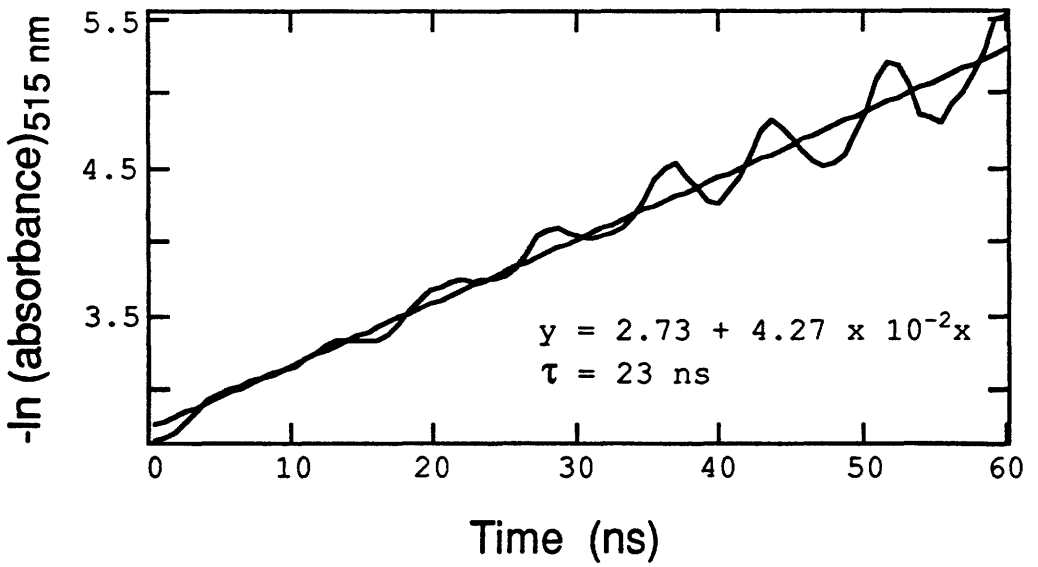
-ln (absorbance)515 nm
5.5
4.5
3.5
y = 2.73 + 4.27 x 10-2x
τ = 23 ns
0
10
20
30
40
50
60
Time (ns)

Figure 5-3. Transient absorption decay at 515 nm following 3 ns 416 nm excitation of **II**. Fitting the decay curve gives the lifetime of the charge-separated state of 15 ns.

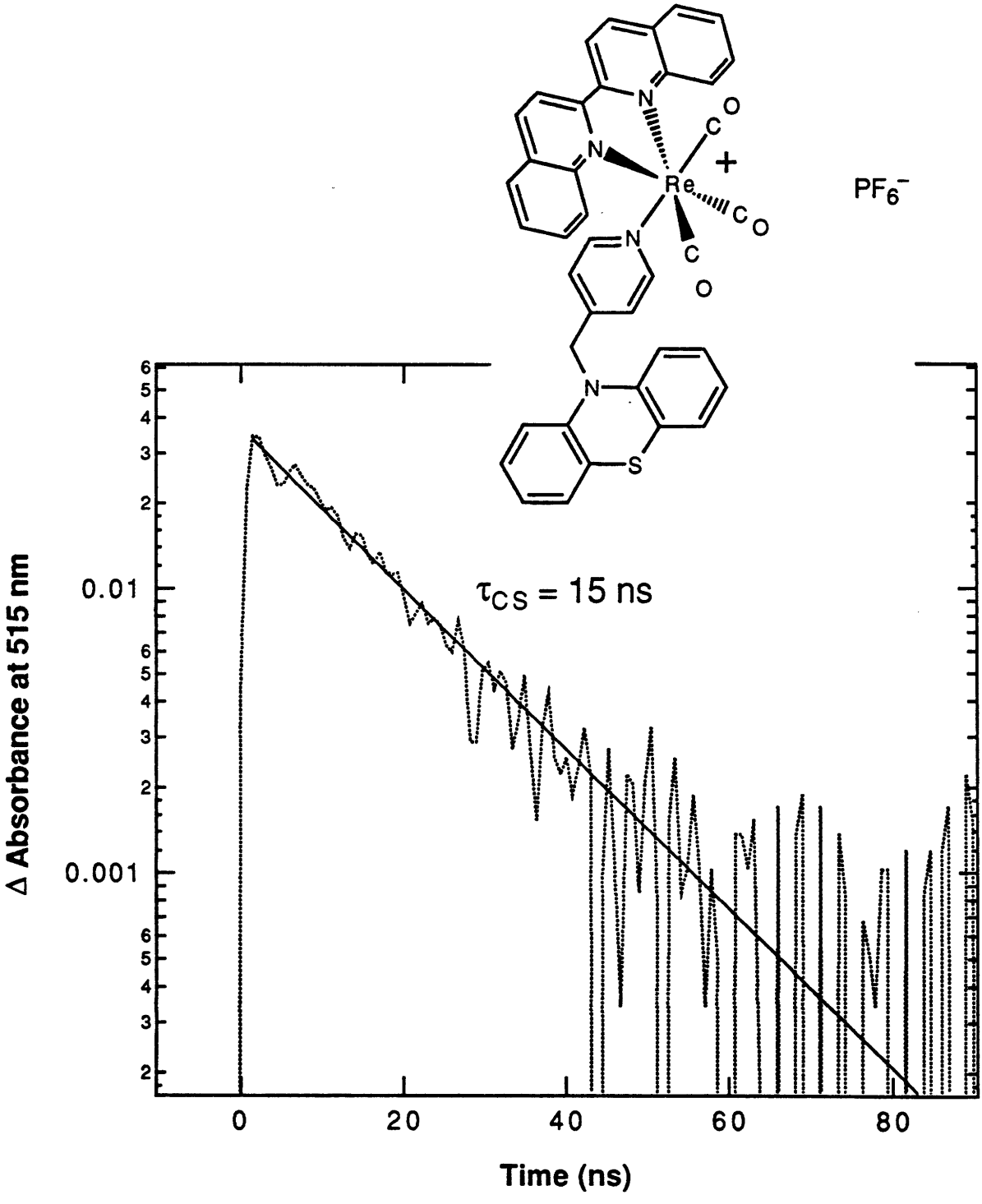
N
N
Re
C
O
C
O
C
O
+
PF6−
N
N
S
τCS = 15 ns
Δ Absorbance at 515 nm
0.01
0.001
0
20
40
60
80
Time (ns)

Figure 5-4. Absorption spectra of the first oxidation product of **III** obtained either by electrolysis at 0.4 V vs SCE in CH_3CN/0.1M [*n*-Bu_4N]PF_6 or by adding $Fc^+BF_4^-$ in CH_3CN solution of **III**.

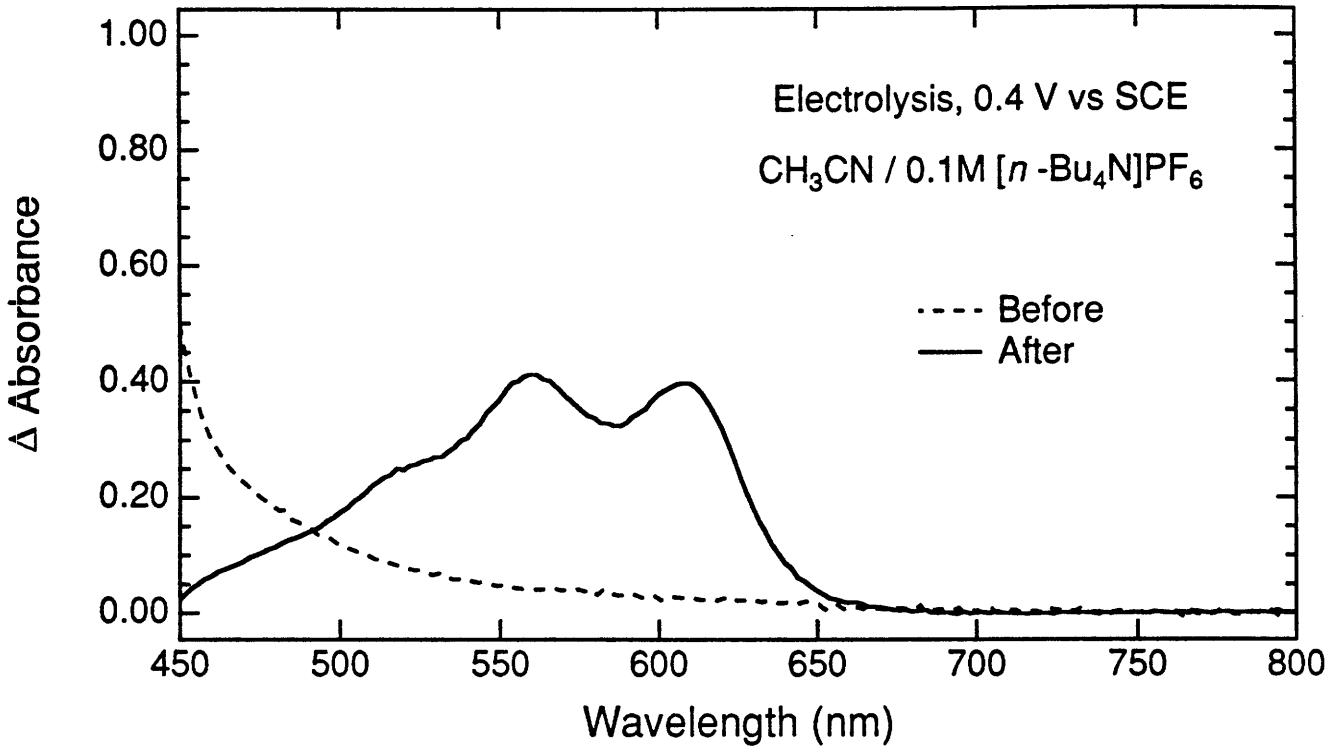
Electrolysis, 0.4 V vs SCE
CH3CN / 0.1M [n -Bu4N]PF6
Before
After
Δ Absorbance
Wavelength (nm)
1.00
0.80
0.60
0.40
0.20
0.00
450
500
550
600
650
700
750
800

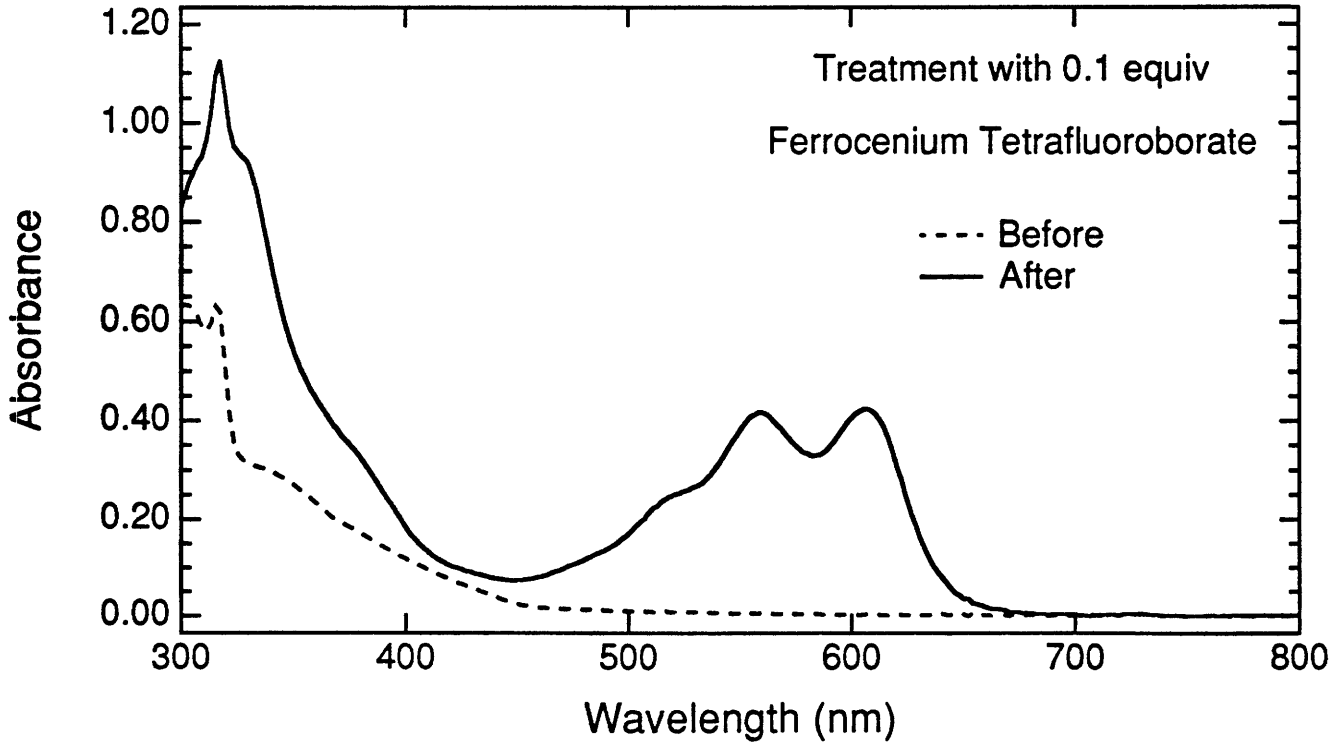
Treatment with 0.1 equiv
Ferrocenium Tetrafluoroborate
Before
After
Absorbance
Wavelength (nm)
1.20
1.00
0.80
0.60
0.40
0.20
0.00
300
400
500
600
700
800

Figure 5-5. Transient absorption spectrum of **III** in CH_3CN accumulated during 3 ns excitation pulse at 416 nm and the absorption decay at 568 nm following the photoexcitation of III. Fitting the decay curve produces the lifetime of the charge-separated state of ~6 ns.

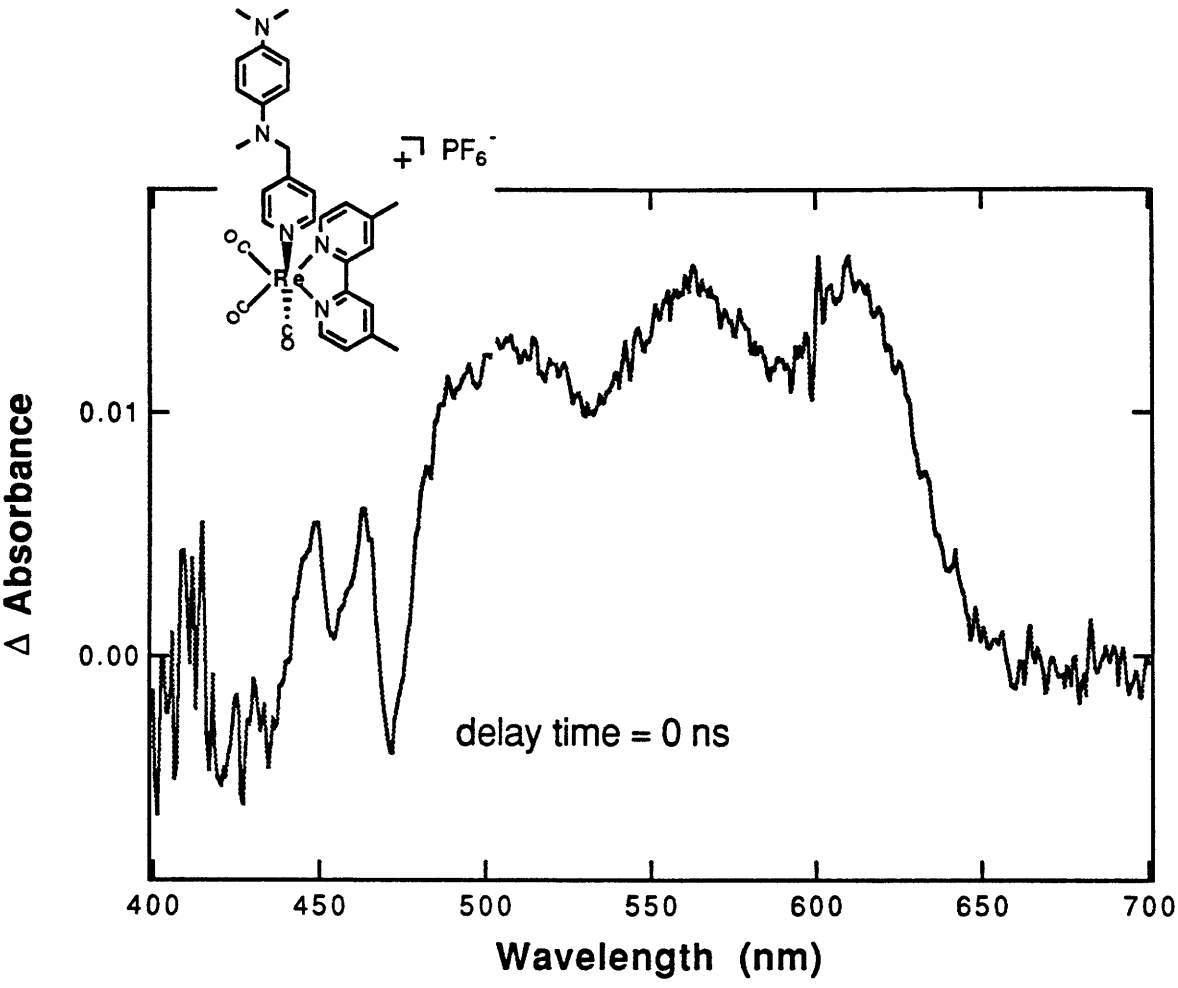
PF6-
Δ Absorbance
0.01
0.00
delay time = 0 ns
400
450
500
550
600
650
700
Wavelength (nm)

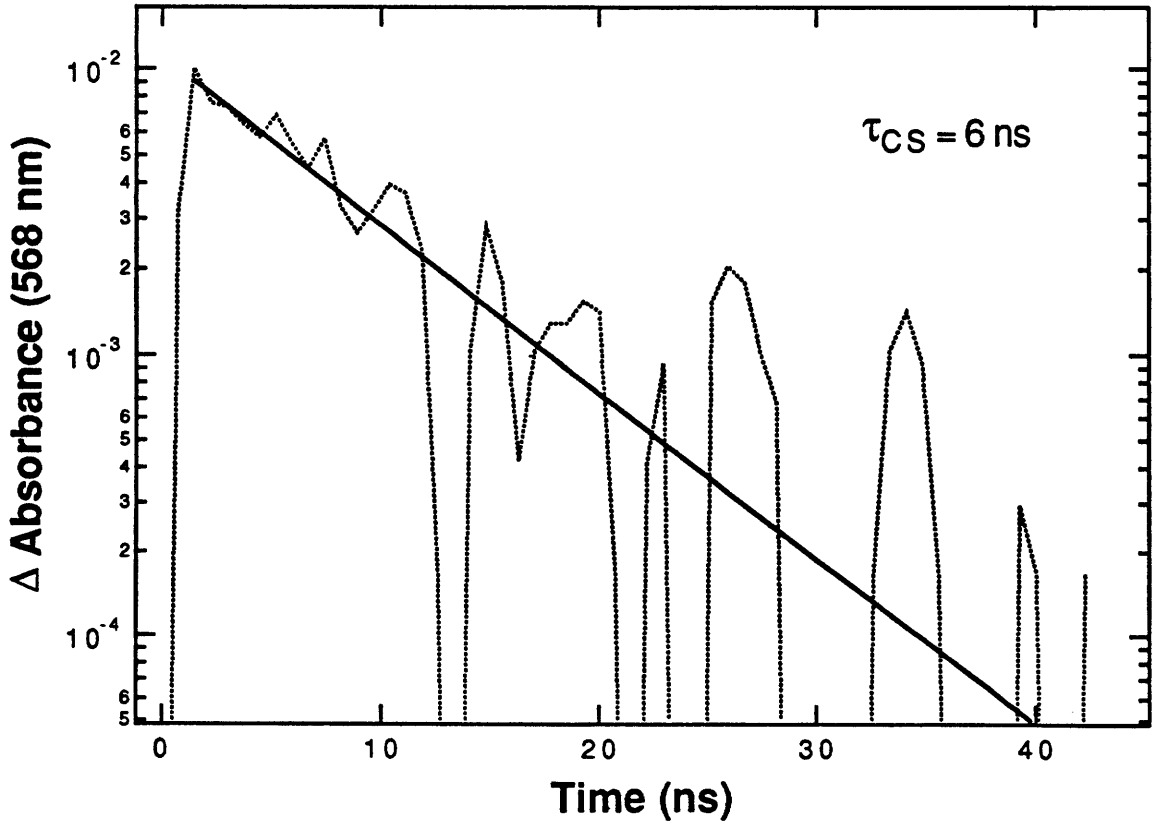
Δ Absorbance (568 nm)
τCS = 6 ns
Time (ns)

Figure 5-6. Steady-state emission spectroscopy of $Re(mtd)_x(PTZ)_{10}$ (x = 5, 20, 50, 100) block polymers excited at 380 nm in toluene.

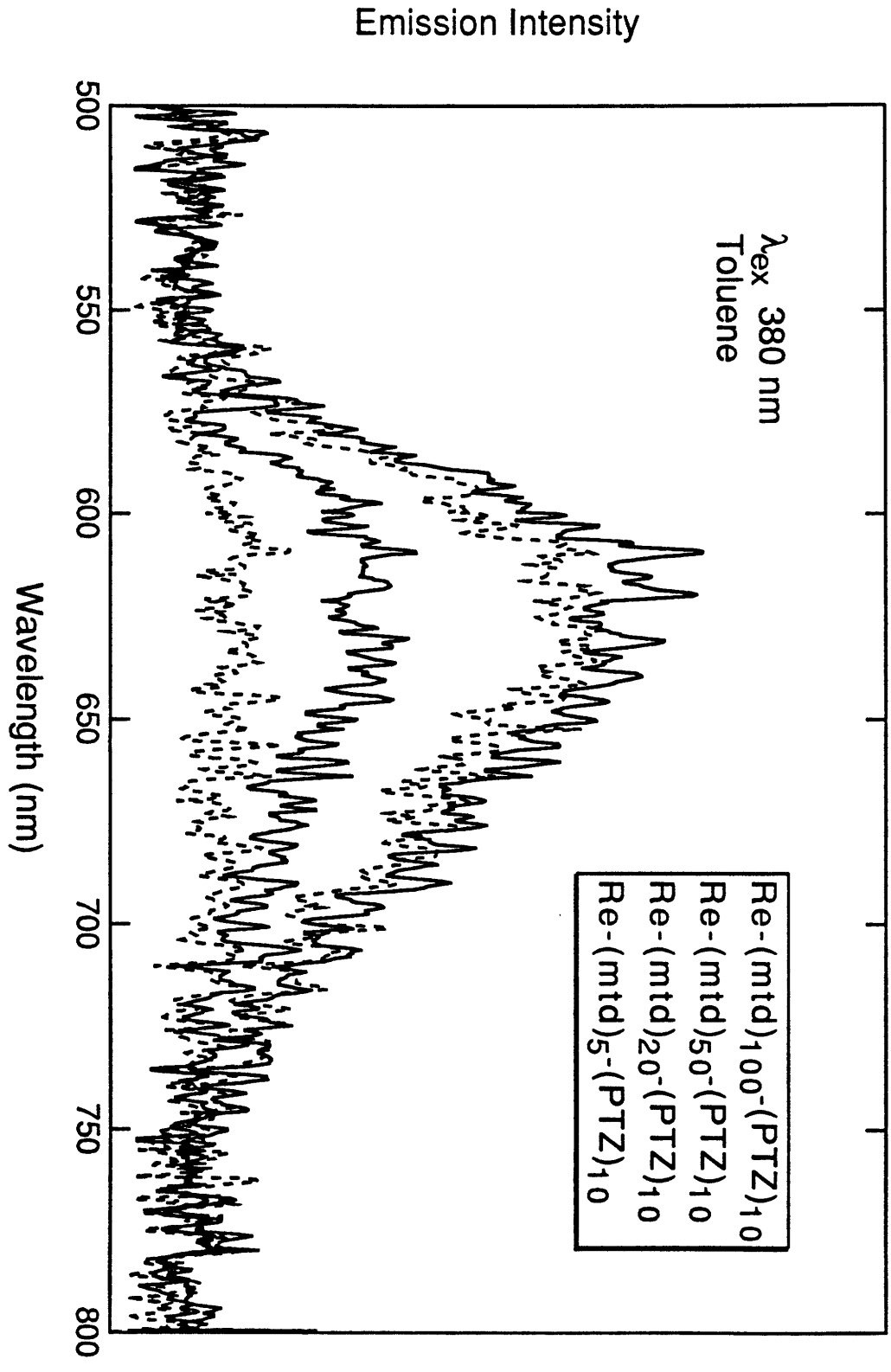
Emission Intensity
λex 380 nm
Toluene
Re-(mtd)100-(PTZ)10
Re-(mtd)50-(PTZ)10
Re-(mtd)20-(PTZ)10
Re-(mtd)5-(PTZ)10
500
550
600
650
700
750
800
Wavelength (nm)

Figure 5-7. Transient absorption spectrum of $Re(PTZ)_{25}$ in toluene taken 50 ns after a 3 ns 416 nm excitation and the absorption decay at 515 nm following the photoexcitation of $Re(PTZ)_{25}$. Fitting the decay curve produces the lifetime of the charge-separated state of 38 ns.

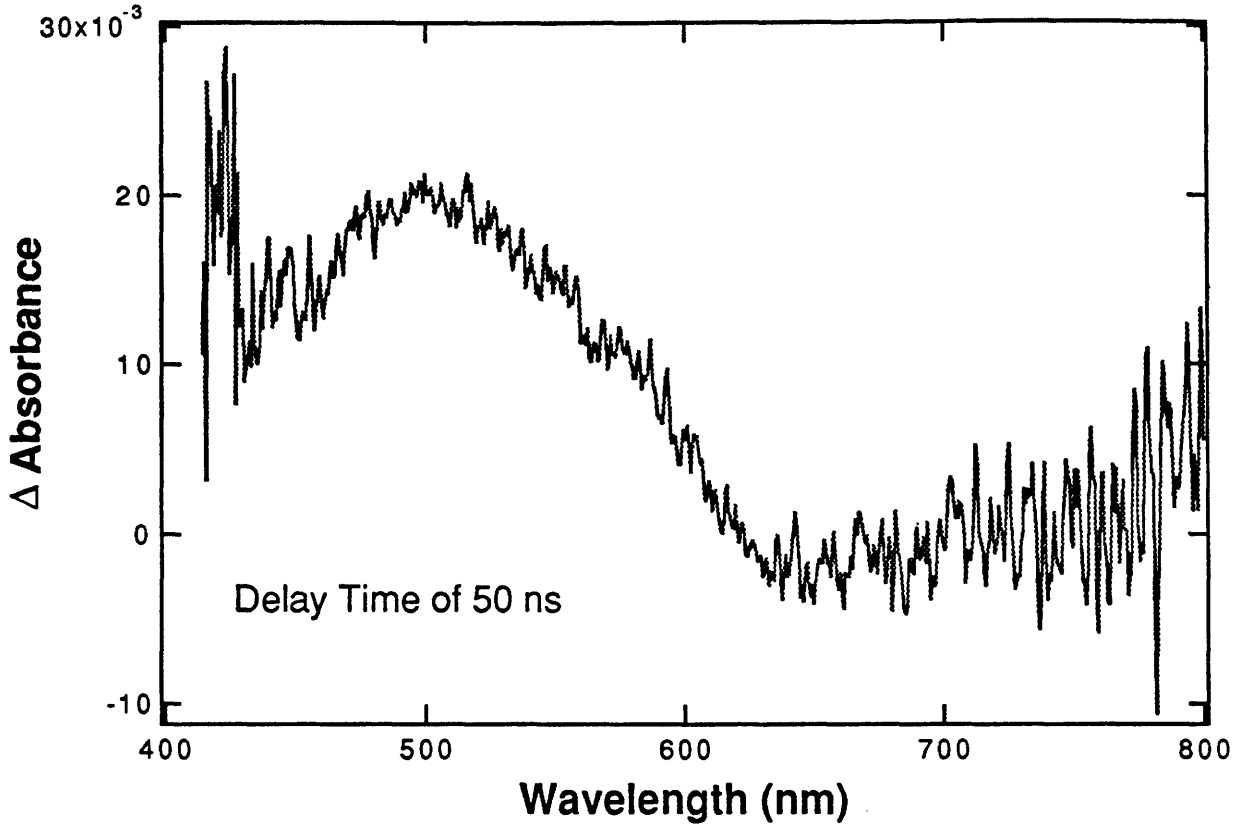
30x10-3
20
10
0
-10
Δ Absorbance
Delay Time of 50 ns
400
500
600
700
800
Wavelength (nm)

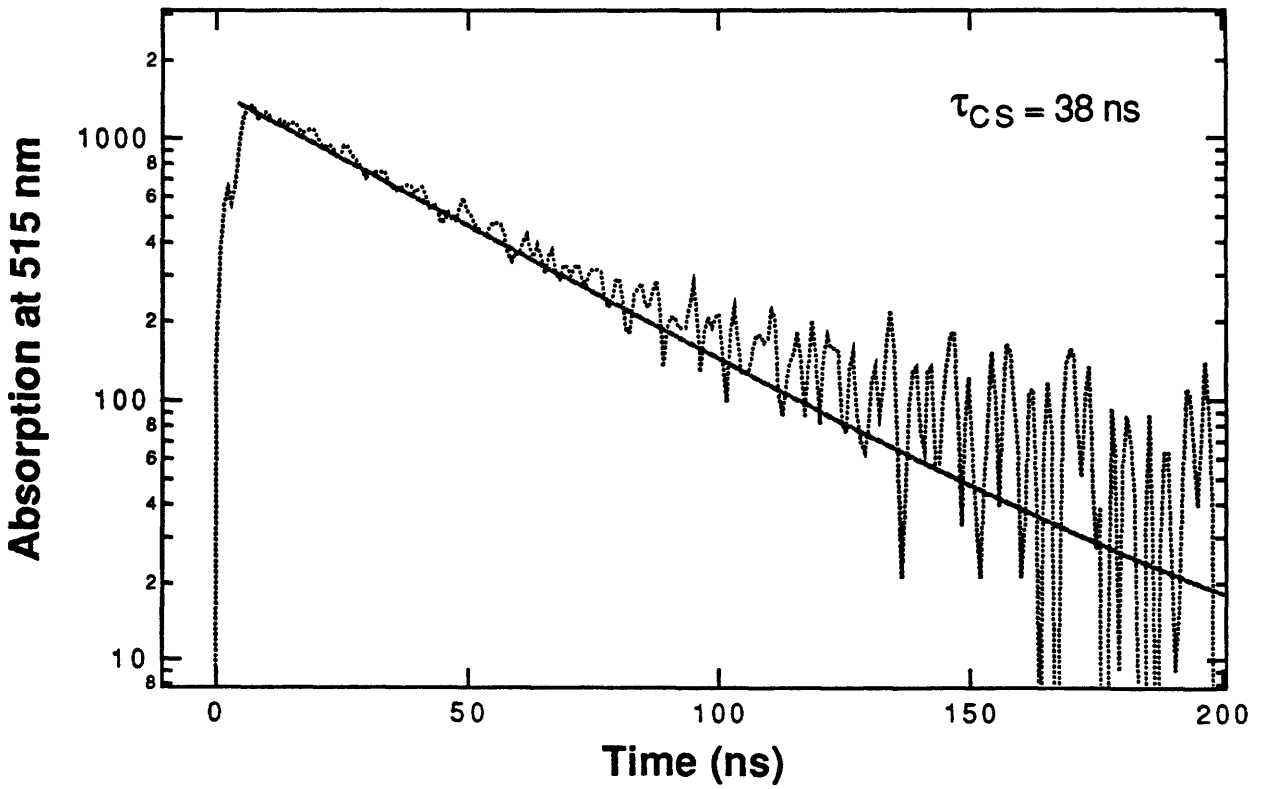
τCS = 38 ns
Absorption at 515 nm
1000
100
10
0
50
100
150
200
Time (ns)

Figure 5-8. Transient absorption spectrum of $Re(mtd)_{100}(PTZ)_{10}$ in toluene taken 100 ns after a 3 ns 416 nm excitation and the absorption decay at 515 nm following the photoexcitation of $Re(mtd)_{100}(PTZ)_{10}$. Fitting the decay curve produces the lifetime of the charge-separated state of 111 ns.

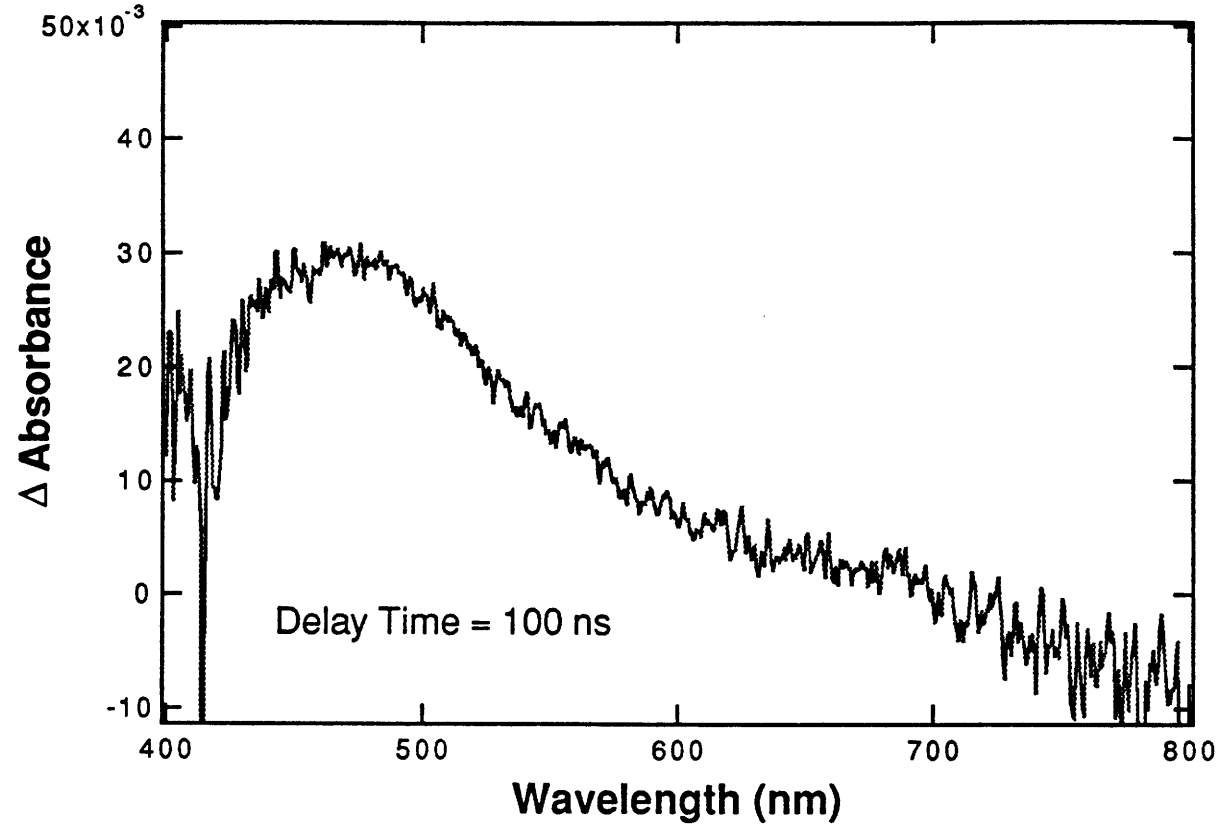
50x10-3
40
30
20
10
0
-10
Δ Absorbance
Delay Time = 100 ns
400
500
600
700
800
Wavelength (nm)

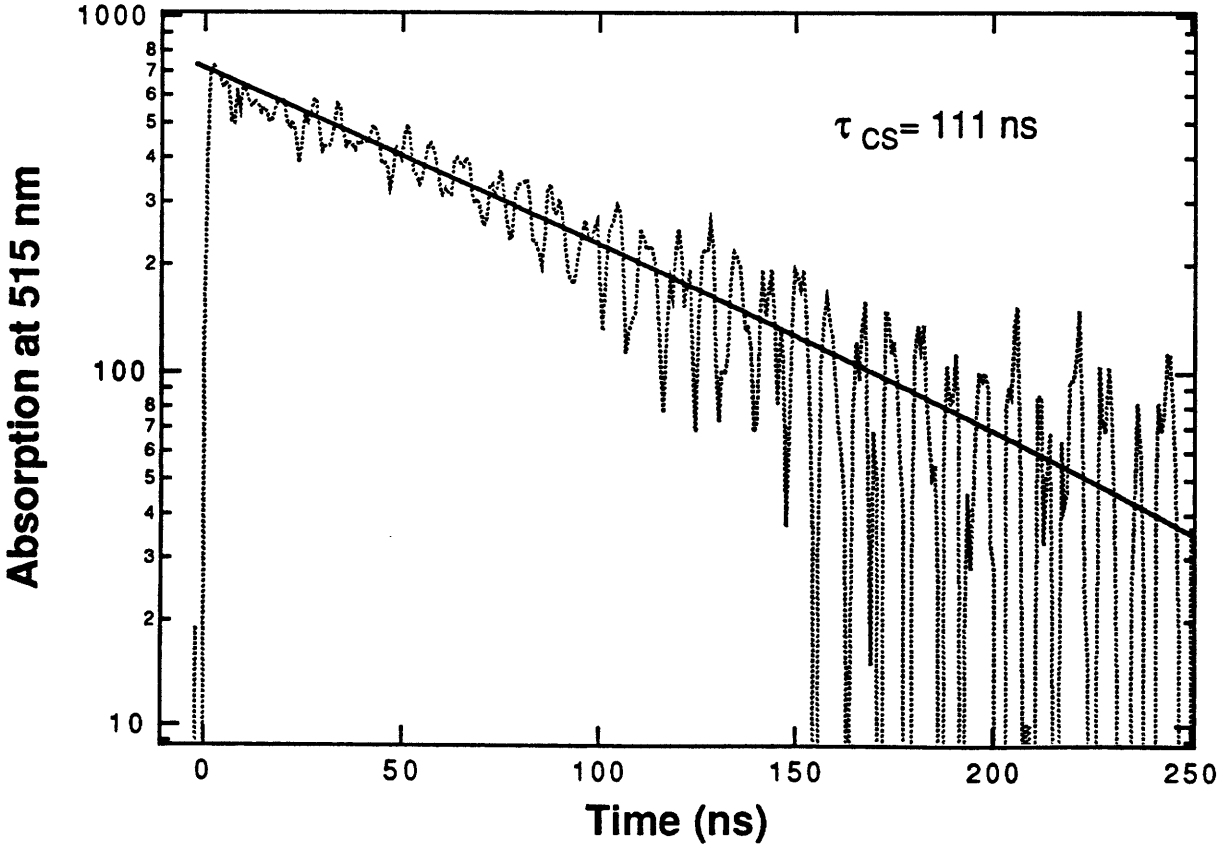
1000
100
10
Absorption at 515 nm
τ CS= 111 ns
0
50
100
150
200
250
Time (ns)

Figure 5-9. Transient absorption spectrum of $Re(mtd)_{50}(PTZ)_5$ in toluene taken 100 ns after a 3 ns 416 nm excitation and the absorption decay at 515 nm following the photoexcitation of $Re(mtd)_{50}(PTZ)_{50}$. Fitting the decay curve produces the lifetime of the charge-separated state of 95 ns.

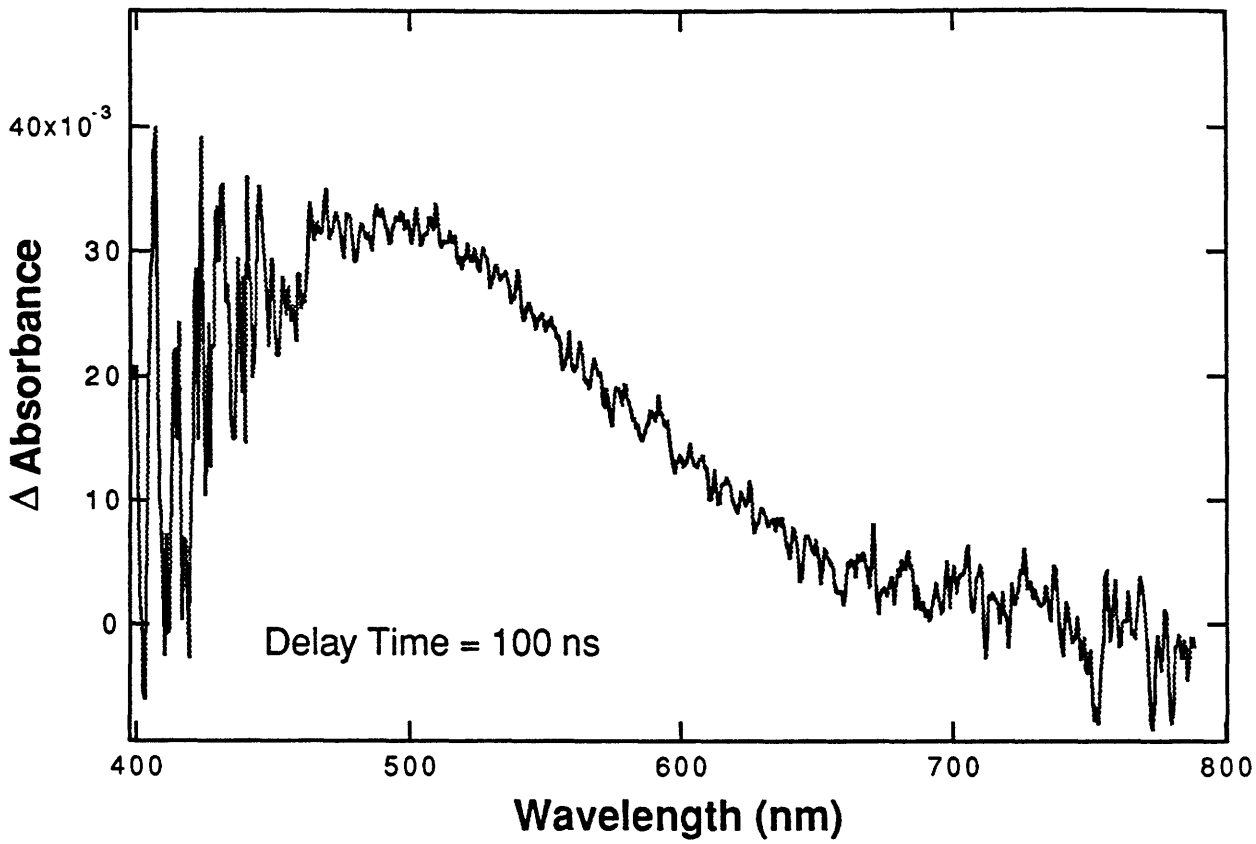
40x10-3
30
20
10
0
Δ Absorbance
Delay Time = 100 ns
400
500
600
700
800
Wavelength (nm)

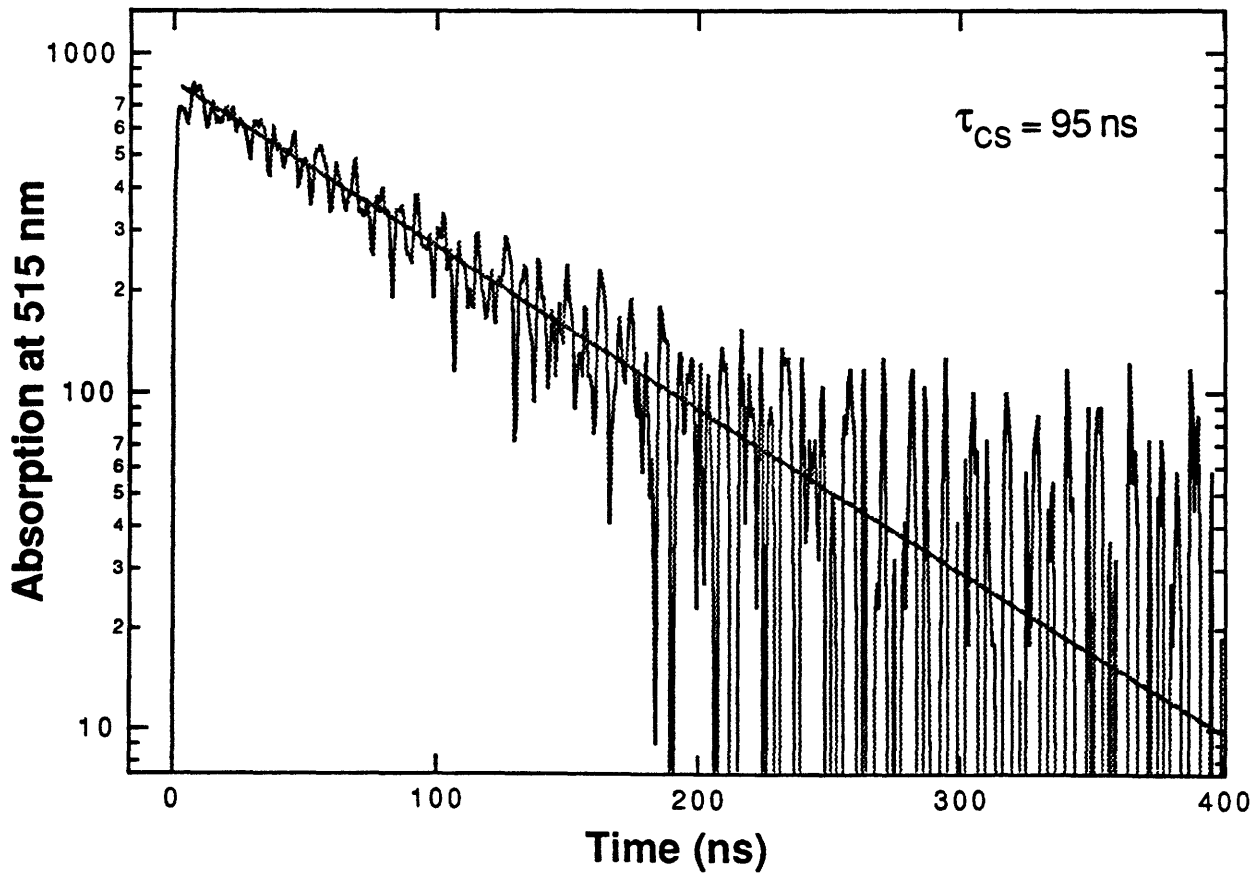
1000
100
10
Absorption at 515 nm
τcs = 95 ns
0
100
200
300
400
Time (ns)

Figure 5-10. Transient absorption spectrum of $Re(TMPD)_{25}$ in toluene taken 20 ns after a 3 ns 416 nm excitation and the absorption decay at 568 nm following the photoexcitation of $Re(TMPD)_{25}$. Fitting the decay curve produces the lifetime of the charge-separated state of 14 ns.

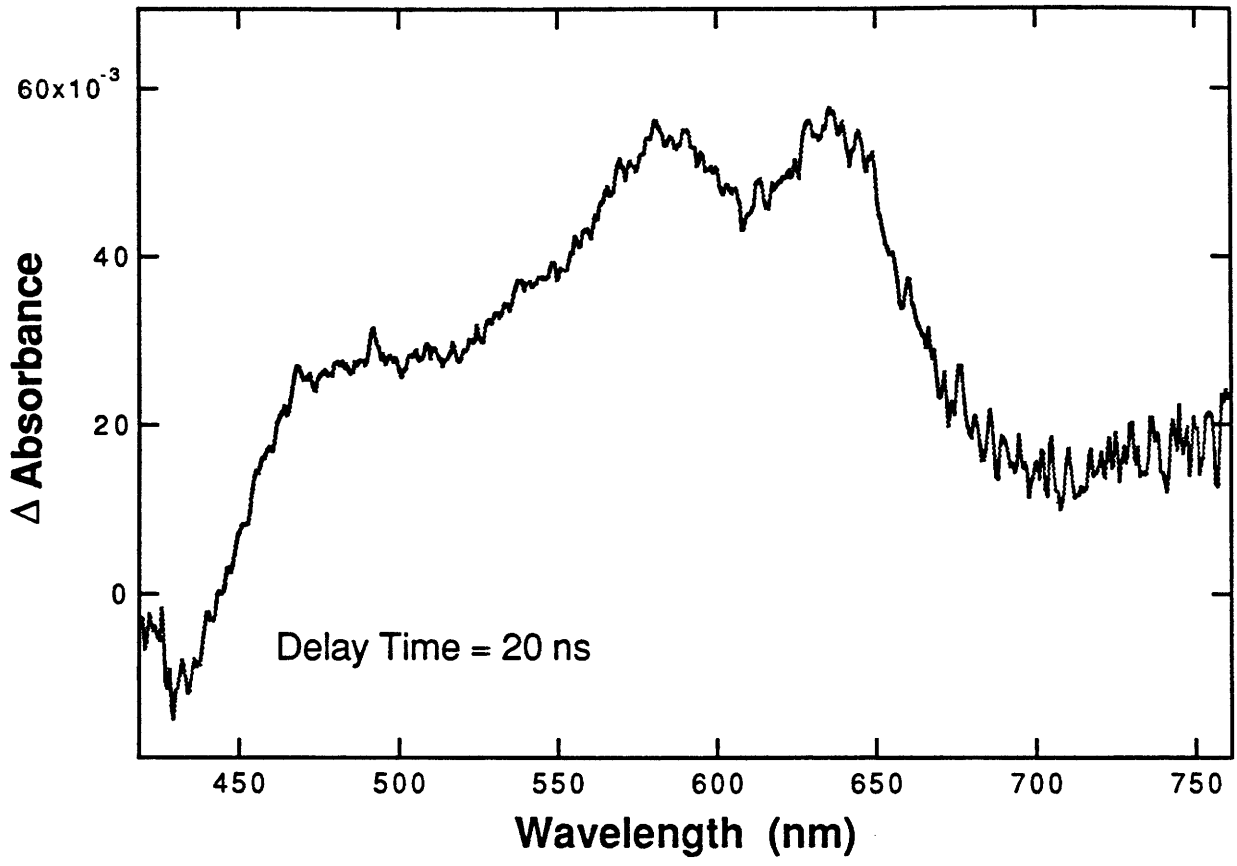
60x10-3
40
20
0
Δ Absorbance
Delay Time = 20 ns
450
500
550
600
650
700
750
Wavelength (nm)

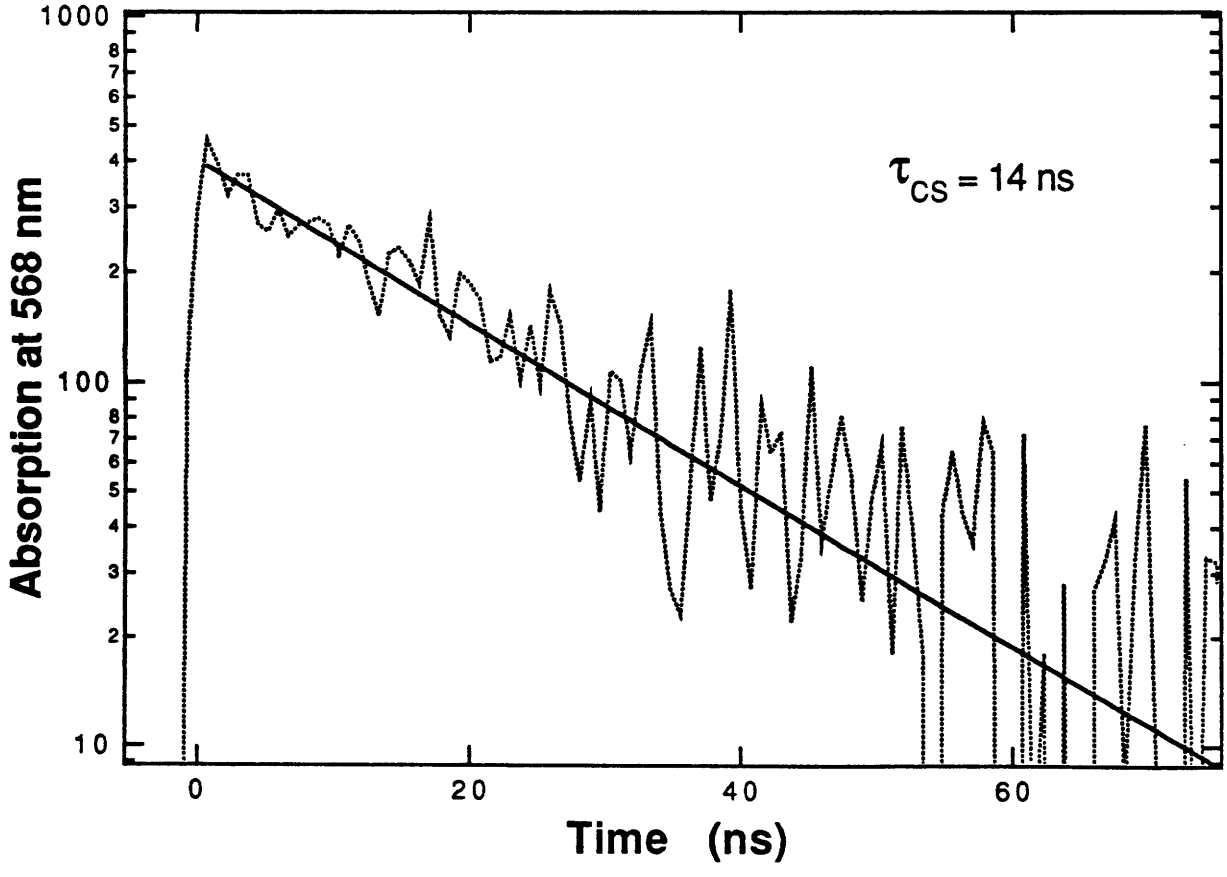
1000
100
10
Absorption at 568 nm
τCS = 14 ns
0
20
40
60
Time (ns)

Figure 5-11. Transient absorption spectrum of $Re(mtd)_{25}(TMPD)_5$ in toluene taken 150 ns after a 3 ns 416 nm excitation and the absorption decay at 568 nm following the photoexcitation of $Re(mtd)_{25}(TMPD)_5$ accompanying with the absorption decay of **III**. Fitting the decay curve produces the lifetime of the charge-separated state of 92 ns.

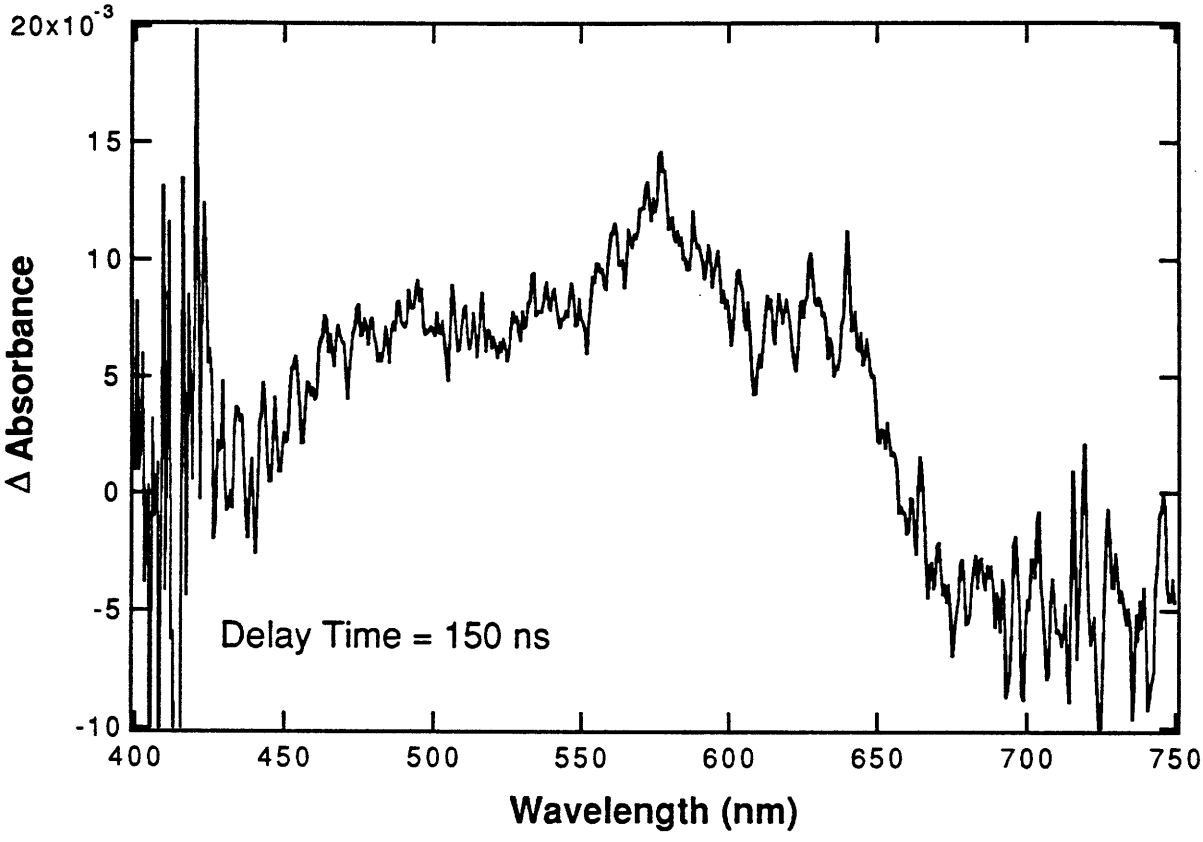
20x10-3
15
10
5
0
-5
-10
Δ Absorbance
Delay Time = 150 ns
400
450
500
550
600
650
700
750
Wavelength (nm)

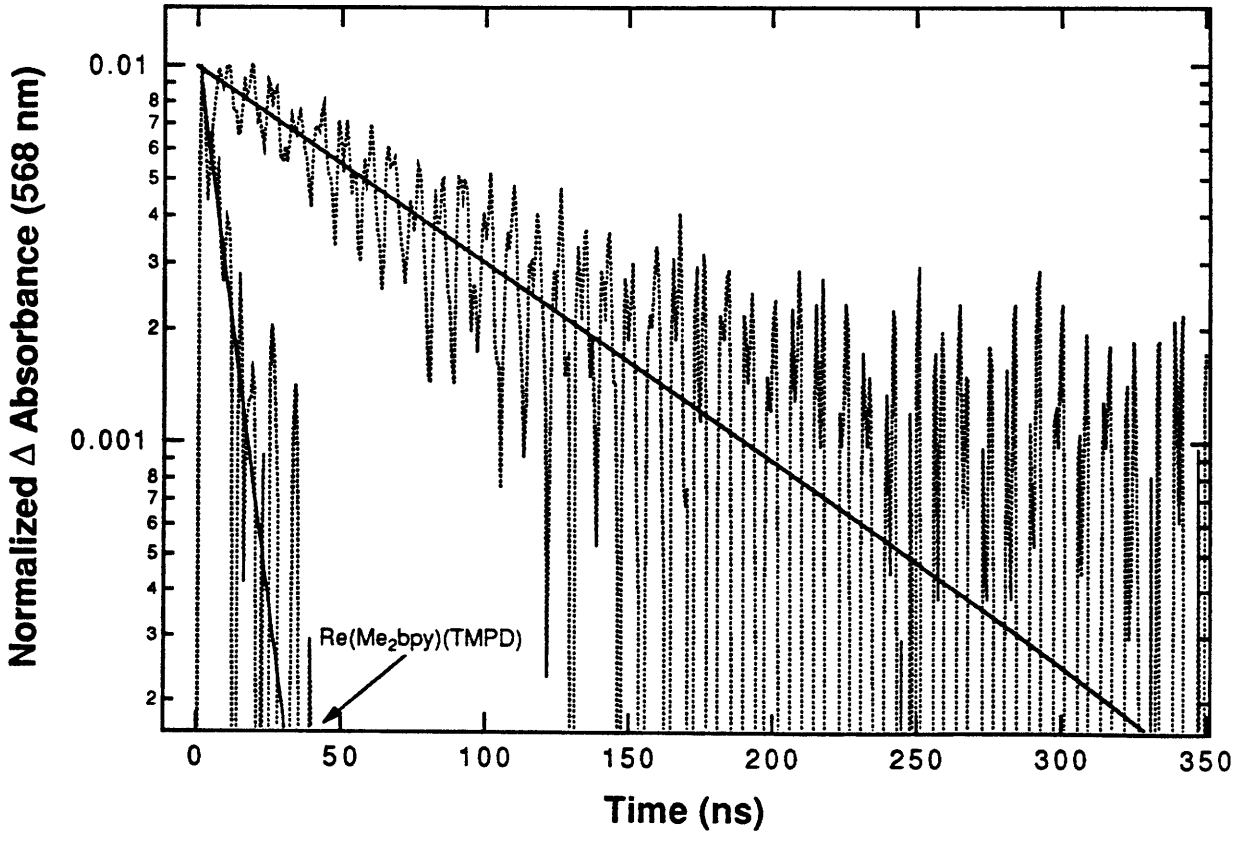
0.01
0.001
Normalized Δ Absorbance (568 nm)
Re(Me2bpy)(TMPD)
0
50
100
150
200
250
300
350
Time (ns)

Figure 5-12. Transient absorption spectra of $Re(mtd)_{100}(PTZ)_{10}(TMPD)_{10}$ in toluene taken 230 ns after a 3 ns 416 nm excitation. The spectral fingerprinting of $PTZ^{+\cdot}$ and $TMPD^{+\cdot}$ are shown in the spectra.

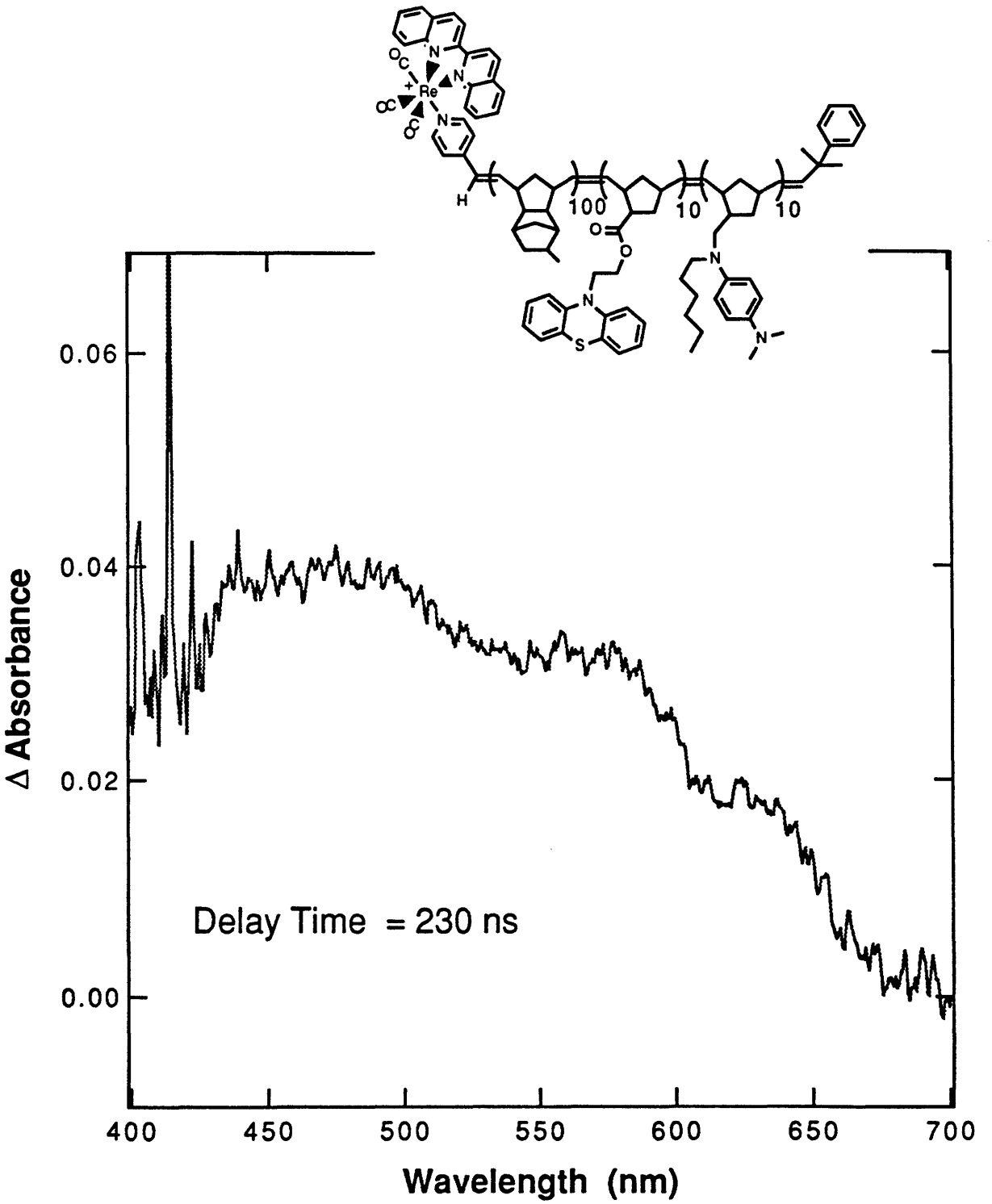
Re
100
10
10
Δ Absorbance
0.06
0.04
0.02
0.00
Delay Time = 230 ns
400
450
500
550
600
650
700
Wavelength (nm)

Figure 5-13. The absorption decays at 515 and 568 nm following the photoexcitation of $Re(mtd)_{100}(PTZ)_{10}(TMPD)_{10}$ in toluene. Fitting the decay curves give τ_{cs} (515 nm) of 88 ns and τ_{cs} (568 nm) of 85 ns.

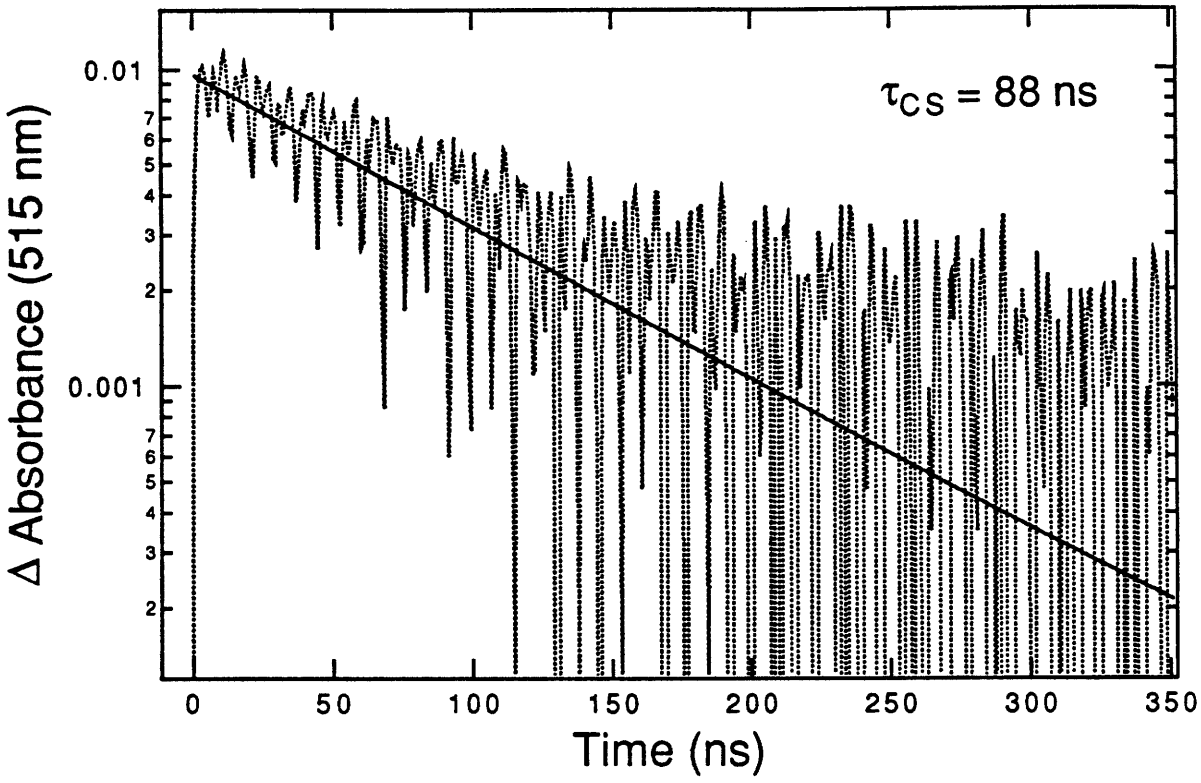
Δ Absorbance (515 nm)
0.01
0.001
τ_{CS} = 88 ns
0
50
100
150
200
250
300
350
Time (ns)

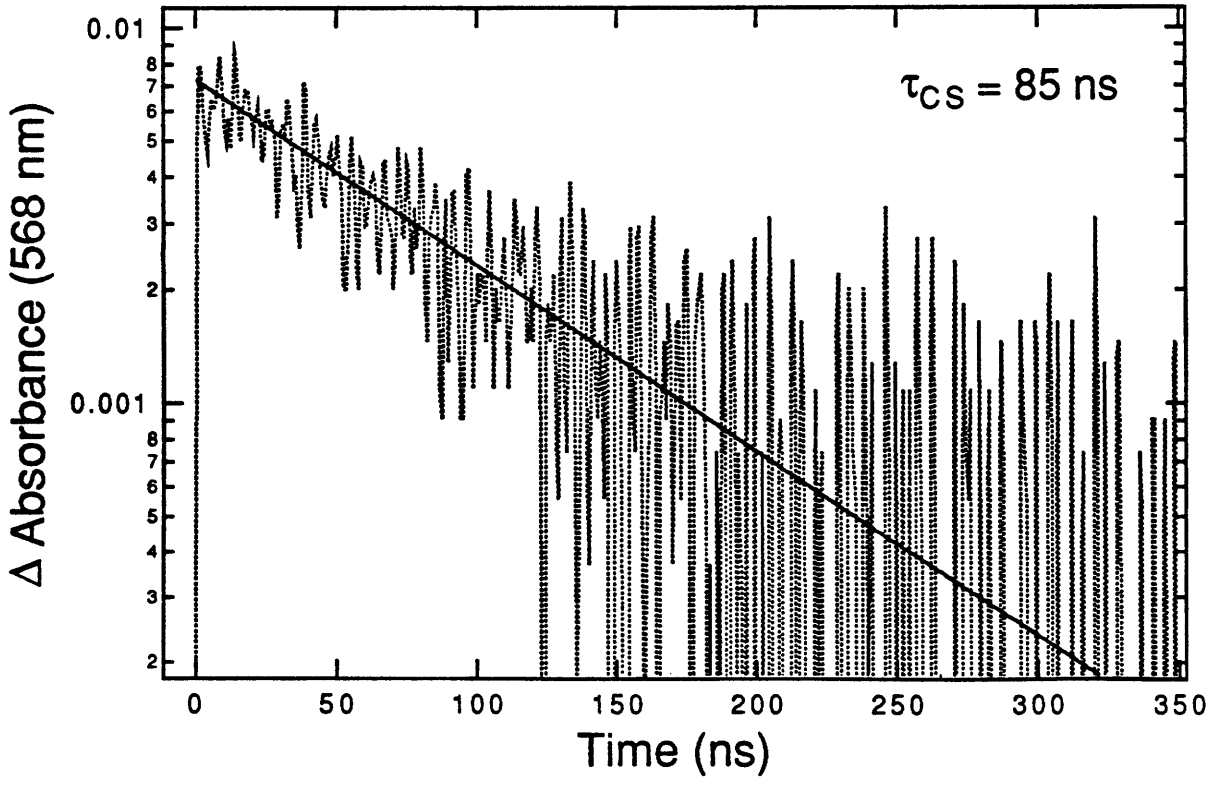
Δ Absorbance (568 nm)
0.01
0.001
τ_{CS} = 85 ns
0
50
100
150
200
250
300
350
Time (ns)

Figure 5-14. Transient absorption spectra produced at the indicated times following the quenching of Re(biq), [(pyridine)$Re(CO)_3$(2,2′-biquinoline)]$^+$ by 10^{-2} M MePTZ and 10^{-5} M TMPD CH_3CN/0.1 M [*n*-Bu_4N]PF_6. The top spectra show immediate appearance of $PTZ^{+\cdot}$ absorption. In the 20 ns to 3 μs time regime show in the middle spectra TMPD electron transfers to $PTZ^{+\cdot}$. The bottom spectra show the diffusion-controlled back reaction of $TMPD^{+\cdot}$ and $Re(biq^-)$. This figure is from ref.18.

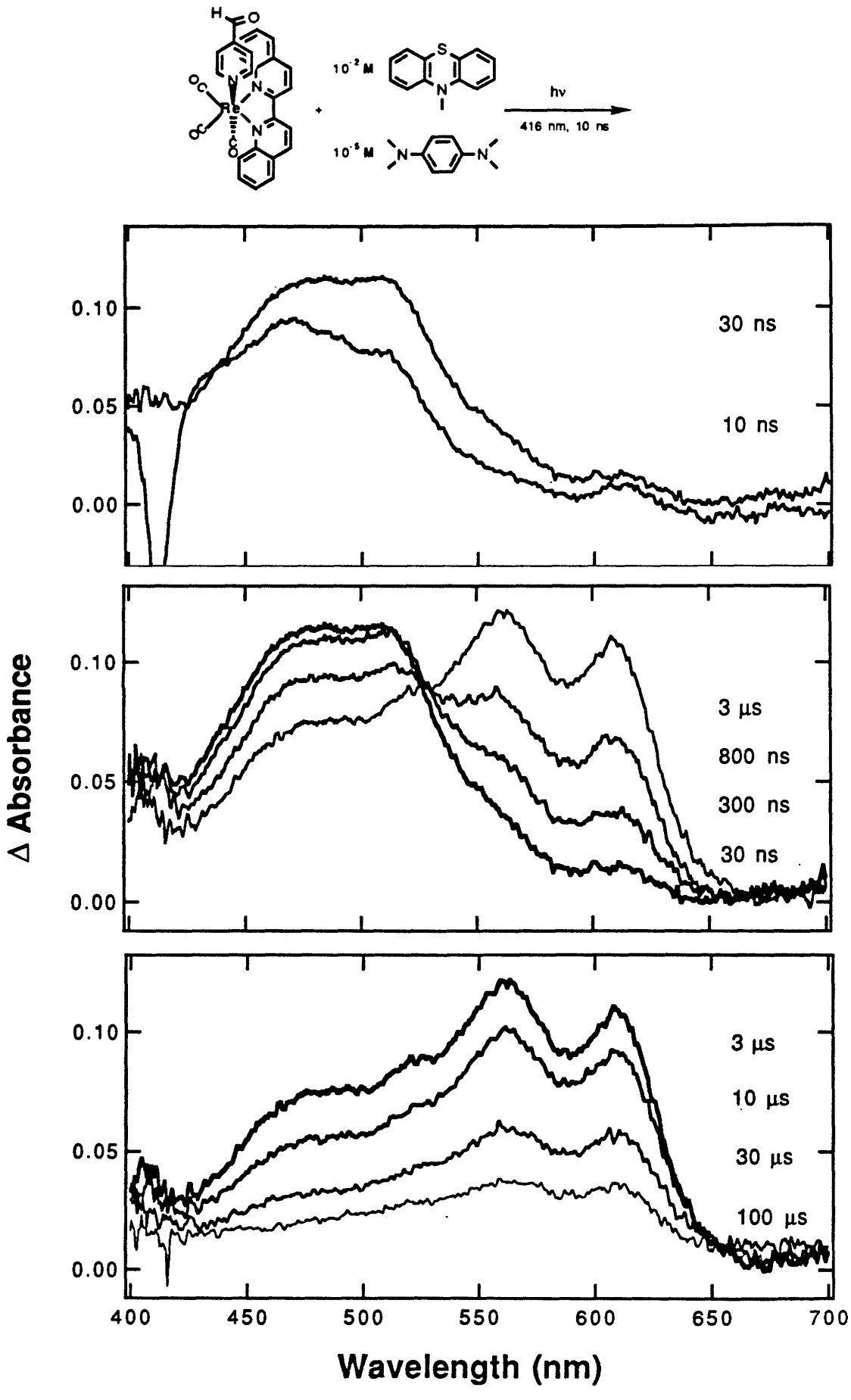
10⁻² M
10⁻⁵ M
hv
416 nm, 10 ns
30 ns
10 ns
3 µs
800 ns
300 ns
30 ns
3 µs
10 µs
30 µs
100 µs
0.10
0.05
0.00
Δ Absorbance
400
450
500
550
600
650
700
Wavelength (nm)

Figure 5-15. Transient absorption spectra of the cast film of $Re(mtd)_{100}(PTZ)_{10}(TMPD)_{10}$ taken 20 ns after a 3 ns 416 nm excitation and the absorption decay at 515 nm following the photoexcitation of $Re(mtd)_{100}(PTZ)_{10}(TMPD)_{10}$. Fitting the decay curve gives that τ_{CS}^{1} = 35 ns and τ_{CS}^{2} = 191.

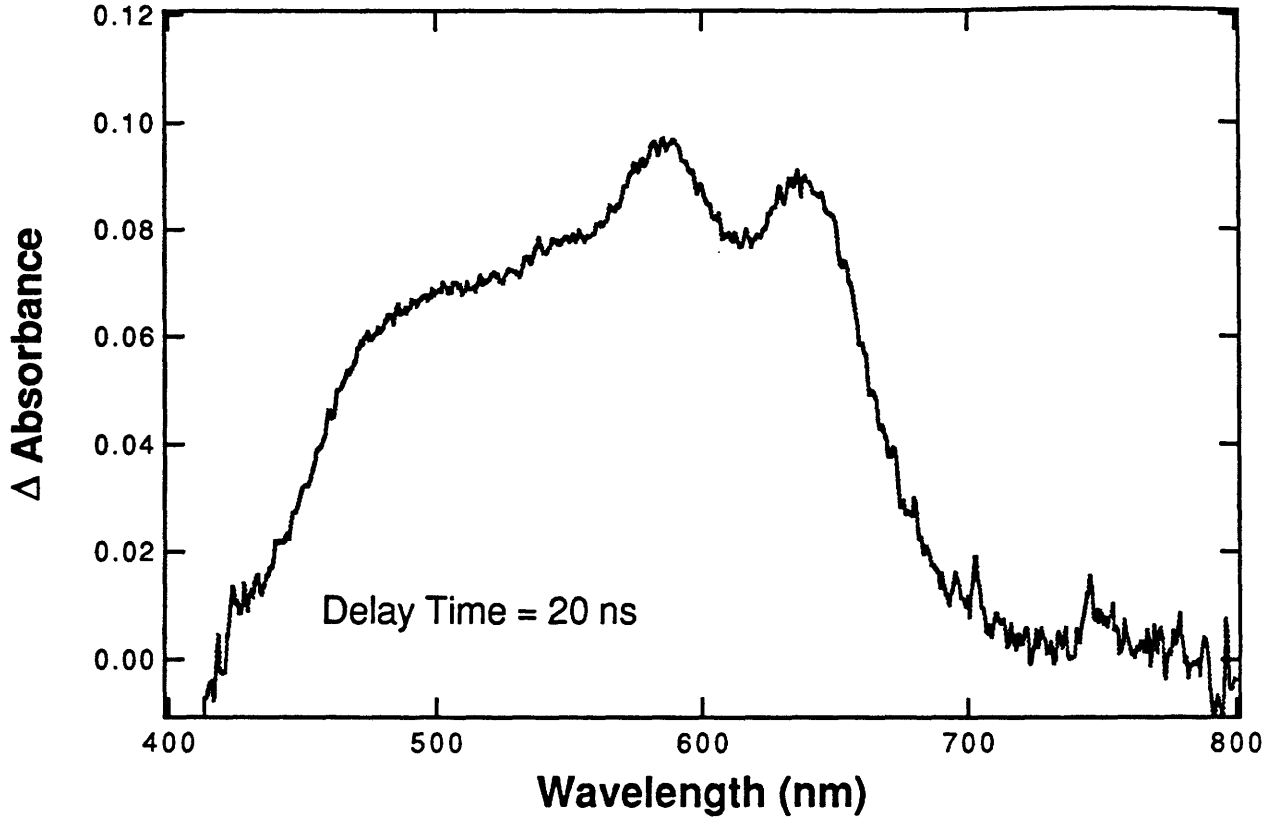
0.12
0.10
0.08
0.06
0.04
0.02
0.00
Δ Absorbance
Delay Time = 20 ns
400
500
600
700
800
Wavelength (nm)

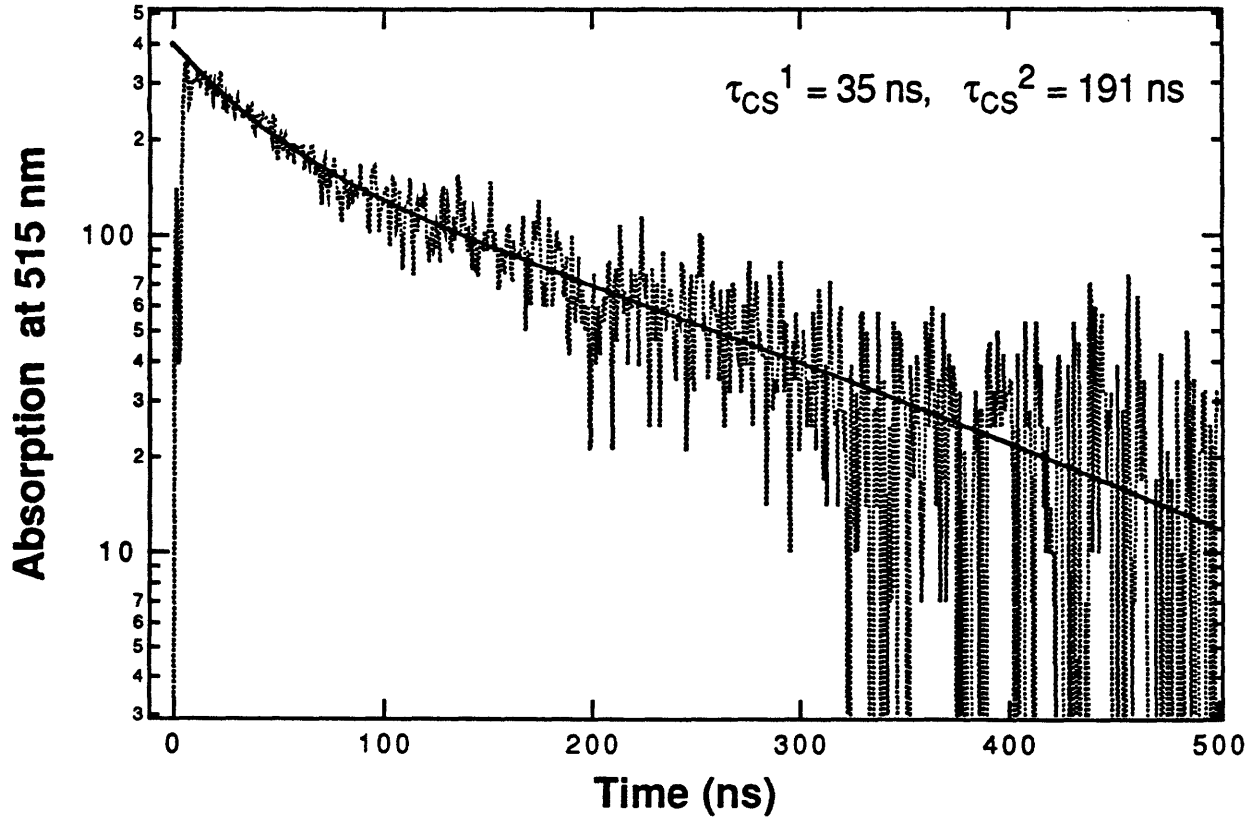
τ_{CS}^1 = 35 ns, τ_{CS}^2 = 191 ns
Absorption at 515 nm
0
100
200
300
400
500
Time (ns)